

THE UNIVERSITY *of* EDINBURGH

This thesis has been submitted in fulfilment of the requirements for a postgraduate degree (e. g. PhD, MPhil, DClinPsychol) at the University of Edinburgh. Please note the following terms and conditions of use:

- This work is protected by copyright and other intellectual property rights, which are retained by the thesis author, unless otherwise stated.
- A copy can be downloaded for personal non-commercial research or study, without prior permission or charge.
- This thesis cannot be reproduced or quoted extensively from without first obtaining permission in writing from the author.
- The content must not be changed in any way or sold commercially in any format or medium without the formal permission of the author.
- When referring to this work, full bibliographic details including the author, title, awarding institution and date of the thesis must be given.

ON

THE ORIGIN OF ACUTE NEUROVASCULAR SYNDROME

BY MEANS OF ^{18}F-SODIUM FLUORIDE POSITRON EMISSION TOMOGRAPHY-MAGNETIC RESONANCE IMAGING

By

JAKUB KACZYNSKI

MBChB (Hons) MRCS (Ed) MSc



THESIS PRESENTED FOR THE DEGREE OF DOCTOR OF PHILOSOPHY

THE UNIVERSITY OF EDINBURGH

2023

To Science

“Knowledge leaves no regrets.
Except for radiation.
I wish I’d never messed with that.”

- Marie Sklodowska-Curie (1867-1934)

ABSTRACT

BACKGROUND

Despite the substantial progress made in understanding that high-risk carotid plaque features can more accurately reflect the risk of acute neurovascular events independently of the degree of stenosis, clinicians around the globe continue to rely on the luminal diameter stenosis of carotid artery as the main parameter that stratifies patients to either surgery or best medical therapy. In effect, non-obstructive (<50% stenosis) carotid plaques are excluded from a stroke preventative intervention despite being highly likely to cause thromboembolic complications. Furthermore, although cross-sectional imaging modalities can provide complementary plaque characteristics, neither of currently available imaging systems can offer a robust insight into the biological status of the clinically culprit plaque. Fluorine 18-labelled sodium fluoride positron emission tomography-magnetic resonance imaging (^{18}F-NaF PET-MRI) is the only imaging technique which facilitates parallel assessment of plaque characterisation; cellular (inflammation), molecular (microcalcification) and morphological (macrocalcification, intraplaque haemorrhage, necrotic lipid core, luminal thrombus, and fibrosis). This thesis focused on the use of ^{18}F-NaF PET-MRI to investigate pathobiological processes of the culprit carotid plaques which are most likely to produce neurovascular syndromes.

METHODS AND RESULTS

Transcranial Doppler: Reproducibility Study (Chapter 3)

This study evaluated the reproducibility of transcranial Doppler ultrasound in healthy volunteers and patients with symptomatic carotid artery stenosis to explore the role of transcranial Doppler in characterisation of clinically culprit carotid plaque. In healthy volunteers (n=20, 31±9 years, 11 male), within-day repeatability of Doppler measurements was 0.880 (95% CI 0.726–0.950) for peak velocity, 0.867 (95% CI 0.700–0.945) for mean velocity, and 0.887 (95% CI 0.741–0.953) for end-diastolic velocity. Between-day reproducibility was

similar but lower: 0.777 (95% CI 0.526–0.905), 0.795 (95% CI 0. 558–0.913), and 0.674 (95% CI 0.349–0.856), respectively. In patients (n=20, 72±11 years, 11 male), within-day repeatability of Doppler measurements was higher: 0.926 (95% CI 0.826–0.970) for peak velocity, 0.922 (95% CI 0.817–0.968) for mean velocity, and 0.868 (95% CI 0.701–0.945) for end-diastolic velocity. Similarly, between-day reproducibility revealed lower values: 0.800 (95% CI 0.567–0.915), 0.786 (95% CI 0.542–0.909), and 0.778 (95% CI 0.527–0.905), respectively. In both cohorts, the intra-observer Bland Altman analysis demonstrated acceptable mean measurement differences and limits of agreement between series of middle cerebral artery velocity measurements with very few outliers. In patients, the carotid stenoses were 30–40% (n = 9), 40–50% (n = 6), 50–70% (n = 3) and > 70% (n =2). No spontaneous embolisation episodes were detected in either of the groups.

^{18}F-NaF PET-MRI: Acute Neurovascular Syndrome (Chapter 4)

In this prospective observational single-centre cohort study, 110 participants were evaluated (mean age, 68 years 6±10 [SD]; 70 men and 40 women). Of the 110, 34 (32%) had prior cerebrovascular disease, 26 (24%) presented with amaurosis fugax, 54 (49%) with transient ischemic attack, and 30 (27%) with stroke. Compared with non-culprit carotids, culprit carotids had greater stenoses (≥50% stenosis: 30% vs 15% [*P* = 0.02]; ≥70% stenosis: 25% vs 4.5% [*P*, 0.001]) and had increased prevalence of MRI-derived adverse plaque features, including intraplaque haemorrhage (42% vs 23%; *P* = 0.004), necrotic core (36% vs 18%; *P* = 0.004), thrombus (7.3% vs 0%; *P* = 0.01), ulceration (18% vs 3.6%; *P* = 0.001), and higher ^{18}F-NaF uptake (maximum tissue-to-background ratio, 1.38 [IQR, 1.12–1.82] vs 1.26 [IQR, 0.99–1.66], respectively; *P* = 0.04). Higher ^{18}F-NaF uptake was positively associated with necrosis, intraplaque haemorrhage, ulceration, and calcification and inversely associated with fibrosis (*P* = 0.04 to *P*, 0.001). In multivariable analysis, carotid stenosis at or over 70% (odds ratio, 5.72 [95% CI: 2.2, 18]) and MRI-derived adverse plaque characteristics (odds ratio, 2.16 [95% CI: 1.2, 3.9]) were both associated with the culprit versus non-culprit carotid vessel.

^{18}F-NaF PET-MRI: Correlation with Histology (Chapter 5)

This study was a subset of the prospective observational single-centre cohort study (Chapter 4) as described above that aimed to assess the correlation between ^{18}F-NaF uptake with *ex vivo* imaging and histological examination. ^{18}F-NaF PET-MRI was evaluated using the maximum standard uptake values (SUV_{max}). A total of 20 participants were evaluated (mean age, 69±9 years; 13 male). *In vivo* 3T MRI demonstrated good to excellent agreement with *ex vivo* 7T MRI (intraplaque haemorrhage, rupture, or erosion, intraplaque haemorrhage) and histology (lipid core, thrombus, calcium) although agreement was poor for lipid core on *ex vivo* 7T MRI and rupture or erosion on histology. The level of agreement between *ex vivo* 7T MRI and histology ranged from good (intraplaque haemorrhage, lipid core) to excellent (calcium), whereas there was a poor agreement for plaque rupture or erosion with no thrombus detection by *ex vivo* 7T MRI. There was a strong correlation between *in vivo* and *ex vivo* ^{18}F-NaF uptake (SUV_{max}, R=0.78, p<0.001), and they both correlated with calcium volume (*in vivo* SUV_{max}, R=0.73, P<0.001; *ex vivo* SUV_{max}, R=0.51, P=0.03) and with calcium index (*in vivo* SUV_{max}, R=0.67, P=0.004; *ex vivo* SUV_{max}, R=0.62, p=0.008). *In vivo* ^{18}F-NaF correlated with elastin index (SUV_{max}, R=0.44, P=0.05), inversely with lipid core (SUV_{max}, R= -0.55, P=0.02) but not with fibrin index (SUV_{max}, R=-0.17, P=0.48) or red blood cell index (SUV_{max}, R=-0.25, P=0.29). *In vivo* SUV_{max} of ^{18}F-NaF uptake predicted histological carotid plaque grade severity (P= 0.04).

CONCLUSIONS

Whilst intracranial Doppler is a reproducible technique, spontaneous embolic episodes are rare and do not provide a clear method for risk stratification in patients with stroke. In contrast, in the largest prospective observational data of acute neurovascular syndromes, ^{18}F-NaF PET-MRI identified clinically culprit carotid plaques that were characterised by adverse plaque features, higher radiotracer uptake and coexistent active aortic vascular lesions. Furthermore, ^{18}F-NaF PET-MRI uptake co-localised with the most severe histological carotid plaque grade severity providing a comprehensive map of

carotid tissue mineralisation supported by relevant *ex vivo* imaging modalities and histological analysis. At present, ^{18}F-NaF PET-MRI is the only imaging modality that enables simultaneous structural and physiological atherosclerotic plaque assessment. This may improve further scientific understanding of atherosclerotic disease and potential therapeutic interventions. Most importantly, hybrid PET-MRI as an ultimate imaging platform could transform the management of patients from the current all-stenosis-based approach to a truly individualised therapeutic dyad centred on the biological plaque activity.

LAY SUMMARY

Most strokes occur when blood clots or other particles block the blood vessels supplying the brain. One such example is hardening of the neck arteries caused by fatty deposits called “plaques”. It occurs because small clots or fatty particles (called microemboli) break off from these hardened areas and reduce the blood supply to the brain. This damages the brain tissue and can cause death. Hardening of the neck arteries usually remains silent for decades and frequently is detected only when an individual presents suddenly with a stroke.

When a stroke is diagnosed, the patient has an ultrasound scan that measures the degree of hardening (narrowing) of a neck artery. If the narrowing of the artery is significant, the patient may undergo an operation that removes the fatty deposit from the neck artery. Conversely, if hardening is not severe, it does not require an operation, and the treatment consists of medications only.

However, it has recently become possible to take pictures highlighting certain biological processes in the hardened arteries that are invisible on an ultrasound scan. ^{18}F-NaF PET-MRI (fluorine 18-labelled sodium fluoride positron emission tomography-magnetic resonance imaging) is a new imaging technique allowing us to examine what is happening in the walls of these narrowed vessels. ^{18}F-NaF PET-MRI detects microscopic calcium deposits (microcalcification), which are linked with the plaques that have a high chance of releasing small clots or fatty particles. This could help to identify more accurately which fatty deposits are more likely to cause strokes, thus, ought to be removed from the arteries, even when narrowing is not severe. In contrast, patients with significantly narrowed vessels without biologically active hardening could avoid surgery.

We tested a simple head ultrasound technique measuring blood flow within the brain circulation. Although we detected no signals corresponding to the small

clots or fatty particles, we showed that this head ultrasound technique was repeatable among patients following a stroke.

Using ^{18}F-NaF PET-MRI, we found a higher level of microcalcification, thus pinpointing biologically active hardening of the neck artery responsible for a stroke. We also confirmed that this new imaging scanner discovered vessel wall components that contribute to the risk of future stroke.

To establish whether ^{18}F-NaF PET-MRI correctly identified microcalcium spots and “ingredients” within the fatty deposits, we examined plaques removed from the neck arteries during surgery under the microscope. We found that ^{18}F-NaF PET-MRI found a high level of microcalcification in the areas of fatty deposits, which consisted of the same components found on the images. This indicated that this new imaging technique could one day be used to identify future patients at particular risk of stroke, hence should undergo surgery.

This largest ^{18}F-NaF PET-MRI study may give us valuable insights into why hardening of the arteries develops and pave the way for new treatments for stroke conditions.

DECLARATION

This thesis has been composed by myself and represents the research work that I have undertaken between August 2016 and August 2020 at the British Heart Foundation Centre for Cardiovascular Science, University of Edinburgh. I performed literature search, designed and drafted the study proposal under the supervision of Professor David Newby. I obtained the Clinical Research Training Fellowship grant (FS/17/50/33061) which funded this research project from the British Heart Foundation with the support from Professor David Newby. I applied for relevant regulatory approvals (ethical, research and development) and I registered the study on a publicly open domain (ClinicalTirials.gov) prior to the patients recruitment. I was personally involved in all aspects of the research process, including recruitment, consent, clinical assessment, transcranial Doppler imaging, development of PET-MRI imaging protocol, image analysis, compilation of results with statistical data analysis and authoring publications arising from this research, as reported in this thesis. Chapters 1, 2, 3, 4, 5 and 6 have been either published in peer-reviewed journals or manuscripts are currently drafted (Chapter 5). The thesis has not been submitted elsewhere in the application for any other degree or qualification.

Jakub Kaczynski, 2023

ACKNOWLEDGEMENTS

I undertook this research and other related studies under the primary supervision of Professor David Newby at the University of Edinburgh. The entirety of this research, including thesis would not have been possible without Professor Newby's vision and patience. Throughout the years, his academic work enriched the scientific field and inspired numerous research fellows. Professor Newby has certainly lit the flame of my own desire to continue a lifelong tour of academia that in my opinion, is an essential part of a well-rounded vascular surgeon. I wish to express my profound appreciation and gratitude to Professor Newby for his wisdom and generous support. I feel very fortunate that I had this incredible research opportunity that shaped me professionally and personally. The journey of my research has been challenging and uplifting. It helped me to crystalise some of the central aspects of science, its professional conduct and interpretation of data. I hope this thesis will continue to advance scientific discoveries and I am glad that I made some progress towards this ambition.

I would like to thank my secondary supervisors for their time and ideas to enable successful completion of this research, Professor William Whiteley, and Mr Andrew Tambyraja. I would also like to acknowledge guidance from the stroke team, including Professor Joanna Wardlaw, Professor Martin Dennis, Professor Rustam Al-Shahi and Dr Fergus Doubal.

I could not thank enough my collaborators at the Edinburgh Imaging Facility regarding the development of complex imaging protocols and subsequent image analysis. The input that I have received from Professor Edwin van Beek, Dr Gillian Macnaught, Dr Christophe Lucatelli, Dr Calum Gray, Dr Chengjia Wang, Dr Tom McGillivray, Dr Scott Semple and David Senyszak was invaluable. Particularly, I would like to thank David Brian and the entire team of radiographers without whom this research would not have been possible.

I acknowledge a debt of gratitude to the staff of the Clinical Research Facility for their participation in study visits. I am also grateful to the vascular team, theatre and vascular laboratory staff at Edinburgh Royal Infirmary for their help in this project.

I would like specially thank Dr Stephanie Sellers and Dr Jonathon Leipsic in Canada for their contribution and histopathological analysis. Similarly, I would like to acknowledge the contribution from Dr Adriana Tavares, Carlos Corral Alcaide, Dr Maurits Jansen and Ross Lennen that have played a crucial role in ex vivo imaging of carotid tissue.

I would like to extend my gratitude to my fellow colleagues for their help, discussions and successful collaborations including Rachael Forsythe, Maaz Syed, Alex Fletcher, Alastair Moss, Alex Vesey and especially I wish to thank Michelle Williams who provided me with advice and ongoing support.

I would like to acknowledge the role of outstanding vascular surgery frontiers, academics, and trainers: Mr L Fligelstone, Mr C Gibbons, Professor I Pallister (orthopaedic trauma surgeon), Mr R Holdsworth and Mr J Nagy who have presented me with a contrasting perspective on vascular surgery conditions including trauma, their clinical implications and richness of various preventative surgical manoeuvres that benefit patients. I intend to continue their legacy.

Above, all I would like to thank all patients who have agreed to participate in the research. Their contribution was second to none and I appreciate their willingness in helping to advance research for the benefit of *others*.

Last, I am enormously grateful to Maria for her patience and steady support over the past four years and beyond.

ABBREVIATIONS

1.5T	1.5 Tesla
^{11}C	Carbon-11
^{123}I	Iodine-123
^{125}I	Iodine-125
^{15}O	Oxygen-15
^{18}F	Fluorine-18
^{18}F-FCH	^{18}F-labelled fluorocholine
^{18}F-FDG	^{18}F-Fluorodeoxyglucose
^{18}F-FIMSO	^{18}F-fluoromisonidazole
^{18}F-GP1	Thrombus-specific radiotracer
3T	3 Tesla
^{64}Cu	Copper-64
^{68}Ga	Galluim-68
7T	7 Tesla
^{99}Tc	Technetium-99
AMA	Aortic microcalcification activity
ATLO	Arterial tertiary lymphoid organs
CD68+	Cluster of Differentiation 68
CETC	Carotid Endarterectomy Trialists Collaboration
CMA	Coronary microcalcification activity
COX-1	Cyclooxygenase-1
COX-2	Cyclooxygenase-2
CT	Computed tomography
$CXCL_{12}$	Chemokine ligand 12
$CXCR_4$	Chemokine receptors 4
dB	Decibels
ECST	European Carotid Surgery Trial
FAPI	Fibroblast Activation Protein Inhibitor
GPIIb/IIIa	Glycoprotein IIb/IIIa receptor
ICAM-1	Intercellular adhesion molecule
ICC	Intra-class correlation coefficient
keV	Kiloelectronvolt
LDL	Low-density lipoproteins

mAb	Monoclonal antibodies
MBq	Megabecquerels
MCA	Middle cerebral artery
MES	Microembolic signals
Micro-PET-CT	Micro positron emission tomography-computed tomography
MMP	Matrix metalloproteinases
MRI	Magnetic resonance imaging
^{18}F-NaF	Fluorine 18–labelled sodium fluoride
NASCET	North American Symptomatic Carotid Endarterectomy Trial
PCSK9	Proprotein Convertase-Subtillisin/Kexin type 9
PD	Proton density
PDGF	Platelet derived growth factor
PET	Positron emission tomography
PET-CT	Positron emission tomography-computed tomography
PET-MRI	Positron emission tomography-magnetic resonance imaging
RF	Radiofrequency
Runx2	Runt-related transcription factor 2
SPACE	Sampling Perfection with Application optimized Contrasts using different flip angle Evolution
SPECT	Single-photon emission computerised tomography
SUV_{max}	Standardized uptake values max
SUV_{mean}	Standardized uptake values mean
T1W	T1-weighted
T2W	T2-weighted
TBR_{max}	Tissue-to-background ratio max
TBR_{mean}	Tissue-to-background ratio mean
TE	Echo time
TIA	Transient ischaemic attack
TOF	Time-of-flight
TR	Repetition time
TSPO	Translocator protein
USPIO	Ultrasmall paramagnetic particles of iron oxide
UTE	Ultrashort echo time
VCAM-1	Vascular cell adhesion molecule

CONTENTS

	Pages
ABSTRACT	iv-vii
LAY SUMMARY	viii-ix
DECLARATION	x
ACKNOWLEDGEMENTS	xi-xii
ABBREVIATIONS	xiii-xiv
CONTENTS	xv-xvii
CHAPTER 1:	1-97
INTRODUCTION	
1.1 Background	
1.2 Aetiology of carotid territory acute neurovascular syndrome	
1.3 Pathogenesis of the atherosclerotic carotid disease	
1.4 Carotid plaque progression	
1.5 Clinical neurovascular events	
1.6 Current evaluation of carotid atherosclerosis	
1.7 Current imaging modalities of carotid artery stenosis	
1.8 Summary	
1.9 Aims and hypotheses	
CHAPTER 2:	98-132
METHODS	
2.1 General	
2.2 Transcranial Doppler Ultrasound	
2.3 Positron Emission Tomography	
2.4. Magnetic Resonance Imaging	
2.5 Hybrid Positron Emission Tomography- Magnetic Resonance Imaging	
2.6 Ex vivo Imaging	
2.7 Histopathology	
2.8 Statistical Analysis	

CHAPTER 3: 133-151

REPRODUCIBILITY STUDY OF TRANSCRANIAL DOPPLER IN THE MIDDLE CEREBRAL ARTERY

3.1 Introduction

3.2 Methods

3.3 Results

3.4 Discussion

3.5 Conclusions

CHAPTER 4: 152-181

^{18}F-SODIUM FLUORIDE POSITRON EMISSION TOMOGRAPHY-MAGNETIC RESONANCE IMAGING IN PATIENTS WITH ACUTE NEUROVASCULAR SYNDROME

4.1 Introduction

4.2 Methods

4.3 Results

4.4 Discussion

4.5 Conclusions

CHAPTER 5: 182-211

^{18}F-SODIUM FLUORIDE POSITRON EMISSION TOMOGRAPHY-MAGNETIC RESONANCE IMAGING IN PATIENTS UNDERGOING CAROTID ENDARTERECTOMY – CORRELATION WITH HISTOLOGY

5.1 Introduction

5.2 Methods

5.3 Results

5.4 Discussion

5.5 Conclusions

CHAPTER 6: 212-248

CONCLUSIONS AND FUTURE DIRECTIONS

6.1 Introduction

6.2 Summary of thesis findings

6.3 Limitations
6.4 Future directions
6.5 Final conclusions

BIBLIOGRAPHY OF ADDITIONAL WORKS 249-257
REFERENCES 258-297

CHAPTER ONE

INTRODUCTION

1.1 BACKGROUND

"This apoplexy is, as I take it, a kind of lethargy…
a kind of sleeping in the blood…"

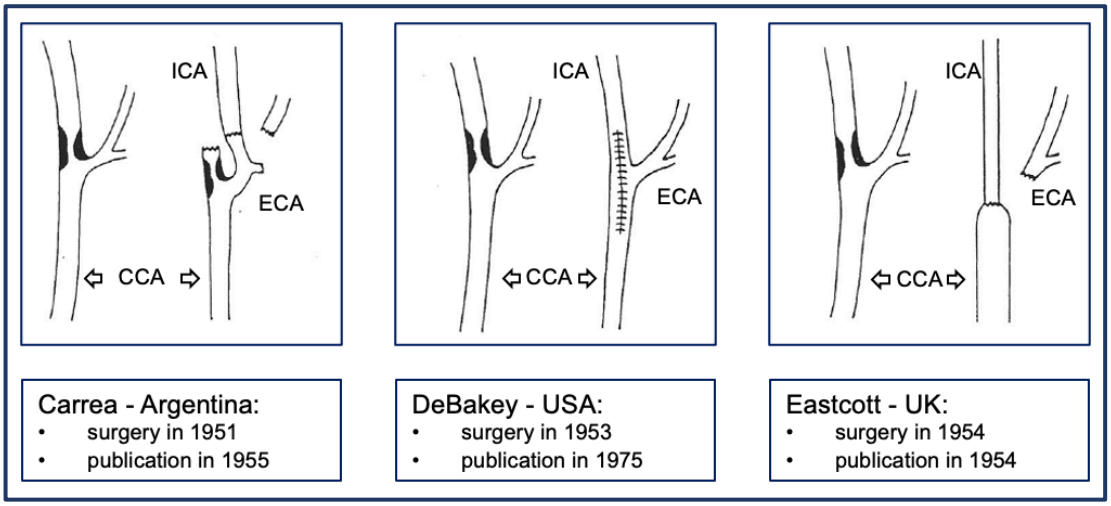
- William Shakespeare (1564-1616)

The history of stroke spans many centuries and is paved with the names of many important pioneers. Their milestone discoveries allow us to comprehend why it has taken us so long to recognise and understand the nature of the acute neurovascular syndromes. The first description was made by Hippocrates (460-370 BC) who documented loss of consciousness caused by occluded stout arteries that were named *carotid* from the Greek word Karos meaning *deep sleep* [Caplan, 2016]. At this time, stroke related paralysis *plexe* was referred to as *apoplexy* [Donkor, 2018]. Next, Galen (131-201 AD) with the first description of animal brain circulation dominated medical knowledge for more than 1300 years [Nilsen, 2010; Caplan, 2016]. Finally, in 16th century Andreas Vesalius broke the Galenic dogma by creating detailed neuroanatomical diagrams of the human brain by conducting cadaveric dissections [Caplan, 2016]. Whilst the most notable discovery of 17th century was the eponymous *circle of Willis* described by Thomas Willis in Oxford in the United Kingdom [Caplan, 2016]. Successive clinical and pathological observations have many scientific fathers including Giovanni Battista Morgagni, Rudolf Virchow, William Osler, and others [Donkor, 2018; Caplan, 2016]. During the 20th century, Chiari in 1905 and later Hunt in 1914 correlated clinical cerebral embolisation with ulcerated carotid plaques at post-mortem examinations [Estol, 1996]. Whereas Moniz in 1937 performed the first angiography as a novel tool to investigate carotid artery pathology [Cronenwett et al., 2014]. However, these conclusions met with a substantial rebuttal from the scientific community, and for more than a decade, stroke was still attributed to a vasospasm. In effect, the treatment options aimed to "reduce reflex spasm in the cerebral vessels" by performing sympathectomy [Estol, 1996]. In 1951

C. Miller Fisher published autopsy findings from over 1100 carotid arteries concluding that “indeed it may well prove to be one of the major causes of apoplexy” [Fisher, 1951]. This formulated the long-awaited explanatory model for cerebral embolisation from the carotid arteries that was finally universally accepted. The conclusions made by C. Miller Fisher were neither new nor original, but by connecting the missing neurovascular dots together, he foresaw what nobody else had. Thus, his scientific breakthrough was the product of discovering a link between established aspects of knowledge. In 1954 carotid revascularisation done by Eastcott, Pickering and Rob at St. Mary’s Hospital in London in the United Kingdom gained its momentum, and carotid surgery followed to remove carotid plaques to prevent future ischaemic strokes [Eastcott et al., 1954]. The authorship of the first carotid arterial reconstructions is somewhat shared among several surgical figures. Undoubtfully, the first carotid reconstruction for occlusive carotid disease was performed by Carrea (neurosurgeon) in 1951 in Argentina [Friedman, 2014]. The operation involved arterectomy (partial resection of the diseased carotid segment) with *carotid-carotideal* anastomosis (end-to-end anastomosis of the external to the internal carotid arteries) and the report was published in 1955 (Figure 1.1) [Carrea et al., 1955]. This surgical technique was modified by Eastcott, Pickering and Rob by re-establishing arterial continuity following arterectomy by anastomosing the common carotid to the distal internal carotid artery (Figure 1.1) [Eastcott et al., 1954]. However, the credit for the first carotid endarterectomy including primary arteriotomy closure thus avoiding arterectomy, belongs to DeBakey (vascular surgeon) who performed this operation in 1953 in the United States of America. Unfortunately, because of the delayed publication this fact went unnoticed for 22 years [DeBakey, 1975]. Lastly, in 1956 Cooley (an American cardiac surgeon) performed closure of arteriotomy following carotid endarterectomy using Dacron velour patch [Cooley et al., 1956; Cooley, 1988]. Nevertheless, it was the prompt publication by Eastcott that marked a quantum leap within the vascular surgery arena establishing a permanent place of carotid surgery in the treatment of carotid thromboembolic disease. Almost half a century later, the two most prominent

randomised control trials; North American Symptomatic Carotid Endarterectomy Trial (NASCET) and European Carotid Surgery Trial (ECST) have fundamentally influenced vascular practice. These trials established carotid endarterectomy as the gold standard in stroke prevention in patients with symptomatic carotid artery stenosis.

Figure 1.1: The first carotid artery reconstructions.



Reproduced and updated from the "Historical Vignettes in Vascular Surgery" [Friedman, 2014]. CCA: common carotid artery; ECA: external carotid artery; ICA: internal carotid artery; USA: United states of America; UK: United Kingdom

The evolution in the understanding of carotid thromboembolism, including treatment options such as medical, surgical, and endovascular techniques, represents a tremendous achievement of vascular medicine as a scientific discipline. More importantly, carotid related research demonstrated the importance of understanding the pathophysiological origin of disease prior to formulating any treatment strategy because as Professor Janet Powell said, "only with such understanding and collaborative research can one obtain the evidence for improvements in patients care" [Powell, 2015]. Additional work of the brilliant Professor Peter Rothwell, Professor Alison Halliday, Professor Martin Brown, Professor Ross Naylor and two outstanding researchers at the Centre for Clinical Brain Sciences, University of Edinburgh namely Professor Joanna Wardlaw and Professor Charles Warlow contributed significantly to the greater understanding of pillars of evidence-based medicine such as

randomised control trials, systematic reviews, and meta-analyses [Qiu, 2008]. Ultimately, the technological revolution from an invasive angiography to non-invasive anatomical and molecular imaging modalities produced major advances in the imaging field that enabled visualisation of vascular lesions including their morphological and cellular elements akin to sub-atomic particles. The novel and truly sophisticated imaging modalities allowed us to bridge the theoretical and practical gap by explaining how interconnected factors come together to craft the culprit carotid plaque and the forces that drive its instability. Finally, these innovations permitted the discovery of new medical therapeutic strategies for survivors of acute neurovascular syndromes.

Despite these advances, many aspects surrounding the management of ischaemic stroke remain unresolved. The disease is the second leading cause of death and disability around the globe, with approximately 2.7 million deaths a year [Johnson et al., 2019; Gorelick, 2019; World-Stroke-Organization, 2019]. In the United Kingdom, the rate of stroke decreased between 1990 and 2010 by almost 20% because of better prevention, earlier and more advanced treatment rather than a decline in the incidence [Feigin et al., 2014]. Yet still, over 100,000 individuals suffer a stroke with almost 60,000 reported deaths each year [King et al., 2020; Davies et al., 2006]. Furthermore, predicted stroke related illness, including death, is set to double in the next 15 years [Feigin et al., 2014; Johnson et al., 2019]. This may translate into the astonishing spending rise (250%) in the health and social care costs, which currently in the United Kingdom are around £26 billion a year [King et al., 2020].

Additionally, even with the meticulous surgical technique that overall has halved the 30-day peri-operative stroke and death rate to 1-2% in the United Kingdom from the recommended 6-7% threshold reported by NASCET, carotid endarterectomy remains a high-risk vascular procedure [Ferguson et al., 1999; Waton et al., 2020; Paraskevas et al., 2016; Rothwell et al., 2003b]. Thus, the

ability to accurately select patients who would benefit from surgery is of paramount importance.

This historical context of stroke broadens our perspective on the disease. Equipped with this knowledge, we can choose a path towards future research and novel discoveries. And if this “brief” history of stroke has taught us anything, it is that successful ischaemic stroke management starts with an accurate detection of clinically culprit carotid plaque. Otherwise, identification of carotid plaque will continue to be an Achilles heel of vascular surgery. Only when we fully integrate the biology of the plaque with simultaneous validation of clinical outcomes, will we transform the management of patients from the current *stenosis-based* approach to truly individualised medicine. Therefore, the focus of this thesis is on the pathobiological processes and identification of the plaques which are most likely to produce neurovascular symptoms.

1.2 AETIOLOGY OF CAROTID TERRITORY ACUTE NEUROVASCULAR SYNDROME

Atherosclerosis of the carotid bifurcation and the internal carotid artery are the principal cause of thromboembolism responsible for the major acute neurovascular events such as ischaemic stroke, transient ischaemic attack, or retinal ischaemia (amaurosis fugax). It is a complex disease characterised by the interplay of many factors including metabolic, behavioural, hereditary, and histopathological determinants. The atherosclerotic disease can remain clinically silent for decades or can present aggressively in early life with serious cardiovascular consequences. Moreover, our understanding of why some develop carotid atherosclerosis early, whilst others with similar risk factors retain disease-free carotid arteries is incomplete.

1.2.1 DEMOGRAPHY AND GENES

Age is the strongest determinant of acute neurovascular event. Although ischaemic stroke usually affects patients over 70-75 years of age, the risk

doubles every decade above age 55 [Donkor, 2018]. Furthermore, recent data suggest that the average age of major cerebral events has decreased and up to a quarter of neurovascular events occur in the individuals of working age [Donkor, 2018; Johnson et al., 2019]. These data reflect the natural history of atherosclerotic disease progression that regardless of age, can remain asymptomatic until luminal atheroma ruptures and flowing blood over the culprit lesion washes away embolic material distally.

The worldwide incidence of ischaemic stroke is greater in men (52%) compared with women (48%) [Gorelick, 2019; World-Stroke-Organization, 2019]. Men also tend to suffer from a stroke at a younger age, although the death rate is higher among women who live longer [Feigin et al., 2017; Stroke-Association, 2020]. Higher prevalence of cardiovascular complications among men has been widely attributed to the negative effects of androgens and behavioural factors such as tobacco use and increased alcohol consumption [Cronenwett et al., 2014]. Whilst oestrogens in women appear to offer a beneficial lipid profile until the onset of menopause [Cronenwett et al., 2014], oestrogen replacement therapy is disappointingly associated with an increased risk of stroke (hazard ratio 1.6) [Roach et al., 2015].

There is increasing evidence that genetic factors contribute to a risk of stroke, but no genetic markers have been identified that would enable population screening. Although genome-wide association studies have identified a wide range of genes associated with ischaemic stroke, some of these genes are also associated with the traditional risk factors of stroke [Ikram et al., 2009]. A meta-analysis of 12 genome-wide association studies that included European 10,307 stroke cases and 19,326 controls from European populations, found loci that were associated with ischemic stroke [Malik et al., 2016]. Recently, the largest study which involved a meta-analysis of 521,612 individuals (67,162 cases and 454,450 controls) including those with European and non-European ancestry groups (America, Asia, Africa, and Australia) identified 32 stroke risk loci, including 22 novel ones [Malik et al., 2018].

Ethnic differences may also contribute to ischaemic stroke risk. In general, cardiovascular atherosclerotic diseases are more prevalent in developed countries [Donkor, 2018]. However, individuals of Sub-Saharan Africa descent have a significantly higher rate of stroke compared to Caucasians [Connor et al., 2007; Johnston et al., 2009]. This may be related to the increased frequency among African populations of the sickle cell disease, which is a known haematological cause of the stroke but also risk factors such as hypertension, diabetes, and obesity [Beard et al., 2009].

Finally, other carotid artery diseases that are associated with acute neurovascular events include fibromuscular dysplasia, Takayasu's arteritis, carotid body tumour, aneurysm, and dissection. However, these conditions are non-atheromatous and frequently of unknown origin and are beyond the scope of this thesis.

1.2.2 METABOLIC AND BEHAVIOURAL RISK FACTORS FOR ACUTE NEUROVASCULAR SYNDROME

Acute neurovascular syndrome shares numerous risk factors associated with atherosclerotic disorders including hypertension, hyperlipidaemia, type 2 diabetes, smoking, alcohol consumption and obesity. Hypertension is the single strongest risk factor after age that can triple the risk of stroke, followed by smoking and diabetes that double the risk of an adverse neurovascular event [Chobanian et al., 2003; Stroke-Association, 2020]. Diabetes induces reactive oxygen species in vascular cells that in turn, activate pro-inflammatory pathways that lead to the production of pro-inflammatory cytokines, and it is the inflammation that plays a key role in the pathobiology of atherosclerosis [Guerci et al., 2001]. Smoking mediates its adverse atherosclerotic effects by invoking endothelial cell injury that stimulates adhesion of leucocytes, exacerbates inflammation, impairs nitric oxide availability, and increases levels of potent vasoconstricting endothelin-1 [Yuan, 2019]. Addition of unfavourable lipid profile, pro-coagulant state and increased sympathetic drive are the foundation bricks for the development of another risk factor such as

hypertension. Hypertension mimics tabaco induced endothelial cell injury primarily by reducing nitric oxide bioavailability which translates into reduced vasodilation response and aggravates pro-inflammatory and pro-coagulant responses [Cronenwett et al., 2014]. Furthermore, hypertension with increased arterial wall stiffness deforms vasa vasorum, thereby reduces microvascular flow which results in the intramural oxygen malnutrition leading to plaque hypoxia [Tarbell et al., 2020]. Other elements including poor diet, low physical activity and high alcohol consumption are the most common modifiable risk factors making ischaemic stroke a highly preventable disease [Beard et al., 2009].

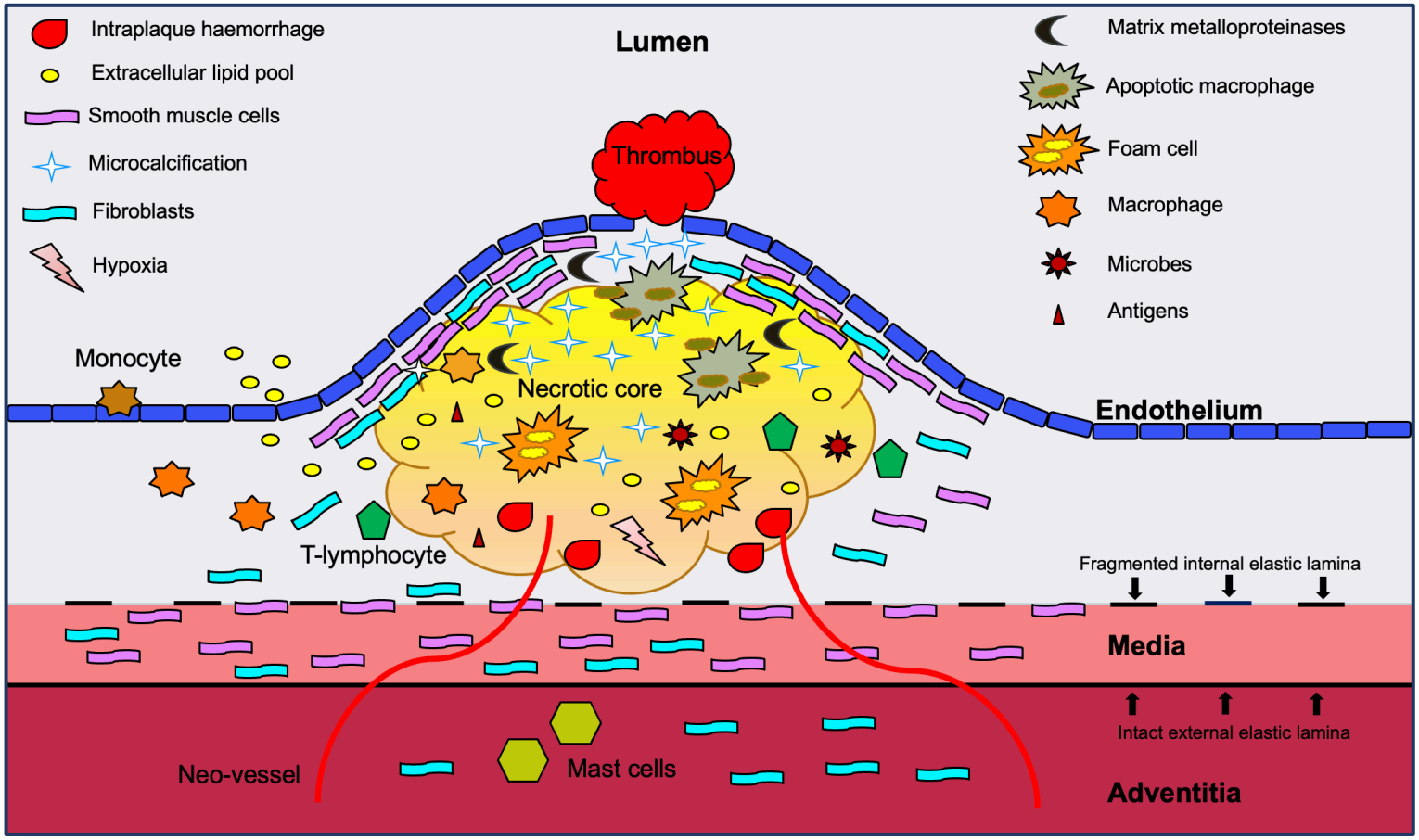
1.3 PATHOGENESIS OF ATHEROSCLEROTIC CAROTID DISEASE

The pathogenesis of carotid atherosclerosis is multifactorial and is caused by endothelial cells injury that is driven by chronic degenerative inflammation. Atherosclerosis is a complex biochemical and cellular process that results in structural and functional arterial abnormalities. Although subendothelial space is the key location for in situ atheroma where acellular lipid debris is encapsulated by proliferated smooth muscle cells, all three layers of the arterial wall are involved in the development of atherosclerosis [Libby et al., 2015].

Histologically, the arterial wall consists of highly organised connective tissue (cells and matrix fibres of elastin and collagen) arranged in three distinct layers; *intima*, *media* and the *adventitia* (Figure 1.2) [Cronenwett et al., 2014]. The *intima* is a single layer of endothelial cells resting on a thin extracellular matrix of elastic and collagen fibres. Endothelial cells have anti-thrombotic properties that, in part, relate to its glycocalyx coating [Cronenwett et al., 2014]. Whereas the tight intercellular seal forms a barrier that prevents cellular migration and inhibits proliferation [Aird, 2007]. In contrast, the tunica *media* is

a porous layer containing organised layers of smooth muscle cells embedded within elastic and collagenous extracellular matrix. All these elements ensure arterial stability and distensibility. The contractile state of smooth muscle cells is guarded by the internal elastic lamina that shields the media from the shear forces of flowing blood. Whist disruption of the internal elastic lamina is observed in atherosclerotic lesions that are predisposed to rupture (Figure 1.2) [Bentzon et al., 2014]. The innermost portion of the *media* layer receives nutrients from the circulating blood, while vasa vasorum feed the outer parts [Cronenwett et al., 2014]. More importantly, the tunica *media* displays unique immunosuppressive properties. Smooth muscle cells produce anti-inflammatory indoleamine dioxygenase which halts immune responses [Tellides et al., 2015]. Thus, the immuno-privileged media which is sandwiched between the internal (separates *intima* from *media*) and external (separates *media* from *adventitia*) elastic laminae protects arterial wall integrity by buffering the spread of intimal inflammation [Libby et al., 2015; Hans, 2018]. Finally, although thinning of tunica *media* predominates beneath a plaque, an outward enlargement of this layer facilitates geometric remodelling which preserves luminal cross-sectional area of an atherosclerotic vessel despite high-volume disease [Libby et al., 2015]. The *adventitia*, with high elastic and collagen content, provides overall strength of the vessel. It contains vasa vasorum with nerves that help regulate smooth muscle cells function as well as fibroblasts and mast cells that have been implicated in the process of atherosclerotic disease [Bot et al., 2011]. In particular, the adventitial vasa vasorum that govern the entry of variety of immune cells, accelerate inflammatory cascade further.

Figure 1.2: Pathophysiology of atherosclerosis.



A complex interplay between endothelial cells, macrophages, smooth muscle cells and arterial layers that take place within the fibroatheroma with fragmentation of the internal elastic lamina culminating in the loss of the immunoprotective properties of the media.

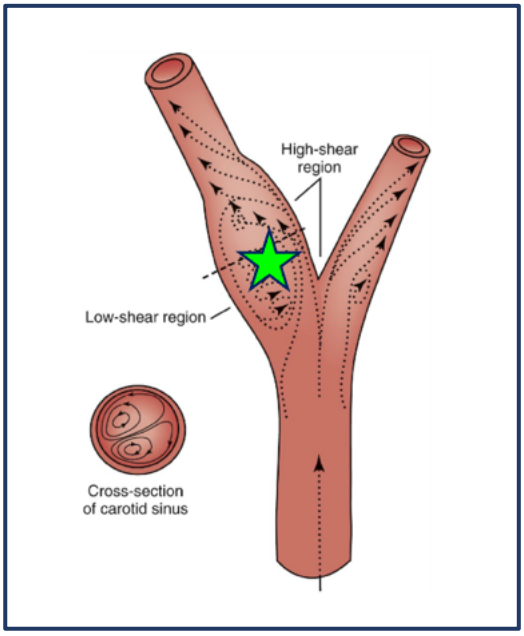
There are four hypotheses of carotid plaque formation, including a response to injury, lipid deposition, inflammatory and monoclonal mechanisms. This implies our incomplete understanding of the disease and translates into the challenges with prevention and treatment. However, regardless of the model of atheroma formation, all hypotheses seem to coalesce around the endothelial cell injury that is central to the pathogenesis of atherosclerosis and marks the beginning of the disease before any histological evidence can be detected. Various chemical (smoking, hyperlipidaemia, diabetes) and mechanical (cyclic strain, low shear stress, hypertension) factors induce inflammation that play a pivotal role in the endothelial cell injury leading to its dysfunction. Ultimately, inflammation driven deposition of lipids within foam cells and migration of smooth muscle cells into the subendothelial space leads to the formation of atherosclerotic plaque with gradual luminal stenosis, thrombosis and embolisation.

1.3.1 RESPONSE TO INJURY

The carotid arterial system is a highly organised structure that withstands cyclic strain and shear stress [Davies et al., 1999]. Cyclic strain is determined by the blood pressure and represents circumferential deformation of the vascular wall caused by the pulsatile changes in systole-diastole cycle. In contrast, the shear stress results from the parallel blood flow against the arterial wall. These two haemodynamic forces modulate cells differentiation and proliferation; cyclic strain affects all cell types, and shear stress exerts friction on endothelial cells. Interestingly, it is not the high but low shear stress that is associated with atherosclerosis. Blood flow in the centre of the carotid vessel is rapid and laminar. Whereas carotid bifurcation with unique geometry contains areas of turbulent blood flow containing areas of flow separation and stasis [Beard et al., 2009]. The flow can be even locally reversed, especially if an atherosclerotic lesion is present (Figure 1.3). This results in a low velocity recirculating blood and convective flow away from the arterial wall, thereby leading to the formation of fluid based mechanical barrier for the intramural oxygen transport followed by ischaemia of arterial wall [Tada et al., 2006]. In

effect, abnormal blood flow and low shear stress predominantly affect the outer wall of the carotid artery, and at this specific site, carotid plaques tend to form [Markl et al., 2010].

Figure 1.3: Anatomy of the carotid artery bifurcation.



Adapted from Rutherford's Vascular Surgery [Cronenwett et al., 2014] and updated (green star) to highlight the area of flow reversal.

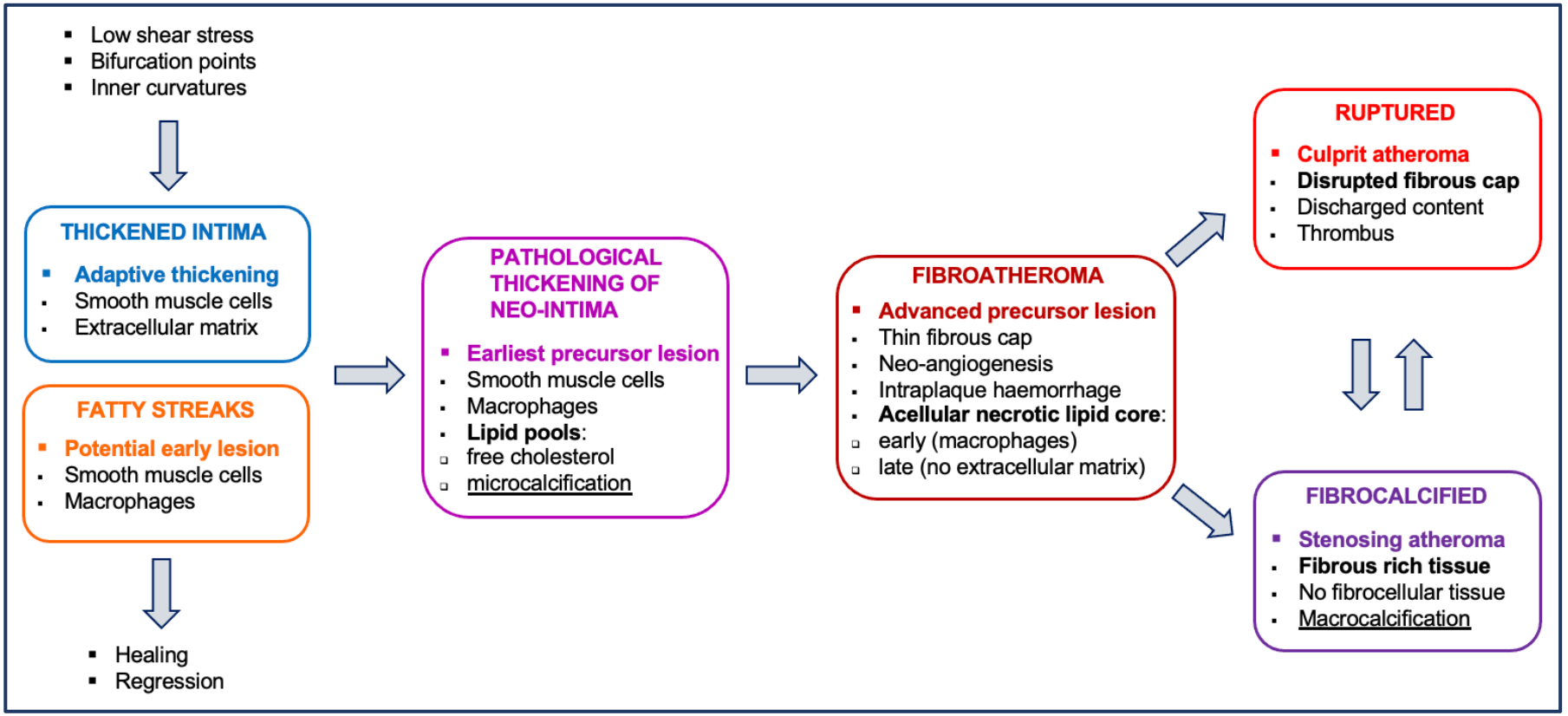
The local haemodynamic environment that injures the endothelium represents the primacy of endothelial involvement in the initiation of atheroma formation followed by all stages of atheroma evolution with the two earliest precursor changes in the arterial wall such *as intimal thickening* and *fatty streaks* (Figure 1.4). The intimal thickening is the earliest and adaptive vascular change that is characterised by selective and focal accumulation of smooth muscle cells within the extracellular matrix [Yuan, 2019; Mori et al., 2017]. Injured endothelial cells are characterised by reduced nitric oxide levels (normally inhibits smooth muscle cell proliferation), increased endothelial permeability and amplified pro-inflammatory adhesion molecules such as: intercellular adhesion molecule (ICAM-1), vascular cell adhesion molecule (VCAM-1) and toll-like receptors (TLR1, TLR2 and TLR4) [Cronenwett et al., 2014; Virmani et al., 2005; Davies et al., 2006]. Added chronic exposure to cyclic strain and low

shear stress provokes further a pro-inflammatory palette of responses from the endothelial cells. Smooth muscle cells undergo hypertrophy, proliferation and change their contractile phenotype into the immature synthetic form, which synthesises connective tissue components (collagen, elastin, proteoglycans) at the site of endothelial injury [Cronenwett et al., 2014]. These elements synergistically result in the progressive and pathological intimal thickening [Bentzon et al., 2014]. In addition to smooth muscle cells, these lesions also contain macrophages and small areas of lipid pools within the *media* but without evidence of a lipid core [Yuan, 2019]. Crucially this pathological intimal thickening is particularly prone to erosion [Libby et al., 2019].

Dysfunctional endothelial cells upregulate platelet derived growth factor (PDGF). In effect, activated platelets lead to an influx of low-density lipoproteins (LDL) particles into the subendothelial space. At this location LDL particles are protected from the plasma antioxidants; hence they undergo oxidative modification and exhibit pro-inflammatory functions [Libby et al., 2019]. Subsequent and aberrant phagocytosis by foam cells along with lipid-laden smooth muscle cells [Mori et al., 2017] results in the formation of *fatty streaks* which represent a seminal event of the first histologically detectable atherosclerotic lesion. *Fatty streaks* are devoid of lipid core and fibrous cap, may also regress or progress to a complex fibroatheroma (Figure 1.4).

A self-perpetuating cycle of endothelial pro-inflammatory and immunogenic responses culminates in apoptosis (endothelial, foam and smooth muscle cells), adventitial fibroblasts activation and formation of a complex fibro-atheroma with acellular necrotic lipid core and overlying fibrous cap that can be degraded by matrix metalloproteinases (MMP-2 and MMP-9), cathepsins, plasminogen activators resulting in plaque rupture [Cronenwett et al., 2014; Yuan, 2019] (Figure 1.2 and Figure 1.4). The clinical neurovascular complications that may arise mark the final stage of the fibroatheroma development.

Figure 1.4: Types of atherosclerotic lesions and their development.



Adaptive intimal thickening is described as a focal but low smooth muscle cells accumulation within extracellular matrix and is frequently observed at atherosclerosis-prone arterial sites including carotid, coronary, iliac and aortic circulations.

Fatty streaks are potentially early atherosclerotic lesions that contain deposits of lipids within macrophages and smooth muscle cells which can either regress or progress to an advanced fibroatheroma.

Pathological intimal thickening is the earliest precursor of atherosclerotic lesion consisting of smooth muscle cells (including their proliferation, hypertrophy, synthetic phenotypic modulation, and apoptosis), extracellular lipid pools without necrosis containing free cholesterol with apatite crystals (microcalcification) and macrophages accumulation towards the luminal part of the affected vessel.

Fibroatheroma is an advanced atherosclerotic lesion characterised by a large acellular necrotic lipid core that in early stages is protected by a fibrous cap. At first, macrophages infiltrate areas of lipid pools and contribute to the breakdown of extracellular matrix. Whereas the late stage is characterised by a complete absence of collagen type IV, extensive cellular debris and numerous cholesterol clefts that synergistically lead to a thin-cap fibroatheroma (collagen type I and III, macrophages, lymphocytes, absent smooth muscle cells and thickness < 165-200μm in carotid arteries, <65μm in coronary arteries) which is a prerequisite lesion to rupture. Addition of intraplaque haemorrhage and neo-angiogenesis can lead to a rapid necrotic lipid core expansion.

Ruptured atheroma: disrupted fibrous cap with exposed necrotic lipid core and/or intraplaque haemorrhage results in a thrombus formation with a potential to embolise.

Fibrocalcific atheroma represents healed and latent stage of fibroatheroma that consists of fibrous intima composed of distorted collagens and macrocalcium deposits. Repeated cycles of ruptures followed by tissue repairs lead to a progressive fibrous tissue deposition which results in a constrictive remodeling culminating in a stenosis formation, as opposed to the expansive remodeling which initially preserves and maintains the luminal vessel area.

1.3.2 LIPID DEPOSITION

Once the integrity of endothelial cells is compromised, oxidised LDL particles including lipoprotein(a) enter a subendothelial space triggering a localised inflammatory response [Waissi et al., 2020; Spence et al., 2012]. Accumulation of lipids within the subendothelial space marks the development of the atherosclerotic plaque. It has been suggested that the permeable endothelium mediates lipid ingress in the areas of intimal thickening as healthy *intima* does not retain LDL particles [Cronenwett et al., 2014]. Thus, factors favouring LDL oxidisation that become chemotactic to monocytes and subsequent uptake by macrophages (endocytosis) via scavenger receptor pathways that form foam cells guard the process of lipid trafficking into the arterial wall [Antonov et al., 2004]. Interestingly, smooth muscle cells also accumulate lipids by similar mechanisms to macrophages. These include scavenger receptor mediated uptake of oxidised LDL particles, hydrolysis of free cholesterol from aggregated LDL in extracellular compartments, direct uptake of native LDL particles and remnant lipoproteins [Bentzon et al., 2014]. The notion of the lipid induced process of atherogenesis has been supported by numerous statin trials that proved beneficial in the prevention of major cardiovascular clinical events, including adverse events associated with carotid endarterectomy or carotid artery stenting [Crouse et al., 1998; Amarenco et al., 2006; Perler, 2007]. However, novel pharmacological therapies such as Cholesteryl Ester Transfer Protein Inhibitors disappointingly did not reduce cardiovascular events [Armitage et al., 2019]. Despite a raise in the levels of high-density lipoproteins particles, these medications did not alter the traffic of lipids out of the *intima*. In effect, Cholesteryl Ester Transfer Protein Inhibitors did not have any impact on positron emission tomography-computed tomography (PET-CT) measured arterial inflammation [Ishai et al., 2015]. Similarly, Lipoprotein-Associated Phospholipase A2 did not decreased the rate of adverse atherothrombotic events and failed to demonstrate reduction of atherosclerotic inflammation on PET-CT imaging [Ishai et al., 2015]. Contradictory results were demonstrated by randomised controlled trials that investigated the effect of monoclonal antibodies agents such as Proprotein Convertase-

Subtillisin/Kexin type 9 (PCSK9). Some demonstrated reduction in LDL particles with minimal effect on lipoprotein(a) levels and had no effect on attenuation of inflammatory carotid signal on PET-CT [Stiekema et al., 2018]. Whereas others, demonstrated potent effect of PCSK9 not only on LDL particles but also reduction of carotid inflammation on PET-CT images [Hoogeveen et al., 2019]. This implies that although build-up of lipids in the arteries is an important contributor to plaque development, the process is more complicated and involves several parallel pathways.

1.3.3 INFLAMMATION

Inflammation is a reparative process that aims to “wall off” the area of injury from the remaining tissue. Therefore, as a process of normal arterial wall biology, it aims to restore the vessel wall integrity. However, when endothelial inflammation fails to arrest but instead becomes dysregulated and degenerative, it results in an adverse arterial remodelling characterised by an excessive fibrous tissue deposition that alters arterial wall geometry and biochemistry.

Monocytes play a key role in the process (Figure 1.2). Once they infiltrate the subintima, monocytes differentiate into predominantly M1 pro-inflammatory macrophages that express scavenger receptors and take up oxidised LDL particles [Johnson et al., 2009]. These macrophages also embark on micropinocytosis of native LDL particles [Kruth, 1997]. Consequently, lipid-overloaded macrophages turn into foam cells which as *fatty streaks* are the hallmark of the earliest stage of plaque development that can be observed on histological samples. This triggers a further pro-inflammatory cascade that had led to the monocyte recruitment in the first place and stimulates the transmission of other cells including T-cells, dendritic and B-cells into the vascular lesion as well as arterial tertiary lymphoid organs [Briley-Saebo et al., 2007; Thompson, 2016]. The arterial tertiary lymphoid organs (ATLO) are complex adventitial and peri-adventitial conglomerates of immune cells that modulate interfaced immune and inflammatory pathways. These ATLO

immune like structures contain germinal B-cells centres, thus contribute to antibodies production and mast cells that are a source of basic fibroblast growing factor which is a potent angiogenic mediator that targets fibroblasts, endothelial and smooth muscle cells [Thompson, 2016; Lappalainen et al., 2004]. Furthermore, ATLO activate macrophages via stimulated innate toll-like receptors as a response to endogenous molecules (LDL particles components and intestinal microbiome), β-glucan (fungal cell walls) and liposaccharides (endotoxin component) from Gram-negative and Gram-positive bacteria [Thompson, 2016; Alquraini et al., 2020; Libby et al., 2018; Kol et al., 1998]. Moreover, synergistic action of scavenger receptor expressed by endothelial cell-I with the toll-like receptors (TLR3/TLR9, TLR-2 and in particular TLR-4), enhances inflammatory responses (cytokines production, leucocyte endothelial invasion and procoagulant activation with impaired fibrinolysis) to numerous pathogen-derived molecules ensuing immune responses that exacerbate inflammation within a pre-existing atherosclerotic lesion [Murshid et al., 2016; Libby et al., 2001]. Pathogens affect arteries directly or indirectly by targeting a trio of key cells found within atheroma such as endothelium, smooth muscle cells and macrophages [Libby et al., 2018]. Direct infection of vascular cells may lead to either lethal cells lysis or their damage [Libby et al., 1997]. In particular, the latter enables microbial agents to latently survive within altered but viable vascular cells. Subsequent local or systemic infection could reactivate pathogens which may promote evolution of arterial lesions including thromboembolic consequences via further release of inflammatory mediators. In contrast, indirect microbial effects involve humoral immune responses consisting of deposition of immune complexes on endothelium and leucocyte recruitment [Libby et al., 2018]. This can lead to arteritis but could potentially initiate or aggravate atherosclerotic lesion formation [Kol et al., 1998]. The link between pathogens and acceleration of atherosclerotic disorder involves intricate network of innate and adaptive immune pathways. Although variety of pathogens have been detected in human atherosclerotic plaques including carotid lesions [Campbell et al., 2015], the results of trials examining the role of vaccinations and antibiotics aiming to reduce recurrent cardiovascular

events have been disappointing [Libby et al., 2018]. Thus, the infectious agents' contribution in precipitating atherosclerotic pathology remains unclear and ought to be evaluated in future scientific research.

When inflammation is reduced, T_H2 sub-population with M2 macrophages dominate in the atheroma. Their anti-inflammatory cytokines stimulate smooth muscle cell migration, proliferation and synthesis of collagen that ensures thickness and tensile strength of the fibrous cap. Hence, stable plaque is formed [Libby et al., 2015; Libby et al., 2009]. In contrast, the presence of M1 macrophages, and T_H1 cells that secrete pro-inflammatory cytokines results in further inflammatory activation [Cronenwett et al., 2014]. This milieu of inflammatory mediators along with released proteinases leads to degradation of elastic and collagen fibres. In effect, weakening of the fibrous cap promotes an unstable state of the plaque that is at greater risk of rupture. Persistent inflammatory process sheds the anti-thrombotic glycocalyx from the endothelium and with procoagulant tissue factor expressed by smooth muscle cells sets the foundations for potential thrombotic complication.

1.3.4 MONOCLONAL HYPOTHESIS

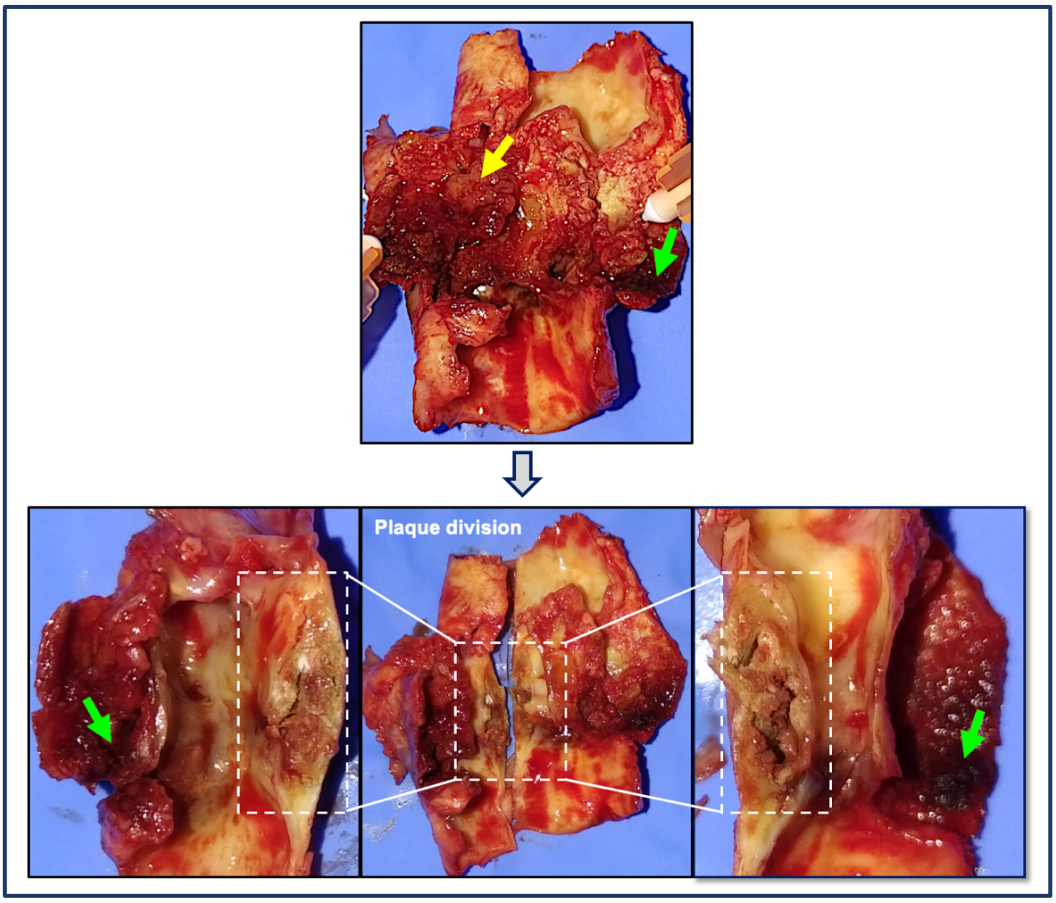
The proliferation of smooth muscle cells that produce extracellular matrix is responsible for the evolution of *fatty streaks* into more complex fibrotic plaques [Benditt et al., 1973]. The monoclonal hypothesis advocates that each atherosclerotic lesion is a result of clonal multiplication of a single precursor smooth muscle cell within the intima [Cronenwett et al., 2014]. Theory of monoclonality is based on the research evidence that the proliferating smooth muscle cells within an atheroma have only one of the two isoforms of glucose-6-phosphate dehydrogenase isoenzyme [Cronenwett et al., 2014], while the areas free of atheroma contain both isoforms. Three stages of the above hypothesis have been proposed. At first, a mutation occurs in a cell due to genetic and extrinsic factors including viral infections, tobacco use or ionising radiation [Poole et al., 1977]. Subsequently, chemical or physical factors provoke inflammation that induces smooth muscles cell proliferation [Pearson

et al., 2018]. The final stage involves cell degeneration [Poole et al., 1977]. However, many disagree with these conclusions. Although smooth muscle cells within thickened intima are monoclonal in origin, the genes that give them a proliferative advantage in the abnormal atherosclerotic environment may outnumber other cells giving an impression of a single cell progeny [Pearson et al., 2018]. Furthermore, plaques develop in layers with ongoing cells turn over (proliferation and cell death) that may lead to a dominant smooth muscle cells phenotype to be present in a vascular lesion [Cronenwett et al., 2014]. Overall, the monoclonal hypothesis has not found many supporters, but it certainly brought more focus towards the genetic basis of atherogenesis.

1.4 CAROTID PLAQUE PROGRESSION

The typical carotid plaque represents a culmination of a staccato life cycle that consists of periods of chronic inflammation (progression) and healing response (regression) within the arterial wall (Figure 1.5a and Figure 1.5b). This interesting pattern was demonstrated by histological data that showed high-risk plaque features to predominate within the early pre-operative (< 14 days) period, followed by a decline in these features in those who underwent delayed surgery (< 28 days) [Salem et al., 2013a]. Crucially, high-risk plaque characteristics re-appeared again beyond 29 days [Salem et al., 2013a] suggesting that following an acute and initial discharge of an atheromatous content, atherosclerotic lesions re-build its core features (Figure 1.5a and Figure 1.5b). Furthermore, other histopathological data also showed *buried fibrous caps* [Libby et al., 2019] indicative of the previous rupture followed by the healing process (Figure 1.5a).

Figure 1.5a: Complex culprit carotid plaque.

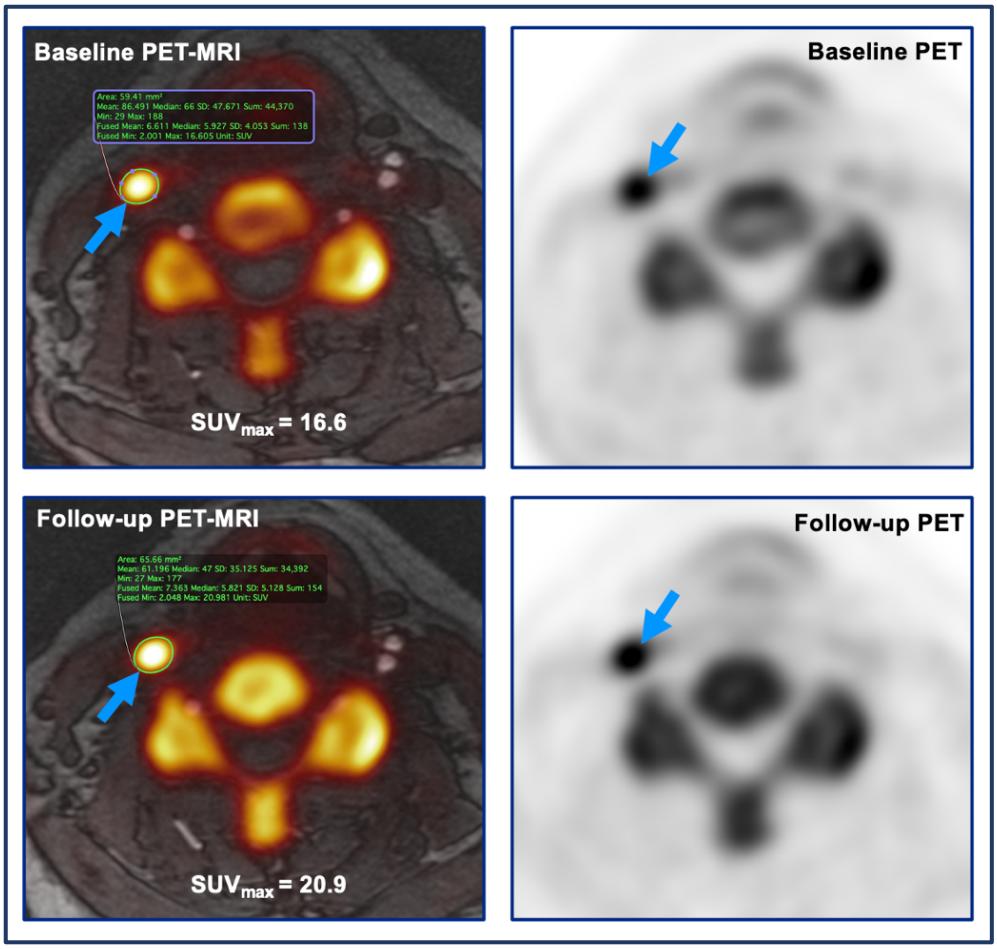


Carotid plaque consisting of:

- acutely ruptured fibroatheroma with thrombus (green arrows) with exposed lipid core (yellow arrow) containing intraplaque haemorrhage
- healed fibrocalcified regions (white dashed boxes)

The incubation period of an atherosclerotic plaque may take several decades before it becomes clinically apparent. Unsurprisingly, atherosclerosis starts in childhood or early adulthood as *fatty streaks* that represent lipid deposits within the macrophages and smooth muscle cells. The next stage involves the formation of complex fibrotic plaques that gradually compromise arterial lumen and consist of lipid core, inflammatory cells, neo-vessels and thick fibrous cap. Whether fibrous cap undergoes a gradual or more dynamic degradation remains unknown. Ultimately, plaques complicated by intraplaque haemorrhage, necrotic lipid core, ulceration, and fibrous cap rupture with thrombus formation, mark the end stage of the disease associated with the acute neurovascular syndrome.

Figure 1.5b: Persisting ^{18}F-NaF PET-MRI uptake on follow-up scan in right carotid artery.



Example of a patient with right amaurosis fugax and >70% stenosis of the right internal carotid artery with high-grade focal ^{18}F-NaF PET-MRI uptake (blue arrows) on baseline scan (SUV_{max}= 16.6) and higher radiotracer uptake after 3 months (blue arrows) on follow-up imaging (SUV_{max}= 20.9). ^{18}F-NaF PET-MRI: Fluorine 18–labelled sodium fluoride positron emission tomography-magnetic resonance imaging; SUV_{max}: max Standardised Uptake Value.

1.4.1 NECROTIC LIPID CORE

Continued lipid infiltration of the arterial wall that overwhelms foam cell formation, leading to their ultimate fate of necrosis. This coupled with the impaired clearance of the cellular debris (efferocytosis) of native and oxidised lipids, creates a vicious cycle of increasing chronic inflammation and cell death. These processes generate extracellular pools of lipid that become acellular necrotic lipid cores (Figure 1.6) that increase the plaque mass

[Cronenwett et al., 2014]. However, the release of MMP by the macrophages leads to a fibrous cap degradation; both directly and indirectly via the death of smooth muscle cells that produce the extracellular matrix (collagen and elastin). In effect, scaffold provided by the fibrous cap is weakened and prone to a rupture.

1.4.2 VASA VASORUM AND PLAQUE HYPOXIA

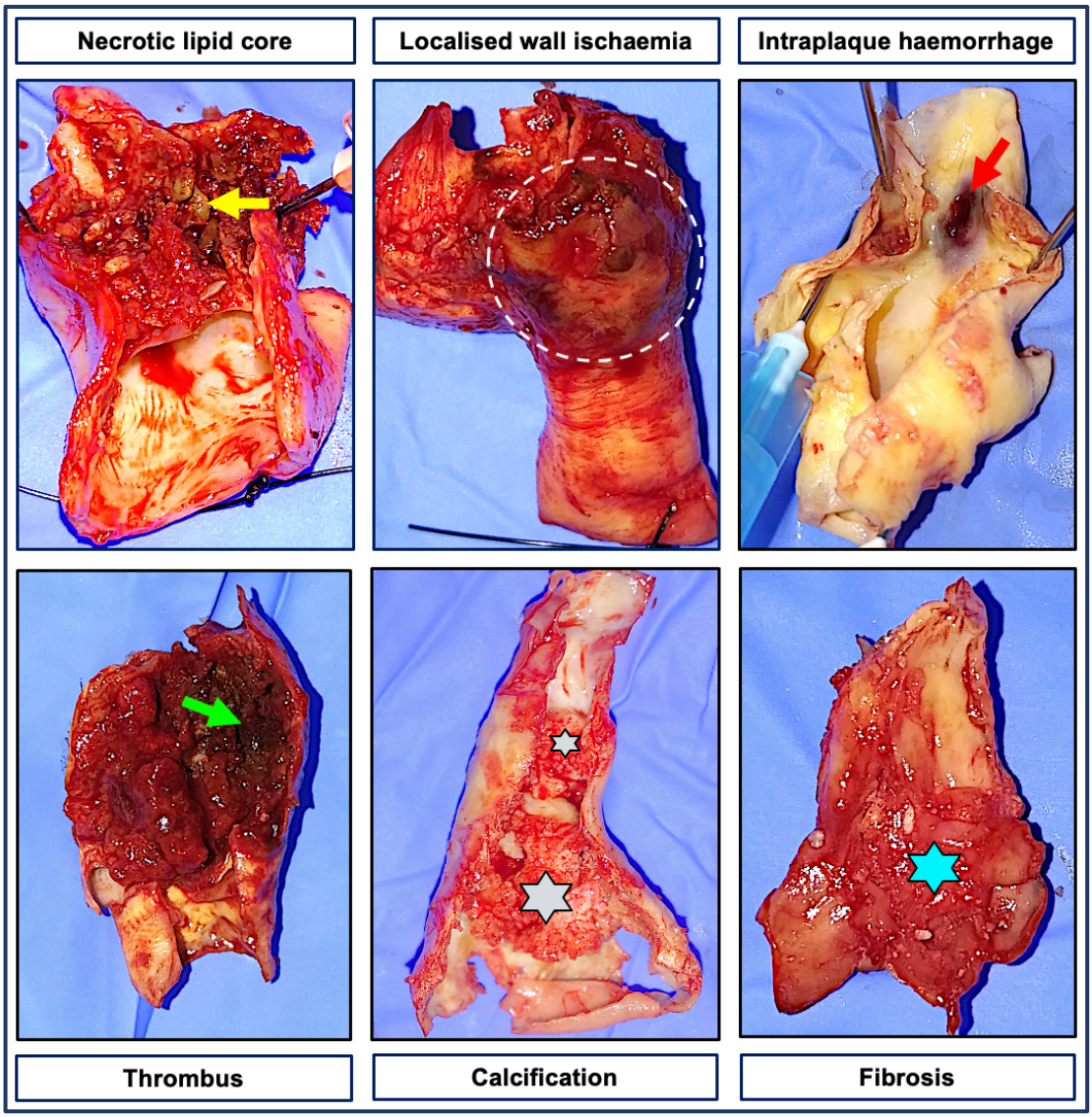
The term vasa vasorum encompasses the microvascular wall system that consists of the venous and arterial components. The *venous* vasa vasorum are frequently omitted in the literature despite their pivotal role in regulating microvascular arterial blood flow and clearance of oxidised LDL particles with inflammatory cells [Tarbell et al., 2020]. Instead, the focus is given to the arterial counterparts: vasa vasorum *interna* (originate from the main lumen and create intramural microvessels network) and vasa vasorum *externa* (originate and are localised outside the vessel wall). However, this is a rather simplistic explanation of a complex intramural oxygen delivery system as vasa vasorum are a heterogenous microvascular system that differs at anatomically separate vascular locations. For example, internal mammary artery is characterised by a low density of microvessels, while normal coronary artery lacks intimal vasa vasorum [Virmani et al., 2005].

Several factors shape the oxygen distribution including, lipid-rich atheroma, vascular anatomy (bifurcations, tortuosity, location), thickness of the arterial wall and specific pattern of microvascular supply. The latter was already described, as two distinct microcirculation zones deliver essential nutrients to the three-layered arterial wall resembling watershed areas within the brain. In effect, junctional common zone (mid *media*) is particularly susceptible to ischaemia. Therefore, even positive arterial remodelling that preserves the lumen, due to increased wall thickness and localised tissue stress reduces oxygen diffusion from the luminal blood to the vessel wall. This results in mechanical compression of distal vasa vasorum that predominate in the regions close to the *media* layer [Tarbell et al., 2020]. Furthermore, pre-clinical

research based on carotid models showed interesting data regarding anatomical aspects that influence oxygen supply to a vessel wall. First, normal oxygen tension across healthy common carotid artery (canine) exhibits a bimodal reduction: an abrupt drop (from the lumen towards the inner *media* layers) is followed by a gradual fall within the outer *media* and *adventitia* due to oxygen consumption by various cells (fibroblasts, smooth muscle cells) [Santilli et al., 1995]. Second, canine carotid arteries contain only vasa vasorum externa and lack penetrating intramural branches [Tarbell et al., 2020]. This is particularly relevant to carotid bifurcation due to its unique flow divider region which is a hypoxic zone.

Locally aberrant blood flow (low shear stress) results in a diminished oxygen influx to the outer aspect of the carotid bifurcation wall via inhibited degradation of hypoxia-inducible factor-1α [Bitto et al., 2010; Evans et al., 2016]. The activated hypoxia-inducible factor-1α is expressed by upregulated macrophages and is responsible for a metabolic shift to anaerobic glycolysis [Semenza, 2012]. Furthermore, histological examination of atherosclerotic aortas (rabbit model) revealed hypoxia (upregulated hypoxia-inducible factor-1α) to be located deep within the macrophage loaded lipid core, whilst areas at luminal boundary contained hypoxia-negative macrophages [Mateo et al., 2018]. Ultimately, hypoxia becomes the most powerful factor that drives compensatory, albeit dysfunctional neovascularisation by mediating a vicious cycle of inflammation, endothelial damage, lipid infiltration and cell death [Bitto et al., 2010; Evans et al., 2016; Mateo et al., 2018].

Figure 1.6: Excised culprit carotid plaques.



Carotid plaques with various high-risk plaque features:

- necrotic lipid (yellow arrow)
- localised wall ischaemia (white dashed circle)
- intraplaque haemorrhage (red arrow)
- thrombus (green arrow)
- calcification (grey stars)
- fibrotic tissue (turquoise star)

1.4.3 NEOVASCULARISATION

As expanding plaque becomes starved of its oxygen supply due to insufficient perfusion from vasa vasorum, neovascularisation of the media and intima begins. This neo-microvascular invasion represents a carefully orchestrated

pattern of arborisation as the secondary and tertiary branches of vasa vasorum enter the *intima* from the *adventitia* to surround necrotic lipid core at specific breakpoints within the *media* [Virmani et al., 2005]. A dense network of neovessels originating from the vasa vasorum of the *adventitia* ensures oxygen delivery. This process can arrest cell death and necrotic core development, thus may promote plaque growth [Aikawa, 2015]. However, at the same time, new vessels form microvascular channels that allow entry of immune cells exacerbating the inflammatory process further. Furthermore, these neovessels are susceptible to metabolic changes caused by their dysfunctional endothelium leading to their apoptosis, blood stasis and in turn, to localised arterial wall ischaemia (Figure 1.6) [Cronenwett et al., 2014; Aikawa, 2015]. Finally, disruption of fragile and porous (inadequate endothelial cell junctions) neovessels that lack smooth muscle cells strut, culminates in the intraplaque haemorrhage which is an important factor in plaque destabilisation.

1.4.4 INTRAPLAQUE HAEMORRHAGE

Ruptured neovessels trigger localised extrinsic coagulation cascade with thrombin generation and fibrin deposition. This also serves as an entry point for erythrocytes and other immune cells. Oxidised LDL particles and reactive oxygen species lead to erythrocytes lysis, and free haemoglobin with subsequent hemosiderin deposition increases the oxidative stress response [Balla et al., 2018]. Degradation of red blood cells membrane is a substantial contributor to the necrotic core volume because 40% of their weight is attributed to cholesterol [Virmani et al., 2005]. It is, therefore, possible that repeated cycles of erythrocytes accumulation which increase lipid core volume may represent a critical point of plaque transition from the *stable* to *unstable* phenotype [Virmani et al., 2005]. These processes result in further endothelial cells damage, macrophages apoptosis and ongoing accumulation of necrotic lipid cores [Aikawa, 2015]. Thrombin generation within the atheroma and the PDGF stimulates smooth muscle cells migration and further proliferation [Cronenwett et al., 2014]. Intraplaque haemorrhage promotes atheroma

infiltration by neutrophils which release proteases that degrade fibrous cap components and facilitate plaque rupture [Ionita et al., 2010].

1.4.5 CALCIFICATION

Atherosclerotic calcification shares a common pathway with the development of atherosclerotic carotid plaque through the recruitment of inflammatory cells and pro-calcific responses. *Intimal* calcification involves a process resembling osteogenesis, including osteoblastic induction, thus bone formation [Cronenwett et al., 2014; Rashdan et al., 2020]. This also mirrors the calcific response seen in tuberculosis. Caseating tuberculous granulomas provide a survival niche from which the bacteria may disseminate due to sustained necrotic inflammation that cannot be permanently halted due to a dynamic interplay of immune cells with the micro-organisms [Ehlers et al., 2013]. Inability to control the pathogen induces calcification that encapsulates affected areas and transforms these granulomas into an indolent deposit of calcium. This suggests that calcification is a healing response and within the arterial wall, it effectively *walls off* inflamed atheroma and prevents the discharge of its pro-thrombotic elements into the bloodstream. In effect, this macrocalcification which is visible on standard imaging modalities, such as magnetic resonance imaging, computed tomography or Duplex ultrasound scan, represents a contained and quiescent state of the atherosclerotic disease.

As already described, chronic and degenerative inflammation serves as fertile soil for macrophages and smooth muscle cells. These cells play a crucial role in the development of intimal calcification via direct calcification of the extracellular matrix. Furthermore, cellular and acellular necrotic debris acts as a nidus for microscopic calcium formation [Bentzon et al., 2014]. Macrophages are a source of the matrix vesicles that induce calcification and promote smooth muscle cells migration [New et al., 2013b; Niu et al., 2016]. Smooth muscle cells, under the influence of transforming growth factor-beta, loose synthetic capabilities and transition into the osteogenic phenotype [Rashdan

et al., 2020] initiating mineralisation by increased release of matrix vesicles [Cronenwett et al., 2014; New et al., 2013a]. These calcified vesicles or micronodules found in the lipid pools [Mori et al., 2017] are precursors to microcalcification which foster a further pro-inflammatory state [Tzolos et al., 2020]. More importantly, microcalcification within the fibrous cap increases local stress and promotes microfractures, and this in turn, can trigger carotid plaque rupture [New et al., 2013b; Adamson et al., 2016]. Finally, these hotspots of micro-calcium are indicative of inflammation and necrosis, which are the key drivers of atherosclerotic plaque instability and rupture [Vesey et al., 2017]. Unlike, macrocalcification, this early stage of mineralisation (<50 μm) is beyond the resolution of currently available imaging techniques. Therefore, the ability to detect micronodules of calcium by molecular imaging modalities may identify carotid plaques that are at high-risk of either progression or symptomatic transformation before the vessel displays morphological change.

1.4.6 FIBROSIS

An efficient healing response of any damaged tissue consists of four overlapping stages of haemostasis, inflammation, proliferation, and remodelling, with the latter culminating in the restoration of the connective tissue network that aims to maintain the structural integrity of an injured arterial wall [Diegelmann et al., 2004]. The above can be achieved only when each reparative step is completed in an orderly and neatly fashion [Diegelmann et al., 2004]. However, when numerous cell-signalling events (persistent cytokines production) sustain chronically degenerative inflammation, the dysregulated healing pathway leads to an excessive matrix deposition with unsuccessful vascular remodelling [Artlett, 2013]. Therefore, positive tissue repair relies on a finely tuned equilibrium between restorative regeneration of the new cross-linked collagen matrix and fibrosis which is a pathological form of healing resulting in excessive deposition of distorted collagens (scar tissue) [Artlett, 2013]. Activated *adventitial* fibroblasts (mesenchymal cells) maintain the focal atherosclerotic plaque structural integrity through the balanced

deposition of the new extracellular matrix, which supports other cells associated with the complex healing process [Evrard et al., 2016; Wu et al., 2021]. However, at the other end of the healing spectrum, fibroblasts instigate a fibrosing-type reparative process which involves excessive accumulation of scar tissue (thickened neo-intima) (Figure 1.5a) that results in adverse biochemical (hypoxia), structural (arterial wall stiffness) and haemodynamic (stenoses) changes [Iking et al., 2021]. Eventually, a vicious cycle is established where thickened neo-intima which impairs diffusion of oxygen and nutrients to an already compromised atherosclerotic tissue, parallelly stimulates fibroblasts and neo-angiogenesis as a response to the hypoxia caused by the thickened neo-intima in the first place.

Activated fibroblasts navigate vascular lesion repair either by differentiation into myofibroblasts with subsequent migration to the *intima* [Xu et al., 2007] or by an *endothelial-to-mesenchymal* cellular transition which derives fibroblast-like cells with co-expressed endothelial and fibroblast specific proteins that correlate with unstable plaque phenotype [Evrard et al., 2016]. Moreover, fibrotic lesions are characterised by an increased density of mast cells that, once recruited into the tissues, mature into connective tissue-type mast cells and release several mediators contributing to matrix degradation, apoptosis and ongoing inflammation [Bot et al., 2015].

1.5 CLINICAL NEUROVASCULAR EVENTS

Atherosclerosis of the carotid arteries has a diverse set of neurovascular presentations including ischaemic stroke, transient ischaemic attack (TIA) and amaurosis fugax. Although atherosclerosis is a systemic disorder, specific vascular territories are characterised by locally different mechanical and biological variables that do not operate parallel mechanisms that surround plaque disruption. Thromboembolism caused by an acute carotid plaque disruption leads to an abrupt reduction in oxygen and nutrients delivery to

brain tissue that is physiologically characterised by high metabolic demand. This mechanism differs from a progressive stiffening and restriction in the cross-sectional vessel area that results in the gradual outflow obstruction and therefore an incongruent oxygen delivery against the actual requirement by an endpoint tissue. This formulates the basis of the coronary, visceral or peripheral (intermittent claudication) events which can be treated on an elective basis by endovascular, surgical or hybrid interventions that aim to restore the flow to ease downstream ischaemia.

Non-carotid plaques frequently undergo silent rupture owing to the vascular remodelling that restores the fibrous cap with endothelial cover. However, this process may also lead to a significant plaque expansion, due to for example, intraplaque haemorrhage which stimulates the synthesis of collagen and induces fibrosis [Cronenwett et al., 2014]. In effect, flow-limiting stenosis that develops with time may nurture compensatory collateral circulation.

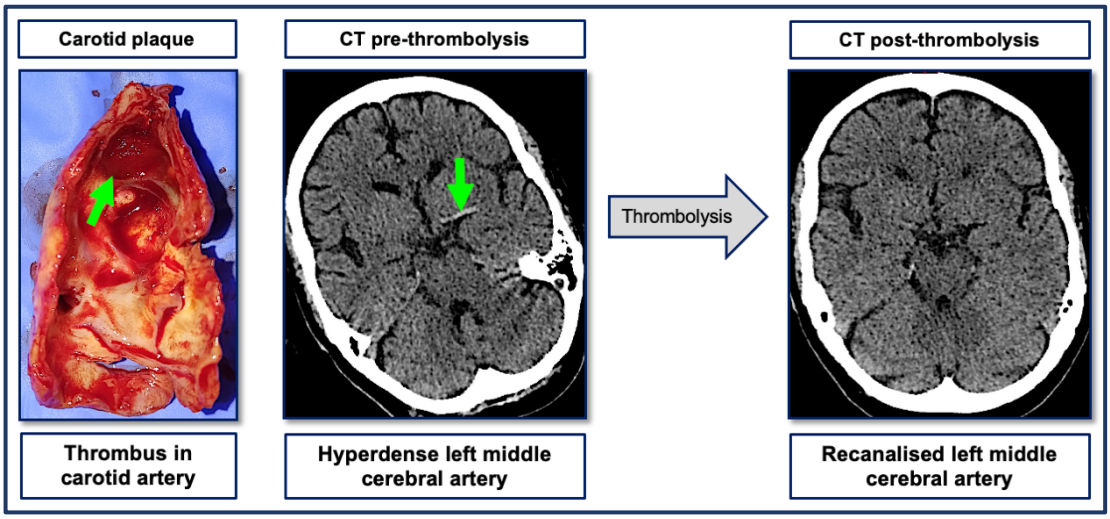
In contrast, acute neurovascular presentations are often sudden and catastrophic because they result from an acute thrombus development that may embolise. Thrombus formation necessitates a thrombogenic environment which is produced by direct contact of carotid plaque content with arterial blood. The primary mechanism for this to occur is the disruption of the physical barrier that separates these two environments, namely fibrous cap, through either acute rupture or erosion. The secondary factors, such as inflammation, microcalcification, necrotic lipid core and intraplaque haemorrhage, are thrombogenic substrates that along with the pro-thrombotic cardiovascular risks, trigger the extrinsic coagulation cascade. At the same time, endogenous fibrinolytic mechanisms attempt to combat the process of thrombosis and if successful, then an individual may spontaneously improve. However, when fibrinolysis fails, established thrombosis at the level of the microcirculation prevents effective reperfusion, and causes tissue infarction leading to persistent neurovascular symptoms.

1.5.1 PLAQUE RUPTURE

Plaque rupture is defined as a through-and-through disruption of the fibrous cap and is the most common mechanism of acute neurovascular syndromes [Libby et al., 2005]. Several factors mediate plaque disruption, including microcalcification, cholesterol crystals (alter pH and hydration of tissue), endothelial shear stress, necrotic apoptosis of macrophages and smooth muscle cells [Giannakou et al., 2020]. Exposure of the highly pro-thrombotic necrotic lipid core with or without intraplaque haemorrhage that is normally sequestered from the bloodstream leads to embolisation in two ways. Most typically, neurovascular events result from embolisation by a thrombus that originates in the carotid bulb. At first, platelet aggregation forms white non-occlusive thrombus, typically in plaques that undergo erosion [Libby et al., 2019]. However, with sufficient time, blood stasis in the carotid bulb (despite high velocities due to underlying stenosis) with ongoing coagulation and impaired thrombolysis leads to the creation of fibrin network that traps erythrocytes [Spence et al., 2012]. This marks the development of a red thrombus (Figure 1.7) associated with ruptured plaques [Libby et al., 2019] that can either embolise distally (Figure 1.7), cause thrombosis in situ or propagate further culminating in total vessel occlusion.

The composition of a thrombus determines its response to a thrombolytic therapy. Therefore, prompt best medical therapy is of essence because white and fresh thrombus is susceptible to anti-platelet medications, whilst organised red thrombus is resistant to thrombolytic agents. Another mechanism of embolisation involves a direct discharge of atherogenic debris from the ruptured plaque. An expelled carotid atheroma either lodges in the vessels (brain or retina) or induces an in-situ thrombosis at the level of intracerebral microcirculation. The latter is feasible because atheroma is a rich source of tissue factor itself, thus easily induces coagulation cascade with predictable neurovascular consequences.

Figure 1.7: Total anterior circulation stroke caused by thromboembolisation of the middle cerebral artery.



A red thrombus in the carotid bulb (green arrow) occluding left middle cerebral artery (green arrow) on brain CT with full recanalisation of the left middle cerebral artery following thrombolysis. CT: computed tomography.

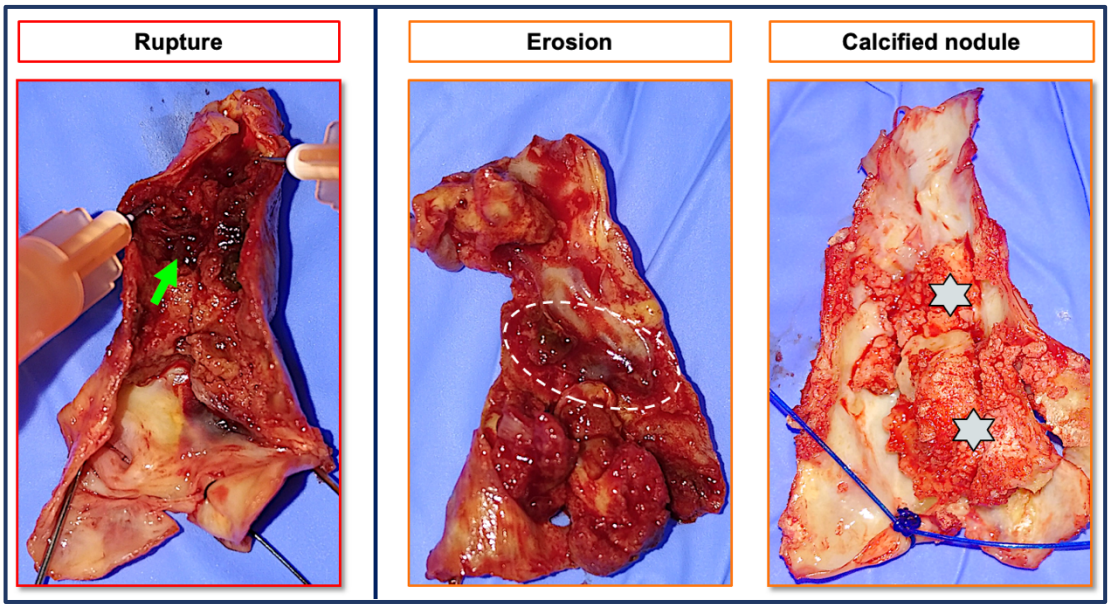
Different forces act on the fibrous cap. As already described, ongoing inflammation destabilises the cap through degradation of its matrix by various proteolytic enzymes whilst microcalcification exerts physical stresses that may induce biomechanical inhomogeneity and predisposes to fibrous cap fractures [Alexopoulos et al., 2009]. Smooth muscle cells undergo apoptosis and are absent at the site of a rupture [Yuan, 2019]. The shoulder region of the plaque is the most vulnerable point where fibrous cap is thinnest (<65 µm) and can be affected by the shear forces of flowing blood [Aikawa, 2015]. This scenario is typically observed in plaques with large lipid cores that occupy >40% of the total plaque area [Aikawa, 2015]. Finally, intraplaque haemorrhage can result in a rapid plaque expansion due to a mass effect which weakens the fibrous cap and ultimately can lead to its rupture.

1.5.2 PLAQUE EROSION

Plaque erosion manifests as a localised loss of endothelium in the presence of a thick fibrous cap (Figure 1.8) [Aikawa, 2015]. However, the exact mechanisms leading to erosion are not fully understood. Some propose that in

situ inflammation or a cytolytic attack by activated killer T cells cause endothelial cells death [Cronenwett et al., 2014; Libby et al., 2009; Libby et al., 2002]. Others suggest a dominant role of activated MMP by oxidised LDL that degrades the extracellular matrix to which endothelial cells normally adhere [Davies et al., 2006]. While *in vitro* studies propose the role of myeloperoxidase and hydrochloric acid in endothelial apoptosis [Sugiyama et al., 2004]. Overall, this results in exposed collagen, and von Willebrand factor promotes platelets adhesion [Faggiotto et al., 2018]. Subsequently, platelets aggregate or alternatively thrombus forms and distal embolisation causes ischaemia. This type of plaque complication is predominantly seen in young females with hypercholesterolaemia and diabetes [Arbab-Zadeh et al., 2012]. Another mechanism culminating in plaque disruption and thrombosis is an erosion of a calcium nodule (Figure 1.8). A calcified nodule that protrudes through the fibrous cap as a foreign body is devoid of an endothelial covering [Naghavi et al., 2003]. When in contact with circulating blood coagulation proteins may activate and aggregate platelets leading to formation of a white (platelet rich) thrombus. As expected, this may lead to a thromboembolisation. Severe calcification may lead to the formation of cauliflower-like structures (Figure 1.8) that project into the arterial lumen. Still, these are thought to be more common in peripheral vessels, for example in femoral artery plaques which tend to be fibrotic [Cronenwett et al., 2014].

Figure 1.8: Three principal mechanisms of acute plaque events.



Possible acute plaque events:

- plaque rupture with thrombus (green arrow)
- endothelial erosion (white dashed oval)
- heavily calcified nodule (grey stars)

1.5.3 CULPRIT (HIGH-RISK PLAQUE) - A TICKING TIME BOMB?

The nomenclature defining rupture prone carotid plaques include the following descriptions: culprit, high-risk, unstable and vulnerable plaques. All these terms refer to the complex vascular lesion that has a high probability of a rupture, thus leads to the clinical neurovascular manifestations. A quartet of pathological features characterises such culprit plaques (inflammation, microcalcification, necrotic lipid core and intraplaque haemorrhage) that ultimately result in thinning or rupture of the fibrous cap. The precise trigger for the plaque disruption is unclear, but most likely, it involves a multifaceted interplay of parallel atherogenic pathways. Undoubtedly, degenerative inflammatory activity is the key to the transition from a *stable* to *unstable* carotid plaque. For example, constant exposure to pro-inflammatory irritants, such as tobacco use, excessive alcohol consumption which exacerbates hypertensive effects, untreated hypertension or hypercholesterolaemia and diabetes, provoke the inflammatory and thrombogenic processes to dominate.

Another potential explanation is that plaque rupture resembles the formation of an abscess which is a localised collection of neutrophils and dead tissue. The process involves liquefication of harmful tissue or agents leading to a subsequent discharge of necrotic tissue through a path of the least resistance [Chen et al., 2017]. Analogously, the cargo of necrotic atheroma that includes overexpressed active collagenases (MMP-1, MMP-2, MMP-8, MMP-9, MMP-13) supersedes endogenous inhibitors of metalloproteinases leading to collagen degradation [Cronenwett et al., 2014]. The dissolved collagenous skeleton weakens the fibrous cap, creating a focal point releasing atheromatous content into the bloodstream.

On the other hand, some plaques exhibit discontinuous growth. The repeated cycle of ongoing inflammation and healing or repair reflects periods of atheroma expansion and dormancy. When intraplaque haemorrhage is contained with the atheroma, and endogenous fibrinolytic mechanisms successfully dissolve thrombus, plaque healing is feasible. This repair is augmented by anti-inflammatory mediators and the tissue inhibitors of MMPs that together counterbalance degenerative inflammation [Cronenwett et al., 2014]. In effect, a fibrocalcific stable plaque emerges that is unlikely to result in neurovascular events.

1.6 CURRENT EVALUATION OF CAROTID ATHEROSCLEROSIS

"We are too much accustomed to attribute to a single cause
that which is the product of several, and the majority of
our controversies come from that."

-Marcus Aurelius Antoninus (121-180 AD)

At present, the evaluation of carotid atherosclerosis is based on the simplistic measurement of luminal stenosis. Basic assessment is performed by Duplex ultrasound scan that is inexpensive, radiation-free and most accessible

imaging modality. When in doubt or when vascular intervention is considered, more complex cross-sectional imaging techniques such as computed tomography angiography or magnetic resonance angiography are utilised. However, one must remember that the degree of luminal stenosis was the only available target for treatment in the NASCET and ECST era due to the lack of advanced cross-sectional and molecular imaging. Although the severity of stenosis is reflective of the burden of atherosclerotic disease and can be the target for therapeutic decisions, comprehensive histological and imaging data demonstrated that the morphology of the plaque is a more important determinant of future neurovascular events [Howard et al., 2015]. Furthermore, high-risk plaque features add to the independent risk of ipsilateral transient ischaemic attack or ischaemic stroke provided by the severity of carotid artery stenosis alone [Archie, 2016; Howard et al., 2013; Howard et al., 2015]. Thus, having recognised the complexity of atherosclerotic carotid disease, we cannot continue to rely on a simplistic anatomic measure to guide our treatment choices. If we are to prevent future strokes, we must replace our myopic view that the severity of stenosis and treatment of it, have no room for improvement. Instead, we must acknowledge different aspects of carotid plaque composition to achieve more accurate prediction regarding the vascular intervention for an individual patient.

1.6.1 CAROTID ARTERY STENOSIS MEASUREMENT

All patients who are suspected of having an ischaemic stroke, transient ischaemic attack or retinal ischaemia undergo carotid artery stenosis evaluation. Subsequently, patients with a surgical grade of carotid artery stenosis (>50%) are considered for carotid endarterectomy as at this threshold, the recurrent risk of stroke equals or exceeds the risk of surgery. This threshold is based on the results from the three major randomised controlled trials: North American Symptomatic Carotid Endarterectomy Trial (NASCET), European Carotid Surgery Trial (ESCT) and Veterans Affairs Cooperative Study. Ultimately, re-analysis of more than 6000 pre-randomisation angiograms using NASCET principles of stenosis

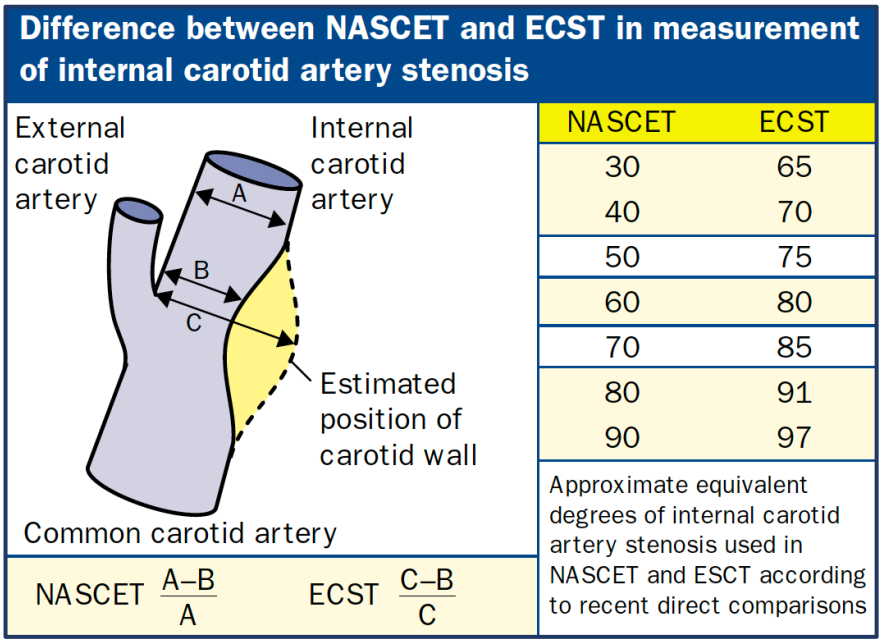
measurement performed by the Carotid Endarterectomy Trialists Collaboration (CETC) provided the most comprehensive summary of results [Rothwell et al., 2003a; Beard et al., 2009]. The CETC identified several principal observations. First, the trials unequivocally established carotid endarterectomy as a highly effective vascular intervention in reducing the risk of future stroke. The cumulative risk for ipsilateral stroke at 2 years was 26% in those treated with best medical therapy only, while in the surgical group the risk was 9% [Barnett et al., 1991]. The major reduction in ipsilateral stroke following carotid endarterectomy was conferred in patients with moderate (50-69%) to severe (>70%) symptomatic carotid artery stenosis [Ferguson et al., 1999; Rothwell et al., 2003a; Rothwell et al., 2004]. Whereas the vascular intervention was found to be harmful when arterial stenosis was <50%.

Second, the carotid trials highlighted the importance of early intervention. However, it is worth highlighting those randomised controlled trials did not collect any details about the timing of index neurovascular syndromes [Rothwell et al., 2004]. Therefore, the delay between the index neurovascular symptoms and carotid endarterectomy was much longer than currently used two-week operative window [Rothwell et al., 2004]. Nevertheless, the NASCET and ESCT data demonstrated clear benefit from early randomisation (hence early intervention) with an impressive absolute reduction in 5-year stroke risk following carotid surgery in severe (30.2%) and moderate (14.8%) stenoses [Rothwell et al., 2004]. In contrast, surgical intervention beyond 12 weeks from the randomisation process presented less benefit in severe (8.9%) stenoses and was harmful in moderate (-2.9%) degree of stenoses [Rothwell et al., 2004]. These findings were subsequently reiterated by natural history studies which demonstrated that the highest risk of stroke is within two weeks of symptoms onset and can be as high as 25% [Shahidi et al., 2015; Coull et al., 2004]. Ultimately, consecutive nation-wide audits conducted by the Vascular Society of Great Britain and Ireland augmented the notion of maximum benefit from carotid endarterectomy within two weeks of the index neurovascular event. Third, CETC data showed that gain from carotid endarterectomy in women was found in those with high-grade stenoses who were promptly

intervened upon, contrary to men who benefited from the intervention even beyond two weeks [Rerkasem et al., 2011; Rothwell et al., 2004]. Finally, NASCET and ESCT identified factors associated with a higher risk of stroke in patients treated with best medical therapy only. These included elderly men with severe stenosis (>90%) demonstrating surface irregularity or ulceration who suffered from hemispheric symptoms (multiple cerebral events) and had contralateral carotid occlusion [Rothwell et al., 2004; Rothwell et al., 2003b]. In contrast, predominantly women, with moderate and smooth stenoses (<70%) or with near occlusion who presented with amaurosis fugax presented a lower risk of subsequent stroke [Rothwell et al., 2004].

Whilst the ESCT results are complementary to the NASCET outcomes, both trials used fundamentally different methodological angiographic assessment of the carotid stenoses. In NASCET, the degree of stenosis was determined by comparing the residual lumen at the narrowest point of the stenosed area with the lumen of the normal distal internal carotid artery (at least 1 cm distal to the carotid bifurcation) [Rothwell et al., 2003a]. In contrast, ESCT used the residual luminal diameter of the internal carotid artery in relation to the estimated carotid bifurcation diameter [Rothwell et al., 2003b]. Consequently, ESCT overestimated the degree of carotid stenosis (Figure 1.9). Hence, 75% ESCT measured stenosis was comparable to 50% NASCET based assessment and 85% ESCT stenosis translated into 70% NASCET equivalent. Although, NASCET measurement method has been widely adopted as a default one, clinicians ought to remember that in symptomatic patients with large volume plaques contained within the dilated carotid bulbs, NASCET method is inferior to ESCT measurement [Naylor et al., 2018]. In this scenario, residual carotid diameter may be very similar to the distal internal carotid artery resulting in <50% stenosis assessment by NASCET method and this could potentially lead to an exclusion from carotid intervention, whilst ESCT measure of >70% stenosis would advocate carotid revascularisation [Naylor et al., 2018].

Figure 1.9: Two methods of measurement of the degree of carotid artery stenosis.



The NASCET and ECST trails used different methods of reporting the degree of carotid stenosis on carotid angiograms [Donnan et al., 1998]. NASCET: North American Symptomatic Carotid Endarterectomy Trial; ESCT: European Carotid Surgery Trial.

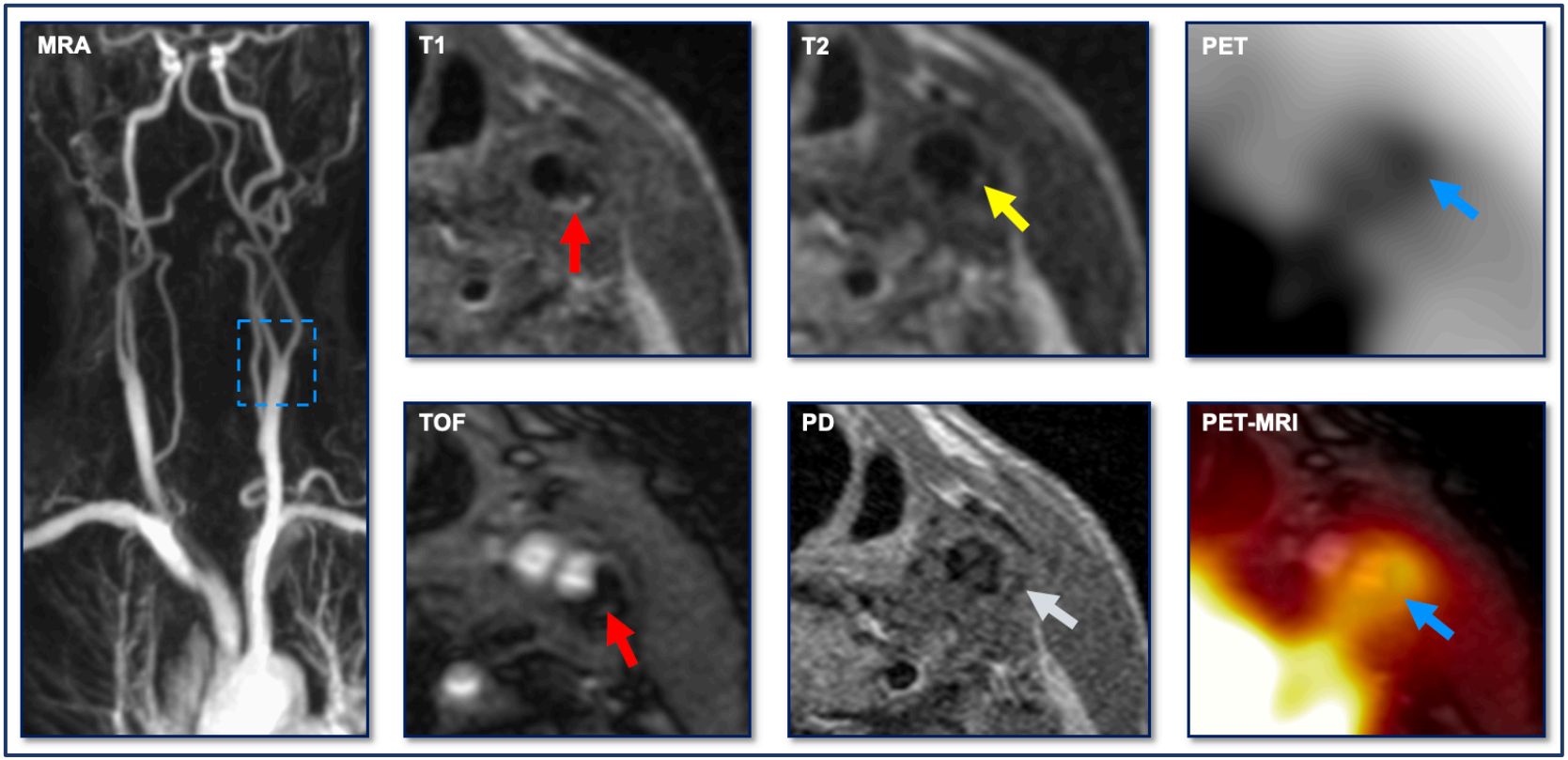
However, there are many limitations related to these ground-breaking carotid trials. Both NASCET and ESCT were conducted three decades ago when best medical therapy lacked the routine combination of anti-hypertensives, statins and consisted of aspirin only. Since then, dedicated transient ischaemic attack (TIA)/Stroke pathways with rapid outpatient access have been developed. These measures along with the routine and prompt implementation of best medical therapy reduced 90-day stroke risk from 10% to 2% following the TIA and minor stroke [Rothwell et al., 2007]. Furthermore, clinical stroke pathways facilitated fast-tracked broader population recruitment including this carotid research. On the other hand, despite these advances in standard care, including dual antiplatelet therapy, the risk of stroke following a transient ischaemic attack or stroke remains high implying that a considerable number of patients suffer from a thrombus fragmentation with subsequent embolisation [Salem et al., 2011]. Also, grading of the severity of carotid artery stenosis in NASCET and ECST trials was performed with outdated intra-arterial

angiography that was inept of characterising plaque morphology, and itself carried a risk of stroke [Cronenwett et al., 2014]. As already mentioned, the frequently quoted two-week operative rule that spans the time between symptoms onset and surgery has never actually been exercised in the original trials. Unsurprisingly many clinicians argue that these results are obsolete and express a desire to move beyond this old body of knowledge, suggesting novel endovascular technologies as a way forward. However, we should value the contributions of these trials that have immensely helped to advance our understanding of the symptomatic carotid artery stenosis. Crucially, it is still the NASCET data that consistently maintains the gold standard treatment position of carotid endarterectomy when faced with carotid artery stenting trials that aim to replace this unique vascular operation, so far unsuccessfully.

1.6.2 LOOKING BEYOND CAROTID ARTERY STENOSIS

Since the publication of NASCET and ECST trials, we have made significant progress in understanding the imperfections of using the degree of carotid artery stenosis when selecting patients for vascular revascularisation. We have known for decades that majority of ischaemic strokes are attributable to culprit ruptured plaques with <50% stenoses (Figure 1.10) and perhaps unsurprisingly only about half of excised recently symptomatic carotid plaques demonstrate rupture [Naghavi et al., 2003; Howard et al., 2015; Kim et al., 2016]. Also, with application of sophisticated molecular probes [Evans et al., 2016; Aizaz et al., 2020] we have gathered compelling and irrefutable information that plaque morphology is a far better predictor of future neurovascular events than carotid stenosis alone [Howard et al., 2015; Saba et al., 2021].

Figure 1.10: ^{18}F-NaF PET-MRI of <30% stenosed left carotid artery.



Example of a patient with left hemispheric ischaemic stroke and <30% stenosis of the left internal carotid artery (MRA blue dashed box). MRI plaque analysis identified intraplaque haemorrhage (red arrows), necrotic lipid core (yellow arrow) and calcification (grey arrow). ^{18}F-NaF PET-MRI showed focal uptake (blue arrows) in the region of the intraplaque haemorrhage and necrotic lipid core. MRA: magnetic resonance angiography; ^{18}F-NaF PET-MRI: Fluorine 18–labelled sodium fluoride positron emission tomography-magnetic resonance imaging; T1 and T2 weighted imaging; TOF: time-of-flight; PD: proton density.

Furthermore, compensatory outward (expansive) remodelling index that preserves the lumen [Khenkina et al., 2023], results in non-stenotic lesions ensuring no adverse haemodynamic effects. Arguably, this may be a more prevalent scenario in carotid arteries which are characterised by greater distensibility than coronary vessels [Degnan et al., 2012]. Moreover, plaques resulting in <50% stenosis exert greater tension within the fibrous cap than lesions with higher degree of stenoses based on the Laplace's law [Wasserman et al., 2005; Ballotta et al., 2014]. These low-grade arterial lesions or mild stenoses (<50%) with high-risk plaque features predominate on the ipsilateral carotid side to the presenting stroke when compared with the contralateral carotid artery [Kamtchum-Tatuene et al., 2021]. Unsurprisingly, mild stenoses rupture more frequently than the severe ones [Ballotta et al., 2014] and were responsible for >40% of recurrent strokes during NASCET trial follow up [Saba et al., 2021]. In effect, risks associated with mild stenoses have been underestimated by NASCET trial. An interesting perspective on this was demonstrated by a retrospective study which showed that patients with symptomatic mild (20-49%) carotid artery stenosis treated with best optimal medical therapy had a higher risk of recurrent ipsilateral stroke of 7.4% when compared with both an asymptomatic group with a similar degree of stenosis and a symptomatic cohort with moderate or severe stenoses [Karlsson et al., 2016]. Finally, several vascular surgery frontiers published seminal surgical reports on safety and efficacy of carotid endarterectomy in patients with <50% carotid artery stenosis whose benefit was dismissed by the original NASCET data. Three publications performed revascularisation in patients if they experienced recurrent neurovascular event (despite maximal best medical therapy), additional investigations excluded other potential sources of emboli and MRI demonstrated high-risk plaque features with subsequent histological validation: n=7 [Yoshida et al., 2012], n=14 [Takai et al., 2018], n= 17 [Yoshida et al., 2019]. Whilst an Italian study n=57 [Ballotta et al., 2014] recruited patients after their first or recurrent neurovascular event similarly performing MRI with histopathological validation of excised carotid tissue. Although these surgical results are limited by small sample sizes, single institution and

surgeon experiences, they reinforce the notion that mild stenoses are not benign lesions. This suggests that it is high time that we refine our notion of selecting patients for carotid surgery based solely on the severity of stenosis. Although relieving haemodynamic impairment is important, prevention of thromboembolism that drives acute neurovascular events regardless of the stenosis severity is paramount for an individual's welfare.

Therefore, knowledge of high-risk plaque morphology should be the lead point when selecting patients for carotid endarterectomy. Conversely, patients with highly stenosed carotid arteries with no evidence of high-risk plaque features could avoid surgery, including procedural risks. This, to a degree, is controversial. However, it is the only way that vascular discipline can in the future collectively introduce a more holistic and plaque-based approach into a routine clinical practice where a detailed identification of individual plaque components would start from the original ictus and determine the appropriate treatment strategy. This would constitute an authentic *look* beyond the anatomical level of carotid artery stenosis.

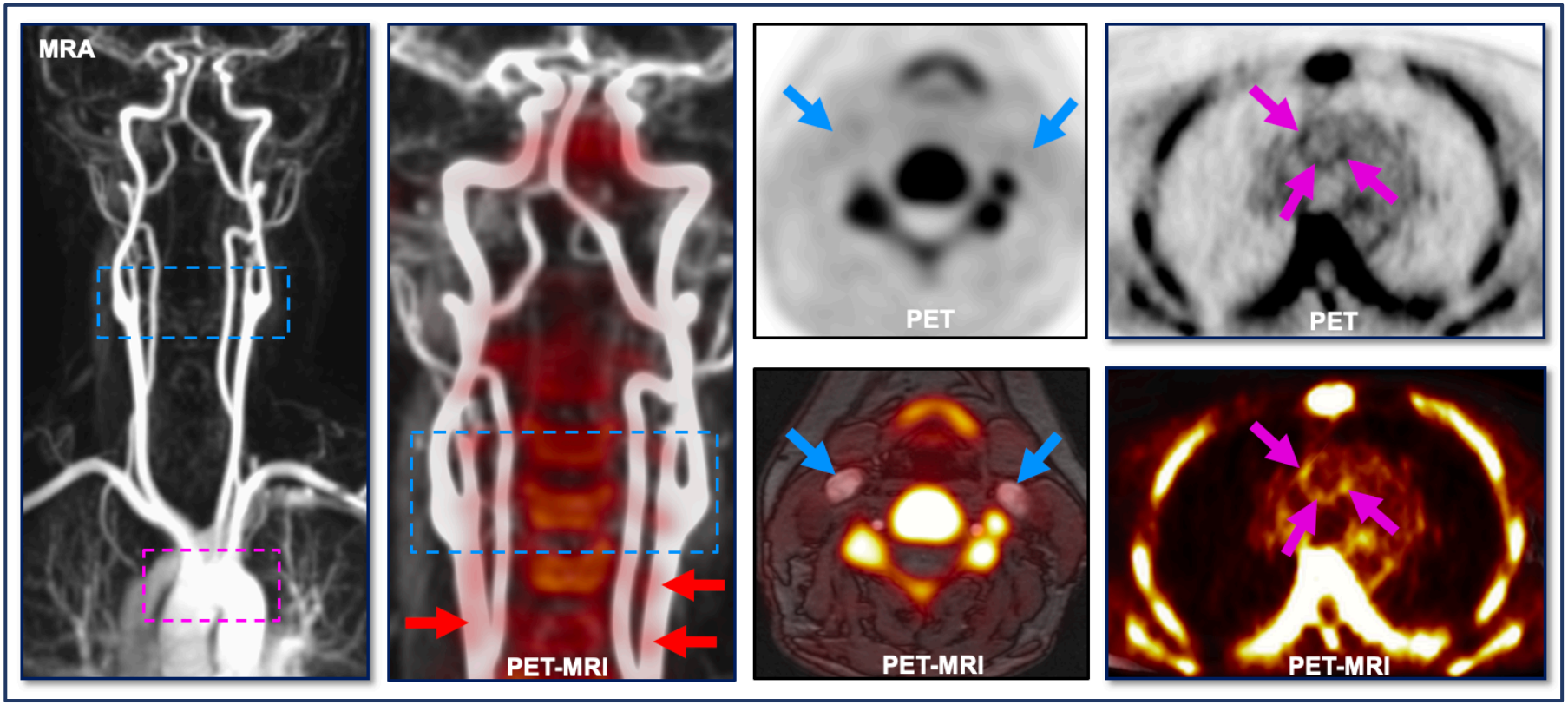
1.7 CURRENT NON-INVASIVE IMAGING MODALITIES OF CAROTID ARTERY STENOSIS

Current guidelines use the severity of carotid artery stenosis to stratify neurovascular syndrome management. However, there are many pitfalls with this traditional approach. Firstly, anatomical quantification of stenosis does not take account of positive remodelling which preserves the lumen and delays clinical presentation of atherosclerotic disease [Saito et al., 2002; Labropoulos et al., 2000]. Thus, it may underestimate the degree of cross-sectional area stenosis, including associated risks. Second, arterial stenosis provides no information on the biological activity of the plaque. Whereas, histological data show that inflammation, necrotic lipid core, intraplaque haemorrhage, thin fibrous cap and microcalcification are key features in driving both carotid

plaque formation and instability [Howard et al., 2015; Redgrave et al., 2006; Vesey et al., 2017; Salem et al., 2013b]. Third, only 50-60% of recently symptomatic carotid plaques removed during carotid endarterectomy demonstrate rupture [Howard et al., 2015]. This creates uncertainty as to whether excised plaque was indeed a clinically culprit one. Furthermore, up to a quarter of ischaemic strokes are cryptogenic in nature and thromboembolism from other large arteries with non-occlusive lesions (aortic arch) is deemed responsible for many adverse neurovascular events (Figure 1.11) [Castellanos et al., 2001; Wehrum et al., 2017]. Therefore, reliable detection of culprit carotid plaque that may be not necessarily obstructive would ensure appropriate selection of patients to a vascular procedure. This would also facilitate the assessment of novel pharmacological therapies.

Four different imaging modalities are available to image carotid artery such as ultrasound scan, computed tomography (CT), magnetic resonance imaging (MRI), and hybrid positron emission tomography (PET) combined either with CT or MRI.

Figure 1.11: ^{18}F-NaF PET-MRI uptake in ascending aorta.



Example of a patient with amaurosis fugax, disease-free bilateral carotid arteries on Duplex ultrasound, MRA (coronal-blue dashed box) and no ^{18}F-NaF uptake on PET-MRI (coronal-blue dashed box and axial-blue arrows). Moderate ^{18}F-NaF PET-MRI uptake (axial-pink arrows) in the ascending aorta on MRA (coronal-pink dashed box). Radiotracer overspill from the adjacent cervical spine demonstrated on PET-MRI (coronal-red arrows) images. ^{18}F-NaF PET-MRI: Fluorine 18–labelled sodium fluoride positron emission tomography-magnetic resonance imaging; MRA: magnetic resonance angiography.

1.7.1 ULTRASOUND SCAN

B-MODE and DOPPLER

Stenosis measurement

Ultrasound is a repeatable and low-cost tool that is well tolerated by patients. Traditional B-mode ultrasound is the most used first-line imaging modality in the pre-operative carotid artery stenosis assessment that is often combined with colour Doppler flow [Cronenwett et al., 2014]. It facilitates a rapid evaluation of carotid arteries that is vital in stroke prevention because it avoids unnecessary delays due to imaging when carotid endarterectomy is indicated [Wardlaw et al., 2006b]. Doppler ultrasound offers reliable quantification of a severe (70-99%) luminal carotid artery stenosis with a less accurate assessment of 50-69% categories (Figure 1.12) [Tsuruda et al., 1991; Carroll, 1991; Mitchell et al., 2017; Naylor, 2015a]. Therefore, in those with <70% stenosis, the diagnosis should be confirmed by either a repeated ultrasound performed by another operator or different imaging modality to avoid unnecessary carotid endarterectomy and vice versa [Wardlaw et al., 2006b; Chappell et al., 2009]. Several studies have found that Doppler ultrasound may overestimate the degree of stenosis when the peak systolic velocity that is indicative of the severity of stenosis is increased on the ipsilateral artery in the presence of the contralateral occlusion [Naylor, 2007; Fujitani et al., 1992; Cronenwett et al., 2014]. Finally, ultrasound can fail to detect near occlusion of the carotid artery, and excessive carotid artery calcification may impede stenosis measurements [Devuyst et al., 2005; Dawson et al., 1993; Sabeti et al., 2004].

Morphological assessment

In general, ultrasound can differentiate lipid-rich plaques with intraplaque haemorrhage (echolucent) from fibro-calcific atherosclerotic lesions (echogenic) [Hjelmgren et al., 2013; Arnold et al., 1999; Golledge et al., 2008]. Additionally, it measures fibrous cap thickness and detects features of plaque rupture such as ulceration and thrombus [Huibers et al., 2015; Lammie et al., 2000; Gronholdt et al., 2001]. Fibrous cap is identified as an echogenic

structure with a reported sensitivity of 73% and specificity of 67% [Huibers et al., 2015]. Whereas plaque rupture manifests as a focal depression (ulcer) with an irregular surface that measures at least 2 mm (depth) x 2 mm (length) [Huibers et al., 2015]. Thrombus can be identified with specificity and sensitivity as high as 90% [Kawasaki et al., 2001; Noritomi et al., 1997]. However, sensitivity and specificity demonstrate significant differences across studies with values of 33-75% regarding the former and 33-92% for the latter [Huibers et al., 2015]. Both, intraplaque haemorrhage or thrombus produce echolucent images on ultrasound. Similarly, the differentiation between intraplaque haemorrhage and necrotic lipid core is poor because these features also appear as echolucent areas [Lammie et al., 2000; Skagen et al., 2016a]. Again, presence of carotid artery calcification can obscure plaque features [Devuyst et al., 2005; Russell et al., 2010]. Thus, the role of ultrasound in evaluating plaque morphology remains controversial because the interpretation is subjective, has moderate specificity, and potential clinical usefulness is still debatable [Cronenwett et al., 2014; O'Donnell et al., 1985; Hunink et al., 1993].

Figure 1.12: Non-invasive imaging of carotid artery stenosis.

	DUS	CTA	MRA	CEMRA
70–99% stenosis				
Sensitivity (95% CI)	0·89 (0·85–0·92	0·77 (0·68–0·84)	0·88 (0·82–0·92)	0·94 (0·88–0·97)
Specificity (95% CI)	0·84 (0·77–0·89)	0·95 (0·91–0·97)	0·84 (0·76–0·97)	0·93 (0·89–0·96)
50–69% stenosis				
Sensitivity (95% CI)	0·36 (0·25–0·49)	0·67 (0·30–0·90)	0·37 (0·26–0·49)	0·77 (0·59–0·89)
Specificity (95% CI)	0·91 (0·87–0·94)	0·79 (0·63–0·89)	0·91 (0·78–0·97)	0·97 (0·93–0·99)
0–49% stenosis or 100% occluded				
Sensitivity (95% CI)	0·83 (0·73–0·90)	0·81 (0·59–0·93)	0·81 (0·70–0·88)	0·96 (0·90–0·99)
Specificity (95% CI)	0·84 (0·62–0·95)	0·91 (0·74–0·98)	0·88 (0·76–0·95)	0·96 (0·90–0·99)

Meta-analysis results reproduced from [Wardlaw et al., 2006a]:

- US: Ultrasound Scan
- CTA: Computed Tomography Angiography
- MRA: Magnetic Resonance angiography
- CEMRA: Contrast Enhanced Magnetic Resonance Angiography

TRANSCRANIAL DOPPLER ULTRASOUND

Transcranial Doppler is a non-invasive ultrasound technique that facilitates detection of microembolic signals (MES) in the middle cerebral artery (MCA) through the skull (via the temporal bone acoustic window) with the use of a head fixation device [Nicolaides et al., 2012]. The international consensus criteria defined MES as short-duration high-intensity signals associated with a specific audible *chirp* sound (>6 dB threshold) [Ringelstein et al., 1998]. The recommended time of transcranial Doppler monitoring is between 30-60 minutes because the rate of detectable MES increases with ultrasound duration. Also, bilateral MCA monitoring should be performed owing to the possibility of cross hemispheric embolisation from the contralateral asymptomatic carotid plaque [Nicolaides et al., 2012].

The composition of solid emboli includes plaque debris or fragmented thrombus, and these MES predominantly occur during the dissection of a carotid artery or wound closure at the surgery. Whilst gaseous MES can result from the release of carotid cross-clamps or insufficient venting of repaired arteriotomy site. The clinical significance of MES in symptomatic carotid artery stenosis is associated with an increased risk of a recurrent ipsilateral focal ischaemia [Markus, 1993; Imray et al., 2005]. Numerous studies have demonstrated that the presence of MES translates to a 40-fold increased risk of future neurological events [Dellen et al., 2008; Verhoeven et al., 2005b; Wolf et al., 2004a; Kimura et al., 2001; Saedon et al., 2014]. More importantly, patients following carotid endarterectomy remain at greater risk of MES-induced postoperative stroke [Stork et al., 2002b; Abbott et al., 2007a] and this was confirmed by brain imaging data that showed a greater number of MRI detectable cerebral infarcts in patients with detected emboli compared with those who were free from MES [Wolf et al., 2004a; Kimura et al., 2001]. However, one must remember that published data demonstrate considerable differences regarding methodology, lack of standardised imaging protocols, imaging equipment, therefore, it should be interpreted with caution. Although transcranial Doppler is a safe, portable and repeatable, several aspects make

it a rather unfriendly imaging modality that precludes a routine clinical use. Transcranial Doppler requires expertise, prolonged monitoring and lack of temporal window prevents its use [Marinoni et al., 1997; Markus, 2000a]. In the context of symptomatic carotid artery stenosis and stroke preventative surgery which requires urgency, this ultrasound technique has not found many vascular enthusiasts. On the other hand, a compelling data showed that intra-operative application of transcranial Doppler leads to almost a complete eradication of intra-operative stroke in the vascular centres that use it routinely [Naylor et al., 2000; Lennard et al., 1999b]. This phenomenon's explanation lies in the prompt detection of reduced or absent MCA flow at an operation that allows for the immediate rescue of brain tissue. Two concurrent mechanisms lead to the intra-luminal thrombus formation at the site of endarterectomised carotid artery that carry the potential to embolise distally. First, endarterectomised area is a highly pro-thrombotic surface because it is devoid of any endothelial cover. Second, transected vasa vasorum leak intraluminally and form a thrombus, resistant to manual irrigation with heparinised normal saline [Naylor, 2021]. Additional benefits of intra-operative transcranial Doppler use relate to the assessment of sufficient haemodynamic cerebral perfusion. This is achieved by real-time MCA velocity assessment and patency control of a shunt that may be kinked against distal internal carotid artery, indicating no shunt flow. However, until transcranial Doppler is part of a routine vascular training, its role will remain limited even during carotid revascularisation.

NOVEL AND EXPERIMENTAL ULTRASOUND IMAGING

Grey Scale Median

To overcome the aforementioned ultrasound deficiencies, some propose to use the grey-scale median, which is a computerised measurement of plaque echogenicity. The low value of grey-scale-median (<40) implies the presence of echolucent plaque (thin fibrous cap, high lipid and/or intraplaque haemorrhage content) and it has been associated with increased risk of acute neurovascular events [Degnan et al., 2012]. Furthermore, the grey-scale

median is a measure of an overall plaque brightness evaluated as discrete white areas compared to the black vessel wall (adventitia). Therefore, it does not reflect the homogeneity or heterogeneity of the individual plaque components. Unsurprisingly, due to the lack of the standardised imaging protocols, the technique has not found its use in routine clinical practice.

Juxta-luminal Black Area

The juxta-luminal black area is defined as a hypoechoic plaque area adjacent to the arterial lumen without a visible echogenic fibrous cap (pixels with grey-scale values $\geq$ 25) [Griffin et al., 2010]. The latter implies that the fibrous cap is either absent or too thin to produce reflected echoes, thus is beyond the resolution of ultrasound. The *black-and-white* image normalisation of the juxta-luminal black area, similarly to the grey-scale median, utilises two reference points such as blood (area free of noise, grey-scale value = 0) and adventitia (the brightest part adjacent to the plaque) [Kakkos et al., 2013]. The largest juxta-luminal black area (pixels with grey-scale values < 25) is then delineated and automatically calculated by a dedicated software research package. Despite some promising findings this imaging approach did not find many enthusiasts likely due to the discrepancies among available data which are still to be addressed in large and prospective clinical studies. Some demonstrated that the juxta-luminal black area cut-off value of >8 mm^2 is an independent predictor of symptomatic plaques regardless of the degree of stenosis with neurovascular symptoms [Griffin et al., 2010]. Whist others showed that smaller area of >6 mm^2 identified unstable carotid plaques [Salem et al., 2014]. Other potential confounding factors include heterogenous populations consisting of asymptomatic and symptomatic patients as well as retrospective imaging databases analyses. More importantly, published results lacked basic information on the time scale between the index event and actual imaging [Griffin et al., 2010], while other studies had a long recruitment window (up to 6 months from index event) [Salem et al., 2014]. Both these scenarios could potentially provide a sufficiently long interval for the plaque morphology to change. Another limitation relates to the arbitrary grey-scale pixel values of

0-25 that define the juxtaluminal black areas as these reflect limitations of a human eye that cannot distinguish any plaque features under an average ambient light [Griffin et al., 2010]. Therefore, to determine the diagnostic value of this approach with the potential role in risk stratification of patients more data are required including extended analyses using grey-scale pixel values below and above 25. Until then, the juxta-luminal black area will remain one of many research tools enhancing characterisation of plaque texture features.

Intimal Medial Thickness

The rationale for this form of imaging is based on the hypertensive thickening of the smooth muscles in the media layer [Johri et al., 2013]. Some reported increased thickness of tunica intima-media to be predictive of future cerebral and cardiovascular events when assessing the efficacy of pharmacological therapy in managing atherosclerosis [Yu et al., 2007; Goldberger et al., 2010; Skagen et al., 2016b]. While others did not find this association [Chambless et al., 2004; Sol et al., 2001; Simon et al., 2010]. However, one must remember that atherosclerosis is a subintimal process [Libby et al., 2009]. Hence, this pathological feature, in conjunction with small annual changes of the intimal-medial-thickening that are beyond the resolution of ultrasound, make this imaging modality far from accurate. Until larger prospective studies prove that even minimal changes in the intimal-medial-thickening translate into a reduced clinical risk, the overall clinical applicability will remain debatable.

Plaque Thickness and Volume

Plaque thickness is a simple measurement obtained from the intima to the maximal point of atheroma protrusion into the vessel's lumen that was found to be an independent predictor for cardiovascular risk [Johri et al., 2013]. Furthermore, measurements of plaque area (volume) assessed by two-dimensional ultrasound showed that it was a strong predictor of stroke [Johri et al., 2013]. As such evaluation of a focal increase in arterial wall thickness or volume indicate regions of atherosclerosis more reliably compared to medial hypertrophy investigated by the intimal-medial-thickening [Cronenwett et al.,

2014]. This may be reflective of a pathophysiological feature that plaque grows faster in a longitudinal plane compared to the process of arterial wall thickening [Spence, 2008]. At present, however, assessment of plaque thickness is primarily performed to observe plaque regression following pharmacological therapy.

3-Dimensional Ultrasound

This next generation ultrasound may permit more comprehensive volumetric plaque assessment because it could facilitate not only detection of the atherosclerotic carotid disease but also provide a platform for monitoring response to novel treatments [Johri et al., 2013; Huibers et al., 2015]. Another advantage over the two-dimensional ultrasound is the improved detection of plaque ulceration (16.1% versus 6.5% respectively) [Huibers et al., 2015]. Unfortunately, 3-dimensional ultrasound has not overcome problems with imaging areas of calcification. In effect, it can underestimate the severity of stenosis [Wessels et al., 2004]. Also, this enhanced plaque assessment is time consuming, and considerable inter-observer variability (6-15%) has been demonstrated across different studies [Spence, 2015; AlMuhanna et al., 2014]. Therefore, the lack of standardised protocols and robust histological validation, makes this imaging technique a useful research tool only.

Contrast-Enhanced Ultrasound

Contrast-enhanced ultrasound provides improved visualisation of the fibrous cap, ulceration and neovascularisation with or without intraplaque haemorrhage when compared with the standard ultrasound imaging [Skagen et al., 2016b]. This technique involves an injection of a microbubble contrast which localises within the plaque. The reflected ultrasound beam graded on a 4-point scale indicates the degree of neovascularisation. Although several studies have demonstrated a good correlation between assessment of ultrasound contrast uptake in the plaque with histological examination, such visual assessment is highly user dependent [Huibers et al., 2015]. Even semi-automated methods at best offer moderate inter-observer agreement [Huibers

et al., 2015]. Most importantly, artefacts generated by breathing and small movements of transducer complicate robust quantification of the neovascularisation [Skagen et al., 2016b]. Finally, use of contrast-enhanced ultrasound is limited by the presence of calcified-echogenic plaques that preclude evaluation of the contrast uptake [Huibers et al., 2015].

Superb Microvascular Imaging Ultrasound

Superb microvascular imaging ultrasound is a Doppler technology that allows the visualisation of microvascular bed with low flow signals without the use of contrast agents [Artul et al., 2017; Lu et al., 2017]. The technique effectively separates flow signals from overlying tissue motion artefacts which allows preserving low flow components [Skagen et al., 2016b]. To date, the technique has been studied in small and heterogeneous populations of patients presenting with various malignancies [Artul et al., 2017]. In these scenarios, superb microvascular ultrasound aimed to detect microvascular flow patterns to differentiate between benign and malignant lesions [Lu et al., 2017; Zhu et al., 2018]. Similarly, limited data are available on the potential use of this technique in detecting neovascularisation and thereby in assessing intraplaque haemorrhage in patients who suffered a stroke [Wang et al., 2019; Yang et al., 2020]. Most recent meta-analysis revealed promising results of superb microvascular imaging compared with contrast enhanced ultrasound in detecting intraplaque haemorrhage [Yang et al., 2020]. However, data were based on low quality studies with small sample sizes. Furthermore, most studies that were evaluated originated from one country. Therefore, the results ought to be interpreted with caution. Until larger, multicentre, and international studies are available, the technique will remain an interesting research tool.

Shear Wave Elastography

Shear wave elastography is a new ultrasound method that exploits acoustic radiation forces to generate shear wave propagation in tissues [Skagen et al., 2016b]. Recent data suggest that plaque ruptures when the peak stress within the fibrous cap exceeds a certain threshold level. Hence knowledge about the

stress distribution within the fibrous cap may predict the risk of plaque rupture. Shear wave elastography can identify features of plaque vulnerability and enables the assessment of tissue stiffness by quantifying Young's modulus of elasticity [Skagen et al., 2016b]. The speed of propagation of the shear waves depends on the local density and elastic modulus of tissue [Zamani et al., 2020]. Although, some authors reported the ability to identify vulnerable plaques, the data were based on a small number of patients (n=25) [Garrard et al., 2015]. The presence of intra-plaque haemorrhage and thrombus were associated with a significantly lower Young's modulus [Garrard et al., 2015]. However, there was also an overlap in Young's modulus values between stable and unstable plaques. Therefore, this aspect requires further research before this imaging modality could be used in a clinical setting. To date, the technique has been evaluated in different tissues including thyroid, breast, liver and prostate and, as such, is in its infancy stage [Zamani et al., 2020].

Carotid Plaque Risk Index

Carotid plaque risk index combines quantitative measures of carotid plaque echogenicity and surface irregularities with the degree of stenosis [Kanber et al., 2015]. This index was found to be a better predictor of cerebrovascular symptoms and could aid in the identification of vulnerable carotid artery stenoses [Kanber et al., 2015; Rafailidis et al., 2019]. Most importantly, this approach is based on quantitative measures of carotid plaque delineation with a combined assessment of stenosis. This has undoubtedly limited applicability and validity due to varying assessment methods that were used between centres [Kanber et al., 2015]. However, published data is based on a few reports with limited number of participants. Thus, it must be considered as preliminary and requires further validation.

Limitations

Unfortunately, like with most real-time imaging techniques, Doppler and 2-dimentional ultrasound are primarily limited by high operator dependency. This results in a high variability of imaging quality that is performed by different

vascular laboratories globally. Another disadvantage is the anatomy of carotid arteries including tortuosity, vessel depth, high bifurcation, excessive calcification and near occlusion.

1.7.2 MAGNETIC RESONANCE IMAGING

Stenosis Measurement

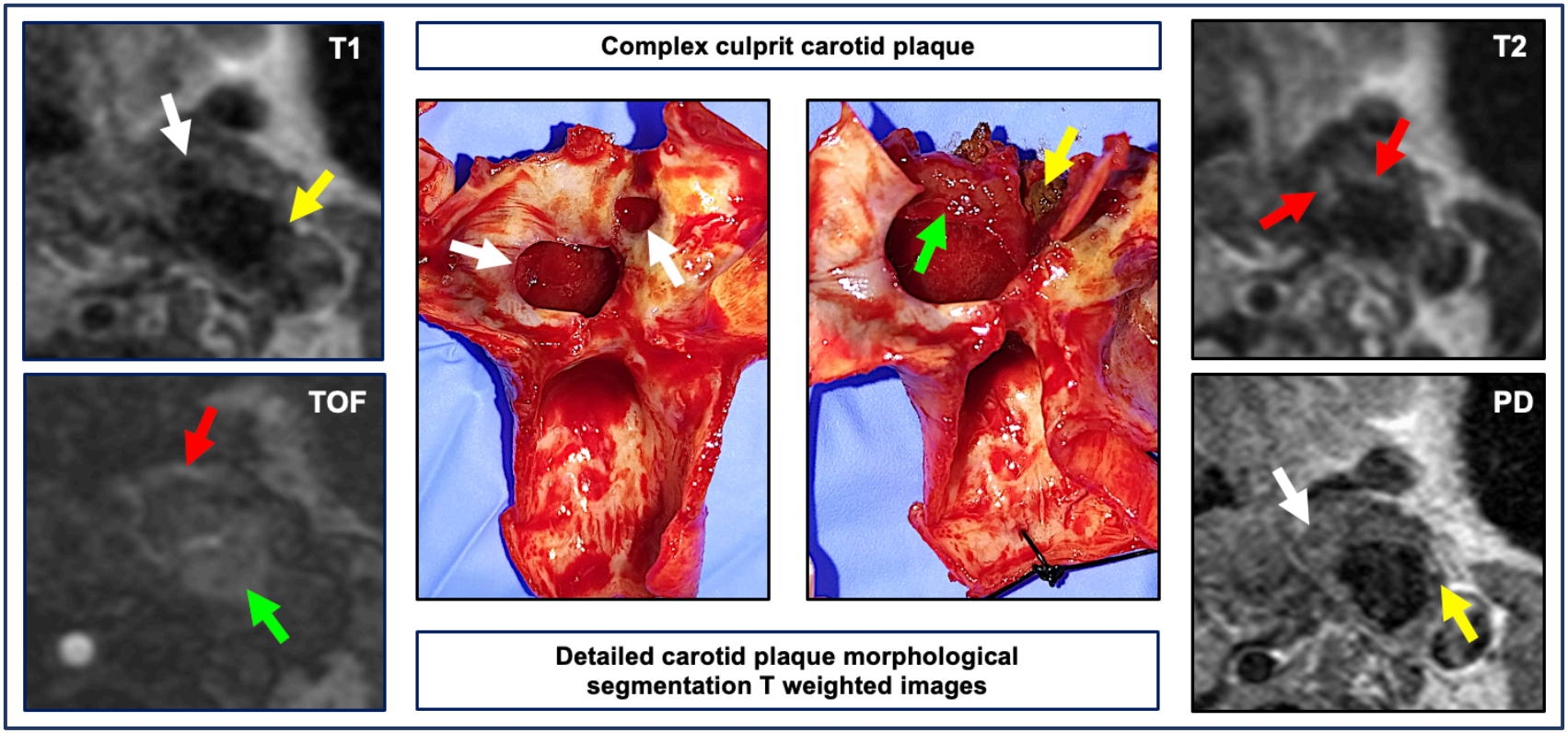
Magnetic resonance angiography used for evaluating carotid arteries most commonly utilises two techniques: time-of-flight imaging (contrast free) and contrast-enhanced magnetic resonance angiography. Although, both time-of-flight imaging and contrast-enhanced magnetic resonance angiography assess carotid stenosis accurately, the latter produces higher quality images that are less prone to artefacts due to the use of paramagnetic contrast media [Syed et al., 2019]. Meta-analyses demonstrated that contrast-enhanced magnetic resonance angiography was the most sensitive (94%) and specific (93%) technique for detection of symptomatic 70-99% carotid artery stenosis when compared with magnetic resonance angiography, Doppler ultrasound and computed tomography angiography (Figure 1.12) [Wardlaw et al., 2006a]. Whereas magnetic resonance angiography produced low sensitivity (37%) when evaluating moderate (50-70%) carotid artery stenosis [Chappell et al., 2009]. These findings highlight that a misdiagnosis due to an imprecise calculation of the degree of stenosis could either lead to the exclusion of a patient from having carotid endarterectomy or indicate an unnecessary surgical intervention [Wardlaw et al., 2006b; Wardlaw et al., 2006a].

Morphological assessment

Magnetic resonance imaging is a reproducible modality that that allows for detailed carotid plaque morphology evaluation with moderate to a good agreement [Huibers et al., 2015; Lovett et al., 2004a]. It detects lipid-rich necrotic core, intra-plaque haemorrhage, cap thickness, ulceration and plaque rupture (Figure 1.13) [Sitzer et al., 1993; Hartog et al., 2013]. Magnetic resonance imaging offers superior soft tissue detail at high resolution that can better segment plaque by exploiting the varying T1/T2 properties and proton

density (PD) of different lesion constituents. In particular, intra-luminal thrombus or intra-plaque haemorrhage may be identified as regions of high signal on non-contrast T1-weighted (T1W) echo gradient sequences. Such signal has been observed in the culprit plaques of patients who have suffered a recent stroke, corresponding to acute thrombus on histology and localising to complex carotid lesions with evidence of surface rupture or intra-plaque haemorrhage [Lovett et al., 2004a; Huibers et al., 2015]. Depending on the age of the haemorrhage, intensity signals can vary across T-weighted images due to the presence of methaemoglobin, a breakdown product of haemoglobin (Table . However, similarly to ultrasound, differentiation between intraplaque haemorrhage and lipid core is challenging because the former is often contained within the larger area of a lipid core.

Figure 1.13: Non-invasive carotid plaque imaging.



MRI identified high-risk carotid plaque features:

- T1 - ulcer (white arrow) and necrotic lipid core (yellow arrow)
- TOF - thrombus (green arrow) and intraplaque haemorrhage (red arrow)
- T2 - intraplaque haemorrhage (red arrows)
- PD - ulcer (white arrow) and necrotic lipid core (yellow arrow)

MRI: magnetic resonance imaging; T1 and T2: T weighted images; TOF: time of flight; PD: proton density.

Necrotic lipid core presents as hyperintense signals on T1W and PD images [Saam et al., 2005]. Detection of lipid core differs between individual studies with reported sensitivity from 82% to 100% and specificity ranging between 40% to 100% [Hartog et al., 2013; Saam et al., 2005]. There are several potential explanations including the manual segmentation of regions, the low resolution of 1.5T scanners, and the lack of dedicated T2 mapping techniques [Chai et al., 2017]. These aspects make detection of small areas of lipid pools difficult. However, increasing understanding of the importance of reliable detection of necrotic lipid cores led to development dedicated T2 mapping sequences on a voxel-by-voxel basis using 3T scanners [Chai et al., 2017]. This allowed the quantification of lipids and thereby detect recently symptomatic plaques with high sensitivity and specificity [Chai et al., 2017]. Most importantly, reduction in lipid core has been reported without simultaneous changes in the carotid plaque volume [Underhill et al., 2008; Xia et al., 2017]. Thus, in the future, this may allow for a more precise assessment of lipid lowering therapies, identification of high-risk lesions and ultimately the risk of future cerebrovascular events [Deng et al., 2019].

Magnetic resonance imaging detects the fibrous cap defined as a layer of connective tissue covering necrotic lipid core [Ota et al., 2009]. The fibrous cap appears as a juxta-luminal band characterised by isointense signals at T1, T2 and PD weighted images and hypointense signal on time-of-flight [Huibers et al., 2015]. However, differentiation between a ruptured or thin fibrous cap remains problematic, and there is no consensus whether the absence of a hypointense band is indicative of either of the above [Cai et al., 2002]. Ulceration can be identified with moderate sensitivity as a surface defect on all T-weighted and PD images [Huibers et al., 2015] Finally, calcification can be identified as a hypointense signal on all T-weighted images with a sensitivity of 76-84% and specificity of 86-94% [Cai et al., 2002]. Although existing literature on the imaging of *in vivo* carotid plaque features with histological data is vast and promising, all studies lack standardised histological analysis as well as imaging protocols [Hartog et al., 2013]. This precludes a meta-analysis.

Nevertheless, magnetic resonance angiography is, at present the most multifaceted technique to assess the breadth of culprit plaque characteristics.

ADDITIONAL MAGNETIC RESONANCE IMGING

Arterial Wall Thickness and Plaque volume

The primary role of measuring arterial wall thickness is to assess plaque regression following medical treatment. A significant reduction in vessel wall thickness has been reported after long-term statin therapy, [Degnan et al., 2012] although others found no change in relation to wall thickness [Underhill et al., 2008]. Most commonly, this parameter is assessed concurrently with other volumetric measurements of atherosclerotic lesions. Several recent studies have shown that magnetic resonance imaging is a reliable technique to monitor the disease progression by measuring arterial wall and lumen volume (a sum of which comprises a total plaque area) and the normalised wall index (wall area divided by total plaque area) [Hayashi et al., 2010; Aidi et al., 2009; Chorath et al., 2020]. In general, studies demonstrate a reduction in wall area with an increase in lumen area approximately at least after 1 year of stain therapy [Degnan et al., 2012]. Although, these are promising results, current data are limited and require further validation in larger and longer clinical trials [Huibers et al., 2015].

Magnetic Resonance Spectroscopy

Magnetic resonance spectroscopy combines the spatial localising of MRI with information of chemical composition from spectroscopy by detecting a range of atoms including 1-hydrogen (most used due to high natural abundance and nuclear magnetic sensitivity), 13-Carbon, 19-Fluorine, 23-Sodium and 31-Phosphours [Castillo et al., 1996; Vinitski et al., 1991]. In effect, magnetic resonance spectroscopy identifies and quantifies various metabolites in tissues including liquid phase cholesteryl ester in atherosclerotic plaques [Castillo et al., 1996; Duivenvoorden et al., 2013; Zajicek et al., 1987]. This is of particular importance since the early stages of atherosclerosis are characterised by the deposition of cholesteryl ester in the foam cells [Guyton,

2013; Pearlman et al., 1988] whilst the liquid cholesteryl ester is the major class of lipids found within the atheroma lipid-rich necrotic cores associated with plaque rupture [Ruberg et al., 2006]. Moreover, plaque lipids can undergo thermotopic transitions between liquid and solid phases, and the physical state of cholesteryl ester influences enzymatic activities, lipids transport, and storage; all which are essential in atherogenesis [Pearlman et al., 1988]. Hence, quantification of specific lipid content can provide vital information central to the pathophysiology of atherosclerosis and potentially aid in the identification of culprit carotid plaque. However, MRI lacks the capacity to differentiate specific lipid plaque components because lipid regions are inhomogeneous, and cholesterol crystals create a signal void in proton-density MRI [Ruberg et al., 2006; Guyton, 2013]. This, to a degree, has been overcome by gadolinium contrast-weighted sequences that allow to distinguish various signal intensities within plaque components including lipid-rich tissue. However, these signals are non-specific, hence do not permit an individual lipid identification. In contrast, magnetic resonance spectroscopy detects liquid cholesteryl ester by providing a spectrum of proton resonances from lipid-rich or poor regions in a volume (lumen, plaque and perivascular tissue) during a routine MRI at the cost of additional 15 minutes of scanning [Guyton, 2013]. The obtained proton spectra are detected through their inherent frequency shift relative to water and interpreted as ratio of individual chemical components (plaque cholesteryl ester relative to perivascular triglyceride). The feasibility of this imaging technique has been demonstrated by several studies that obtained consistent cholesteryl ester chemical composition and physical state from *ex vivo* human carotid and aortic plaques specimens that have been confirmed on histology [Duivenvoorden et al., 2013; Zajicek et al., 1987; Pearlman et al., 1988; Ruberg et al., 2006; Guo et al., 1998; Moreno et al., 2002]. Although an *in vivo* study (n=35) reported promising data obtained from human carotid arteries, unfortunately only half of the obtained proton spectra were adequate for the analysis due to limited spatial resolution [Duivenvoorden et al., 2013]. Therefore, this form of spectral imaging remains challenging and further work is required to better understand the arterial

plaque lipid constituents that may form the basis for future treatment strategies and provide a means of assessing response to a pharmacological treatment.

Future Directions

Molecular MRI can be performed with ultrasmall paramagnetic particles of iron oxide (USPIO). USPIO are 30nm iron oxide nanoparticles stabilised with low-molecular-weight dextran that accumulate in areas of macrophage infiltration within atherosclerotic carotid plaques [Syed et al., 2019]. A small study (n=11) demonstrated accumulation of USPIO in culprit carotid plaques that was associated with a decrease in the signal intensity on T2* weighted sequences and histological evidence of high macrophage content [Kooi et al., 2003; Dweck et al., 2016]. A reduction in USPIO uptake was observed after treatment with high dose statin indicating diminished plaque inflammation [Calcagno et al., 2020]. New developments involve fluorinated nanoparticles such as ^{19}F-fluorine that focus on immunometabolism. However, at present its utility is limited to pre-clinical applications due to challenges related to detection and quantification of ^{19}F-fluorine signal from low concentrations of nanoparticles [Wüst et al., 2019]. Ultimately, these contrast agents capable of detecting cellular activity or specific markers, such as elastin, fibrin or VCAM-1 may enable identification and phenotyping of high-risk carotid plaques [Huibers et al., 2015].

Limitations

Several obstacles prevent a routine use of magnetic resonance imaging in patients with stenosed carotid arteries. First, this imaging modality is expensive, takes longer to perform, and is not widely available. Second, the use of magnetic resonance imaging is limited by the exclusion of patients with certain metallic implants and claustrophobia. Furthermore, it requires a greater degree of co-operation than either Doppler ultrasound or computed tomography angiography [Huibers et al., 2015]. Difficulties in precise identification of individual plaque components are multifactorial. At present, segmentation is performed manually, hence the process is time consuming

and subject to a considerable inter and intra-observer variability [Huibers et al., 2015]. Furthermore, most available scanners are 1.5T that offer an inferior signal-to-noise ratio. This may improve with scanners using higher field magnet such as 3T that reduce background noise and artefact [Gonzalez et al., 2016].

1.7.3 COMPUTED TOMOGRAPHY ANGIOGRAPHY

Stenosis measurement

Computed tomography angiography is another confirmatory investigation that can be performed before carotid vascular intervention. It is particularly useful when Doppler ultrasound cannot image high carotid bifurcation, tortuous vessels, short necks and severe calcification [Huibers et al., 2015]. Furthermore, it is an easily accessible imaging technique that visualises the entire carotid arterial system form the origin to the base of the skull and three-dimensional reconstruction facilitates accurate measurement of carotid artery stenosis. Two techniques permit vascular imaging, dual-source and multidetector computed tomography. Dual-source is also known as dual-energy or spectral computed tomography that uses two separate x-ray sources at two different photon energy spectra to discriminate between various attenuation properties (Hounsfield Units at two energy spectra) in the same tissue [Brinjikji et al., 2016]. This translates into a higher spatial and temporal resolution which improves visualisation of vessels. Dual source computed tomography differentiates iodine contrast from the calcified plaque by utilising bone subtraction algorithms and multiplanar reformats. Conversely, row of multiple detectors, enables multiplanar reconstructions with a submillimetre spatial and contrast resolution. Multidetector computed tomography is widely available and plaque imaging is achieved with a bolus tracking computed tomography angiography. While detailed plaque characterisation is based on the voxel Hounsfield Units [Brinjikji et al., 2016]. A meta-analysis showed that computed tomography angiography had the highest specificity (95%) when assessing >70% stenoses but lowest specificity (63%) for evaluating 50-69%

category compared to other imaging modalities (Figure1.12) [Wardlaw et al., 2006a].

Morphological assessment

Computed tomography angiography can delineate a heterogeneous, calcified, ulcerated atheroma and can identify intra-plaque haemorrhage, lipid core and intra-luminal thrombus [Oliver et al., 1999; Thapar et al., 2013; Eesa et al., 2010]. Hounsfield units are used to define the density of individual plaque components. However, the Hounsfield Units cut-off attenuation values often overlap between morphological features and different ranges have been described in the literature. Intraplaque haemorrhage can be detected with sensitivity approaching 100% and specificity between 64%-70% with reported Hounsfield Units values from -17 to 31 [Walker et al., 2002]. However, it is impossible to reliably differentiate between acute intraplaque haemorrhage and intra-luminal thrombus because computed tomography angiography is limited by poor soft tissue contrast [Syed et al., 2019]. Lipid core is detected at as a hypodense area with Hounsfield units ranging from 25 to 32 [Wintermark et al., 2008]. Although others assigned 17-70 Hounsfield units density values [Lavra et al., 2017] or presented a simplistic description of a *soft plaque* with Hounsfield units <50 [Cronenwett et al., 2014]. Although there is some evidence to support computed tomography angiography use in detection of lipid core robust research data are lacking.

Identification of both intraplaque haemorrhage and lipid core on computed tomography angiography showed good correlation with histological examinations [Huibers et al., 2015]. Thickness of fibrous cap can be assessed, and fissured fibrous cap has been associated with neurovascular symptoms [Saba et al., 2009]. However, published data lacked histological validation. In comparison, ulceration is identified as an intimal defect with contrast presence within the plaque. Detection of ulceration, when compared with histology, has been reported with sensitivity between 60-94% and specificity ranging from 70% to 99% [Huibers et al., 2015]. Finally, computed tomography angiography

is the best imaging modality in the analysis of plaque calcification which is recognised as high density areas (> 120 Hounsfield units) within the plaque. Yet again, one must remember that intraluminal constrast agent can overlay calcification, whilst heavy calcification can produce artefact that limits overall image interpretation.

ADDITIONAL COMUPTED TOMOGRAPHY ANGIOGRAPHY IMAGING

Arterial Wall Thickness and Plaque Volume

There are no reports of carotid arterieal wall assessment using computed tomography angiography except for one study that found a good agreement of the imaging technique with measurements obtained by Doppler ultrasound [Degnan et al., 2012]. The same report demonstrated the ability of computed tomography angiography ability to perform volumetric plaque assessment with a difference between ipsilateral and contralateral carotid arteries [Degnan et al., 2012]. This reflects the limitations and risks associated with this imaging modality described below. Evaluation of treatment response with this imaging technique seems very unlikely given the risks related to cumulative radiation exposure.

Future Directions

In view of the above limitations, one way to advance the role of computed tomography angiography in detailed plaque assessment is the removal of bone and calcification pixels [Huibers et al., 2015]. However, the process is time consuming, and perhaps automated methods will be able to move this area of research forward. There are also suggestions for using 3-dimensional geometry of the plaque to investigate the impact of shear stress on plaque progression [Huibers et al., 2015]. However, research data are sparse, and these ideas have not found any clinical relevance.

Limitations

Two factors primarily restrict computed tomography angiography. First, plaque segmentation is one-dimensional (based purely on photon attenuation), and

there is a significant overlap between Hounsfield Units values which limit soft tissue contrast differentiation. Second, as already eluded above, morphological assessment is complicated by blooming artefact from dense calcification that often precludes any form of plaque analysis. This restricts morphological evaluation in routine work. Furthermore, the utility of computed tomography angiography is diminished by radiation exposure and iodinated contrast administration.

Table 1.1: Imaging modalities with their inherent advantages and disadvantages.

Imaging modality	Advantages	Disadvantages
ULTRASOUND	▪ No radiation, available, low cost ▪ Tolerated by patients ▪ Reliable quantification of severe stenosis ▪ Ulcer identification	▪ Operator dependent, inter-observer variability ▪ Less accurate assessment of moderate stenosis ▪ Poor differentiation between intraplaque haemorrhage and necrotic lipid core
TCD	▪ No radiation, portable, repeatable ▪ Tolerated by patients ▪ Real-life microembolic signals detection	▪ Time consuming ▪ Requires expertise ▪ Absent temporal window
MRA	▪ No radiation ▪ High spatial and contrast resolution ▪ Excellent at measurement of severe stenosis ▪ Detailed plaque morphology	▪ Limited availability, costly, long acquisition time, exclusion of metal implants ▪ Not tolerated by all patients ▪ Potential gadolinium related toxicity ▪ Less accurate assessment of moderate stenosis
CTA	▪ Widely available, rapid cross-sectional assessment ▪ High acceptability by patients ▪ High specificity when assessing severe stenosis ▪ Best modality in analysis of plaque calcification	▪ Radiation, iodine contrast related complications, beam hardening artefact from dense calcification ▪ Low specificity for evaluation of moderate stenosis ▪ Inability to differentiate between high-risk plaque features due to poor soft tissue contrast and overlap in Hounsfield Units

TCD: Transcranial Doppler; MRA: Magnetic Resonance Angiography; CTA: Computed Tomography Angiography.

1.7.4 MOLECULAR IMAGING

Although anatomical imaging based on a simple measure of carotid artery stenosis alone has been the mainstay of clinical neurovascular syndrome management, such an approach limits accurate identification of those with symptomatic but non-stenotic atheroma who could potentially benefit from stroke preventative vascular intervention. Therefore, new strategies are needed that will facilitate accurate plaque assessment with subsequent stroke risk prediction, improved clinical management and monitoring of treatment effects. Molecular imaging techniques with various radiotracers offer new insights into the biology of atherosclerotic plaques across different cardiovascular regions including carotid, aortic, coronary and peripheral arteries. Successful molecular imaging requires a specific *probe* (radiotracer) that can bind to a biological *target* in the form of a particular cell or a pathophysiological pathway. However, due to the complexity of atherosclerotic processes, a molecular tracer that binds to a pre-defined cell, can identify more than one pathobiological process impeding precise identification and localisation of disease activity. For example, macrophages that accumulate at sites of inflammation can be targeted by various molecular probes as they are also involved in different pathological processes such as microcalcification and neo-angiogenesis. Therefore, radiotracers that selectively target specific pathophysiological corridors rather than cells may define premature and evolving disease states with greater precision including identifying culprit carotid plaques.

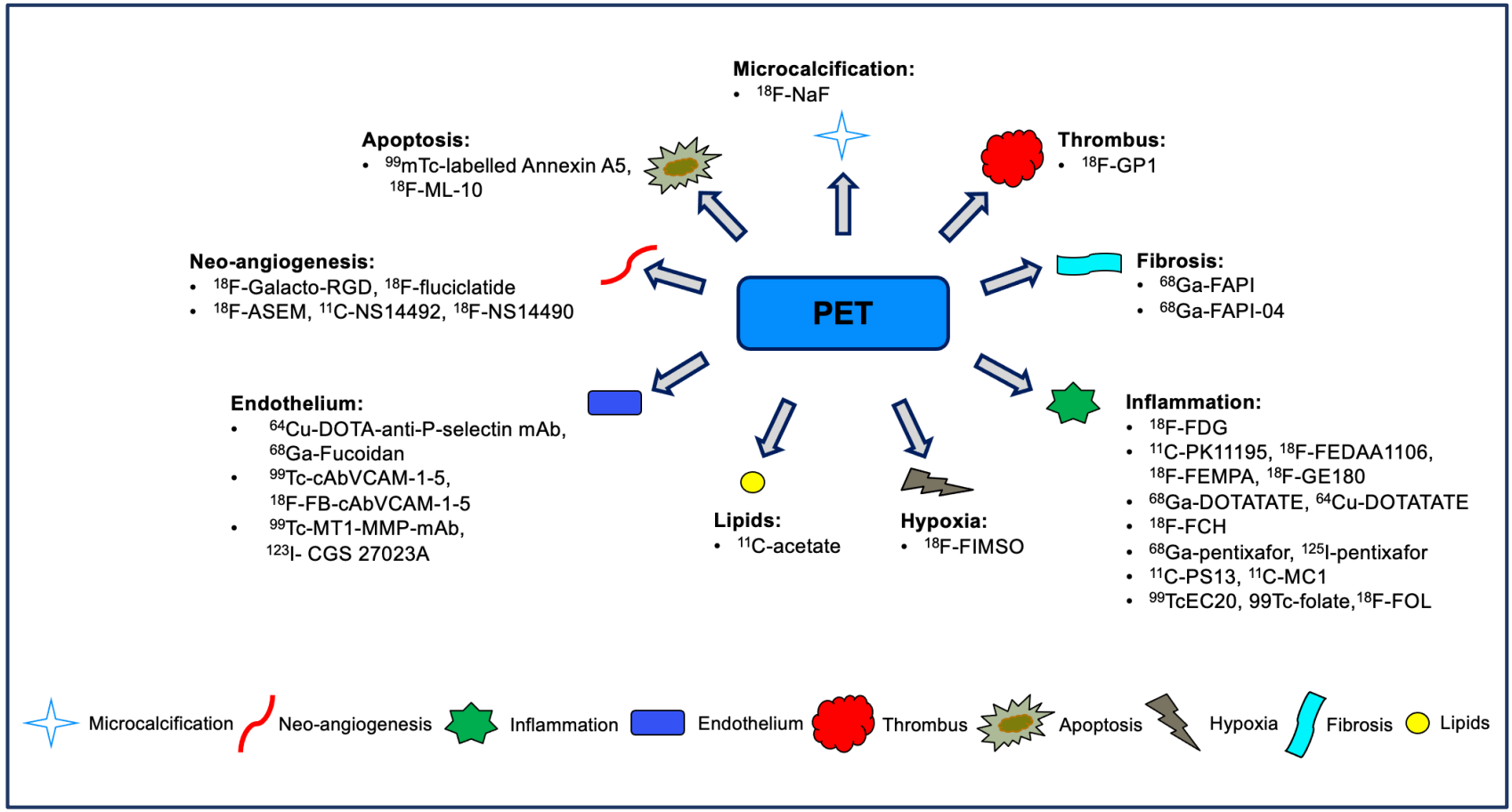
POSITRON EMISSION TOMOGRAPHY

A whole array of positron emission tomography (PET) tracers can target different atherosclerosis features that predispose to plaque rupture including inflammation, microcalcification, intraplaque haemorrhage, lipids deposition, neo-angiogenesis, fibrosis, and hypoxia. Although PET can localise radiotracer with very high sensitivity even in small areas of disease activity, it is disadvantaged by a low spatial resolution of 4-5mm. Therefore, PET alone is unable to provide detailed anatomical information that could facilitate robust

plaque assessment. Traditionally, PET has been combined with CT as PET-CT, but recently, novel hybrid systems combining PET and MRI, have become available. These systems have been developed with the specific intention of combining PET with the generic advantages that MRI holds over CT; principally improved soft-tissue contrast, lack of radiation exposure or requirement for iodine-based media, and the potential for full-motion correction of PET data. MRI offers multiple other key advantages over CT when explicitly considering the carotid arteries that have been already described above.

Among many available tracers (Figure 1.14), two have shown a particular promise in the carotid atherosclerosis assessment, Fluorine 18–labelled sodium fluoride and ^{18}F-fluorodeoxyglucose. Many other radiotracers primarily hold the experimental status due to the limited data from pre-clinical and clinical studies that are often small and publish conflicting results. Nevertheless, these novel radiotracers continuously expand and refine technological PET discoveries allowing for a more holistic *in vivo* carotid plaque assessment.

Figure 1.14: Molecular targets of PET tracers in atherosclerosis.



High-risk plaque features associated with culprit carotid plaque (microcalcification, necrotic lipid core, intraplaque haemorrhage, neo-angiogenesis, and thrombus) resulting from hypoxia, cell death and inflammation driven stimuli.

MINERALISATION

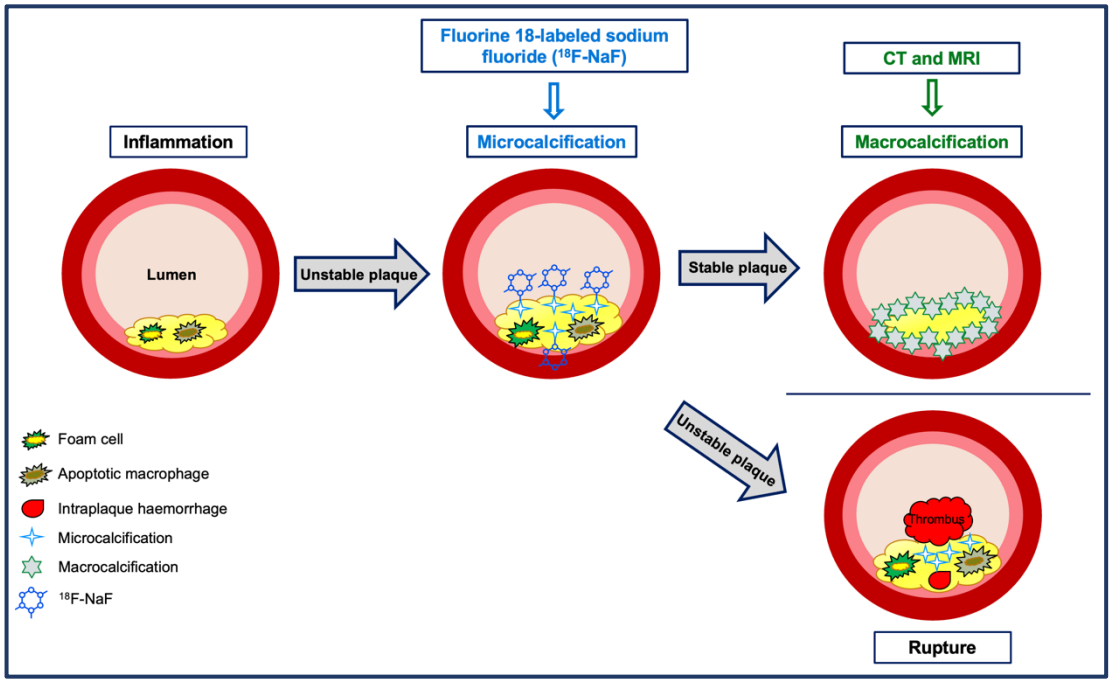
Microcalcification:

- *18–labelled sodium fluoride*

The PET radiotracer fluorine 18-labelled sodium fluoride (^{18}F-NaF) was first developed for the assessment of bone metabolism [Kairemo et al., 2020]. Subsequently, an incidental finding of ^{18}F-NaF arterial uptake on cancer-staging PET scans expanded its use into the field of atherosclerotic calcification [Evans et al., 2017]. This has fundamentally reshaped our views on the pathophysiology of intimal calcium dystrophy that consists of two principal phases. In phase one (initiation), macrophages and other inflammatory cells secrete numerous pro-osteogenic cytokines including tumour necrosis factor-α, insulin-growth like factor-1, transforming growth factor-β and interleukins. The osteoblast-like cells derived from the smooth muscle cells [Rashdan et al., 2020] and macrophages release extracellular vesicles of hydroxyapatite that coalesce into organised areas of microcalcification. This is a direct response to unresolved chronic inflammation within plaque attempting to contain it. The second phase culminates in forming the dense and confluent layers of macrocalcium deposits that isolate the necrotic plaque area, thus preventing plaque rupture with its thrombo-embolic consequences. However, detection of this early vascular calcification is difficult because we can only monitor the disease's late stages when calcium deposition has become large enough (macrocalcification, diameter >50 μm) to be detected by either computed tomography or magnetic resonance imaging. ^{18}F-NaF can identify early microcalcification (binds to exposed and high surface area of hydroxyapatite crystals) well beyond the resolution of the traditional cross-sectional imaging modalities (<50 μm) (Figure 1.15). Thereby radiotracer localises to the areas of biologically active plaque (*unstable* plaque) rather than merely to the macrocalcification sites (*stable* plaque) where the process of mineralisation has resolved. ^{18}F-NaF uptake has been found to localise to plaque rupture that showed greater immunostaining for macrophage infiltration markers and cell death [Irkle et al., 2015]. Moreover, ^{18}F-NaF PET-CT was able to identify high-risk ruptured carotid plaques in

patients with carotid stenosis and recent cerebrovascular events [Vesey et al., 2017]. Therefore, ^{18}F-NaF identification of high-risk atherosclerotic plaques could facilitate a specific evaluation of a vascular lesion with the potential prediction of future neurovascular events.

Figure 1.15: Atherosclerotic sequence of inflammation, microcalcification and macrocalcification.



High-risk plaque features including microcalcification lead to plaque rupture, while macrocalcification confers plaque stability and reduced risk of rupture.

TRACERS TARGETTING INFLAMMATION

Macrophages:

- *^{18}F-Fluorodeoxyglucose*

^{18}F-Fluorodeoxyglucose (^{18}F-FDG) is the most widely used radiotracer for assessment of plaque inflammation. This glucose analogue actively competes with glucose to enter the cell, and once inside, it becomes trapped without undergoing any further metabolism [Andrews et al., 2018]. Hence, the metabolically active tissue by taking up the ^{18}F-FDG is reflecting glycolytic cellular activity specifically within macrophages [Dweck et al., 2016]. Over the last decade, the radiotracer demonstrated not only the ability to detect culprit

carotid plaques, but increased uptake has been found to correlate with high-risk plaques features confirmed on histology [Rudd et al., 2002; Howard et al., 2015]. Furthermore, increased ^{18}F-FDG uptake in symptomatic carotid plaques was associated with recurrent ischaemic stroke independently of the degree of carotid artery stenosis [Marnane et al., 2012]. However, some studies have failed to show the discriminatory role of ^{18}F-FDG in distinguishing between symptomatic versus asymptomatic carotid lesions [Degnan et al., 2012; Vesey et al., 2017]. This reflects the radiotracer's several drawbacks, including non-specific uptake by other actively metabolising cells that hinder identification of the high-risk plaques due to spill-over [Evans et al., 2017]. Moreover, despite promising results found with attenuation of atherosclerotic inflammation evidenced by decreased ^{18}F-FDG uptake following statin therapy, their anti-inflammatory effect can mitigate the uptake of radiotracer [Tahara et al., 2006; Tawakol et al., 2013]. On the other hand, precisely because of that attenuating effect,^{18}F-FDG is a useful metabolic endpoint in trials testing new pharmacological agents such as Cholesteryl Ester Transfer Protein inhibitors, Lipoprotein-Associated Phospholipase A2 and Mitogen Activated Protein Kinase (P38); all these novel lipid-lowering medications failed to reduce ^{18}F-FDG uptake including cardiovascular events [Andrews et al., 2018]. Finally, ^{18}F-FDG uptake has been correlated with cellular hypoxia making it difficult to confidently detect a true source of uptake in atherosclerotic plaques [MacAskill et al., 2019]. Therefore, the ambiguous role of ^{18}F-FDG due to the above confounding factors prompted the development of additional tracers targeting inflammation.

18 kDa translocator protein:

- *^{11}C-PK11195*
- *^{18}F-FEDAA1106*
- *^{18}F-FEMPA*
- *^{18}F-GE180*

The 18 kDa translocator protein (TSPO) is also known as the peripheral benzodiazepine receptor that is a targeted by more than 80 radiotracers

[MacAskill et al., 2019]. Among them, 11C-PK11195, 18F-FEDAA1106, 18F-FEMPA and ^{18}F-GE180 have provided the most useful research data. Macrophages highly express the TSPO, therefore, TSPO can be used as a biomarker for localised inflammation [MacAskill et al., 2019]. The ^{11}C-PK11195 uptake showed co-localisation with macrophages on histology, and more importantly, the uptake of radiotracer has been increased in symptomatic carotid plaques [Gaemperli et al., 2012; Bird et al., 2010]. However, pre-clinical atherosclerotic models failed to demonstrate any difference in the uptake between atheromatous and healthy vessel wall [Laitinen et al., 2008]. Similar results were obtained by ^{18}F-FEMPA and ^{18}F-GE180 radiotracers. Although both demonstrated increased macrophage binding, they have failed to discriminate between atherosclerotic and disease-free arteries [MacAskill et al., 2019].

An upgrade of ^{11}C-PK11195, the ^{18}F-FEDAA1106 in animal studies revealed significantly higher uptake in the induced atherosclerosis in carotid artery lesions compared to normal arteries [Cuhlmann et al., 2014]. The uptake of ^{18}F-FEDAA1106 was also more specific than the uptake of ^{18}F-FDG, thus consistent with inflammation [MacAskill et al., 2019]. However, two main barriers prevent the wider application of the above radiotracers. First, the TSPO genetic polymorphism significantly affects the binding affinity of TSPO [MacAskill et al., 2019]. Therefore, subsequent developments need to overcome the issues surrounding the binding heterogeneity. Second, the radiotracers have short half-life time of approximately 20 minutes; thus, their production requires an on-site cyclotron precluding a remote delivery [Andrews et al., 2018].

Somatostatin receptor type 2:

- *^{68}Ga-DOTATATE*
- *^{64}Cu-DOTATATE*

The Gallium 68 and Copper 64 labelled DOTATATE specifically bind to somatostatin receptors type 2 that are up regulated in activated macrophages. Like many inflammatory radiotracers, both ^{68}Ga-DOTATATE and ^{64}Cu-

DOTATATE originated from the field of neuroendocrine tumours imaging [Li et al., 2012; Kayani et al., 2009; Pfeifer et al., 2012]. Subsequently, ^{68}Ga-DOTATATE demonstrated superior macrophages specificity over the ^{18}F-FDG activity [Li et al., 2012; Kayani et al., 2009]. These findings were particularly important in coronary circulation where ^{18}F-FDG myocardial uptake often precludes vessels imaging analysis. A clinical study demonstrated ^{68}Ga-DOTATATE ability to differentiate symptomatic from asymptomatic carotid plaques with improved focal signal-to-noise ratio compared to ^{18}F-FDG [Tarkin et al., 2017]. On histological examination of carotid plaques, the radiotracer uptake correlated with CD68+ macrophages and revealed specific binding to M1-macrophages (pro-inflammatory) [Tarkin et al., 2017]. In contrast, other researchers did not demonstrate higher ^{68}Ga-DOTATATE activity in symptomatic carotid plaques compared to asymptomatic contralateral carotid lesions [Wan et al., 2017]. Furthermore, except for a variable CD68+ staining, histological validation failed to report any somatostatin receptors type 2 expression in all excised carotid specimens [Wan et al., 2017]. However, the study's small size (n=20) raises the possibility of a false negative result that could potentially be explained by somatostatin receptors expression variability. Of note, atherosclerotic popliteal arteries express somatostatin receptors type 1, -2 and -4 [Curtis et al., 2000].

An alternative radiotracer, ^{64}Cu-DOTATATE is characterised by the longer half-life (greater than 12 hours) with a shorter positron range, hence providing an improved spatial resolution which is important in imaging small carotid tissue [Pedersen et al., 2015]. An increased uptake was reported in symptomatic carotid arteries prior to carotid endarterectomy versus asymptomatic contralateral carotid vessel [Pedersen et al., 2015]. The early radiotracer uptake was associated with a biomarker of macrophage accumulation (CD68+) and with their activation (CD163+). The CD163+ gene expression is up-regulated in M2-macrophages found in the areas of intraplaque haemorrhage [Boyle et al., 2009]. M2-macrophages have anti-inflammatory properties; they clear haemoglobin-haptoglobin complexes that

reduce oxidative stress [Paoli et al., 2014]. However, delayed imaging demonstrated reduced standardised uptake values (SUVs) of ^{64}Cu-DOTATATE and diminished co-localisation with macrophage markers (CD68+ and CD163+). This implies that radiotracer's binding to the somatostatin receptor subtype-2 declines over time; hence researchers advocate early imaging at 80 minutes post-injection. In summary, both radiotracers represent a promising tool in atheroma imaging that does not require a cyclotron-based production, significantly reducing the scanning costs. Additional long shelf-life of ^{64}Cu-DOTATATE of 24 hours make it particularly attractive molecular probe for large prospective clinical studies.

Choline receptor:

- *^{18}F-Fluorocholine*

^{18}F-labelled fluorocholine (^{18}F-FCH) is another potential molecular marker of inflammation driven by the macrophages. Choline is a precursor of phosphatidylcholine (lecithin) which is a major phospholipid component of the cellular membranes [Vöö et al., 2018]. Increased ^{18}F-FCH uptake has been found in cancer cells and proliferating macrophages [Andrews et al., 2018]. Promising data have been shown in the murine atherosclerotic plaques model where enhanced uptake of ^{18}F-FCH correlated better with macrophage accumulation than ^{18}F-FDG [Matter et al., 2006; Andrews et al., 2018]. More importantly, an albeit small (n=10) prospective study of stroke patients who underwent carotid endarterectomy revealed that ^{18}F-FCH discriminated between symptomatic and asymptomatic carotid lesions [Vöö et al., 2018]. Furthermore, histological validation demonstrated that the uptake of radiotracer correlated with plaque CD68+ macrophages in the excised carotid specimens [Vöö et al., 2018]. Thus, ^{18}F-FCH is potentially a viable alternative in the imaging of atherosclerosis. However, more comprehensive and prospective clinical data is required to assess ^{18}F-FCH suitability in the atherosclerotic plaque imaging.

Chemokine receptor 4:

- *^{68}Ga-pentixafor*
- *^{125}I-pentixafor*

The chemokine receptors 4 ($CXCR_4$) expressed on the macrophages, endothelial, smooth muscle cells play crucial role in chemotactic recruitment of these cells to inflamed or injured areas via its chemokine ligand 12 ($CXCL_{12}$) [Derlin et al., 2018]. Stimulation of macrophages via $CXCR_4$ led to increased formation of foam cells, while in endothelial cells, it boosted recruitment of progenitor endothelial cells to the plaque [Vorst et al., 2015]. In contrast, stimulated smooth muscle cells exert a beneficial effect by producing a thicker fibrous cap [Yao et al., 2012; MacAskill et al., 2019]. Therefore, the $CXCR_4$ - $CXCL_{12}$ axis may be a useful target for molecular imaging of atherogenic pathways. Recently, two specific and highly selective radiotracers that with nanomolar affinity acting as $CXCR_4$ ligands have been developed to investigate processes that contribute to atherosclerotic plaque evolution: ^{68}Ga-pentixafor and ^{125}I-pentixafor. A pre-clinical study demonstrated that ^{68}Ga-pentixafor uptake was increased in atherosclerosis induced vessels (carotid and aorta) compared with healthy controls [Hyafil et al., 2017]. In comparison, ^{125}I-pentixafor binding co-localised with macrophage rich (CD68+) regions in the plaques and $CXCR_4$ expression on corresponding cryosections [Hyafil et al., 2017]. Of note, one retrospective clinical study revealed that ^{68}Ga-pentixafor uptake was increased in patients who have recently suffered from myocardial infarction and uptake correlated with cardiovascular risk factors [Derlin et al., 2018]. However, the precise role of ^{68}Ga-pentixafor and ^{125}I-pentixafor radiotracers in the identification of cell- specific atherogenesis and potential therapeutic opportunities is yet to be established.

Cyclooxygenase 1 and 2:

- *^{11}C-PS13*
- *^{11}C-MC1*

Cyclooxygenase is the rate limiting enzyme responsible for converting arachidonic acid into prostanoids that are implicated in a variety of

pathophysiological processes, including inflammation [MacAskill et al., 2019]. The two isoforms have different functional roles, cyclooxygenase-1 (COX-1) is primarily involved in homeostasis, whilst cyclooxygenase-2 (COX-2) is linked with pro-atherogenic cellular inflammatory players. COX-2 leads to the production of Prostaglandin E2 that causes up-regulation of MMP production by the monocytes, which subsequently cause degradation of fibrous cap [Cuccurullo et al., 2007; Baroncini et al., 2011]. Up to date, only two radioligands have been tested in rhesus monkeys to assess COX-1 and COX-2. The ^{11}C-PS13 which targets COX-1 demonstrated generalised uptake in most organs, whereas ^{11}C-MC1 did not specifically bind to any viscera in healthy controls [Kim et al., 2018b]. However, available research data is sparse and requires further exploration to establish its utility in the field of atherosclerosis.

Folate receptor-β:

- *^{99}TcEC20*
- *^{99}Tc-folate*
- *^{18}F-FOL*

Folate receptor-β is a surface receptor for the folic acid that is selectively expressed by activated macrophages [Paulos et al., 2006]. At present, folate imaging has been carried out primarily in rheumatoid arthritis and like many other inflammatory radiotracers was also first developed for oncology use. Therefore, limited pre-clinical and *ex vivo* human tissue data exists on its use in atherosclerosis. A murine model of aortic atherosclerosis imaging with single-photon emission computerised tomography (SPECT) revealed increased uptake of folate-targeted chelate (^{99}TcEC20) in plaques of mice on a high-fat diet [Ayala-López et al., 2010]. The radiotracer ^{99}TcEC20 uptake co-localised with the macrophage accumulation on histological tissue sections. Macrophage selective ^{99}TcEC20 uptake was confirmed by treatment with clodronate liposome that depleted macrophages and resulted in reduced radiotracer uptake in plaque lesions [Ayala-López et al., 2010]. In carotid plaques following endarterectomy imaging with SPECT showed that

radiotracer ^{99}Tc-folate was able to discriminate between M1 and M2-macrophages and was found with increased binding in areas rich in M2-macrophages [Jager et al., 2014]. Finally, ^{18}F-FOL had increased uptake in excised carotid plaques in patients who had recently neurovascular symptoms and correlated with macrophage density in carotid plaques [Silvola et al., 2018]. In the same study increased accumulation of ^{18}F-FOL was revealed in the atherosclerotic murine and rabbit models compared with healthy controls. Furthermore, the ^{18}F-FOL was compared with ^{18}F-FDG and demonstrated lower myocardial uptake [Silvola et al., 2018]. Folate receptor-β is a promising novel tool for imaging atherosclerotic inflammation. But the next level of evidence needs to come from the clinical *in vivo* data.

Fibroblast activation protein inhibitor:

- *^{68}Ga-FAPI*
- *^{68}Ga-FAPI-04*

Fibroblasts are mesenchymal cells principally located within the *adventitial* arterial layer [Xu et al., 2007] that regulate inflammation, matrix with collagen production, and atherosclerotic plaque structural integrity [Evrard et al., 2016; Wu et al., 2021]. Their cellular origins within the complex atherosclerotic lesions are not fully understood, however, fibroblasts proliferation followed by differentiation into myofibroblasts with subsequent migration to the *intima* have been previously described [Xu et al., 2007]. Recent scientific evidence points towards an *endothelial-to-mesenchymal* cellular transition resulting in the derived fibroblast-like cells with co-expressed endothelial and fibroblast specific proteins that correlate with unstable plaque phenotype [Evrard et al., 2016]. The process of fibrotic tissue deposition by the fibroblasts is frequently coined as remodelling which reflects scarring of injured tissue that when excessive, contributes to the myriad of cardiovascular disorders including vascular calcification, myocardial infraction, transplant arteriopathy, vascular malformations and pulmonary hypertension [Evrard et al., 2016]. Activated fibroblasts with upregulated expression of fibroblasts activation protein-α (transmembrane serine protease) are common at the sites of intimal

atherosclerotic plaques [Iking et al., 2021]. The visualisation of activated fibroblasts requires the use of fibroblast activation protein inhibitors (FAPI) because this allows to mitigate slow clearance of radiolabelled antibodies resulting in high background signal with limited detection of small lesions which is particularly important in atherosclerotic plaques [Iking et al., 2021]. Two PET-CT studies evaluated ^{68}Ga-FAPI-04 radiotracer in the Ig-G4 autoimmune disorder characterised by a diffuse inflammatory reaction consisting of lymphoplasmacytic infiltrates and fibrosis that can affect any organ including aorta. One of these studies demonstrated higher fibroblasts ^{68}Ga-FAPI-04 uptake than ^{18}F-FDG and greater detection of organ involvement in half of the examined participants (n=13) [Luo et al., 2020]. Whereas the other study provided histological validation for the discriminatory role of ^{68}Ga-FAPI-04 in detecting fibrotic activity; ^{18}F-FDG uptake co-localised with cellular infiltration of IgG4^{+} whilst ^{68}Ga-FAPI-04 signal correlated with activated fibroblasts [Schmidkonz et al., 2020]. Furthermore, anti-inflammatory treatment reduced ^{18}F-FDG activity to a greater degree than ^{68}Ga-FAPI-04 implying that more customised anti-fibrotic treatment may be required to address fibrotic disease activity rather than traditional broad-spectrum anti-inflammatory medications [Schmidkonz et al., 2020]. Pre-clinical micro-PET-CT models have shown promising results in the carotid atherosclerotic plaques detection (murine model) by ^{68}Ga-FAPI [Wang et al., 2021] and ^{68}Ga-FAPI-04 accumulation within the infarcted myocardium (rats) that correlated with immunofluorescent staining of FAPI-positive myofibroblasts [Varasteh et al., 2019]. Finally, ^{68}Ga-FAPI-04 PET-CT imaging of human carotid walls demonstrated greater FAPI expression within thin fibrous caps than within thick fibrous caps indicating association of activated fibroblasts with complex atherosclerotic plaques [Wu et al., 2021]. Although FAPI directed PET imaging represents diagnostic and therapeutic potential, current data is limited to pre-clinical studies and clinical imaging of broad range of non-cardiovascular inflammatory conditions including variety of cancer-associated fibroblasts. Therefore, larger studies with histopathological correlation are needed to validate these preliminary findings.

ENDOTHELIAL ACTIVATION

Anti-P-selectin monoclonal antibody

- *^{64}Cu-DOTA-anti-P-selectin mAb*
- *^{68}Ga-Fucoidan*

Atherosclerotic inflammation is characterised by extensive infiltration of the arterial wall by recruited monocytes and lymphocytes. Several adhesion molecules have been implicated in the migration of immune cells such as the family of selectins and VCAM-1. Additionally, various proteases (cathepsins, serine proteases) and in particular MMPs expressed by macrophages, T-lymphocytes, mast cells and smooth muscle cells are crucial in fragmentation of extracellular matrix [Reimann et al., 2017]. All these molecules represent potentially novel imaging targets of biologically active plaques. Among the members of selectin family (E-expressed by leucocytes and L-expressed by activated endothelial cells), P-selectin that is stored by the endothelial cells is pivotal in recruiting monocytes with leucocytes to the site of injury and is highly expressed on activated endothelium and platelets [Nakamura et al., 2013; Li et al., 2014].

Anti-P-selectin monoclonal antibody radiolabelled with ^{64}Cu via DOTA (^{64}Cu-DOTA-anti-P-selectin mAb) in a murine model of aortic atherosclerosis revealed increased uptake of radiotracer predominantly in the aortic root on PET-CT [Nakamura et al., 2013]. While scanty uptake of ^{64}Cu-DOTA-anti-P-selectin mAb was detected in the control group. These findings were validated by *ex vivo* autoradiography which demonstrated that uptake of radiotracer co-localised with corresponding atherosclerotic regions identified by immunohistochemistry [Nakamura et al., 2013].

^{68}Ga-Fucoidan is a conjugate of Fucoidan which is a polysaccharidic ligand for P-selectin and gallium. ^{68}Ga-Fucoidan showed increased uptake in the atherosclerotic murine aortic model and was able to identify high-risk atherosclerotic plaques [Li et al., 2014]. An increased tracer accumulation in the aorta correlated with increased P-selectin expression, high-density

macrophage accumulation on histological examination and high-risk plaque morphology on *ex vivo* MRI [Li et al., 2014].

Anti-VCAM-1 nanobody:

- *^{99}Tc-cAbVCAM-1-5*
- *^{18}F-FB-cAbVCAM-1-5*

VCAM-1 is another molecular target for radiolabelled molecules that is present on the endothelial surface of luminal endothelium of neo-vessels, macrophages and smooth muscle cells [Broisat et al., 2012]. VCAM-1 can be detected using nanobodies which are the smallest antigen-binding fragments derived from the heavy-chain-only antibodies naturally occurring in camelids [Bala et al., 2016]. They have a nanomolar affinity, high specificity and fast blood clearance. Pre-clinical SPECT study demonstrated increased uptake of ^{99}Tc-labelled anti-VCAM-1 nanobody cAbVCAM-1-5 (^{99}Tc-cAbVCAM-1-5) in the atherosclerotic aortic arch (murine model) which correlated with VCAM-1 positive lesions on immunohistochemistry [Broisat et al., 2012]. At the same time, no uptake was seen in the control aortic vessels. However, the tracer was also taken up by lymphoid tissue (bone marrow, spleen, thymus, lymph nodes) in both mice groups.

Another radiotracer targeting VCAM-1 is anti-VCAM-1 nanobody based on the lead compound cAbVCAM-1-5 that is radiolabelled with ^{18}F-Fluorine (^{18}F-FB-cAbVCAM-1-5). Similarly, to the previous pre-clinical studies, increased binding of ^{18}F-FB-cAbVCAM-1-5 was detected in the ascending aorta and aortic arch compared with aortic control vessels [Bala et al., 2016]. This was also confirmed on *ex vivo* analyses.

Monoclonal Antibodies MTP-1-MMP and MMP inhibitor:

- *^{99}Tc-MT1-MMP-mAb*
- *^{123}I- CGS 27023A*

A dynamic balance between synthesis and degradation of collagen and elastin fibres results from a complex interplay between MMP and their endogenous

inhibitors. Monoclonal antibodies (mAb) specific for membrane type 1 (MTP-1) activate MMP to their active forms and when labelled with ^{99}Tc, yield ^{99}Tc-MT1-MMP-mAb. This radiotracer in a rabbit atherosclerotic model showed an increased uptake of the aortic atheromas compared with the control group, which revealed no marked radiotracer accumulation [Kuge et al., 2010]. ^{99}Tc-MT1-MMP-mAb correlated with plaque regions characterised by high MT1-MMP on histological validation [Kuge et al., 2010].

In contrast, a whole range of agents based on small molecules, peptides, antibodies, nanoparticles with several radioisotopes such as ^{11}C,^{18}F, ^{123}I, ^{125}I, and ^{99}Tc are available for imaging of the MMP inhibitors [Rangasamy et al., 2019]. Most commonly studies modify a generic MMP inhibitor- CGS 27023A by performing radiolabelling with a specifically chosen radioisotope [Schäfers et al., 2004]. Pre-clinical murine carotid atherosclerotic model (high-fat diet combined with ligation of carotid artery) demonstrated increased uptake of ^{123}I-CGS 27023A on *in vivo* scintigraphy with no specific radiotracer signal uptake in the non-ligated carotid vessels [Schäfers et al., 2004]. Immunostaining and *ex vivo* micro-autoradiography confirmed binding of the radiotracer to the plaque regions with high MMP activity. Others reported radiolabelling of the MMP inhibitor with ^{99}Tc. In this rabbit model of aortic atherosclerosis, radiotracer uptake (on SPECT) was increased in aortic lesions and correlated with histologically high expression of macrophages, MMP-2 and MMP-9 [Fujimoto et al., 2008]. However, MMP inhibitors have been so far tested in pre-clinical studies due to problems with toxicity, venous thrombo-embolism and bone marrow suppression [Rangasamy et al., 2019]. Therefore, more selective inhibitors with improved biodistribution and acceptable toxicity are needed.

There are many molecular candidates for cardiovascular related research as potential diagnostic biomarkers. Although pre-clinical data proved its feasibility, clinical translation is lacking. Therefore, future research requires

clinical utility assessment to validate these molecular probes and their role in atherosclerosis.

NEO-ANGIOGENESIS

Integrin αVβ3 receptor:

- *^{18}F-Galacto-RGD*
- *^{18}F-fluciclatide*

Intraplaque neo-angiogenesis creates an environment that makes a carotid plaque susceptible to a rupture. The process is mediated by the proliferating and fragile medial vasa vasorum that lead to extravasation of red blood cells and subsequent intraplaque haemorrhage [Laitinen et al., 2009]. The adhesion surface glycoprotein receptor integrin αVβ3 is a potential marker of angiogenesis and inflammation in atherosclerotic lesions. Integrin αVβ3 is expressed on the surface of a various cells during neo-angiogenesis, regulates the migration of smooth muscle cells and differentiation of macrophages into foam cells [Hoshiga et al., 1995; Antonov et al., 2004]. Two novel radiotracers that bind with high specificity to integrin αVβ3 include ^{18}F-Galacto-RGD and ^{18}F-fluciclatide. A murine model of atherosclerosis showed higher focal biodistribution of ^{18}F-Galacto-RGD in the diseased aorta compared to the normal vessel and co-localised with calcified lesions in the aortic arch seen on computed tomography angiography [Laitinen et al., 2009] However, this pre-clinical model lacked the actual intraplaque neo-angiogenesis. This was demonstrated by *ex vivo* imaging with histological immunostaining which revealed scanty endothelial cells and macrophages consistent with high inflammation sites. While in a small PET-CT study (n=10) of patients with symptomatic carotid artery stenosis before surgery ^{18}F-Galacto-RGD uptake was increased at stenotic areas compared with non-stenotic parts and correlated with integrin αVβ3 but only in half of the participants [Beer et al., 2014]. Whereas in the remaining 5 individuals there was a wide distribution of radiotracer with little or no uptake in stenosed areas. Also, no correlation was found with macrophage and microvessels density [Beer et al., 2014]. Another integrin αVβ3 radiotracer, ^{18}F-fluciclatide that is primarily used in neuro-

oncology and showed a reduction in uptake following treatment before any changes in tumour volume were detected allowing for assessment of the tumour angiogenesis response to the therapy [Battle et al., 2011]. A limited data exists on the role of ^{18}F-fluciclatide in the area of atherosclerosis, although some encouraging results were demonstrated in patients following myocardial infarction. The radiotracer uptake was increased at the site of recent myocardial infarction, potentially acting as a marker of cardiac repair and predicting regions that could recover contractile function [Andrews et al., 2018]. Moreover, in patients following a recent myocardial infarction, uptake of ^{18}F-fluciclatide increased with atherosclerotic aortic plaque burden compared to patients without cardiac adverse events [Jenkins et al., 2019]. In the same study *ex vivo* imaging of carotid plaques showed that radiotracer co-localised to the sites of integrin $\alpha V\beta 3$ receptor expression, endothelial cells at regions of angiogenesis and macrophages adjacent to the necrotic lipid core [Jenkins et al., 2019]. Carotid specimens free of atheroma demonstrated no ^{18}F-fluciclatide uptake with low levels of integrin $\alpha V\beta 3$ receptor expression. Overall, targeting integrin $\alpha V\beta 3$ could help to unravel complex pathways that play a role in the progression of atherosclerosis to control macrophage dependant responses in the arterial wall. However, better pre-clinical models with evidence of neo-angiogenesis are needed before research could expand to the high-risk human lesions.

POTENTIAL NOVEL NEO-ANGIOGENESIS TRACERS

α-7-Nicotinic acetylcholine receptor:

- *^{18}F-ASEM*
- *^{11}C-NS14492*
- *^{18}F-NS14490*

The acetylcholine is an endogenous agonist of the nicotinic acetylcholine receptors that are composed of numerous subunits [Conti-Fine et al., 2000; Lee et al., 2013]. The α-7-nAChR receptor is one subtype and is primarily expressed on neuronal cells, thereby conveniently serving as a molecular target for neuroimaging (neuropsychiatry and oncology). More importantly,

α-7-nAChR is also expressed in non-neuronal tissue including bronchial epithelial cells, skin keratinocytes, macrophages, smooth muscle cells and endothelial cells [Conti-Fine et al., 2000; Heeschen et al., 2002]. This is particularly relevant to the atherogenesis as the α-7-nAChR is involved in the pathway of pathological neo-angiogenesis and therefore plays an active role in proliferation and differentiation of cells [Heeschen et al., 2002]. Furthermore, α-7-nAChR being sensitive to the nicotine, which is a potent stimulus for neovascularisation, mediates tobacco toxicity in the cardiovascular system and may increase a plaque burden [Boswijk et al., 2017]. Similarly, to the integrin αVβ3, the α-7-nAChR up-regulates M2-macrophages, thus contributes to the formation of foam cells [MacAskill et al., 2019; Lee et al., 2013]. However, current data is limited to pre-clinical studies that have assessed the role of α-7-nAChR in atherosclerosis models again without the actual neovascularisation. In a murine model varenicline which is a full agonist of α-7-nAChR enhanced formation of aortic atherosclerotic plaques through the up-regulated expression of α-7-nAChR in macrophages [Kanaoka et al., 2017]. However, the potential role of α-7-nAChR as a marker of plaque vulnerability has not been investigated, and present data is limited to few studies examining the role of radiotracers in neuronal tissue that confirmed the feasibility of imaging quantification of α-7-nAChR. Two studies that evaluated ^{18}F-ASEM in human brains with the animal data include, imaging of human along with mouse [Wong et al., 2014] and humans with non-human primates [Hillmer et al., 2017]. Other tracers that have been suggested as potential new means of imaging were assessed in porcine brains. ^{11}C-NS14492 was assessed in porcine brain structures (frontal cortex) [Magnussen et al., 2015]. ^{18}F-NS14490 was used in mice and porcine brain tissue. ^{18}F-NS14490 was detected in the carotid arteries and circle of Willis in pigs suggesting expression of α-7-nAChR receptors on endothelial and smooth muscle cells [Rötering et al., 2013; Rötering et al., 2014]. However, further research is needed before its application in the imaging of human circulation.

INTRAPLAQUE HAEMORRHAGE AND THROMBUS

Glycoprotein IIb/IIIa:

- *^{18}F-GP1*

The glycoprotein IIb/IIIa (GPIIb/IIIa) receptor is highly expressed on activated platelets and is crucial for their adherence and aggregation [MacAskill et al., 2019]. The ^{18}F-GP1 is a radiolabelled ligand that specifically binds with high affinity to the GPIIb/IIIa receptor, making it a promising target for imaging platelet-rich thrombi. Pre-clinical murine model of aortic plaque formation quantified activated platelets on the atherosclerotic endothelium non-invasively using ultrasound molecular imaging with microbubbles targeted to GPIIb/IIIa receptor [Guo et al., 2015]. A phase 1 study demonstrated ^{18}F-GP1 high detection rate of acute arterial thrombosis foci across different vascular beds in 10 patients who underwent a whole-body PET-CT [Chae et al., 2019]. Similarly, ^{18}F-GP1 successfully identified all thromboembolic lesions in patients with recently formed deep venous thrombi (n=10) and pulmonary embolism (n=10) [Kim et al., 2019]. More importantly, binding was not altered by anticoagulation therapy (aspirin and heparin). However, inhibitors of glycoprotein IIb/IIIa could potentially alter radiotracer binding to activated platelets, hence limit the clinical use of this new tracer. Nevertheless, so far, the radiotracer performed favourably regarding its metabolism, pharmacokinetics and dosimetry profile [Chae et al., 2019]. It's binding in a stable and specific manner to in vivo arterial and venous human thrombi offers significant potential in the evaluation of atherosclerotic disease and beyond the arterial tree.

The process of haemostasis is complex. It involves the expression of activated membrane proteins and coagulation factors dynamically changing throughout. Moreover, platelet expression of GP IIb/IIIa falls with the maturation of a thrombus, hence it is a potential pharmacological target for anti-thrombotic therapies. An improved understanding of how various clinical presentations relate to platelet activation could alter the decisions when choosing appropriate anti-thrombotic regimes.

HYPOXIA

Hypoxic cells:

- *^{18}F-FIMSO*
- *^{18}F-HX4*

The inability of macrophages to engulf apoptotic cellular debris with oxidised lipids leads to the formation of necrotic lipid core which stimulates further plaque growth that becomes progressively depleted in oxygen. Ongoing inflammation and neo-angiogenesis aiming to alleviate hypoxia paradoxically worsen these conditions. In effect, plaque necrosis and rupture occur. The ^{18}F-fluoromisonidazole (^{18}F-FIMSO) is a novel radiotracer that becomes trapped within the hypoxic cells. Pre-clinical study of atherosclerosis model in a rabbit demonstrated increased ^{18}F-FIMSO uptake in aortic atheroma compared to the non-atherosclerotic controls [Mateo et al., 2018]. The radiotracer uptake co-localised to hypoxia regions characterised by macrophage rich areas within the atheromatous core detected on immunohistochemistry [Mateo et al., 2018]. A clinical study in patients with recent TIA and stroke revealed increased ^{18}F-FIMSO uptake in clinically culprit carotid plaques that correlated with ^{18}F-FDG activity [Joshi et al., 2017]. Radiotracer uptake was only minimally lower in the contralateral carotid vessel. These findings imply that hypoxia is interlinked with inflammation and a hypoxia inducible factor - 1α has been implicated in these two separate pathways [Bitto et al., 2010]. This also suggests that hypoxia confounds a significant portion of the ^{18}F-FDG detectable signal in the plaques. Another radiotracer ^{18}F-HX4 demonstrated increased uptake in carotid plaque segments compared to the regions free from plaque in patients with cardiovascular events [Valk et al., 2015]. It also showed a strong correlation with plaque burden [Valk et al., 2015]. However, the study sample was small (n=8), and ^{18}F-HX4 is yet to be explored.

APOPTOSIS

Cell membranes:

- *99mTc-labelled Annexin A5*
- *^{18}F-ML-10*

Apoptosis of endothelium, smooth muscle cells and macrophages contributes to the plaque instability [Kietselaer et al., 2004]. Hence, molecular detection of a cell undergoing the death process could aid in culprit plaque detection. The radiotracer used for apoptosis imaging is 99mTc-labelled Annexin A5. Annexin A5 is a plasma protein with high affinity for phosphatidylserine, which is found on the apoptotic cells [Andrews et al., 2018]. The process of apoptosis changes the distribution of phospholipid constituents of the plasma membrane leading to the exposure of phosphatidylserine making it an accessible target for the Annexin A5 [Aloya et al., 2006; Hyafil et al., 2015b].

A small pilot study of patients with recent (n=2) and late TIA (n=2) who underwent SPECT reported higher uptake of 99mTc-labelled Annexin A5 in the recently operated patients. The immunohistochemical analysis showed a strong correlation between 99mTc-labelled Annexin A5 binding and macrophages infiltration in the excised lesion [Kietselaer et al., 2004]. Interestingly, patients who presented late (imaged at 3 months from an index event) showed no evidence of 99mTc-labelled Annexin A5 uptake in the carotid artery on in vivo imaging with minimal binding and negligible macrophage infiltration on a histological analysis [Kietselaer et al., 2004].

^{18}F-ML-10 is another radiotracer that binds to cell membranes and selectively accumulates in apoptotic cells while being excluded from viable or necrotic cells [Cohen et al., 2009]. A pre-clinical study in rabbits showed that ^{18}F-ML-10 detected apoptotic cells. The radiotracer uptake was higher in the atherosclerotic aorta and lower in the control artery [Hyafil et al., 2015b]. There was a strong correlation between ^{18}F-ML-10 and aortic segments detected by autoradiography and histological analysis [Hyafil et al., 2015b]. However, more data is required to establish the value of this imaging.

LIPIDS

Fatty acids:

- *^{11}C-acetate*

Lipids accumulation within the subintimal space is key to the development and progression of atherosclerosis. This process, however, is far from just passive lipids deposition. Plaque lipids can undergo thermotopic transitions between liquid and solid phases, thereby influence enzymatic activities, lipids transport, and storage, affecting plaque stability [Zajicek et al., 1987; Pearlman et al., 1988]. Fatty acids are a major component of three main classes of lipids found in the atheromas, including cholesterol (mainly in the form of cholesteryl esters), phospholipids and triglycerides. These fatty acids are essential for monocyte differentiation into macrophages and subsequently to foam cells [Sriranjan et al., 2019]. Most importantly, fatty acids can be synthesised de novo within the arterial wall, and their excessive accumulation decreases structural plaque stability [Derlin et al., 2011]. The process of fatty acids synthesis requires acetyl-coenzyme-A produced from acetate as a substrate [Derlin et al., 2011]. Therefore, ^{11}C-acetate could provide novel information regarding the key lipids pathophysiology that could translate into improved detection of high-risk atherosclerotic plaques. However, current data is limited to feasibility studies that assessed ^{11}C-acetate in oncological patients. A small (n=36) whole-body PET-CT study demonstrated ^{11}C-acetate prevalent binding in large vessels (aorta and iliac arteries). The quantification of radiotracer was feasible, and ^{11}C-acetate uptake colocalised with calcified plaque areas in approximately a third of patients. This could suggest ongoing fatty acids synthesis in asymptomatic plaques that are considered stable due to developed macrocalcification [Derlin et al., 2011]. On the other hand, this could imply that plaques are inhomogeneous and consist of biologically dormant areas with neighbouring zones that may be biologically active, thus actively synthesising fatty acids. However, further data is required to access its clinical applicability. Nevertheless, knowledge of the chemical composition of plaque lipids could provide means of assessing response to novel treatment strategies, such as inhibitors aiming to halt fatty acid synthesis.

Table 1.2: Current and novel PET radiotracers in carotid imaging.

Tracer	Pathophysiology	Target cell	Target molecule	Clinical or research application
^{18}F-NaF	Microcalcification	-	Hydroxyapatite	Oncology
^{18}F-FDG	Inflammation	Macrophage	Glucose analogue	Oncology, Neurology, Cardiology
^{11}C-PK11195 ^{18}F-FEDAA1106 ^{18}F-FEMPA ^{18}F-GE180	Inflammation	Macrophage	18 kDa translocator protein receptor	Research
^{68}Ga-DOTATATE ^{64}Cu-DOTATATE	Inflammation	Macrophage	Somatostatin receptor type 2	Oncology-neuroendocrine
^{18}F-FCH	Inflammation	Macrophage	Choline receptor	Research
^{68}Ga-pentixafor ^{125}I-pentixafor	Inflammation	Macrophage/ Endothelium/ Smooth muscle cells	Chemokine receptor 4	Research
^{11}C-PS13 ^{11}C-MC1	Inflammation	Macrophage	Cyclooxygenase 1 and 2	Research
^{99}TcEC20 ^{99}Tc-folate ^{18}F-FOL	Inflammation	Macrophage	Folate receptor-β	Research
^{64}Cu-DOTA-anti-P-selectin mAb ^{68}Ga-Fucoidan ^{99}Tc-cAbVCAM-1-5 ^{18}F-FB-cAbVCAM-1-5 ^{99}Tc-MT1-MMP-mAb ^{123}I-CGS 27023A	Inflammation	Endothelium	P-selectin P-selectin VCAM-1 VCAM-1 MMP MMP inhibitor	Research Research Research Research Research Research
^{68}Ga-FAPI-04	Fibrosis	Fibroblasts	Fibroblast activation protein	Research
^{18}F-Galacto-RGD ^{18}F-fluciclatide	Neo-angiogenesis	Endothelium	Integrin αVβ3	Oncology
^{18}F-ASEM ^{11}C-NS14492 ^{18}F-NS14490	Neo-angiogenesis	Macrophages/ Endothelium/ Smooth muscle cells	α-7-Nicotinic acetylcholine receptor	Oncology, Psychiatry
^{18}F-GP1	Intraplaque haemorrhage Thrombus	Platelets	Glycoprotein IIb/IIIa (GPIIb/IIIa) receptor	Research
^{18}F-FIMSO ^{18}F-FH4	Hypoxia	Macrophage	Hypoxia inducible factor 1α	Research
99mTc-labelled Annexin A5 ^{18}F-ML-10	Apoptosis	Macrophage/ Endothelium/ Smooth muscle cells	Annexin A5	Research
^{11}C-acetate	Lipids	-	Acetyl-coenzyme-A	Oncology

^{18}F-NaF: Fluorine 18-labelled sodium fluoride;
^{18}F-FDG: [^{18}F]2-fluoro-2-deoxy-D-glucose;
^{11}C-PK11195: 1-(2-Chlorophenyl)-N-methyl-N-(1-methylpropyl)-3-isoquinoline carboxamide;
^{18}F-FEDAA1106: N-(5-fluoro-2-phenoxyphenyl)-N-(2-[(18)F] fluoroethyl-5-methoxybenzyl)acetamide;
^{18}F-FEMPA: (*N*-{2-[2-^{18}F-fluoroethoxy]-5-methoxybenzyl}-*N*-[2-(4-methoxyphenoxy)pyridine-3-yl]acetamide);
^{18}F-GE180: ^{18}F-flutriciclamide: (4S)-*N,N*-diethyl-9-[2-[^{18}F]-fluoroethyl]-5-methoxy-2,3,4,9-tetrahydro-1H-carbazole-4-carboxamide;
^{68}Ga-DOTATATE: (^{68}Ga) 1,4,7,10-tetra-azacyclododecane-1,4,7,10-tetra-acetic acid (DOTA)-TATE**;**
^{64}Cu-DOTATATE: (^{64}Cu) 1,4,7,10-tetra-azacyclododecane-1,4,7,10-tetra-acetic acid (DOTA)-TATE;
^{18}F-FCH: Fluorocholine: fluoromethyl-dimethyl-2-hydroxyethylammonium [FCH];
^{68}Ga-pentixafor: (cyclo(D-Tyr^{1}-D-[NMe]Orn^{2}(AMBS-[^{68}Ga]DOTA)-Arg^{3}-Nal^{4}-Gly^{5}) = [^{68}Ga]DOTA-AMBS-CPCR4);
^{125}I-pentixafor: (cyclo[[125I]D-Tyr-N(hexylguanidino)-D-Ala-Arg-Nal-Gly]);
^{11}C-PS13: 1,5-bis(4-methoxyphenyl)-3-(2,2,2-trifluoroethoxy)-1*H*-1,2,4-triazole;
^{11}C-MC1: 6-methoxy-2-(4-(methylsulfonyl)phenyl)-*N*-(thiophen-2-ylmethyl)pyrimidin-4-amine**;**
^{99}TcEC20: (folic acid-pteroic acid (Pte)-D-Glu-β-L-diaminopropionic acid(βDpr)-Asp-Cys);
^{99}Tc-folate: [(2S)-2-[[4-[(2-amino-4-oxo-1H-pteridine-6-yl) methylamino] benzoyl]amino] pentanedioic acid;
^{18}F-FOL: 1,4,7-triazacyclononane-1,4,7-triacetic acid conjugated folate;
^{64}Cu-DOTA-anti-P-selectin mAb: 1,4,7,10-[(2S,3S,4S,5S,6R)-4,5-dihydroxy-2,6-dimethyloxan-3-yl] hydrogen sulfate;
^{99}Tc-cAbVCAM-1-5: technetium-99-m labelled anti-VCAM1 nanobody;
^{18}F-FB-cAbVCAM-1-5: *N*-Succinimidyl-4-[^{18}F]fluorobenzoate ([^{18}F]-SFB) anti-VCAM1 nanobody;
^{99}Tc-MT1-MMP-mAb: technetium-99-m labelled 6-hydrazinylpyridine-3-carboxylic acid-monoclonal antibody for membrane type 1 matrix metalloproteinase (MT1-MMP);
^{123}I-CGS 27023A: N-Hydroxy-2(R)-[[(4-methoxyphenyl)sulfonyl](3-picolyl)amino]-3-methylbutanamide hydrochloride;
^{68}Ga-FAPI-04: (S)-2,2',2''-(10-(2-(4-(3-((4-((2-(2-cyano-4,4-difluoropyrrolidin-1-yl)-2-oxoethyl)carbamoyl)quinolin-6-yl)oxy)propyl)piperazin-1-yl)-2-oxoethyl)-1,4,7,10-tetraazacyclododecane-1,4,7-triyl)triacetic acid;
^{18}F-Galacto-RGD: 2-[(2S,5R,8S,11S)-5-benzyl-11-[3-(diaminomethylideneamino)propyl]-8-[4-[[(2S,3R, 4R,5R, 6S)-6-[(2-(18F)fluoranylpropanoylamino)methyl]-3,4,5-trihydroxyoxane-2-carbonyl]amino]butyl]-3,6,9,12,15-pentaoxo-1,4,7,10,13-pentazacyclopentadec-2-yl]acetic acid;
^{18}F-fluciclatide:2-[(1R,4S,10R,13S,16R,19S,25S)-10-[2-[2-[2-[2-[[2-(2-amino-2-oxoethoxy)acetyl]amino]ethoxy]ethoxy]ethoxy]ethylcarbamoyl]-13-benzyl-25-[3-(diaminomethylideneamino)propyl]-4-[4-[[2-[2-[2-[2-[2-[2-[2-[2-[[2-[(E)-(4-(18F)fluoranylphenyl)methylideneamino]oxyacetyl]amino]ethoxy]ethoxy]ethoxy]ethoxy]ethoxy]ethylamino]-2-oxoethoxy]acetyl]amino]butyl]-3,6,12,15,18,21,24,27-octaoxo-8,29,30-trithia-2,5,11,14,17,20,23,26-octazabicyclo[14.11.4]hentriacontan-19-yl]acetic acid;
^{18}F-ASEM:(3-(1,4-diazabicyclo[3.2.2]nonan-4-yl)-6-([^{18}F]fluorodibenzo[*b,d*]thiophene 5,5-dioxide;
^{11}C-NS14492: 4-(5-[1-^{11}C-methyl-1*H*-pyrrol-2-yl]-1,3,4-oxadiazol-2-yl)-1,4-diazabicyclo[3.2.2]nonane;
^{18}F-NS14490: (1-(2-fluoroethyl)-6-(5-(1,4-diazabicyclo[3.2.2]nonan-4-yl)-1,3,4-oxadiazol-2-yl)indole);
^{18}F-GP1: 4-(3*S*)-3-[5-(2-[^{18}F]-fluoroethoxy)pyridin-3-yl]-3-[({(3*R*)-1-[3-(piperidin-4-yl)propanoyl]-piperidin-3-yl}carbonyl)amino]propanoic acid;
^{18}F-FIMSO: [1H-1-(3-[18F] fluoro-2-hydroxypropyl)-2-nitroimidazole];
^{18}F-FH4: 3-(18F)fluoranyl-2-[4-[(2-nitroimidazol-1-yl)methyl]triazol-1-yl]propan-1-ol;
99mTc-labelled Annexin A5: technetium-99-m labelled 6-hydrazinylpyridine-3-carboxamide-annexin V;
^{18}F-ML-10: 2-(5-fluoro-pentyl)-2-methyl-malonic acid;
^{11}C-acetate: [(3R,4R,5Z,7E,9S)-3-[tert-butyl(dimethyl)silyl]oxy-4-(4-fluorophenyl)sulfanyl-9-hydroxydodeca-5,7-dien-11-ynyl] acetate

1.7.5 HYBRID IMAGING

POSITRON EMISSION TOMOGRAPHY-COMPUTED TOMOGRAPHY

Hybrid PET-CT imaging detects a range of cellular and pathophysiological mechanisms that are implicated in the atherosclerotic plaque development (Table 1.2). These molecular targets have been already discussed above. ^{18}FDG is the most widely utilised radiotracer in carotid atherosclerosis imaging. Clinical studies demonstrated that in patients following recent acute neurovascular events ^{18}FDG PET-CT identified culprit carotid lesion (higher ^{18}FDG uptake) compared with the asymptomatic contralateral plaque [Rudd et al., 2002; Skagen et al., 2015]. Symptomatic carotid plaques with increased ^{18}FDG uptake were associated with stroke recurrence independently of underlying carotid artery stenosis [Davies et al., 2005; Marnane et al., 2012; Kelly et al., 2019]. Furthermore, ^{18}FDG PET-CT proved to be a useful endpoint in measuring the effects of drug treatment by measuring attenuation of the ^{18}FDG signal [Sriranjan et al., 2019]. More recently, ^{18}F-NaF permitted detection of microcalcification associated with high-risk carotid atheroma [Irkle et al., 2015; Vesey et al., 2017]. Increased uptake of ^{18}F-NaF was demonstrated in the culprit carotid vessels following acute neurovascular events versus non-culprit contralateral plaques [Quirce et al., 2013; Quirce et al., 2016; Vesey et al., 2017; Joshi et al., 2014].

Hybrid PET-CT is a powerful tool that provides a comprehensive insight into the different aspects of the pathophysiology of atherosclerosis, thus allowing for a more accurate evaluation of the high-risk carotid plaques. However, its application remains limited primarily due to high costs of radiotracer production. Therefore, if we want to move beyond traditional structural imaging, these aspects will need to be addressed to permit widespread use of this imaging technique.

HYBRID POSITRON EMISSION TOMOGRAPHY-MAGNETIC RESONANCE IMAGING

Hybrid PET-MRI represents a truly new horizon in molecular imaging which facilitates the simultaneous acquisition of PET and MRI data. This contrasts with PET-CT, where both PET and CT acquisitions are obtained consecutively. The benefits of PET-MRI over PET-CT include superior tissue contrast resolution, which is crucial for the detailed carotid plaque assessment, improved motion correction and reduced ionising radiation dose [Robson et al., 2017]. Addition of gadolinium contrast enhancement, intrinsic relaxation (T weighted imaging) and proton densities allow for improved discrimination between plaque components and surrounding tissues [Briley-Saebo et al., 2007]. This results in a unique morphological and physiological plaque assessment with a potential for early identification (before rupture) of high-risk vascular lesions [Giannakou et al., 2020; Evans et al., 2020].

Although PET-MRI has been increasingly used in cardiovascular imaging, less than a handful of small size studies are available on carotid imaging in patients with acute neurovascular syndromes. ^{18}FDG PET-MRI study (n=18) in patients with acute ischaemic stroke and ipsilateral <50% stenoses carotid artery showed increased ^{18}FDG uptake in the clinically culprit carotid artery compared to the non-culprit contralateral side [Hyafil et al., 2015a]. Higher radiotracer uptake in culprit lesions was associated with MRI detected high-risk plaque features such as intraplaque haemorrhage and necrotic lipid core [Hyafil et al., 2015a]. ^{64}Cu-DOTATATE PET-MRI study (n=10) in patients scheduled for carotid endarterectomy revealed higher radiotracer uptake in the symptomatic carotid plaques that correlated with histologically stained macrophages [Pedersen et al., 2015]. However, no correlation was found between ^{64}Cu-DOTATATE, and plaque burden assessed on MRI [Pedersen et al., 2015]. Similar data was demonstrated by a study (n=25) which performed ^{18}FDG PET-CT followed by MRI before carotid surgery [Saito et al., 2013]. PET-CT accurately identified lesions with necrotic lipid core and inflammation, whilst T1-weighted MRI detected intraplaque haemorrhage [Saito et al., 2013].

Finally, exploratory study of hybrid ^{18}F-NaF PET-MRI that involved 12 participants (6 symptomatic and 6 asymptomatic carotid arteries) demonstrated higher radiotracer uptake in the culprit carotid plaques that did not correlate with MRI detected high-risk plaque features [Mechtouff et al., 2020]. Additionally, no difference in ^{18}F-NaF PET-MRI uptake was found in the aortic arch or major branches between symptomatic or asymptomatic patients [Mechtouff et al., 2020]. Consequently, most published data on ^{18}F-NaF PET is based primarily on the ^{18}F-NaF PET-CT findings. However, there are several drawbacks of this novel hybrid imaging technique. PET-MRI is expensive and not widely available. Despite a reduced dose of ionising radiation compared to PET-CT, hybrid PET-MRI requires longer acquisition times affecting tolerability by individuals. Moreover, the small-bore size of PET-MRI scanner might reduce patient compliance due to claustrophobia. Therefore, until these obstacles are solved the clinical use of hybrid systems will be limited to the research field only.

1.8 SUMMARY

Ischaemic stroke is the leading cause of persisting neurological disability and personal suffering. Despite considerable improvements in the treatment outcomes, each year, the disease claims its high mortality toll. Therefore, the mainstay of management is to prevent a future stroke. However, it's impossible to identify those patients at high risk for plaque rupture and subsequent neurovascular event using current imaging modalities. The development of carotid atheroma results from a complex interplay of disordered biological processes that primarily affect the arterial intima with microcalcification at the very core of the atherosclerotic disease progression. Molecular imaging of microcalcification facilitates evaluation of the biological plaque activity beyond currently available cross-sectional imaging techniques. This has the potential to fundamentally alter our management of patients with acute neurovascular syndromes.

1.9 AIMS AND HYPOTHESIS

1.9.1 AIMS

The primary aim of this thesis was to investigate the role of hybrid ^{18}F-NaF PET-MRI in the detection and evaluation of the acute plaque (clinically culprit) that was deemed responsible for acute neurovascular events. This work follows on from a previous carotid study that demonstrated the role of ^{18}F-NaF PET-CT in detecting microcalcification in the clinically culprit carotid plaques.

1.9.2 HYPOTHESES

TRANSCRANIAL DOPPLER (Chapter 3)

Middle cerebral artery

1. Transcranial Doppler ultrasound will provide reproducible middle cerebral artery blood flow velocity measurements in healthy volunteers and patients with symptomatic carotid artery stenosis.

2. Transcranial Doppler ultrasound will detect microembolic signals (MES) in subjects with symptomatic carotid artery stenosis as an additional marker of unstable carotid plaque.

^{18}F-NaF PET-MRI - ACUTE NEUROVASCULAR SYNDROME (CHAPTER 4)

Carotid Artery

1. ^{18}F-NaF uptake will be increased in clinically culprit carotid plaque compared to the contralateral non-culprit plaque that has not caused a clinical event.

2. ^{18}F-NaF uptake will be increased in the clinically culprit carotid plaque and will correlate with MRI detected high-risk plaque features.

Aorta

1. ^{18}F-NaF uptake will be increased in the non-carotid large arteries (aortic arch) in patients with clinically culprit carotid plaque.

^{18}F-NaF PET-MRI – CORRELATION WITH HISTOLOGY (Chapter 5)

Carotid artery

1. ^{18}F-NaF (*in vivo*) uptake will co-localise with the regions of microcalcification deposition found on *ex vivo* PET-CT, histology, and immunohistochemistry.

2. ^{18}F-NaF (*in vivo*) uptake will correlate with the high-risk plaque morphology on histological examination.

3. MRI (*in vivo*) will demonstrate diagnostic accuracy in high-risk carotid plaque features detection compared with *ex vivo* MRI and histological analysis.

Additional works and achievements relating directly and indirectly to this thesis may be found in the Bibliography.

CHAPTER TWO

METHODS

2.1 GENERAL

2.1.1 ETHICAL REGULATIONS

All aspects of this research project were carried out by the ethical principles outlined in the Research Governance Framework for Health and Community Care (Second Edition, 2006), the World Medical Association Declaration of Helsinki Ethical Principles for Medical Research Involving Human Subjects (1964) and Good Clinical Practice. The studies were approved by the South-East Scotland Research Ethics Committee (17/SS/0097, 17/SS/0098 and 16/SS/0217). Formal written informed consent was obtained from all participants prior to any study-related procedures. All clinical studies were registered on a publicly available domain with ClinicalTrials.gov (NCT 03215550, NCT 03215563 and NCT 03050567).

2.1.2 RECRUITMENT

All participants received a verbal description of the study and written patient information sheet prior to enrolment. All participants were contacted at least 24 hours after the initial approach to establish their willingness to participate and to answer any questions that arose regarding the research process. A written and informed consent was obtained from all participants at the beginning of the first study visit. Participants were free to withdraw from the study at any time without any effect on their standard clinical care. An information letter was provided to the participants' general practitioners.

2.1.3 RECRUITED POPULATIONS

In total, four cohorts were recruited for the two studies (two cohorts per each study):

- *Reproducibility Study of Transcranial Doppler Ultrasound In the Middle Cerebral Artery* involved patients following an acute neurovascular syndrome and healthy volunteers.

- *^{18}F-Sodium Fluoride PET-MRI In Patients with Acute Neurovascular Syndrome* study included surgical and non-surgical patients with acute neurovascular syndrome (acute ischaemic stroke, transient ischaemic attack or amaurosis fugax).

2.1.4 REPRODUCIBILITY OF TRANSCRANIAL DOPPLER ULTRASOUND IN THE MIDDLE CEREBRAL ARTERY STUDY

Population

Two cohorts of subjects including healthy volunteers and those with symptomatic carotid artery stenosis were recruited (Figure 2.1):

- Cohort of healthy volunteers was recruited from the Centre for Cardiovascular Science at Edinburgh University. Healthy volunteers were >18 years old and had no previous history of cerebrovascular disease.

- Cohort of patients consisted of individuals with evidence of an acute neurovascular syndrome (acute ischaemic stroke, transient ischaemic attack, retinal ischaemia) due to carotid artery disease who were recruited from the acute neurovascular clinics at Edinburgh Royal Infirmary within a maximum of 14 days of symptom onset. The inclusion criteria were the symptomatic cerebrovascular event (acute ischaemic stroke, transient ischaemic attack or amaurosis fugax) and radiological confirmation of carotid artery stenosis of > 30%. These included patients scheduled for carotid endarterectomy (>50% by North American Symptomatic Carotid Endarterectomy Trial criteria) or treated conservatively with best medical therapy (if patient declined surgical intervention or was outside surgical criteria for carotid endarterectomy).

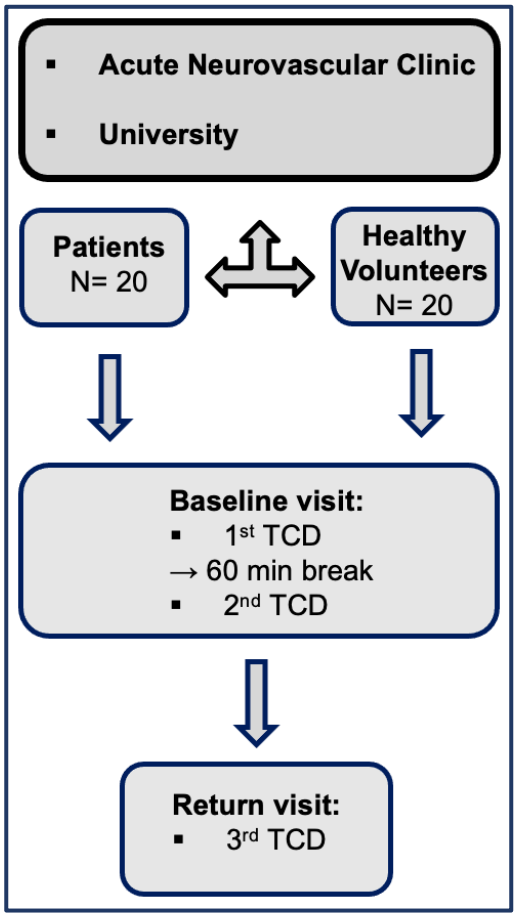
The only exclusion criterion related to the inability to comply with the study procedures.

Clinical Assessments

Transcranial Doppler monitoring took place the Welcome Trust Clinical Research Facility at Edinburgh Royal Infirmary. All subjects underwent clinical evaluation prior to participation. In the patient group, this included assessment of relevant carotid Doppler ultrasound and brain imaging investigations (computed tomography or magnetic resonance imaging).

In both cohorts, three 1-hour transcranial Doppler measurements were performed by the same examiner over two study visits. During the first study visit, two examinations were performed separated by 1 hour. The final (third) examination was obtained on a separate study visit within 14 days of the first examination.

Figure 2.1: Reproducibility of transcranial Doppler ultrasound study flow chart.



TCD: Transcranial Doppler

2.1.6 HYBRID ^{18}F-SODIUM FLUORIDE POSITORN EMISSION TOMOGRAPHY-MAGNETIC RESONANCE IMAGING IN PATIENTS WITH ACUTE NEUROVASCULAR SYNDROME

Population

Patients with evidence of an acute ischaemic stroke, transient ischaemic attack or amaurosis fugax were recruited from the acute neurovascular clinics or hospitalised patients at the Royal Infirmary and Western General Hospital in Edinburgh.

The diagnostic criteria were based on the clinical symptoms and radiological evidence of infarction in line with the American Heart and Stroke Association guidelines. The diagnosis of an acute stroke or amaurosis fugax included a clinically evident episode of an acute neurological dysfunction persisting for >24 hours that was caused by the focal brain or retinal ischaemia identified on brain CT, or MRI [Sacco et al., 2013]. Transient ischaemic attacks were diagnosed when clinical symptoms of focal ischaemia lasted <24 hours with no evidence of infarction on CT or MRI imaging of the brain [Sacco et al., 2013].

Patients over 40 years of age who had suffered a recent neurovascular event and had undergone carotid Doppler ultrasound scan were recruited within 14 days from symptoms onset into one of two cohorts (Figure 2.2) based on the North American Symptomatic Carotid Endarterectomy Trial (NASCET) criteria [Rothwell et al., 2003a; Naylor et al., 2018]:

- Surgical cohort included patients who were scheduled to undergo carotid endarterectomy for symptomatic carotid artery stenosis (≥50% by the NASCET criteria for men, ≥70% for women).

- Non-surgical cohort consisted of patients who either did not meet surgical criteria for carotid endarterectomy (< 50% by the NASCET criteria) or met the criteria but did not undergo surgery as surgery was either declined or considered unsuitable.

Exclusion criteria included patients with new stroke and a modified Rankin score >3, chronic kidney disease with an estimated glomerular filtration rate of <30 mL/min/1.73 m^2, atrial fibrillation, pregnancy, prior ipsilateral carotid intervention or neck radiotherapy, inability to tolerate the supine position, inability to comply with the study requirements, history of allergic reaction attributed to ^{18}F-NaF or gadolinium contrast media, contraindications to MRI, or if the participation in the study would result in a delay to surgery.

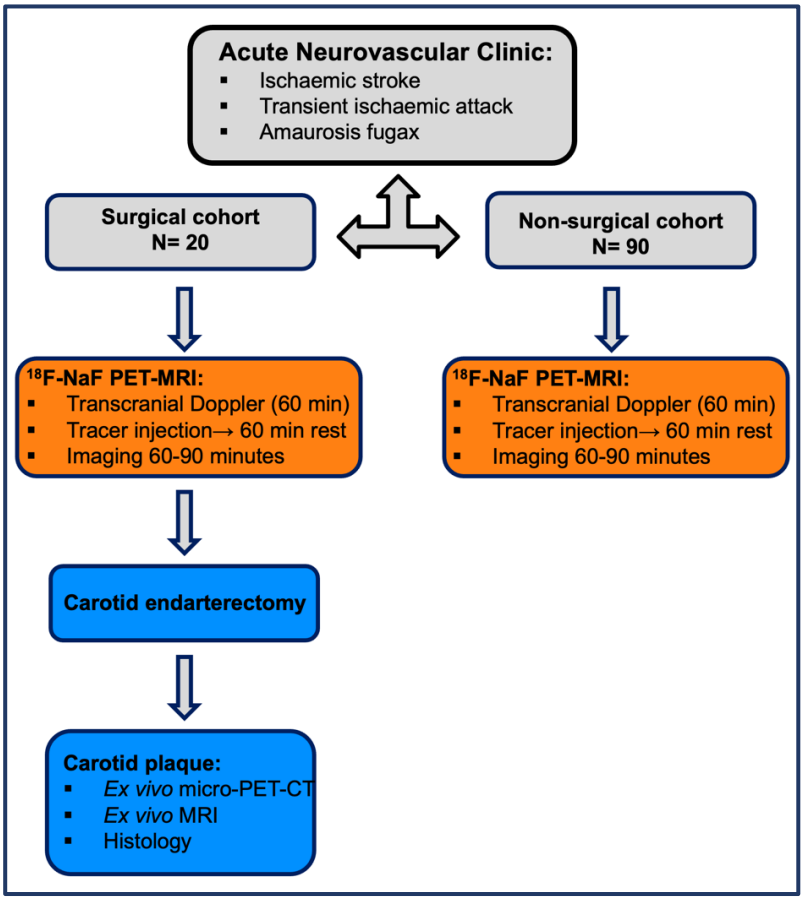
Clinical Assessments

Participants received a baseline assessment within 14 days of the index event incorporating a routine clinical assessment, review of healthcare records and relevant investigations including carotid Doppler ultrasound, brain imaging and clinical laboratory investigations. The attending stroke clinician defined the culprit side at the acute neurovascular clinic as ipsilateral to the hemispheric stroke or transient ischaemic attack.

Follow up Assessments

All acute ischaemic strokes, transient ischaemic attacks or amaurosis fugax following hybrid PET-MRI scan were defined as recurrent and were independently confirmed from the healthcare records by another study researcher at a fixed time point (26th October 2020) that was blinded to the imaging data. These recurrent acute neurovascular events included presentations that were ipsilateral and non-ipsilateral to the index carotid symptoms and were based on the clinical review by attending stroke physician as part of standard care.

Figure 2.2: Carotid study flow chart.



^{18}F-NaF PET-MRI: Fluorine 18-labelled sodium fluoride Positron Emission Tomography-Magnetic Resonance Imaging; Ex vivo micro-PET-CT: Ex vivo micro-Positron Emission Tomography-Computed Tomography; Ex vivo MRI: Ex vivo Magnetic Resonance Imaging.

2.2 TRANSCRANIAL DOPPLER ULTRASOUND

2.2.1 FUNDAMENTALS

Transcranial Doppler ultrasound enables imaging of major intracranial arteries, particularly the middle cerebral artery, using a transtemporal acoustic window, which permits transmission and reception of an ultrasound beam. It relies on a core ultrasound principle that a longitudinal sound wave travels through a medium (tissue) that causes local displacement of particles (in the same direction the wave travels) within the examined matter [Thrush et al., 2023]. The Doppler effect (change in the observed frequency due to the relative motion of the source and the observer) facilitates the assessment of the blood flow and depends on the angle of insonation [Aaslid, 1986], defined as the

angle between the ultrasound beam and the direction of blood flow. M-mode Doppler is another form of transcranial Doppler modality (power-motion) that displays the direction of blood flow Doppler signals, which helps to track microembolic signals within the vessel that produce high-intensity reflections and audible signals [Thrush et al., 2023]. An integral part of transcranial Doppler equipment is the transducer that converts electrical energy to mechanical vibration, which is transmitted into an examined tissue at a resonant frequency at which the transducer is most efficient [Thrush et al., 2023]. In effect, transcranial Doppler ultrasound permits measuring middle cerebral artery velocity and detecting microemboli.

2.1.2 TRANSCRANIAL DOPPLER ULTRASOUND IMAGING PROTOCOL

All examinations were performed in a semi-recumbent position in a quiet temperature-controlled room. The middle cerebral artery was identified through the temporal window and the sample volume adjusted to obtain a stable visually and acoustically optimal signal. In healthy subjects, the side of the middle cerebral artery insonation was randomly allocated. In patients with symptomatic carotid artery stenosis, transcranial Doppler was performed on the symptomatic middle cerebral artery (ipsilateral to the index event). A head frame (Marc 600 Spencer Technologies, United States of America) was fitted to reduce motion and to secure a constant angle of the middle cerebral artery insonation depth at 40-65 mm from the skull surface (Figure 2.3).

2.1.3 TRANSCRANIAL DOPPLER ULTRASOUND IMAGING ANALYSIS

All recordings were made using the ST^3 Transcranial Doppler Ultrasound System (Spencer Technologies, United States of America) with a 2-MHz transducer. Emboli were identified using characteristic short audible sound (range 10-100 ms, intensity threshold above 7 dB) and spectral appearance using the International Consensus Group microembolus identification criteria and assisted by an automated Embolus Detection Software (Spencer Technologies, United States of America) [Ringelstein et al., 1998]. The

Doppler wave forms were reassessed to exclude artefact and confirm the presence of true emboli. The mean of maximal, mean and end-diastolic flow velocities were determined from the mean of measurements obtained over ten cardiac cycles.

Figure 2.3: Head ultrasound: head frame.



Image from the Spencer Technologies manual.

2.3 POSITRON EMISSION TOMOGRAPHY

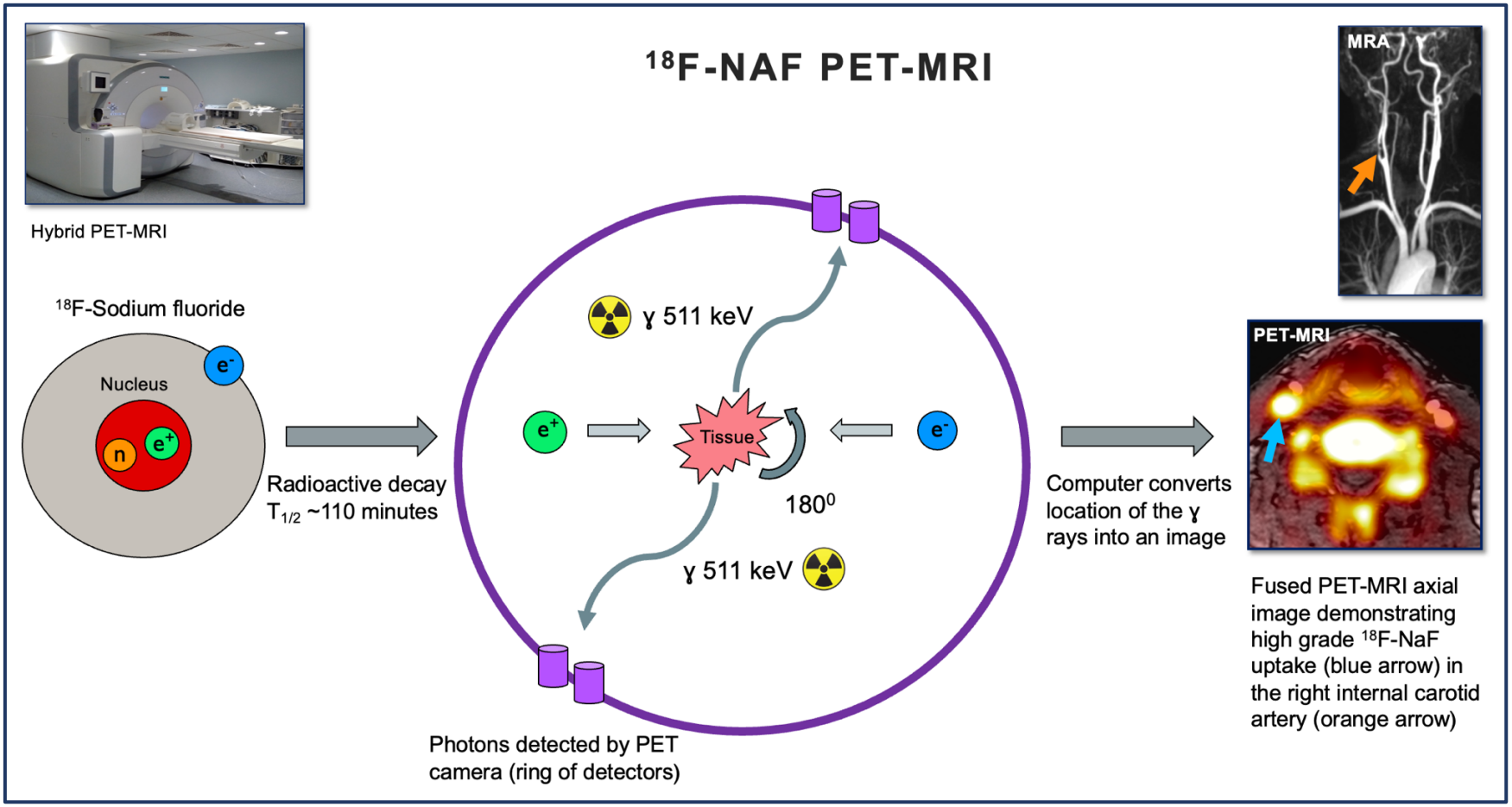
2.3.1 FUNDAMENTALS

Positron Emission Tomography (PET) is non-invasive molecular imaging that enables with picomolar sensitivity detection of radioligands that accumulate at specific tissues, thereby quantify biologically active processes of interest.
The potential of PET imaging is vast and expands rapidly due to the development of new radiotracers targeting an increasing number of different pathophysiological pathways. PET principally relies on photons emission by the positron-emitting radiotracers that do not provide any anatomical detail. Therefore, PET is combined with a traditional cross-sectional imaging

technique such as CT or MRI in a single gantry that provides sufficient anatomical information for image analysis. In effect, hybrid imaging facilitates detection of morphology with concurrent functional information at molecular and cellular levels.

Radiotracer is an indispensable PET element that permits visualisation of biologically active target tissue. PET utilises tracers which are radiolabelled with various isotopes (^{11}C, ^{15}O, ^{18}F, ^{123}I, ^{125}I,^{64}Cu, ^{68}Ga and others) that bind to a molecular or cellular target and decay at a predicted rate with the emission of positrons. These isotopes are generated in a cyclotron where a stable isotope is bombarded with protons. Next, in a radiation-shielded radiochemical laboratory, these radionuclides are incorporated into a chosen biomolecule of interest which as a radiotracer can be administered to a participant. As the radiotracer decays, emitted positrons travel within the tissue for a short distance, ultimately annihilating with electrons in surrounding tissues. This results in the production of two high-energy photons (511keV) at an angle of 180° moving in the opposite direction (Figure 2.4). These photons interact with scintillation crystals within the gantry ring detectors. In effect, each pair of emitted photons is detected simultaneously by two detectors as a single annihilation event (co-incidence event). This means that only photons that strike the scintillator crystals within a short time frame (3-12 nanoseconds) are counted as a true coincidence. Next, all coincidences are recorded as raw data, and the line (line of response) between these paired photons indicates precise localisation of the annihilation events. Thus, the activity of radiotracer can be defined within the area where the positrons were emitted, while reconstructed data creates an image of the radiotracer concentration within the tissue of interest.

Figure 2.4: PET principles.



Hybrid ^{18}F-NaF PET-MRI of the culprit carotid plaque (blue and orange arrows) that caused acute neurovascular event. ^{18}F-NaF PET-MRI: Fluorine 18-labelled sodium fluoride positron emission tomography-magnetic resonance imaging.

As already mentioned, photons prior to annihilation pass through the different tissues on their route to PET detectors. This leads to photons attenuation (Compton scatter), which causes artefacts, and makes the precise assessment of their origin challenging. Furthermore, not all annihilated photons travel in anti-parallel directions, and many represent random coincidences. These aspects diminish spatial resolution of PET, hence, to correct for the reduction of signal and to improve the quality of the PET image, attenuation correction maps are applied. These maps represent the attenuation coefficients of different tissues and adjust the counts of photons absorbed by the body.

2.3.2 ^{18}F-NaF

^{18}F-NaF with a half-life of 110 minutes is a popular radiotracer detecting new calcium formation (microcalcification). This positron-emitting radionuclide is characterised by a high safety profile and pharmacokinetic properties. After intravenous injection, approximately two-thirds of ^{18}F-NaF are plasma-based and remaining third is incorporated in erythrocytes. Most importantly, 60 minutes post-administration, 90% of radiotracer diffuses into the extracellular fluid, while residual 10% is found in the blood [Irkle et al., 2015]. This biodistribution enables an exchange with hydroxyl groups on exposed hydroxyapatite crystals (which incorporates fluoride) at sites of new mineralisation to form fluorapatite [Tzolos et al., 2020].

2.4 MAGNETIC RESONANCE IMAGING

2.4.1 FUNDAMENTALS

ATOM STRUCTURE AND MAGNETIC NUCLEI

Magnetic Resonance Imaging (MRI) is based on the magnetic properties of protons which have their own magnetic field due to a positive electrical charge and rotation around its own axis (spin). Protons and neutrons (have no charge)

are concentrated within the nucleus of an atom, and as nucleons, they define the mass number of an atom. The number of protons equals the number of negatively charged electrons (negligible mass) to maintain electrical neutrality.

The majority of atoms contain protons and neutrons in equal number; therefore, the nucleus has no net spin. However, some atoms have a different number of these subatomic particles resulting in the unopposed spin of one of the nucleons. These atoms are magnetically active (oxygen, carbon, nitrogen and others) and hydrogen, which consist of a single proton is most used for MRI.

Application of an external magnetic field to a proton aligns its own magnetic field with the stronger external magnetic field and produces a secondary spin (precession) around that field. This precession frequency (Larmor frequency) is rapid (42 million per second) and is proportional to the strength of the external magnetic field.

MAGNETISATION

Individual protons can align with the external magnetic field either in a parallel (low energy state) or anti-parallel (high energy state) direction, and they can alternate between these two states. In resting state (individual in MRI scanner), a small excess of protons aligns in a low energy parallel direction creating Net Magnetisation Vector (longitudinal vector) in the same direction as the external magnetic field. With increasing strength of the external magnetic field, more protons align in the parallel direction because they cannot oppose this external field. In effect, the greater magnitude of the Net Magnetisation Vector obtained from more excess protons within the single voxel (volume element), translates into more signal from higher tesla MRI scanners.

RESONANCE

The purpose of the radiofrequency (RF) pulse is two-fold. First, RF induces resonance of protons, and this requires the RF pulse to have the same

frequency as protons. Some protons excited by RF pulse, gain energy and move into the higher anti-parallel energy state resulting in deflection of the longitudinal vector from the external magnetic field. This creates a flip angle between the longitudinal vector from the external magnetic field, and its size depends on the duration of RF pulse. Second, the RF pulse leads to all protons to precess in phase. All above creates a new magnetisation vector that is in the transverse plane to the external magnetic field and is termed Transverse Magnetisation Vector.

SIGNAL

Transverse Magnetisation Vector induces an electrical current due to a conductive coil presence in the fluctuating magnetic field. The voltage within the coil results in the magnetic resonance signal. Subsequent, creation of the magnetic resonance image is based on the application of different strengths of magnetic field to the different body parts of an individual. Produced various frequencies are characterised due to the known specific properties of different body parts.

RELAXATION

Removal of the RF pulse leads to a proportion of anti-parallel protons to return to the parallel low energy state by emitting some of the energy gained from the RF pulse and to a loss of phase of spinning protons. In other words, as the longitudinal magnetisation is regained, the transverse magnetisation diminishes and eventually disappears. This process of return to the original state is called a longitudinal relaxation time or T1. Whist simultaneous decay of transverse magnetisation that occurs independently of T1 results in a transverse relaxation time of T2.

T2* decay is a form of T2 decay combined with the loss of phase due to local magnetic field inhomogeneities created by superimposing an uneven magnetic field on the top of an existing external magnetic field for a short period of time.

These inhomogeneities result in a higher or lower local magnetic field than the external magnetic field and lead to a faster or slower precession of a proton compared to other protons that are in close proximity. When, instead, of 180° RF pulse sequence, the extra magnetic field is switched on and off, re-phased protons exhibit varying rates of precession due to rapid relaxation and decay. This generates a maximum signal intensity which is termed as a gradient echo. In effect, the T2* is shorter than T2.

Although, T1 is longer than T2, these relaxations times vary across different body areas due to various tissue compositions, structures and neighbouring nuclei. These tissue-based factors impact upon energy and pattern of molecules within tissues but also influence molecular tumbling rate, which depends on the size of a molecule. In general, efficient energy transfer occurs if molecules are alike and the tumbling rate is similar to the Larmor frequency resulting in short T1 and T2, which characterises fat. In contrast, water consisting of small and high energy molecules with high tumbling rate (poor matching with the Larmor frequency) has a poor energy transfer; hence the T1 and T2 are long. Overall, tissue components can be distinguished by looking at different T1 and T2 times which result in different signal intensities.

BASIC SIGNAL PARAMETERS

A simple sequence consists of a succession of RF pulses tailed by a relaxation period during which the signal is sampled. The *repetition time* (TR) is the time between RF pulses which guards the degree of T1 recovery process. Hence, by quantifying the various patterns of longitudinal relaxation at 90°, RF pulse sequence provides the T1-weighted image (T1W). Resulting T1W image exploits the T1 differences between fat and water by shortening TR, which translates into a large difference in longitudinal relaxation between fat and water. Whereas the *echo time* (TE) defines the time that elapses between the RF pulse and sampling of the signal, thereby it governs the degree of T2 decay and when followed by a pulse sequence at 180°, it produces T2-weighted image (T2W). Thus, T2W image maximises T2 differences between fat and

water by utilising long TE so that both fat and water decay and a difference can be detected.

CONTRAST AND WEIGHTING

In effect, by adjusting TR and TE, it is possible to obtain an image with predominantly one of the weightings. To minimise T1W images, both TR and TE are long. Conversely, minimising T2W images requires short TR and TE. When T1 and T2 effects are diminished by the application of long TR and short TE, produced image reflects proton density (PD) of tissues. This improves contrast between tissues and enhances detailed analysis, including carotid plaque morphological characterisation.

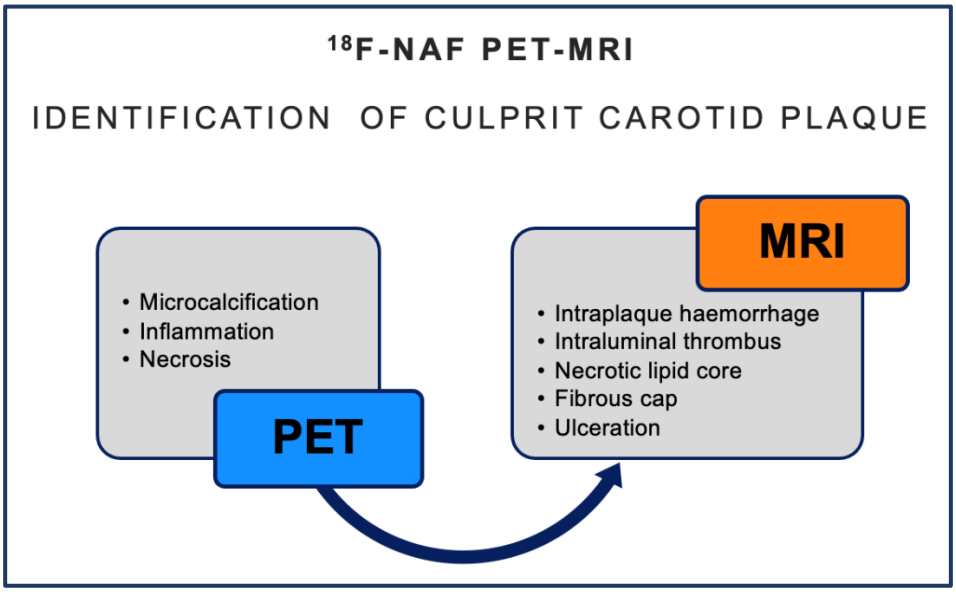
2.5 HYBRID PET-MRI

Hybrid PET-MRI (Positron Emission Tomography-Magnetic Resonance Imaging) is considered the *state-of-the-art* technology that facilitates a simultaneous morphological and functional assessment of disease activity. An injected radiotracer which is a source of ionising radiation accumulates in the area of a biological process of interest. Subsequent detection of this ionising radiation facilitates a direct measure of the underlying disease activity. Thus, identifying ^{18}F-NaF deposition onto hydroxyapatite pinpoints culprit carotid plaques responsible for acute clinical neurovascular events.

As already mentioned, PET is disadvantaged by a low resolution. Therefore, it requires MRI modality that can provide exact anatomical detail. This is essential to co-localise ^{18}F-NaF PET information with specific anatomical structures and allow to correct PET attenuation by different tissues. MRI component of hybrid imaging offers superior soft tissue discrimination, particularly valuable in a detailed carotid plaque analysis. Therefore, MRI identifies the presence of established carotid artery disease, whilst PET imaging provides functional assessment of the atherosclerotic plaque. In

effect, hybrid ^{18}F-NaF PET-MRI offers a broad and powerful spectrum of complementary information (Figure 2.5).

Figure 2.5: ^{18}F-NaF PET-MRI.



Complementary carotid plaque morphological and pathophysiological information obtained by two imaging components of ^{18}F-NaF PET-MRI. ^{18}F-NaF PET-MRI: Fluorine 18-labelled sodium fluoride positron emission tomography-magnetic resonance imaging.

2.5.1 TECHNICAL ASPECTS

The full integration of PET-MRI in a single gantry faced many challenges during the early phases of development. Fortunately, these obstacles have been successfully resolved over the years. However, a few aspects deserve some explanation as they underpin the technical properties of this unique imaging modality and demonstrate a remarkable technological achievement that advanced our understanding of the carotid atherosclerotic disorder.

Photomultiplier Detectors

The development of MRI compatible photomultiplier detectors paved the way for a full PET and MRI integration within the single gantry system. Standard photomultiplier detectors do not function within the strong magnetic field. Therefore, historically the first PET-MRI scans were performed sequentially involving two adjacent but separate rooms because this set up provided

sufficient distance to avoid MRI interference with photomultiplier PET detectors. However, new detectors unaffected by magnetic fields such as avalanche photodiode or silicon photomultiplier detectors eased the path for genuinely simultaneous PET-MRI systems.

Interference of Metal

MRI requires surface coils (invisible on MRI) that improve the quality of imaging data. However, coils located between PET detectors and the imaged individual contain metal parts (conductors, amplifier electronics) and lead to PET photons attenuation producing major artefacts. One solution is to use PET-MRI dedicated coils with reduced metal content [Schulthess et al., 2013]. On the other hand, these issues did not appear to be a major hurdle in cardiovascular imaging due to the low absorption cross-section of the coils including their distance from the imaged tissue [Robson et al., 2017].

Attenuation Correction

The issues surrounding attenuation correction for the reconstruction of PET images are incredibly complex and challenging. An accurate attenuation correction of the tissues is vital for image conversion. Images obtained by CT create attenuation maps because attenuated x-rays are directly converted to attenuation values for the 511 keV photons in PET imaging. In other words, CT images are based on electrons radiodensity and differences in photon attenuation. In contrast, MRI data is not readily available for attenuation correction maps because images are based on varying relaxations times among different tissues, and MRI signal is proportional to proton density [Lairez et al., 2016]. Other problems include difference in the fields of view between MRI and PET. The smaller MRI field of view in the transverse plane can cause truncation artefacts in the off-centre regions [Aizaz et al., 2020]. Furthermore, MRI is characterised by an inferior differentiation between high attenuation of photons by bones and low attenuation by air. In effect, bone is not included in the attenuation correction maps, which may be problematic when assessing structures close to bony tissue.

To generate attenuation correction maps using MRI data, it first needs to be transformed into a pseudo-CT and from there into attenuation correction maps. This is achieved with a Dixon sequence which creates water and fat-based images. Next, these images are segmented into four tissue classes: air, lung, fat and soft tissue. Each segmented tissue is then assigned attenuation coefficients based on their known CT characteristics (attenuation atlas at 511 keV). Subsequently, the MRI atlas data is registered to the images obtained by MRI, followed by a similar transformation of CT based attenuation atlas. Ultimately, low dose pseudo-CT images are used as attenuation correction map to reconstruct PET data.

Although Dixon sequence enabled considerable progress in MRI data conversion, some challenges remain unsolved. Attenuation correction at the edge of the field of view remains problematic because of magnetic field inhomogeneity in the peripheral zones leading to the degradation of estimated attenuation [Robson et al., 2017]. This problem can be observed with the individual's arms beside the body, which is a source of attenuation. Future PET-MRI reconstruction algorithms may use a non-attenuated PET signal to generate both the estimated attenuation and activity [Robson et al., 2017].

Motion Correction

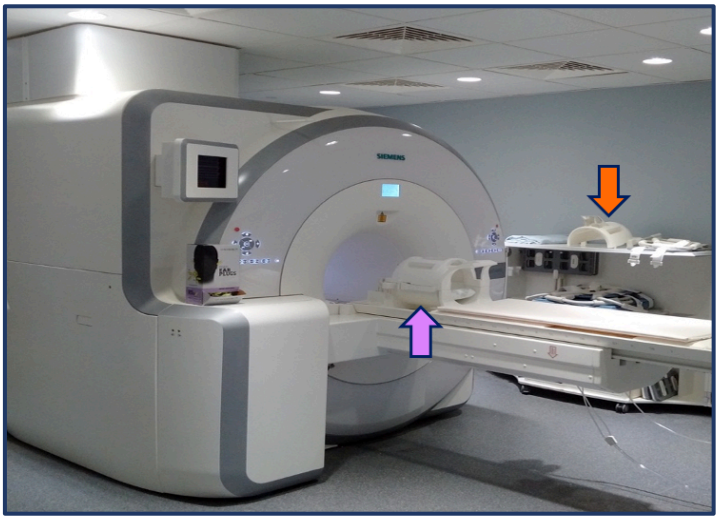
Finally, motion correction is prerequisite for a detailed vessel wall analysis. This is particularly relevant in coronary arteries imaging when cardio-respiratory movement creates motion artefacts. To a degree, it can affect carotid arteries which can experience vessel wall motion caused by swallowing or intrinsic arterial distensibility. However, in most cases with satisfactory patient compliance carotid vessels are subject to a minimal motion. Cardiac imaging utilises electrocardiogram gating, which accepts PET data from diastole only. Whist respiratory movement can be motion-corrected by more sophisticated approaches, including liver-diaphragm navigators that perform respiratory gating with rate tracking [Aizaz et al., 2020].

2.5.2 HYBRID ^{18}F-NaF PET-MRI PROTOCOL

All recruited participants were scanned at the Edinburgh Imagining Facility within the Queen's Medical Research Institute at the Bioquarter campus on the Edinburgh Royal Infirmary site.

Participants received a target dose of 125 MBq of ^{18}F-NaF intravenously and after 60 min of rest were imaged on a hybrid PET-MRI scanner (Biograph mMR, Siemens, Erlangen, Germany) using a dedicated head and neck coil (Figure 2.6). A 3-dimensional ^{18}F-NaF -PET scan was obtained using list-mode acquisitions with two beds positions (15 min each) to ensure coverage of the carotid arteries and aortic arch. MR images of carotid arteries were obtained simultaneously with PET data and included black blood T2-SPACE, 3-dimensional TOF MR angiography and 2-dimensional axial black blood T1W, T2W and PD-weighted stacks. After PET imaging acquisition, a contrast-enhanced MR angiogram (gadobutrol 1 mmol/mL) was performed and centred on the carotid bifurcations and aortic arch. PET-MRI images were reconstructed with corrections applied for attenuation, dead time, scatter and random coincidences using Dixon and UTE sequences.

Figure 2.6: Hybrid PET-MRI scanner at Edinburgh Imaging Facility (Biograph mMR, Siemens, Erlangen, Germany).

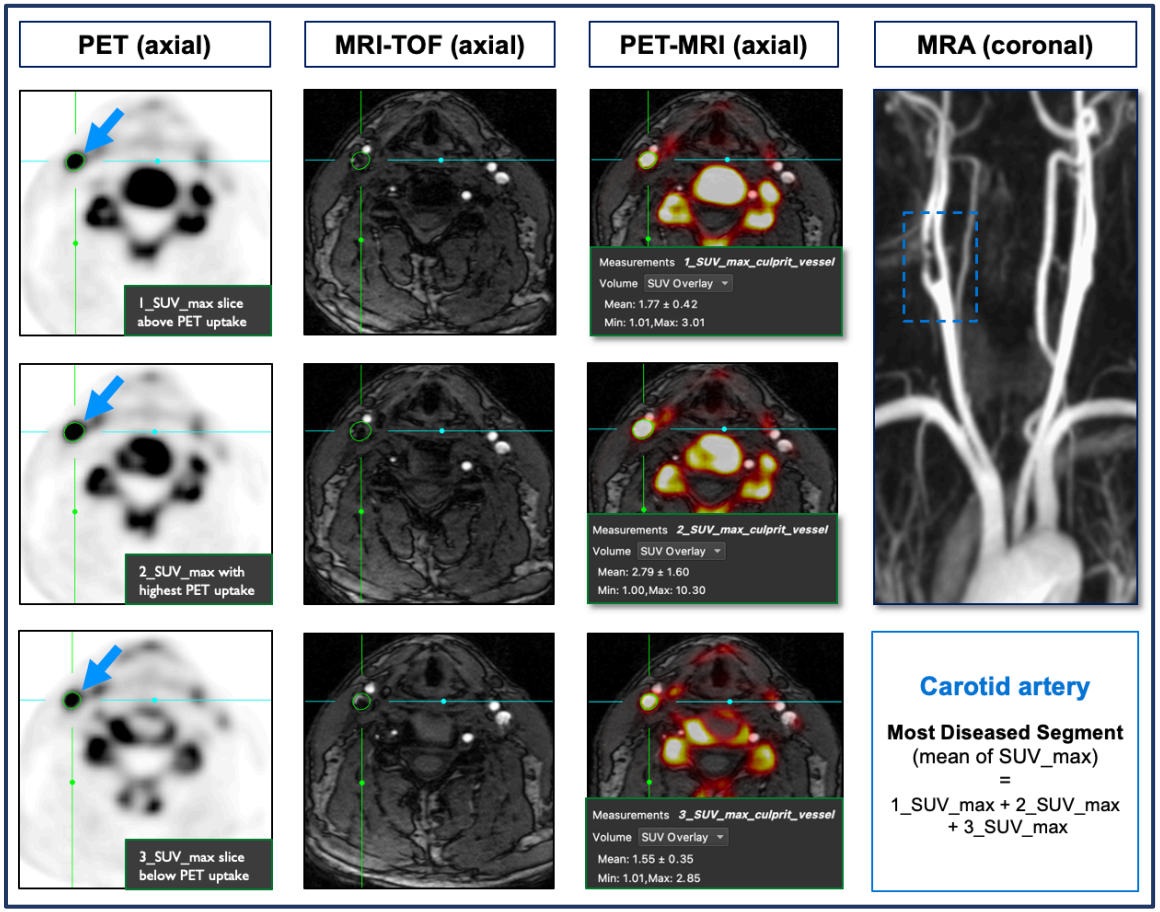


Dedicated Head & Neck coil on the table (purple arrow) and lightweight Chest coil (orange arrow).

2.5.3 HYBRID ^{18}F-NaF PET-MRI - PET IMAGE ANALYSIS

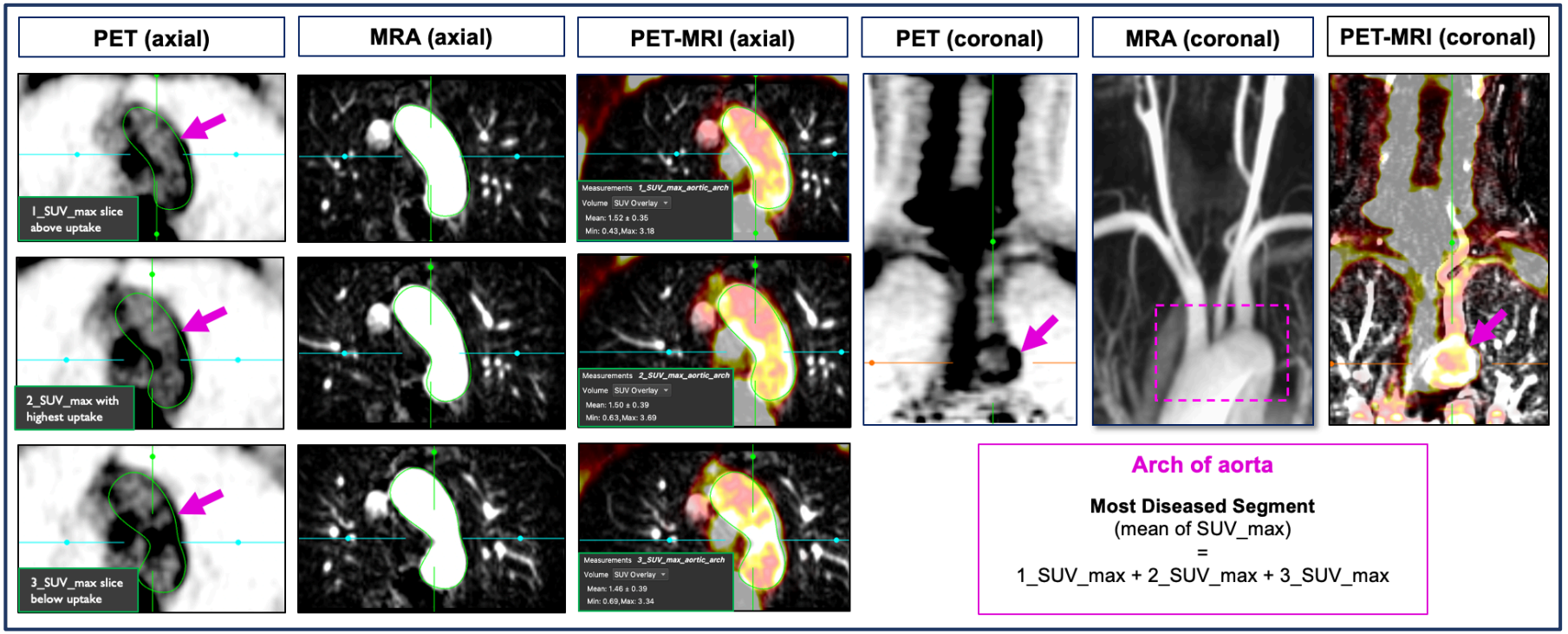
Analysis of ^{18}F-NaF uptake was performed using dedicated image processing software (FusionQuant, Ceders Sinai Medical Centre, United States of America). PET and TOF or magnetic resonance angiography images were fused and co-registered in 3 orthogonal planes. ^{18}F-NaF uptake was measured in a spherical volume of interest centred on the region of most severe carotid stenosis . To quantify ^{18}F-NaF arterial uptake, we used the mean and maximum standardized uptake values (SUV_{mean} and SUV_{max}) of the most diseased segment in the culprit carotid artery (Figure 2.7) compared to the contralateral non-culprit carotid artery and atherosclerotic aortic arch circulation (Figure 2.8) for our primary imaging endpoint [Vesey et al., 2017; Tawakol et al., 2013]. The most diseased segment was derived from the averaged SUV_{mean} and SUV_{max} across three sequential regions of interest centred on the slice with the highest radiotracer activity as described previously [Tawakol et al., 2013]. Background blood pool ^{18}F-NaF activity was measured in 3 regions of interest (area 0.5 cm^3) centred within the brachiocephalic or internal jugular vein as available. Mean and maximum target to background ratio (TBR_{mean} and TBR_{max}) were calculated by dividing the mean or maximum standardised uptake value in the carotid by the background activity. Based on our previous work [Vesey et al., 2017], cut-off values to determine a high TBR_{mean} and TBR_{max} were selected. Values above the 95% confidence interval of controls with carotid atheroma but no history of stroke were considered high (TBR_{mean} >1.95 and TBR_{max} >2.48).

Figure 2.7: Most Diseased Segment method in carotid circulation.



Most Diseased Segment (blue box) was derived from the mean SUV_{max} values across three sequential regions of interest within carotid artery (blue arrows). PET: Positron Emission Tomography; PET-MRI: Positron Emission Tomography-Magnetic Resonance Imaging; MRA: Magnetic Resonance Angiography; SUV: Standardised Uptake Value.

Figure 2.8: Most Diseased Segment method in aortic circulation.



Most Diseased Segment (pink box) was obtained from the mean SUV_{max} values across three consecutive regions of interest within arch of the aorta (pink arrows). PET: Positron Emission Tomography; PET-MRI: Positron Emission Tomography-Magnetic Resonance Imaging; SUV: Standardised Uptake Value.

2.5.4 HYBRID ^{18}F-NaF PET-MRI - MRI IMAGE ANALYSIS

Visual analysis of carotid plaques was performed using Carestream Vue Picture Archiving and Communication System (version 11, Carestream, US). According to previously published criteria, different signal intensities that were detected on T1, T2, PD and TOF sequences allowed for the differentiation of the various plaque components such as intraplaque haemorrhage, lipid core, calcification, thrombus, fibrosis and ulceration (Table 2.1) [Ota et al., 2009; Briley-Saebo et al., 2007; Yuan et al., 2001a; Cai et al., 2002; Saam et al., 2005]. The sternocleidomastoid muscle was used as a reference point when assessing signal intensities from the carotid tissue. A semiquantitative 3-point MRI scoring system was used to assess components of the carotid plaque: 0-none; 1- moderate (<50% of plaque area), and 2 severe (>50% of plaque area).

Table 2.1: MRI signals intensities.

Plaque features	MRI signal intensities			
	T1	**T2**	**PD**	**TOF**
Intraplaque haemorrhage				
▪ **fresh**	high	iso	iso	high
▪ **recent**	high	high	high	high
Necrotic lipid core	high	iso	high	iso
Calcification	low	low	low	low
Thrombus	high	high/low	high	high
Fibrosis	iso	iso	iso	low
Ulcer	*	*	*	*

Different MRI signals intensities of main carotid plaque components; **high** indicates hyperintense signal; **iso** indicates isointense signal; **low** indicates hypointense signal to reference tissue and ***** ulceration was identified as a surface defect on all images.

2.6 EX-VIVO IMAGING

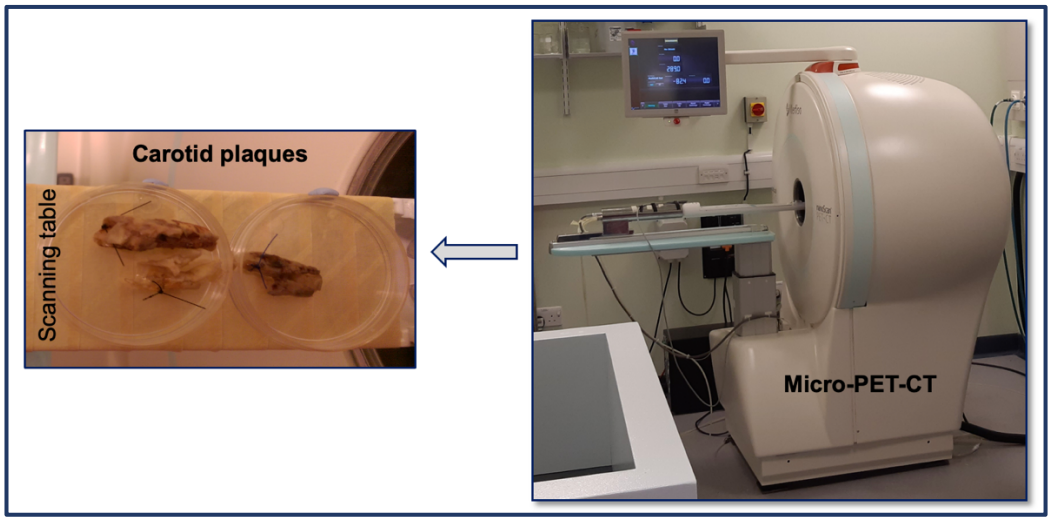
2.6.1 CAROTID PLAQUES

At the time of surgery, carotid plaques were collected from the recruited participants , following written consent. Once carotid endarterectomy was performed, an excised carotid plaque was collected with preservation of lesion integrity and geometry. All specimens were photographed to permit macroscopic assessment by independent and blinded reviewers. Subsequently, carotid plaques were fixed in 10% formaldehyde, and all tissue samples were stored in line with the local regulations.

2.6.2 *EX VIVO* MICRO-POSITRON EMISSION TOMOGRAPHY-COMPUTED TOMOGRAPHY

Carotid plaques were incubated in approximately 100 kBq/mL of ^{18}F-NaF for 30 minutes at 37°C. After incubation, specimens were washed with phosphate-buffered saline and were subsequently stored in a humid environment during the microPET-CT imaging procedure to prevent dehydration. Specimens were imaged using high-resolution (0.5mm) micro-PET-CT (NanoScan PET-CT, Medisco, Budapest, Hungary) (Figure 2.9). At first CT scan was acquired (semi-circular full trajectory, maximum field of view, 480 projections, 50kVp and 1:4 binning) followed by the microPET imaging (3D, list mode, 30 minutes). PET images were reconstructed using 3D Tera-Tomo (4 iterative methods) reconstruction algorithm, including correction for random scatter and attenuation. Regions of regions interest were drawn manually around the carotid plaques' contours and mapped to corresponding fused PET-CT images to measure concentrations of ^{18}F-NaF.

Figure: 2.9: *Ex vivo* micro-PET-CT scan of carotid plaques.



All specimens were marked with a suture at the common carotid artery end to ensure consistent orientation. *Ex vivo* micro-PET-CT: *Ex vivo* micro-Positron Emission Tomography-Computed Tomography.

2.6.3 *EX VIVO* MAGNETIC RESONANSE IMAGING

Carotid plaques were transferred from 10% formaldehyde to phosphate-buffered saline at least 24h before scanning in MRI. Carotid plaques were placed in sample tubes compatible with MRI scanner. Care was taken to remove air bubbles from the sample tubes and retain orientation in the carotid artery axis. Next, imaging was performed on a Varian 7 Tesla (Figure 2.10) horizontal bore MRI system equipped with a 60 mm bore gradient insert (Agilent Technologies, Yarnton, UK, maximum gradient strength 1000 mT/m) or a 140 mm gradient insert (Bruker Biospin, GmbH, Germany, 660 mT/m). All tissue samples were scanned using the same MRI magnet, gradient insert and RF coils. However, due to scanner upgrade, some samples were scanned using different software (Biospec AVANCE neo preclinical imaging system, running Paravision 360, Bruker BioSpin GmbH, Germany). Depending on sample size, variable quadrature volume coil (26 mm, 39 mm or 86 mm) was used for signal transmission and reception (Rapid Biomedical GmbH, Rimpar, Germany or Bruker Biospin GmbH, Germany). Scout images were taken to confirm correct positioning, and the magnetic field was optimised using automated shim routine.

Figure 2.10: *Ex vivo* Varian 7 Tesla MRI scanner.



Ex vivo MRI: *Ex vivo* Magnetic resonance imaging.

Subsequently, 40-50 slices were obtained using the following parameters for all sequences producing: the field of view 19.2 × 19.2 mm (larger for bigger samples), the acquisition matrix 192 × 192 and the slice thickness 0.5 mm. TR and TE varied slightly with the different set-ups used (Table 2.2). For T1W, T2 and PD scans, a fast spin-echo (FSE) protocol was used with an echo train length of 4 T1W or 8 T2W and PD. Thirty-two to sixty-four signal averages were acquired. For T2*-weighted (T2*W) scans, a gradient echo sequence was used with a flip angle of 20° and 32 signal averages.

Table 2.2: MRI scan parameters.

Scan	Type	TR (ms)	TE (ms)	ETL	FA (°)
T1W	FSE	740 - 1340	5.6 – 7.4	4	90-180
T2W	FSE	3000	5.6 – 9.4	8	90-180
PD	FSE	3000	35 - 37	8	90-180
T2*W	Gradient echo	400	3.6 – 4.5	-	20

T1W: T1-weighted; T2W: T2-weighted; PD: Proton Density; T2*W: T2*-weighted; FSE: Fast Spin Echo; TR: repetition time; TE: echo time; ETL: Echo Trian Length; FA: Flip Angle.

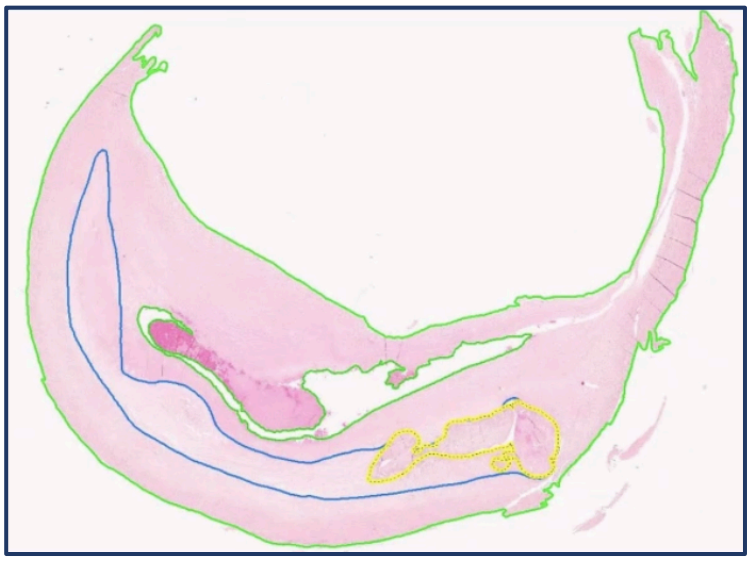
2.7 HISTOPATHOLOGY

All carotid samples were evaluated by histology, immunohistochemistry, and micro-computed tomography (micro-CT). To correct for carotid tissue shrinkage and sample division, the individual carotid plaque components were defined relative to the total plaque area and recorded as '*index* = number of positive plaque component/total plaque area mm^2' (Figure 2.11). An algorithm was used to isolate and quantify elastic fibres and intraplaque haemorrhage (red blood cells and fibrin) (Figure 2.12). Histopathological analysis was performed by a cardiovascular pathologist blinded to patient demographics, clinical history, and imaging.

The following histological stains were performed:

- Haematoxylin and eosin (general morphological analysis)
- Movat's Pentachrome (fibrosis and elastic fibres)
- Martius Scarlet Blue (red stain- fibrin)
- Martius Scarlet Blue (yellow stain-red blood cells)
- Prussian Blue (blue stain- iron (Fe^{3+})

Figure 2.11. Plaque components analysis.



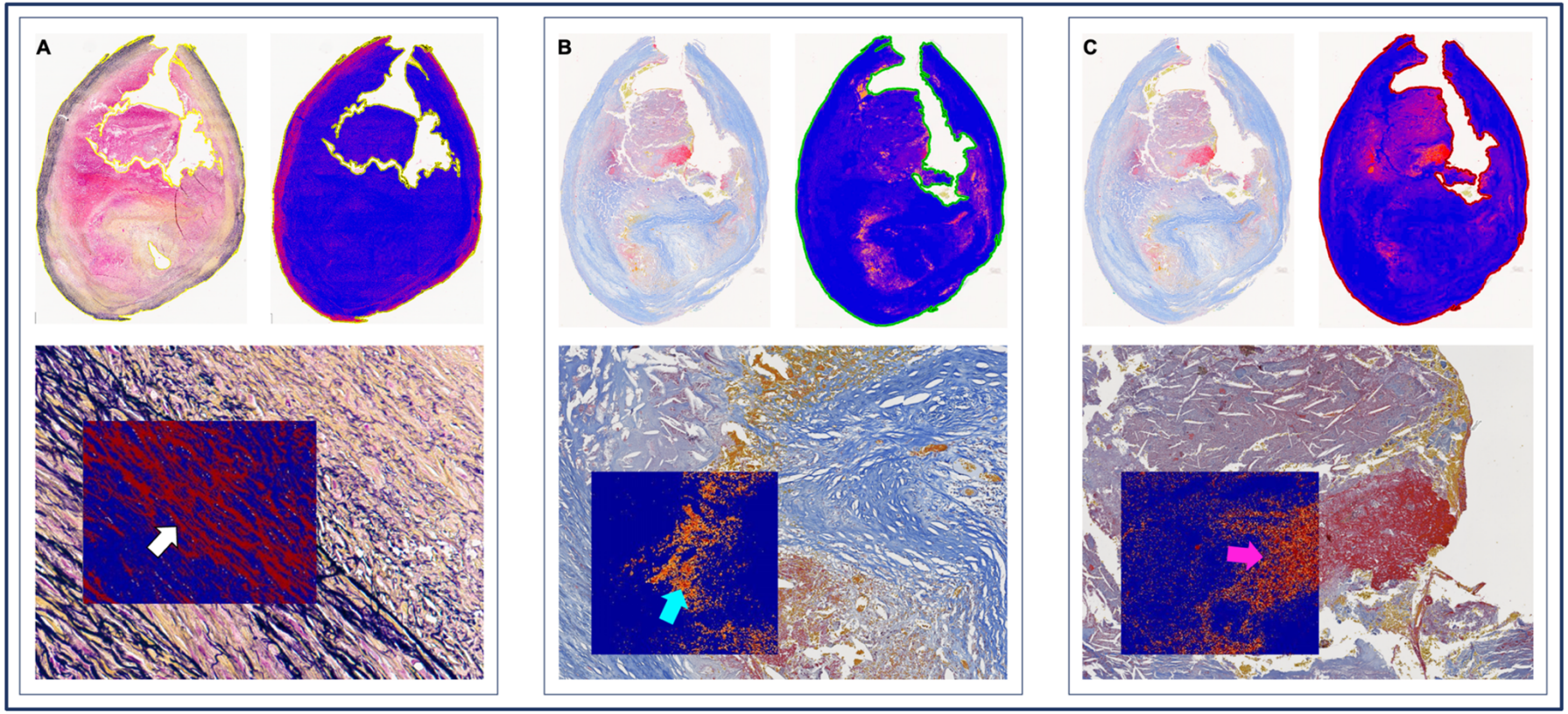
Manual segmentation of plaque components:

- Blue: necrotic lipid core
- Yellow: calcium
- Green: total area

All carotid samples were transversely bisected in regions of plaque (Figure 2.13). One half was decalcified in Cal-Ex II (Fisher scientific, CS511) and then processed for subsequent histology with immunohistochemistry. Immediately prior to embedding, the specimen was cut into approximately 2 mm pieces to facilitate transverse orientation in the block. Following embedding, histologic sections were generated and stained with hematoxylin and eosin (H&E) and Movat's pentachrome stains.

Slides were evaluated for histological features of atherosclerotic plaque, as described in Table 2.3, by a subspecialty cardiovascular pathologist blinded to patient demographics and history on Haematoxylin and Eosin, and Movat's Pentachrome staining. These features were characterised according to criteria used in the Oxford Plaque Study [Lovett et al., 2004a; Redgrave et al., 2006; Lovett et al., 2004b] and in the Athero-Express study [Verhoeven et al., 2004] (Table 2.3), and aggregated into four plaque phenotypes (Table 2.4) using a weighted scoring system for the various plaque features confirming progressively greater "severity" phenotypes from A through to D. The pathologist was blinded to clinical characteristics and imaging findings and confirmed a consistent clustering of the four phenotypes (Figure 2.14). In all cases, images were generated using an Aperio Slide Scanner using Image Scope software (Leica Biosystems, Germany).

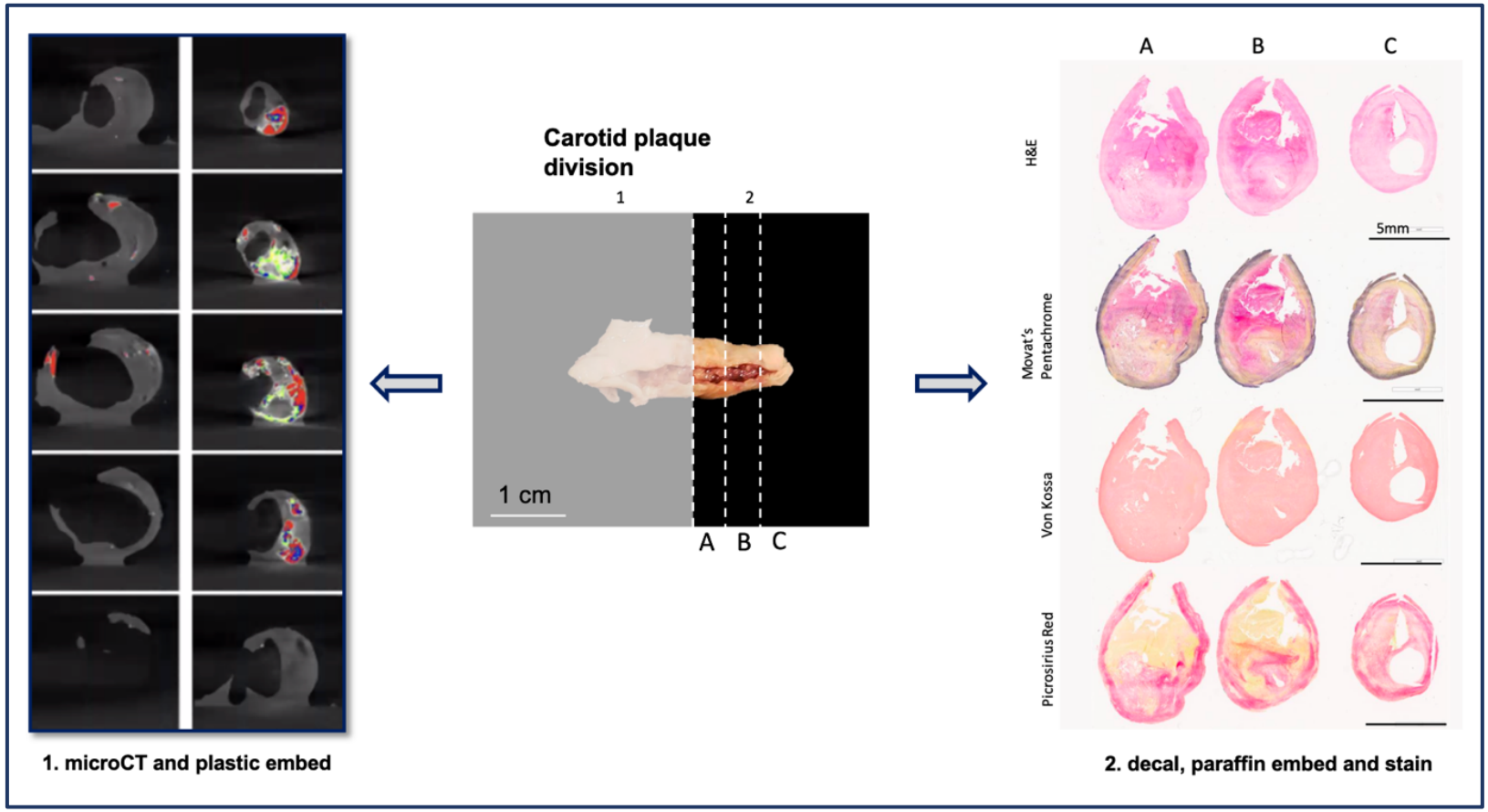
Figure 2.12: Quantification of elastic fibres and intraplaque haemorrhage (red blood cells and fibrin).



An algorithm using different saturation values to isolate and quantify plaque components:

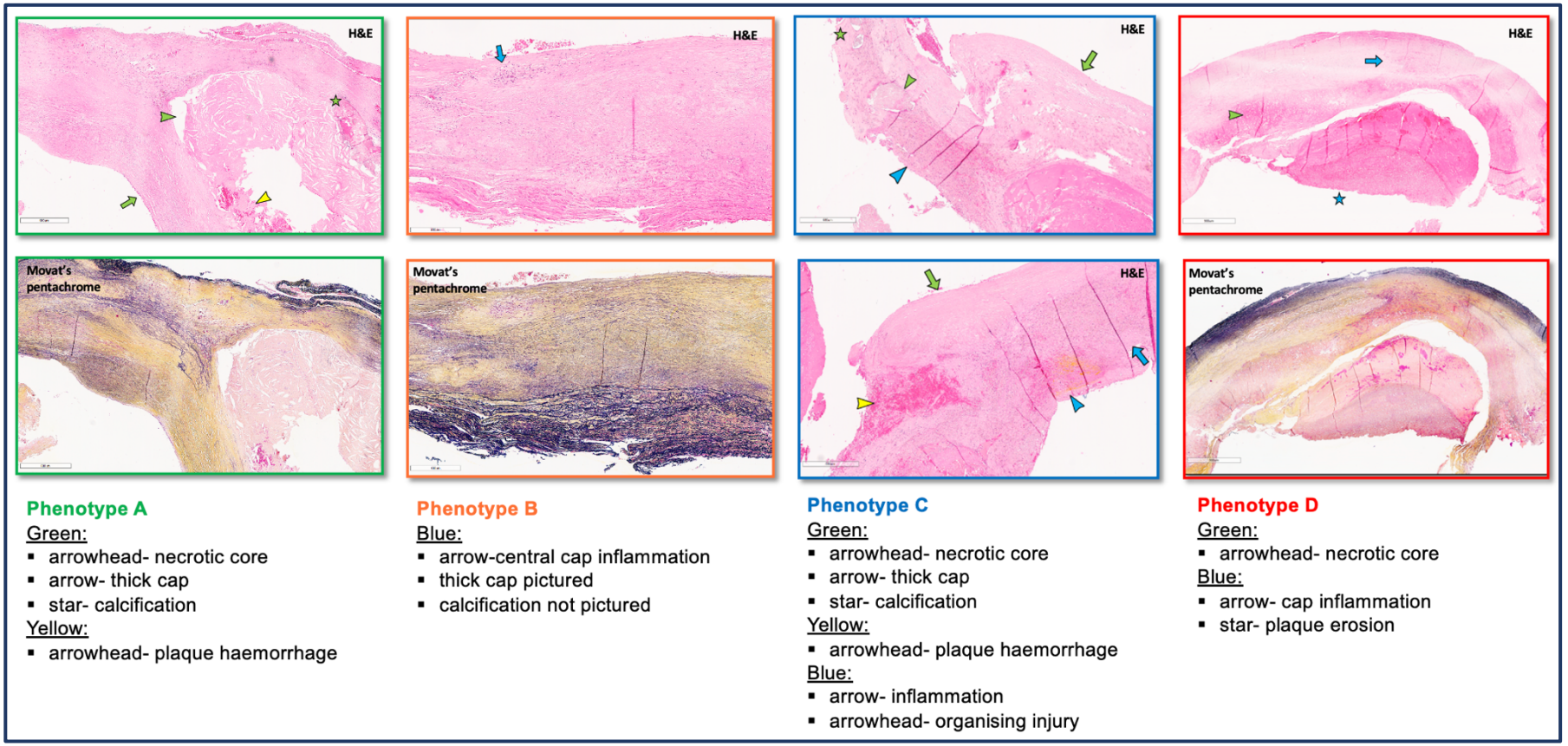
- **A**: Movat's Pentachrome - positively expressed elastin fibres (white arrow)
- **B**: Martius Scarlet Blue (yellow stain) - red blood cells (turquoise arrow)
- **C**: Martius Scarlet Blue (red stain) - fibrin (pink arrow)

Figure 2.13: Division of carotid plaques.



Part 1 of carotid plaque underwent plastic embedding and microCT.
Part 2 of the specimen was decalcified, imbedded in paraffin, and processed histologically.

Figure 2.14: Histological carotid plaques phenotypes (A-D).



Representative images of each phenotype with increasing severity from phenotype A to phenotype D.

Table 2.3: Features of atherosclerotic plaque evaluated in carotid study including weighting in the scoring system and comparison to previous studies.

This carotid study	Levels	Weighting	Oxford Plaque Study	Athero-Express
Calcification	▪ absent (0) ▪ present (+1)	2	included	included
Thin cap	▪ absent (0) ▪ present (+1)	1	included	included
Lipid core and/or necrotic core	▪ absent (0) ▪ present (+1)	1	included, plus foam cells	included, plus lipid distribution
Thrombus and/or Hemorrhage	▪ absent (0) ▪ less than 20% (+1) ▪ more than 20% (+2)	1	included	included
Cap Inflammation	▪ absent (0) ▪ present (+1)	1	included, with subset analysis	included, with subset analysis
Plaque Erosion and/or Rupture	▪ absent (0) ▪ present (+1)	2	included	included
Not assessed	▪ n/a	n/a	smooth muscle, vascularity	smooth muscle

Table 2.4: Carotid plaques phenotypes (A-D).

Phenotype	Description
A	< 4 criteria from Table 2.3, uninflamed, thick cap
B	< 4 criteria from Table 2.3, inflamed, thick cap
C	≥ 4 criteria from Table 2.3
D	plaque erosion and/or rupture

Summary phenotypes derived from features and weighting described in Table 2.3.

2.7.1 IMMUNOHISTOCHEMISTRY

Immunohistochemistry was completed using:

- Osteopontin (bone formation and mineralisation)
- Runt-related transcription factor 2 (Runx2) (osteoblastic calcification and mineralisation on smooth muscle cells)
- Caspase 3 (cell apoptosis)

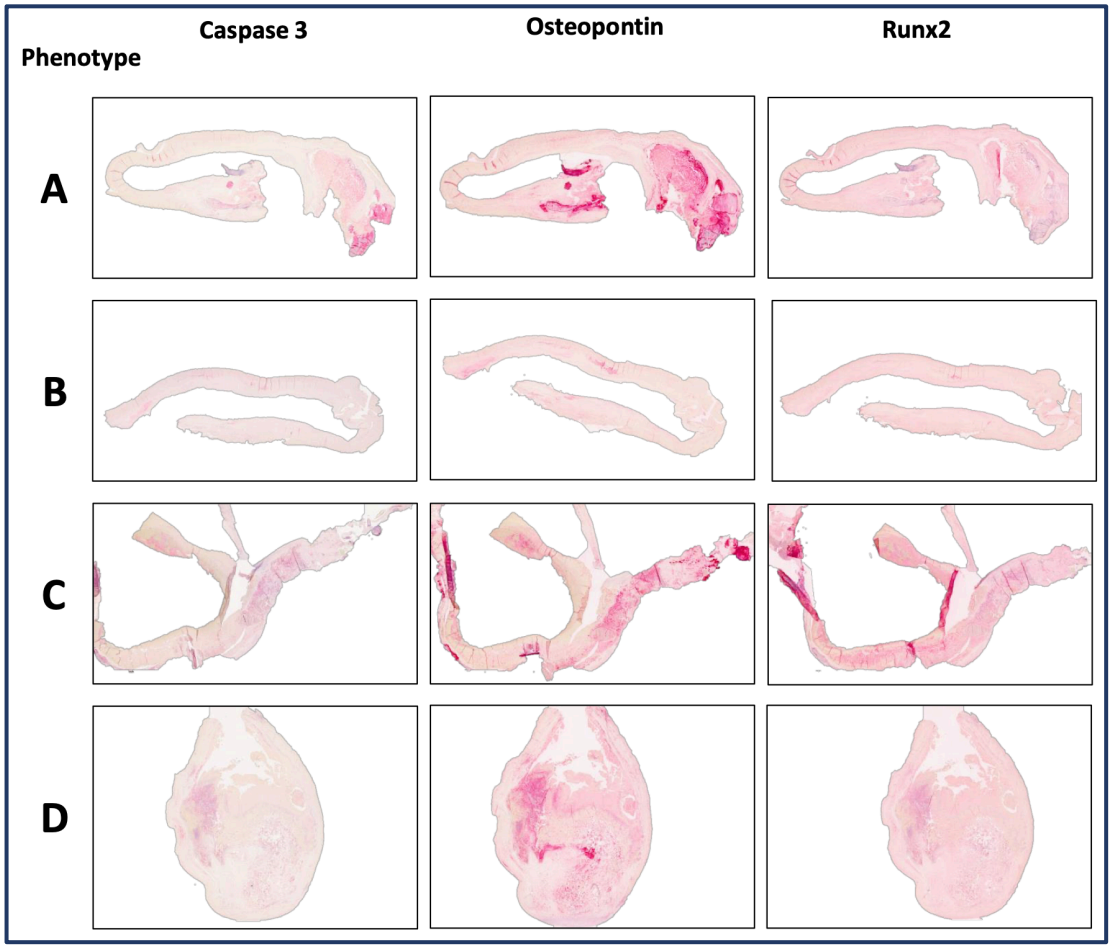
Immunohistochemistry was performed on the selected carotid samples to match the tissue pathology (Figure 2.15). Scoring was completed from high-resolution slide scans. Immunohistochemistry was completed using OPN (osteopontin; catalog No. 07264; 1:100 dilution; Sigma-Aldrich), cleaved Caspase 3 (No. 9664; 1:100 dilution; Cell Signaling), and RUNX2 (Abcam Catalog No: Ab76956, 1:50 dilution). Staining was performed via automated staining with a Leica Bond Rx system using Bond Epitope Retrieval Solution 1 (pH=6, catalog No. AR9961) for Caspase-3, Runx2, and Osteopontin. Background staining was assessed via assessment of sections processed with the omission of primary antibody.

2.8 STATISTICAL ANALYSIS

Baseline characteristics were reported as numbers (percentage) for categorical variables and as mean±standard deviation or median [interquartile range] for continuous variables, as appropriate. Shapiro-Wilk's normality test was used, and skewed datasets were log-transformed (log_{10}) to normalize their distribution when $p< 0.05$. Categorical data were compared using Chi-squared and Fisher's exact tests. Parametric (paired and unpaired *t*-tests) were used for normally distributed data. One-way analysis of variance (ANOVA) was used to compare continuous data across multiple groups, with post hoc analysis using Tukey's test. To quantify intra-observer repeatability and reproducibility of imaging measurements in the transcranial Doppler study, the intra-class correlation co-efficient (ICC) was calculated and Bland-Altman analysis undertaken. In the carotid study, a simple linear logistic regression model was

used to analyse the correlation between radiotracer uptake and MRI-derived plaque features. The correlation was undertaken with either Pearson's or Spearman's as appropriate. To evaluate image-based diagnostic accuracy, the Gwet's AC1 agreement coefficient was calculated and categorised as poor <0.40, good 0.40-0.75, and excellent >0.75 [Dettori et al., 2020; Wongpakaran et al., 2013; Cibulka et al., 2021] Statistical significance was taken as a two-sided 5% level ($p<0.05$). Statistical analysis was undertaken using RStudio Team (2016). RStudio: Integrated Development for R. RStudio, Inc., Boston, MA URL (www. rstudio.com) or with the use of IBM SPSS Statistics for Mac, version 23 (Armonk, New York, IBM Corp, USA).

Figure 2.15: Immunohistochemistry of carotid plaques phenotypes (A-D).



CHAPTER THREE

REPRODUCIBILITY STUDY OF TRANSCRANIAL DOPPLER ULTRASOUND IN THE MIDDLE CEREBRAL ARTERY

3.1 INTRODUCTION

Ischaemic stroke remains a major global cause of disability and death that is associated with an enormous social and economic burden [Naylor, 2015b]. Up to 25% of ischaemic strokes are caused by atherosclerosis of the internal carotid artery [Vavra et al., 2015; Naylor et al., 2018]. Carotid atherosclerosis is a complex disease that is characterised by the deposition of luminal atheroma that may rupture, thrombose and embolise [Vavra et al., 2015]. The resulting thromboembolism can lead to a stroke or transient ischaemic attack (TIA) [Valton et al., 1998]. Transcranial Doppler is a well established real-time imaging modality that evaluates cerebral blood flow velocity and detects microembolic signals in patients who suffer from cerebral or retinal ischaemia [Totaro et al., 1992]. Microembolic signals in symptomatic carotid artery stenosis are associated with an increased risk of a recurrent ipsilateral focal ischaemia [Markus, 1993; Grotta et al., 2001; Lennard et al., 1997a; Abbott et al., 2005; Markus et al., 1997; Markus et al., 2005; Imray et al., 2005; Spence, 2017; Abbott et al., 2007b] and correlate with a greater number of magnetic resonance imaging detectable cerebral infarcts when compared with patients free from microembolism [Sarkar et al., 2007; Kimura et al., 2001; Wolf et al., 2004b; Babikian et al., 2000]. The intraoperative transcranial Doppler has enabled clinicians to lower the rate of the most serious post carotid endarterectomy complication such as thromboembolic stroke from 4% to 0.2% through detection of the middle cerebral artery flow cessation due to the intraluminal carotid artery thrombosis [Lennard et al., 1999a; Naylor et al., 2000]. Whereas transcranial Doppler directed infusion of Dextran 40 has in some centres successfully erased the rate of postoperative thromboembolic cerebral ischaemia from 2.7% to 0% [Lennard et al., 1997b; Lennard et al., 2003]. Despite these benefits from transcranial Doppler, routine use has not been advocated amongst vascular specialists.

Although multiple studies have been conducted on flow velocities in basal cerebral arteries in both healthy volunteers and patients [Demirkaya et al.,

2008; Aaslid et al., 1982] reproducibility data are limited to a hand full of reports. These include four articles involving healthy subjects [Maeda et al., 1990; McMahon et al., 2007; Shen et al., 1999; Baumgartner et al., 1994] and one study that recruited patients with clinical diagnosis of ischaemic stroke (n=3) or TIA (n=7) but provided no information regarding the clinical type of neurovascular event or underlying carotid artery stenosis [Totaro et al., 1992]. In contrast, published data on microembolic signals detection in patients with symptomatic carotid artery stenosis includes systematic reviews, meta-analyses [Best et al., 2016; King et al., 2009a; Ritter et al., 2008a; Udesh et al., 2017] international multicenter reproducibility studies that have described the reproducibility of transcranial Doppler as sufficient for clinical use [Markus et al., 1997; Markus et al., 1996; Cullinane et al., 2000].

Our objective was to assess the intra-observer repeatability and reproducibility of transcranial Doppler for velocimetry measurements and microemboli detection in healthy volunteers and patients with symptomatic carotid artery stenosis that could form the basis for our future study investigating reliable identification of a vulnerable carotid plaque.

3.2 METHODS

3.2.1 STUDY DESIGN

This was an observational investigative study. The study was approved by the local Research Ethics Committee (16/SS/0217), and written consent was obtained from all participants. The research protocol is available on ClinicalTrial.gov (ID NCT 03050567).

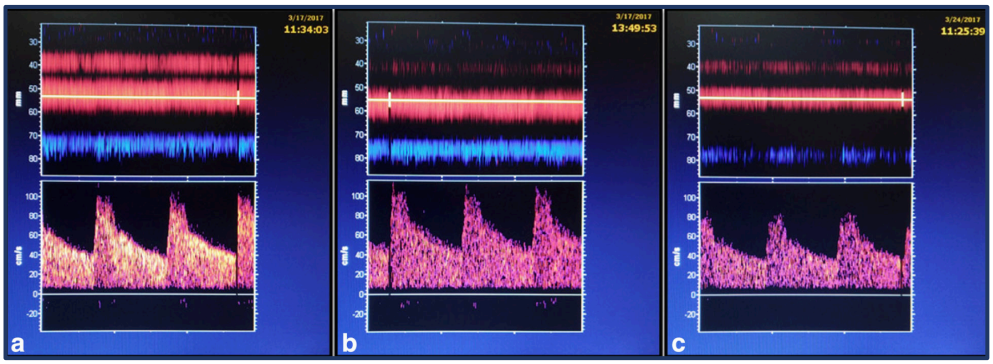
3.2.2 STUDY POPULATION

Cohorts (n=20 per cohort) of healthy volunteers and patients with symptomatic carotid artery stenosis were recruited between March-August 2017. Among the patient group, five patients that were excluded due to an absent temporal window, were subsequently replaced. Healthy volunteers were >18 years old and had no previous history of cerebrovascular disease. Patients with evidence of an acute neurovascular syndrome (stroke, TIA, retinal ischaemia) due to carotid artery disease were recruited from the acute neurovascular clinics at Edinburgh Royal Infirmary within a maximum of 14 days of symptom onset. The inclusion criteria were the symptomatic cerebrovascular event (stroke, TIA or amaurosis fugax) and radiological confirmation of carotid artery stenosis of > 30%. This included patients scheduled for carotid endarterectomy (>50% for men and >70% for women, by North American Symptomatic Carotid Endarterectomy Trial criteria) or treated conservatively with an optimal medical therapy (if patient declined surgical intervention or is outside surgical criteria for carotid endarterectomy) [Naylor et al., 2018].

3.2.3 STUDY PROTOCOL

All subjects underwent clinical evaluation prior to participation. In the patient group, this included assessment of relevant carotid Doppler ultrasound and brain imaging investigations (computed tomography or magnetic resonance imaging). In both cohorts, three 1-hour transcranial Doppler measurements were performed by the same examiner over two study visits. During the first study visit, two examinations were performed separated by 1 hour (Figure 3.1). The final (third) examination was obtained on a separate study visit within 14 days of the first examination (Figure 3.1).

Figure 3.1: Transcranial Doppler.



Three transcranial Doppler examinations of the same participant: (visit 1: images A and B; visit 2: image C).

3.2.4 TRANSCRANIAL DOPPLER

The middle cerebral artery was identified through the temporal window and the sample volume adjusted to obtain a stable visually and acoustically optimal signal. In healthy subjects, the side of the middle cerebral artery insonation was randomly allocated. In patients with symptomatic carotid artery stenosis, transcranial Doppler was performed on the symptomatic middle cerebral artery (ipsilateral to the index event). A head frame (Marc 600 Spencer Technologies, United States of America) was fitted to reduce motion and to secure a constant angle of the middle cerebral artery insonation depth at 40-65 mm from the skull surface. All recordings were made using the ST^3 Transcranial Doppler Ultrasound System (Spencer Technologies, United States of America) with a 2-MHz transducer. Emboli were identified using characteristic short audible sound (range 10-100 ms, intensity threshold above 7 dB) and spectral appearance using the International Consensus Group microembolus identification criteria and assisted by an automated Embolus Detection Software (Spencer Technologies, United States of America) [Ringelstein et al., 1998]. The Doppler wave forms were reassessed to exclude artefact and confirm the presence of true emboli. The mean of maximal, mean and end-diastolic flow velocities were determined from the mean of measurements obtained over ten cardiac cycles.

3.2.5 STATISTICAL ANALYSIS

Continuous variables were expressed as mean ± standard deviation for normally distributed data, and categorical variables were expressed as total and percentage. To quantify intra-observer repeatability and reproducibility of imaging measurements, the intra-class correlation coefficient (ICC) was calculated and Bland-Altman analysis undertaken. Statistical significance was taken as a two-sided $P<0.05$. Statistical analyses were performed with the use of IBM SPSS Statistics for Mac, version 23 (Armonk, New York, IBM Corp, USA).

3.3 RESULTS

All participants tolerated transcranial Doppler examinations well and completed all assessments.

3.3.1 HEALTHY VOLUNTEERS

In total, 60 transcranial Doppler assessments were performed on 20 healthy volunteers who had a mean age of 31±9 years, and 11 were male. All subjects had the temporal window available, and the mean middle cerebral artery insonation depth was 51 mm (Table 3.1) with peak velocities averaging around 70-85 cm/s (Table 3.1).

Table 3.1: Summary of the middle cerebral artery blood flow velocity and insonation depth in healthy volunteers and patients.

Healthy Volunteers			
Velocity (cm/s)	Examination 1	Examination 2	Examination 3
Peak	75.70±23.91	72.00±20.28	82.75±19.93
Mean	49.95±15.30	47.05±12.85	52.60±11.73
Diastolic	34.70±11.28	29.50±10.65	35.45±8.40
MCA depth (mm)	51.75±2.65	51.75±2.94	51.20±2.93
Patients			
Velocity (cm/s)	Examination 1	Examination 2	Examination 3
Peak	73.70±18.94	73.10±16.62	71.20±17.62
Mean	45.40±11.79	45.20±10.83	43.50±9.96
Diastolic	27.30±8.90	27.10±8.14	25.60±6.57
MCA depth (mm)	51.40±5.33	51.55±5.21	51.65±5.24

Data are presented as mean ± standard deviation. MCA, middle cerebral artery.

Overall, the ICC for both repeatability and reproducibility in healthy volunteers group revealed a good reliability (ICC 0.75-0.90) with wider confidence intervals obtained for the peak and mean reproducibility values when compared with the repeatability measurements (Table 3.2).

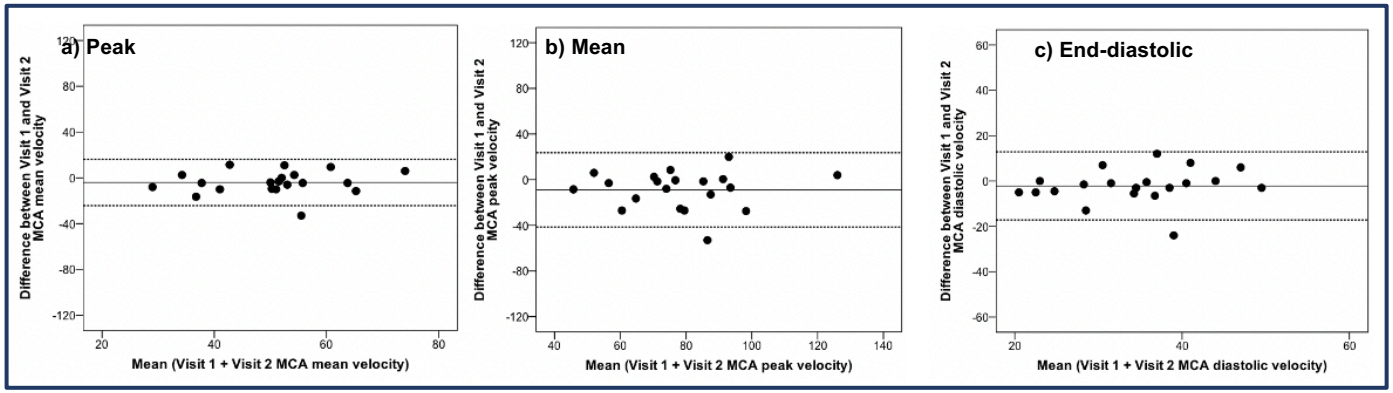
Table 3.2. Summary of ICC velocity values for repeatability and reproducibility assessments in healthy volunteers and patients.

Healthy Volunteers		
Repeatability (Exam 1 vs Exam 2)	ICC	95% CI
Peak	0.88	0.726-0.950
Mean	0.867	0.700-0.945
End-diastolic	0.887	0.741-0.953
Reproducibility (Visit 1 vs Visit 2)	ICC	95% CI
Peak	0.777	0.526-0.905
Mean	0.795	0.558-0.913
End-diastolic	0.674	0.349-0.856
Patients		
Repeatability (Exam 1 vs Exam 2)	ICC	95% CI
Peak	0.926	0.826-0.970
Mean	0.922	0.817-0.968
End-diastolic	0.868	0.701-0.945
Reproducibility (Visit 1 vs Visit 2)	ICC	95% CI
Peak	0.8	0.567-0.915
Mean	0.786	0.542-0.909
End-diastolic	0.778	0.527-0.905

Data are reported as mean with 95% limits of agreement for assessments.

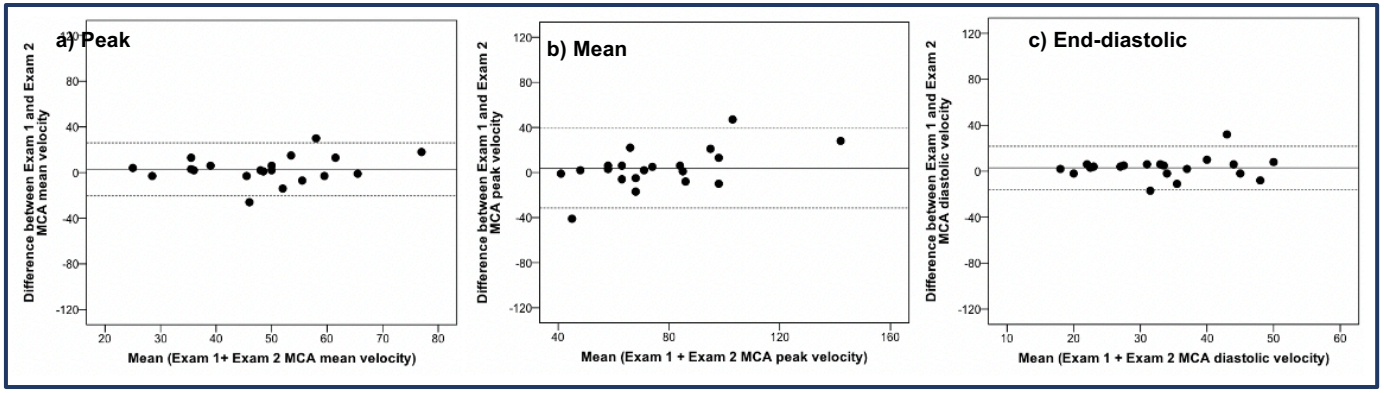
An intra-observer Bland Altman analysis demonstrated acceptable mean measurement differences and limits of agreement between series of middle cerebral artery velocity measurements with very few outliers (Figure 3.2 and Figure 3.3). As expected, no microembolic signals were detected.

Figure 3.2: Transcranial Doppler.



Reproducibility in healthy volunteers (visit 1 vs Visit 2): Bland Altman analysis for middle cerebral artery velocity.

Figure 3.3: Transcranial Doppler.



Repeatability in health volunteers (Examination 1 vs Examination 2): Bland Altman analysis for middle cerebral artery velocity.

3.3.2 PATIENTS

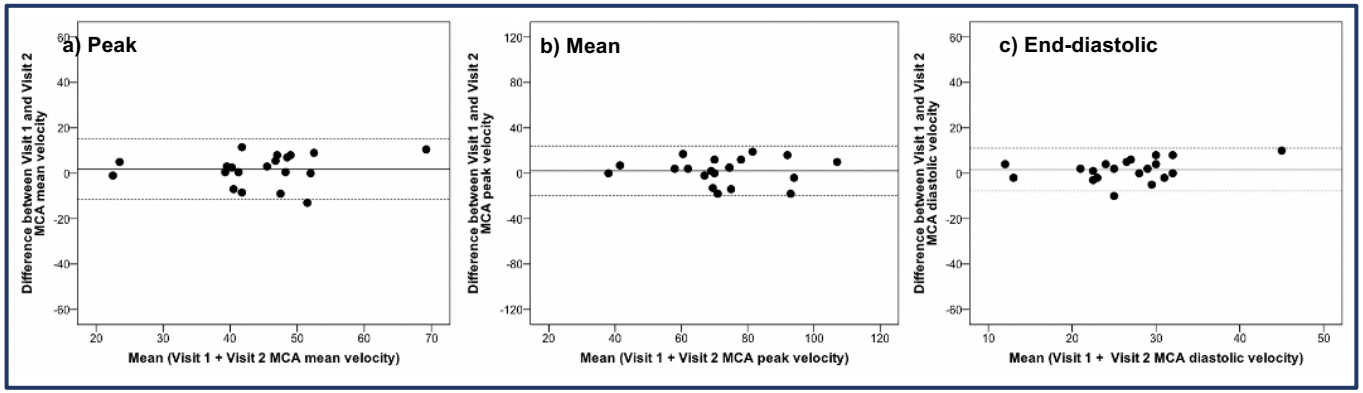
Patients had a mean age of 72±11 years, and 11 were men (Table 3.3). Presenting diagnosis included 18 transient ischaemic attacks (11 cerebral, 7 ocular) and 2 cases of ischaemic stroke. The degree of stenoses measured by Duplex ultrasound scan were: 30-40% (n=9), 40-50% (n=6), 50-70% (n=3) and >70% (n=2). Five patients (4 females, 1 male) had an absent acoustic temporal window. The mean middle cerebral artery insonation depth was 51 mm (Table 3.1) and peak cerebral artery blood flow velocities were 70-75 cm/s (Table 3.1). The overall intra-observer ICC for repeatability and reproducibility displayed at least good (ICC 0.75-0.90) agreement that reached an excellent agreement (ICC> 0.90) for the peak and mean repeatability velocity values (Table 3.2). Similarly, wider confidence intervals were found for the peak and mean reproducibility values when compared with the repeatability assessments. The Bland Altman plots showed acceptable mean measurement differences and limits of agreement between series of middle cerebral artery velocity measurements with very few outliers (Figure 3.4 and 3.5). No microembolic signals were detected during transcranial Doppler assessments.

Table 3.3: Baseline characteristics of patients.

Characteristics	n (%) Total=20
Demographics	
Age, years	72±10.6
Male	11 (55)
Vital signs	
Systolic BP	146.6±27.3
Diastolic BP	77.4±11.0
Heart rate/min	70.15±14.89
Smoker status	
Current smoker	2 (10)
Former smoker	12 (60)
Never smoked	6 (30)
Presenting diagnosis	
Cerebral TIA	9 (45)
Ocular TIA	7 (35)
Stroke	2 (10)
Duplex scan severity of stenosis (%)	
30-40%	9 (45)
4-50%	6 (30)
50-70%	3 (15)
>70%	2 (10)
Duration between index event and 1st transcranial Doppler (days)	11.6±2.4
Relevant medical history	
Hypertension	15 (75)
Hypercholesterolemia	20 (100)
Diabetes Mellitus	3 (15)
Ischaemic Heart Disease	4 (20)
Peripheral Vascular Disease	1 (5)
TIA	4 (20)
Stroke	3 (15)
Chronic Obstructive Pulmonary Disease	3 (15)
Baseline medication therapy	
Antiplatelet (single agent)	18 (90)
Anticoagulant	2 (10)
Statin	20 (100)
Beta-blocker	4 (20)
Angiotensin-converting enzyme inhibitor	7 (35)

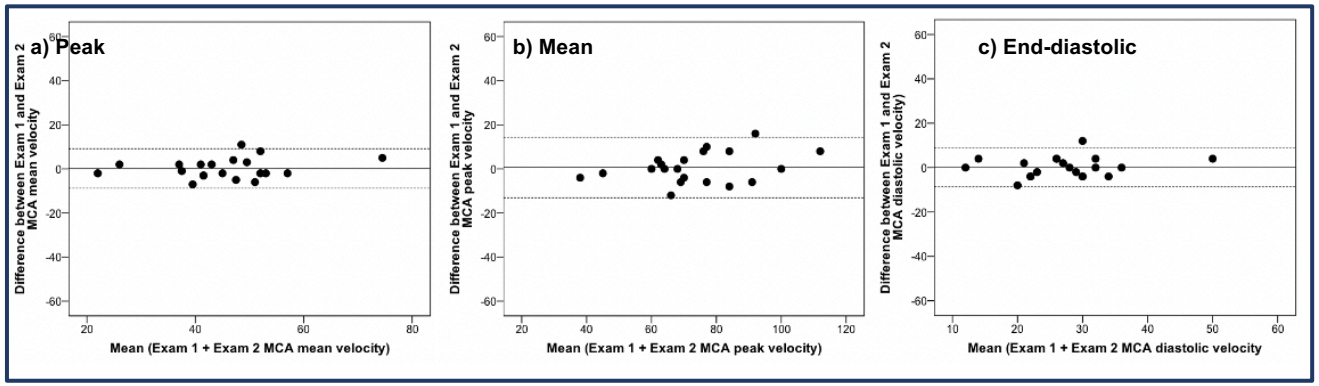
Data are presented as mean (standard deviation) or as percentage (%) where appropriate.

Figure 3.4: Transcranial Doppler.



Reproducibility in patients (visit 1 vs Visit 2): Bland Altman analysis for middle cerebral artery velocity.

Figure 3.5: Transcranial Doppler.



Repeatability in patients (visit 1 vs Visit 2): Bland Altman analysis for middle cerebral artery velocity.

3.4 DISCUSSION

In this study, we have demonstrated that transcranial Doppler generates reproducible data regarding the velocity measurements. Transcranial Doppler utilises an acoustic temporal bone window through which the ultrasound beam can focus on the middle cerebral artery, which receives 80% of an ipsilateral internal carotid artery inflow [Ringelstein et al., 1990]. The obtained middle cerebral artery insonation depth in both cohorts reflects published data [Markus et al., 1997; Alexandrov et al., 2012; Alexandrov et al., 2007]. In general, the success of transcranial Doppler imaging diminishes with an older age due to an increased temporal bone thickness that impairs the transmission of ultrasound waves through the skull [Itoh et al., 1993; Wijnhoud et al., 2008]. This has been observed primarily in approximately 10% of non-Caucasian elderly female participants [Markus, 2000b]. However, others report temporal window failure in almost third of examined subjects [Marinoni et al., 1997].

Multiple studies described substantially different normal reference velocity values of cerebral arteries blood flow [Demirkaya et al., 2008; Arnolds et al., 1986; Krejza et al., 1999; Ringelstein et al., 1990; Lindegaard et al., 1987; Grolimund et al., 1988] but the most frequently quoted normal middle cerebral artery velocity under resting condition ranges from 35-90 cm/sec with a mean of 60 cm/sec [Lindegaard et al., 1987]. Our velocity values mirror the results published by others, except for the lower mean diastolic middle cerebral artery velocity. However, this could be explained by various physiological and technical factors that can affect velocity readings. First, physiological cardiovascular changes such as heart rate, blood pressure, respiratory rate, arterial carbon dioxide tension alter middle cerebral artery blood flow on a daily basis [Stroobant et al., 2001; Vingerhoets et al., 1999]. Second, psychological factors (emotional state, fatigue) by influencing the above physiological cardiovascular autonomic responses can impact on the cerebral blood flow [Stroobant et al., 2001]. Unsurprisingly, changes in the cerebral metabolism due to cognitive activation also affect the middle cerebral artery blood flow.

Some authors demonstrated that arithmetic activity produced very similar values to the resting blood flow values, whereas higher levels of arithmetic difficulty produced smaller changes in the blood flow [Vingerhoets et al., 2002]. Therefore, the above factors could have potentially influenced the obtained velocity values.

The main technical aspect that can impact on velocity measurement is the angle of insonation that is obtained between the middle cerebral artery and ultrasound beam [Totaro et al., 1992; Maeda et al., 1990]. However, this is more relevant when large acoustic window such as the foramen of magnum is used, because it permits significant angle variation [Maeda et al., 1990]. Fortunately, small temporal window with a sharp angle of insonation (0°-30°) that is relatively stable minimises any influence on obtained velocities values [Totaro et al., 1992]. Hence, the maximum error has been estimated to be less than 15% [Maeda et al., 1990; McMahon et al., 2007]. Finally, individual variability of the middle cerebral artery size, length and tortuosity are also contributing to the scattering of the velocity measurements [Lindegaard et al., 1987; Baumgartner et al., 1994].

In general, cerebral flow velocity decreases with age in a bimodal pattern with a first decline above the age of 40 years and a further reduction above 60 years of age [Demirkaya et al., 2008; Hennerici et al., 1987; Ringelstein et al., 1990; Bragoni et al., 1996]. Unsurprisingly, our data demonstrate similar results with lower velocity values in patients cohort when compared with the healthy volunteers. Overall the obtained ICC values in our study represent a good repeatability and reproducibility in both cohorts. However, the peak and mean ICC repeatability values recorded in patients group reached an excellent agreement (ICC>0.90). In both cohorts, the peak and mean ICC reproducibility values decrease with wider confidence intervals when compared to the repeatability values. This likely reflects the combination of technical variation and biological variation which will be much greater when measurements are conducted on separate days rather than within a day. For example, this could

include probe displacement from the original middle cerebral artery segment that was sampled during the first study visit. This may also reflect the well described anatomical variability of the circle of Willis including diameter discrepancy of the individual parts of the middle cerebral artery [Ringelstein et al., 1990; Lindegaard et al., 1987]. In effect, an over or under-estimated velocity values can be reported depending on the diameter of an insonated artery. The slightly higher ICC values obtained in the patients group could be explained by the lower range of physiological fluctuations and more consistent velocity measurements [Venkatesh et al., 2002].

Finally, the equipment characterists such as head frame that supports the transducers could account for some differnces in velocity values. In our study we have used a professional head frame system (Marc 600 Spencer Technologies, United States of America) that minimises the motion and maintains a constant angle of insonation of the middle cerebral artery. Interestingly, no single reproducibility study on velocity measurements described any form of secure fixation of transducers during the examinations [Totaro et al., 1992; Maeda et al., 1990; McMahon et al., 2007; Shen et al., 1999; Baumgartner et al., 1994]. Similarly, systematic reviews and meta-analyses on microembolic signals detection provide no information on any head-frame systems used by individual studies [Best et al., 2016; King et al., 2009b; Ritter et al., 2008b; Udesh et al., 2017]. This raises many questions regarding the methodological aspects of these studies that have been conducted more than 20 years ago.

Although our data regarding transcranial Doppler velocities measurements echoes other researchers findings, it should be interpreted with caution owing to many methodological limitations of the published analyses including a limited number of reproducibility studies that contain small sample size and variable imaging protocols. Furthermore, evidence for the transcranial Doppler criteria to predict the degree of intracranial arteries stenoses remains inconclusive and controversial [Babikian et al., 2000]. Several studies failed to

demonstrate reproducible data on specific cut-off points for the velocities values with the percentage of stenosis [Lindegaard et al., 1985; Niederkorn et al., 1988; Pozo et al., 1990; Feldmann et al., 2007; Lindegaard et al., 1986; Rorick et al., 1994]. Some authors have proposed middle cerebral artery velocity of > 80 cm/sec as a criterion for stenosis [Rorick et al., 1994], whereas others used velocities >100 cm/sec when diagnosing stenosing lesions [Bragoni et al., 1996]. In contrast, some researchers have highlighted the importance of additional measurements such as side-to-side differences in velocities (>30%) or increase in velocity (>50%) along with the assessment of collateral flow using temporary manual occlusions of the common carotid artery [Lindegaard et al., 1985; Niederkorn et al., 1988]. However, one must remember potential pitfalls with such approach because high velocities in collateral circulation can indicate different diameters of the middle cerebral arteries on two sides [Lindegaard et al., 1985]. In effect, high blood flow velocities may be caused simply by the smaller diameter of MCA despite otherwise normal anatomy [Pozo et al., 1990]. Finally, the largest study (The Stroke Outcomes and Neuroimaging of Intracranial Atherosclerosis (SONIA) Trial) that attempted to validate transcranial Doppler findings with magnetic resonance angiography against the standard cerebral digital subtraction angiography regarding the identification of intracranial arterial disease revealed disappointingly low results of positive predictive values for transcranial Doppler (36%) and magnetic resonance angiography (59%) [Feldmann et al., 2007]. In effect, the transcranial Doppler's clinical applicability regarding the abnormal velocity values assessment remains limited.

Despite complete 1-hour transcranial Doppler assessments performed in our study, the lack of microembolic signals in patients with symptomatic carotid artery stenosis was disappointing. The reported incidence varied from 12% to 100% in individual studies [Ritter et al., 2008a; Markus et al., 1995; Stork et al., 2002a]. Nevertheless, considerable differences regarding criteria for microembolic signals detection, timing after stroke, duration of monitoring and

antithrombotic agents used have been identified among many studies [Markus et al., 1997; Ritter et al., 2008a; Markus et al., 1995]. Consequently, the majority of published data described microembolic signals in about 30-40% of individuals with symptomatic carotid artery stenosis when transcranial Doppler was performed for 1 hour [King et al., 2009a; Ritter et al., 2008a; Stork et al., 2002a; Markus, 2000a].

Still, there are several potential explanations for the absent embolisation. Thromboembolism is a dynamic and random process with a generally reported low frequency of microembolic signals during 1-hour long examination [Markus, 2000a; Dittrich et al., 2002]. Although 1-hour long transcranial Doppler evaluation time is recommended for patients with symptomatic carotid artery stenosis, longer assessments increase the chances of successful emboli detection [Markus, 2000a]. This was demonstrated by ambulatory recordings (greater than 5 hours) with portable transcranial Doppler equipment that has yield greater number of microembolic signals when compared with the traditional 60 minutes approach [Mackinnon et al., 2005; Mackinnon et al., 2004]. However, at present, an ambulatory transcranial Doppler recording remains primarily a research tool due to lack of a robust equipment.

Another possible explanation refers to the severity of carotid artery stenosis and plaque morphology. Microembolic signals are more common in patients with the higher degree of carotid artery stenosis, which in turn is associated with specific carotid plaque features reported histologically such as ulceration, intraplaque haemorrhage and surface thrombus [Babikian et al., 2000; King et al., 2009a; Markus, 2000b; Stork et al., 2002a; Markus et al., 2005; Sitzer et al., 1995; Verhoeven et al., 2005a]. These high-risk plaque features are more likely to lead to the development of stroke because they produce larger emboli that consist of thrombi [Stork et al., 2002a]. Whereas small embolic particles comprising of fibrin and platelets aggregates that lodge in small arteriolar branches, may be lysed by endogenous protective haemostatic defences, hence clinically may represent TIA [Stork et al., 2002a]. The majority of our

patients had a non-surgical grade of carotid artery stenosis and presented with TIA. Therefore, these factors could be potentially responsible for no detectable microembolic signals.

The various components of microembolic signals responds differently to treatment [King et al., 2009a]. For example, antiplatelet agents are more effective for emboli originating from the symptomatic carotid artery stenosis and reduce the rate of microembolic signals [Markus et al., 2005; Imray et al., 2005]. On the other hand, anticoagulants deal more effectively with microembolic signals from a cardiac source [Markus et al., 2005; King et al., 2009b]. The majority of participants (90%) in our study have been on an antiplatelet agent at the time of the first transcranial Doppler assessment, and this could represent another potential confounder. Finally, microembolic signals are more likely to be detected within the first week after the index event, and in patients with recent stroke rather than with TIA [Azarpazhooh et al., 2006]. Again, we have performed transcranial Doppler as soon as possible, but due to various logistic factors, only two patients had transcranial Doppler within seven days from their index event.

The main limitations of this study are the small sample size, and single-centre design. However, the main purpose of the study was to demonstrate reproducibility of the transcranial Doppler, and this was achieved. At present, transcranial Doppler remains underutilised in clinical practice due to lack of human expertise, time-consuming recordings with the need for a continuous visual and audible evaluation [Markus, 2000a; Spence, 2017]. Furthermore, unsolved technical and methodological limitations of transcranial Doppler regarding the velocity assessments restrict its clinical applicability. However, its use during carotid surgery has shown that the clinical use of this non-invasive, non-ionising, portable and safe technique could be extended to vascular surgery specialists as part of the routine perioperative strategy that could reduce the risk of neurovascular events even further [Naylor et al., 2000].

3.5 CONCLUSIONS

Our findings indicate that transcranial Doppler provides reproducible data on middle cerebral artery velocities. However, these findings should be interpreted with caution for the many technical and methodological limitations that the transcranial Doppler still presents. Larger studies with the colour transcranial Doppler may enable delivery of a robust data on velocity assessments along with the quantification of intracranial stenoses.

CHAPTER FOUR

^{18}F-SODIUM FLUORIDE POSITRON EMISSION TOMOGRAPHY-MAGNETIC RESONANCE IMAGING OF CAROTID ATHEROMA IN ACUTE NEUROVASCULAR SYNDROME

4.1 INTRODUCTION

The identification of the culprit atherosclerotic plaque represents a key goal in carotid artery imaging. The primary focus of current imaging is stenosis severity, but the detection of high-risk plaque features may aid the identification of patients at risk of future stroke and potential targets for novel therapeutic intervention. Both PET and MRI have shown promise in identifying atherosclerotic plaques with the potential to cause a stroke. In addition to stenosis severity, MRI tissue characterization can identify adverse plaque features, such as lipid-rich necrotic core, intra-plaque hemorrhage, and fibrous cap thickness [Huibers et al., 2015]. The PET radiotracer fluorine 18-lablelled sodium fluoride (^{18}F-NaF) localises to areas of microcalcification activity indicative of inflammation and necrosis and has shown promise in identifying active atherosclerosis across the vascular system [Vesey et al., 2017; Irkle et al., 2015]. Combining these two techniques in PET-MRI would enable the simultaneous assessment of carotid stenosis, adverse plaque features, and plaque biological activity. The addition of the transcranial Doppler ultrasound imaging could help to investigate further downstream consequences of high-risk carotid plaques by detecting microembolic signals as a supplemental imaging marker. This could also explore the relationship between the radiotracer uptake and microembolic signals.

PET-MRI has the potential to provide MRI-based stenosis assessment and soft-tissue characterization alongside PET-based functional evaluation of disease activity. To date, only a few small studies (n=10 to 18) have assessed the feasibility of carotid PET-MRI [Hyafil et al., 2015a; Mechtouff et al., 2020; Pedersen et al., 2015]. The current study assessed ^{18}F-NaF PET-MRI in 110 participants with a broad range of acute neurovascular syndromes. We aimed to evaluate the association between ^{18}F-NaF activity and culprit carotid plaque in acute neurovascular syndrome.

This prospective observational cohort study was approved by the South East Scotland Research Ethics Committee (17/SS/0097, 17/SS/0098). Written informed consent was obtained, and the study was performed in accordance with the Declaration of Helsinki. The study was registered with ClinicalTrials.gov (NCT03215550, NCT03215563).

4.2 METHODS

4.2.1 PARTICIPANTS

Participants over 40 years of age who suffered a recent neurovascular event (14 days) that was compatible with the carotid (anterior) territory and had undergone carotid Doppler ultrasound were recruited consecutively from acute neurovascular clinics (n=2) or hospitals (n=2) between October 2017 and January 2020. Diagnostic criteria for acute neurovascular events were based on symptoms supported by radiological investigations, in line with published guidelines [Sacco et al., 2013]. The diagnosis of acute ischemic stroke or retinal infarct included clinically evident infarction persisting >24 hours [Sacco et al., 2013]. A transient ischemic attack (TIA) or amaurosis fugax (transient retinal ischemia) was diagnosed when clinical symptoms lasted <24 hours [Sacco et al., 2013].

Exclusion criteria were a modified Rankin score >3, chronic kidney disease (estimated glomerular filtration rate <30 mL/min/1.73 m^2), atrial fibrillation, pregnancy, prior ipsilateral carotid intervention or neck radiotherapy, inability to tolerate the supine position, inability to comply with study requirements, prior allergic reaction to study agents, contraindications to MRI, or if participation would delay carotid surgery.

4.2.2 CLINICAL ASSESSMENTS

Participants received baseline assessment within 14 days of the index event incorporating routine clinical assessment, review of healthcare records, and previous investigations. The attending stroke clinician (more than 10 years of experience) defined the culprit carotid artery side based on the clinical presentation and medical records including radiological investigations.

4.2.3 TRANSCRANIAL DOPPLER ULTRASOUND PROTOCOL

All examinations were performed in a semi-recumbent position in a quiet temperature-controlled room. The middle cerebral artery was identified through the temporal window and the sample volume adjusted to obtain a stable visually and acoustically optimal signal. A head frame (Marc 600 Spencer Technologies, United States of America) was fitted to reduce motion and to secure a constant angle of the symptomatic middle cerebral artery (ipsilateral to the index event) insonation depth at 40-65 mm from the skull surface (Figure 2.3, Chapter 2).

4.2.4 TRANSCRANIAL DOPPLER ULTRASOUND IMAGING ANALYSIS

All recordings were made using the ST^3 Transcranial Doppler Ultrasound System (Spencer Technologies, United States of America) with a 2-MHz transducer. Emboli were identified using characteristic short audible sound (range 10-100 ms, intensity threshold above 7 dB) and spectral appearance using the International Consensus Group microembolus identification criteria and assisted by an automated Embolus Detection Software (Spencer Technologies, United States of America) [Ringelstein et al., 1998]. The Doppler wave forms were reassessed to exclude artefact and confirm the presence of true emboli (Chapters 2 and 3).

4.2.5 ^{18}F-NaF PET-MRI PROTOCOL

Participants received a target dose of 125 megabecquerels of ^{18}F-NaF intravenously and after 60 min of rest were imaged on a 3 Tesla PET-MRI scanner (Biograph mMR, Siemens Healthcare GmbH) using a dedicated head

and neck coil. A 3-dimensional ^{18}F-NaF PET scan was obtained using list-mode acquisitions with two 15-min beds positions covering the carotid arteries (aortic arch to skull base). MRI from the aortic arch to the Circle of Willis was obtained simultaneously, including black blood T2-SPACE (TR 2200ms, TE 92ms), 3-dimensional time-of-flight (TOF) MRI angiography (TR 23 ms, TE 3.69 ms), and 2-dimensional axial black blood T1-weighted (TR 764 ms, TE 16ms), T2-weighted (TR 4740ms, TE 73 ms) and proton density (PD) weighted (TR 3000 ms, TE 16 ms) stacks. After PET acquisition, a contrast-enhanced MRI angiogram (gadobutrol 0.1 mL/kg) was performed covering the carotid bifurcations and aortic arch (TR 2.84 ms, TE 1.01 ms). PET images were reconstructed with corrections applied for attenuation, dead time, scatter and random coincidences (matrix size 256x256, ordered subset expectation maximization reconstruction with point spread function modelling [HD PET, Siemens Healthcare], 3 iterations, 21 subsets, 2mm Gaussian filtration). Head and neck coils were part of the attenuation-correction map.

4.2.6 MRI ANALYSIS

Visual analysis of carotid plaques was performed by a cardiovascular radiologist (more than 10 years of experience) using Carestream Vue Picture Archiving and Communication System (version 11, Carestream) blinded to clinical presentation and imaging. The most severe stenosis in each carotid artery was visually assessed on TOF or MRI angiography, and area stenosis was categorized as <30%, 30-49%, 50-69% or >70% stenosis compared with a normal distal reference segment [Naylor et al., 2018]. Consistent with previously published criteria, signal intensities on T1 weighted, T2 weighted, PD and TOF sequences were used to identify intraplaque hemorrhage, lipid core, calcification, thrombus, fibrosis and ulceration (Table 2.1 in Chapter 2) [Ota et al., 2009; Briley-Saebo et al., 2007; Yuan et al., 2001a; Cai et al., 2002; Saam et al., 2005]. The sternocleidomastoid muscle was used as a reference for signal intensities, as per previous studies [Chu et al., 2004].

4.2.7 PET IMAGE ANALYSIS

Visual analysis of ^{18}F-NaF uptake was performed by a cardiovascular radiologist (more than 10 years of experience) using dedicated software (FusionQuant, Ceders-Sinai Medical Center) blinded to clinical presentation and imaging. PET was fused with TOF or MRI angiography for analysis. ^{18}F-NaF uptake was visually assessed as positive or negative in culprit and non-culprit vessels. ^{18}F-NaF uptake was measured in a spherical volume of interest centred on the most severe stenosis in the culprit carotid, contralateral non-culprit carotid and aortic arch. Care was taken to exclude adjacent bony structures, by ensuring accurate co-registration and reviewing MRI and PET images. Mean and maximum standardized uptake values (SUV_{mean} and SUV_{max}) were recorded. Mean and maximum target to background ratios (TBR_{mean} and TBR_{max}) were calculated by dividing by the mean or maximum background activity averaged from 3 regions of interest within the brachiocephalic or internal jugular veins [Vesey et al., 2017; Tawakol et al., 2013].

4.2.8 STATISTICAL ANALYSIS

Statistical analysis was performed using R (version 4.0.3, R Foundation for Statistical Computing). Normally distributed variables are presented as mean ± standard deviation. Non-normally distributed data are presented as median [interquartile interval]. Categorical variables are presented as number and percentage. Statistical significance was derived using Welch two-sample t-test, Wilcoxon rank sum test with continuity correction, Pearson Chi-Square test or Fisher exact test. Threshold values for optimum TBR_{mean} and TBR_{max} to identify culprit versus non-culprit vessels were established using Youden J statistic from receiver operator curve analysis. Multivariable models were constructed to identify culprit compared with non-culprit vessels, which included as covariates the presence of MRI stenosis >70%, one or more MRI adverse plaque characteristics and either TBR_{mean} or $TBR_{max.}$ TBR_{mean} and TBR_{max} were log-transformed for analysis (log base 2). Odds ratios were

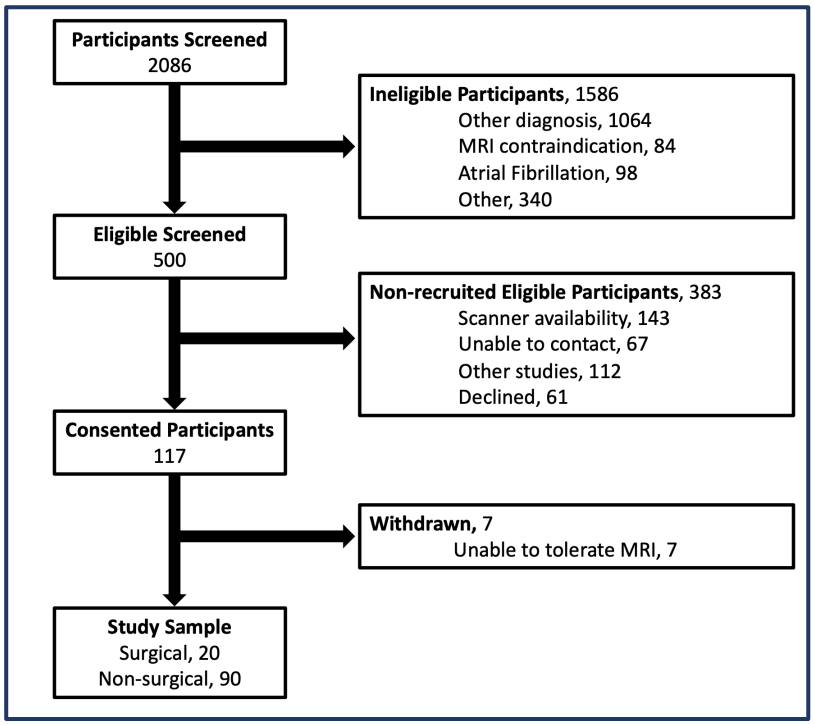
calculated. A 2-sided p-value <.05 was considered statistically significant. Based on PET-CT[Vesey et al., 2017] we estimated that with 80% power and a 2-sided p<.05, 33 patients would be required to identify differences between culprit and non-culprit plaques. To account for differences in quantification with PET-MRI, patient drop-out and multiple comparisons, we recruited 110 patients.

4.3 RESULTS

4.3.1 Participant Characteristics

Of 500 eligible participants, 117 were consented (Figure 4.1). Subsequently, seven withdrew due to an inability to complete the imaging protocol. The final study sample consisted of 110 participants (20 surgical, 90 non-surgical). Imaging of the aortic arch was available in all but two participants.

Figure 4.1: Consolidated Standards of Reporting Trials diagram of participant recruitment.



Participants had a mean age of 68 years ±10 [standard deviation], 70 were men, and 34 of 110 (32%) had a previous history of cerebrovascular disease (Table 4.1). Of the 110 participants, the presenting event was amaurosis fugax for 26 (24%), TIA for 54 (49%) and ischemic stroke for 30 (27%). Compared with those presenting with amaurosis fugax or TIA, participants presenting with ischemic stroke had a higher 10-year cardiovascular risk score (39 [24, 55] versus 26 [17, 43] versus 22 [18, 30] respectively, p=0.01), but most other risk factors were similar between sub-groups (Table 4.2). Twenty-seven participants had stenoses >70% in the culprit carotid vessel and were of a similar age, sex, and risk factor profile compared with those with stenoses <70% (Table 4.1, Table 4.3). We found no evidence of a difference in presentation with stroke between participants with stenoses >70% in the culprit vessel compared to those without (41%, n=11/27 versus 23%, n=19/83, p=0.11). Twenty of the 110 participants (18%) underwent clinically indicated carotid endarterectomy after PET-MRI.

Table 4.1: Clinical characteristics of all participants and those with culprit vessel stenosis above or below 70%.

Characteristic	Overall (n = 110)	Culprit Vessel Stenosis <70% (n = 83)	Culprit Vessel Stenosis ≥70% (n = 27)	P Value
Current acute neurovascular syndrome				.001*
Amaurosis fugax	26 (24)	15 (18)	11 (41)	
Transient ischemic attack	54 (49)	49 (59)	5 (19)	
Stroke	30 (27)	19 (23)	11 (41)	
Age (y)†	68 ± 10	68 ± 10	68 ± 9	.88
Sex				>.99
M	70 (64)	53 (64)	17 (63)	
F	40 (36)	30 (36)	10 (37)	
Ten-year cardiovascular risk score‡§	26 (18–45)	27 (18–44)	26 (22–50)	.36
Systolic blood pressure (mm Hg)†	143 ± 18	144 ± 17	141 ± 20	.49
Diastolic blood pressure (mm Hg)†	81 ± 11	82 ± 12	80 ± 9	.36
Heart rate (beats/min)†	71 ± 9	71 ± 9	71 ± 11	.10
Body mass index (kg/m^2)†	28 ± 5	28 ± 5	29 ± 5	.35
Estimated glomerular filtration rate (mL/min/1.73 m^2)†	59 ± 5	59 ± 5	59 ± 6	.99
Total cholesterol (mmol/L)†	5.2 ± 1.2	5.2 ± 1.2	5.2 ± 1	.88
HDL cholesterol (mmol/L)§	1.2 (1.1–1.6)	1.3 (1.1–1.6)	1.20 (1.1–1.4)	.15
LDL cholesterol (mmol/L)§	2.1 (1.6–3.0)	2.0 (1.6–3.1)	2.2 (1.7–3.0)	.74
Triglycerides (mmol/L)§	1.4 (0.9–2.0)	1.3 (0.9–2.1)	1.5 (1.1–1.8)	.41
Hypercholesterolemia	91 (83)	67 (81)	24 (89)	.50
Smoking status				.32
Nonsmoker	37 (34)	30 (36)	7 (26)	
Former smoker	36 (33)	24 (29)	12 (44)	
Current smoker	37 (34)	29 (35)	8 (30)	
Chronic obstructive pulmonary disease	9 (8.2)	5 (6.0)	4 (15)	.30
Hypertension	77 (70)	56 (67)	21 (78)	.44
Type 2 diabetes mellitus	95 (86)	73 (88)	22 (81)	.60
Ischemic heart disease	15 (14)	10 (12)	5 (19)	.60
Peripheral vascular disease	12 (11)	6 (7.2)	6 (22)	.07
Previous acute neurovascular syndrome				.09
Amaurosis fugax	3 (2.7)	1 (1.2)	2 (7.4)	
Transient ischemic attack	15 (14)	10 (12)	5 (19)	
Stroke	16 (15)	10 (12)	6 (22)	
Family history of cerebrovascular disease	33 (30)	27 (33)	6 (22)	.44

Note.—Unless otherwise specified, data are numbers of participants, with percentages in parentheses. HDL = high-density lipoprotein, LDL = low-density lipoprotein.

* Statistically significant difference.

† Data are means ± SDs.

‡ ASSIGN (or Assessing cardiovascular risk using Scottish Intercollegiate Guideline Network guidelines) score.

§ Data are medians, with IQRs in parentheses.

Table 4.2: Clinical characteristics of all patients presenting with different types of acute neurovascular syndromes.

Characteristic	Overall	AMFX	TIA	Stroke	p
Participants	110	26	54	30	
Age (years)	68 ± 10	65 ± 8	68 ± 10	70 ± 9	.19
Male	70 (64)	16 (62)	32 (59)	22 (73)	.42
10-year cardiovascular risk score	26 [18, 45]	22 [18, 30]	26 [17, 43]	39 [24, 55]	**.01**
Systolic blood pressure (mmHg)	143 ± 18	141 ± 16	144 ± 18	145 ± 21	.68
Diastolic blood pressure (mmHg)	81 ± 11	78 ± 10	82 ± 13	82 ± 9	.30
Heart rate (mean (/min)	71 ± 9	70 ± 8	71 ± 9	73 ± 10	.48
Body-mass index (kg/m^2)	28 ± 5	28 ± 6	28 ± 5	28 ± 4	.96
Estimated glomerular filtration rate (mL/min/1.73m^2)	59 ± 5	60 ± 0	60 ± 1	56 ± 10	**.005**
Total cholesterol (mmol/L)	5.2 ± 1.2	5.2 ± 1.2	5.2 ± 1.2	5.3 ± 1.1	.89
HDL-Cholesterol (mmol/L)	1.2 [1.1, 1.6]	1.3 [1.1, 1.6]	1.4 [1.1, 1.7]	1.2 [1, 1.4]	**.03**
LDL -Cholesterol (mmol/L)	2.1 [1.6, 3]	2.4 [1.9, 3]	2.1 [1.6, 3.1]	1.9 [1.5, 2.5]	.14
Triglycerides (mmol/L)	1.4 [0.9, 2]	1.4 [0.8, 2]	1.3 [0.9, 2]	1.6 [1.1, 2.2]	.34
Hypercholesterolemia	91 (83)	20 (77)	44 (81)	27 (90)	.41
Smoking status					
Non-smoker	37 (34)	10 (38)	18 (33)	9 (30)	.86
Ex-smoker	36 (33)	8 (31)	16 (30)	12 (40)	
Current smoker	37 (34)	8 (31)	20 (37)	9 (30)	
Chronic Obstructive Pulmonary Disease	9 (8)	3 (12)	5 (9)	1 (3)	.49
Hypertension	77 (70)	21 (81)	35 (65)	21 (70)	.35
Diabetes mellitus	95 (86)	24 (92)	48 (89)	23 (77)	.18
Ischaemic heart disease	15 (14)	3 (12)	5 (9)	7 (23)	.19
Peripheral vascular disease	12 (11)	3 (12)	6 (11)	3 (10)	.98
Previous acute neurovascular syndrome					
Amaurosis fugax	3 (3)	1 (4)	1 (2)	1 (3)	.86
Transient ischemic attack	15 (14)	2 (8)	10 (19)	3 (10)	
Stroke	16 (15)	4 (15)	8 (15)	4 (13)	
Family history of cerebrovascular disease	33 (30)	10 (38)	12 (22)	11 (37)	.22
Clopidogrel	99 (90)	24 (92)	48 (89)	27 (90)	.89
Aspirin	27 (25)	5 (19)	13 (24)	9 (30)	.64
Dual antiplatelet therapy	23 (21)	5 (19)	10 (19)	8 (27)	.66
Statin	106 (96)	26 (100)	50 (93)	30 (100)	.12
Anticoagulant	4 (4)	0 (0)	1 (2)	3 (10)	.09
Beta blocker	17 (15)	3 (12)	5 (9)	9 (30)	**.03**
ACE inhibitor	55 (50)	16 (62)	28 (52)	11 (37)	.17
Diuretic	17 (15)	5 (19)	7 (13)	5 (17)	.75
Calcium channel blocker	30 (27)	7 (27)	14 (26)	9 (30)	.92
Hypoglycaemic therapy	12 (11)	2 (8)	4 (7)	6 (20)	.17

Number (%), mean ± standard deviation, or median [interquartile interval]. * ASSIGN score. AMFX: amaurosis fugax; TIA: transient ischemic attack; HDL: high-density lipoproteins; LDL: low-density lipoproteins; ACE: angiotensin converting enzyme.

Table 4.3: Therapy in all participants and those with culprit vessel stenosis above or below 70%.

Therapy	Overall (n = 110)	Culprit Vessel Stenosis <70% (n = 83)	Culprit Vessel Stenosis ≥70% (n = 27)	P Value
Clopidogrel	99 (90)	76 (92)	23 (85)	.56
Aspirin	27 (25)	20 (24)	7 (26)	>.99
Dual antiplatelet therapy	23 (21)	17 (20)	6 (22)	>.99
Statin	106 (96)	79 (95)	27 (100)	.57
Anticoagulant	4 (3.6)	1 (1.2)	3 (11)	.07
β-blocker	17 (15)	13 (16)	4 (15)	>.99
ACE inhibitor	55 (50)	41 (49)	14 (52)	>.99
Diuretic	17 (15)	12 (14)	5 (19)	.84
Calcium channel blocker	30 (27)	21 (25)	9 (33)	.57
Hypoglycemic therapy	12 (11)	8 (10)	4 (15)	.69

Note.—Unless otherwise specified, data are numbers of participants, with percentages in parentheses. ACE = angiotensin-converting enzyme.

4.3.2 TRANSCRANIAL DOPPLER ULTRASOUND

Microembolic signals were detected in one (<1% (n=1/110) participant only during transcranial Doppler ultrasound assessments.

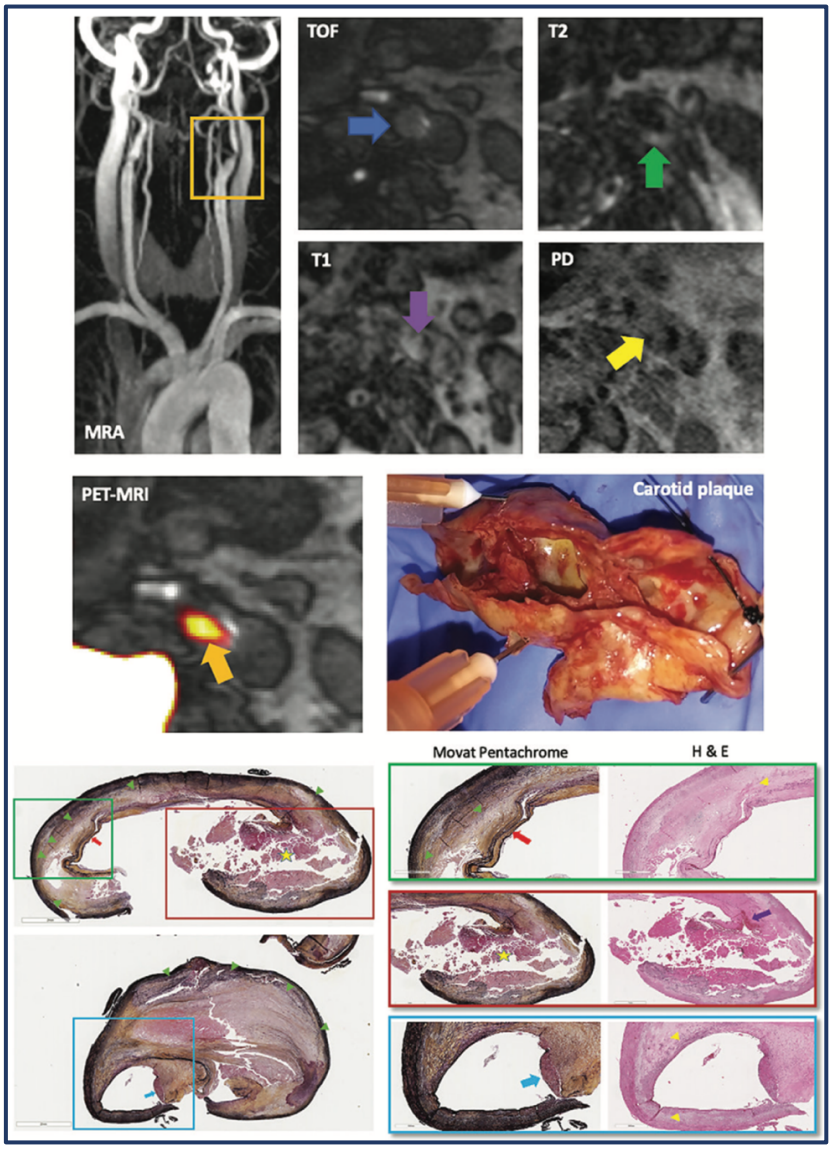
4.3.3 CULPRIT VERSUS NON-CULPRIT VESSELS

MRI

Compared with non-culprit vessels, culprit vessels were more likely to have stenosis >70% (25% (n=27/110) versus 5% (n=5/110), p<0.001) or >50% (30% (n=33/110) versus 15% (n=17/110), p=0.01; Table 4.4). Culprit vessels were more likely to have intraplaque hemorrhage (42% (n=46/110) versus 23% (n=25/110), p=0.004), necrotic core (36% (n=40/110) versus 18% (n=20/110), p=0.004), thrombus (7% (n=8/110) versus 0, p=0.01) and ulceration (18% (n=20/110) versus 4% (n=4/110), p=0.001, Table 4.4, Figure 4.2). We found no evidence of a difference in the presence of fibrosis (32% (n=35/110) versus 44% (n=48/110), p=0.10) or calcification (43% (n=47/110) versus 35% (n=39/110), p=0.33) between culprit and non-culprit vessels (Table 4.4). Compared with participants with <70% culprit stenosis, participants with >70% culprit stenosis were more likely to have thrombus

(26% (n=7/27) versus 1% (n=1/83), p<0.001), calcification (89% (n=24/27) versus 28% (n=23/83), p<0.001) and ulceration (41% (n=11/27) versus 11% (n=9/83), p=0.001) and less likely to have fibrosis (15% (n=4/27) versus 37% (n=31/83), p=0.05) than participants without >70% stenosis (Tables 4.5, 4.6).

Figure 4.2: ^{18}F-NaF PET/MRI carotid scans and ex vivo histologic analysis sample in a patient who experienced a left hemispheric transient ischaemic attack.



MRI angiography in a 60-year-old woman with left hemispheric TIA identified a left carotid artery stenosis of >70% severity (MRA orange box, TOF blue arrow). MRI plaque analysis identified intraplaque hemorrhage (purple arrow), necrotic lipid core (green arrow) and calcification (yellow arrow). ^{18}F-NaF PET-MRI showed focal uptake in the region of the intraplaque hemorrhage and necrotic lipid core (orange arrow). The carotid plaque was excised at operation. Cross sectional images through the carotid plaque are shown, with Hematoxylin and Eosin (H&E) and Movat pentachrome stains. The red arrow indicates the thin fibrous cap, the blue arrow highlights plaque erosion, the yellow star denotes a rupture, the purple arrow shows intraplaque hemorrhage with a thrombus, the yellow arrowheads denote inflammation (shoulder and central regions), and the green arrowhead indicates necrotic lipid core. H&E; Hematoxylin and Eosin; ^{18}F-NaF: fluorine 18-labelled sodium fluoride PD: proton density; MRA: magnetic resonance angiography; TOF: time of flight; T1, T1 weighted imaging; T2, T2 weighted imaging.

Table 4.4: ^{18}F-NaF PET/MRI in culprit and nonculprit vessels.

^{18}F-NaF PET/MRI Finding	Culprit Vessel (n = 110)	Nonculprit Vessel (n = 110)	P Value
Stenosis ≥50% at MR angiography	33 (30)	17 (15)	.02*
Stenosis ≥70% at MR angiography	27 (25)	5 (4.5)	<.001*
Adverse plaque	57 (52)	33 (30)	.002*
Intraplaque hemorrhage	46 (42)	25 (23)	.004*
Necrotic core	40 (36)	20 (18)	.004*
Thrombus	8 (7.3)	0 (0)	.01*
Ulceration	20 (18)	4 (3.6)	.001*
Fibrosis	35 (32)	48 (44)	.10
Calcification	47 (43)	39 (35)	.33
No. of adverse plaque features†	1 (0–2)	0 (0–1)	<.001*
Visual ^{18}F-NaF uptake	78 (71)	41 (37)	<.001*
TBR_{mean} †	2.75 (2.24–3.84)	2.52 (1.99–3.38)	.06
TBR_{max} †	1.38 (1.12–1.82)	1.26 (0.99–1.66)	.04*

Note.—Unless otherwise specified, data are numbers of participants, with percentages in parentheses. ^{18}F-NaF = fluorine 18–labeled sodium fluoride, TBR_{max} = maximum tissue-to-background ratio, TBR_{mean} = mean tissue-to-background ratio.

* Statistically significant difference.

† Data are medians, with IQRs in parentheses.

Table 4.5: MRI findings in participants with culprit vessels stenosis above or below 70%.

MRI Finding	Stenosis <70% (n = 83)	Stenosis ≥70% (n = 27)	P Value
Stenosis ≥50%	6 (7.2)	27 (100)	<.001*
Stenosis ≥70%	0 (0)	27 (100)	<.001*
Adverse plaque	39 (47)	18 (67)	.12
Necrotic core	28 (34)	12 (44)	.44
Intraplaque hemorrhage	30 (36)	16 (59)	.06
Thrombus	1 (1.2)	7 (26)	<.001*
Ulceration	9 (11)	11 (41)	.001*
Calcification	23 (28)	24 (89)	<.001*
Fibrosis	31 (37)	4 (15)	.052
No. of adverse plaque features†	0 (0–2)	2 (0–3.5)	.009*

Note.—Unless otherwise specified, data are numbers of participants, with percentages in parentheses.

* Statistically significant difference.

† Data are medians, with IQRs in parentheses.

Table 4.6: MRI findings in participants with nonculprit vessels stenosis above or below 70%.

MRI Finding	Stenosis <70% (*n* = 83)	Stenosis ≥70% (*n* = 27)	*P* Value
Stenosis ≥50%	5 (6.0)	12 (44)	<.001*
Stenosis ≥70%	0 (0)	5 (19)	<.001*
Adverse plaque	27 (33)	6 (22)	.44
Necrotic core	16 (19)	4 (15)	.81
Intraplaque hemorrhage	19 (23)	6 (22)	>.99
Ulceration	2 (2.4)	2 (7.4)	.54
Calcification	17 (20)	22 (81)	<.001*
Fibrosis	45 (54)	3 (11)	<.001*
No. of adverse plaque features†	1 (0–2)	2 (0–4)	.02*

Note.—Unless otherwise specified, data are numbers of participants, with percentages in parentheses.

* Statistically significant difference.

† Data are medians, with IQRs in parentheses.

PET

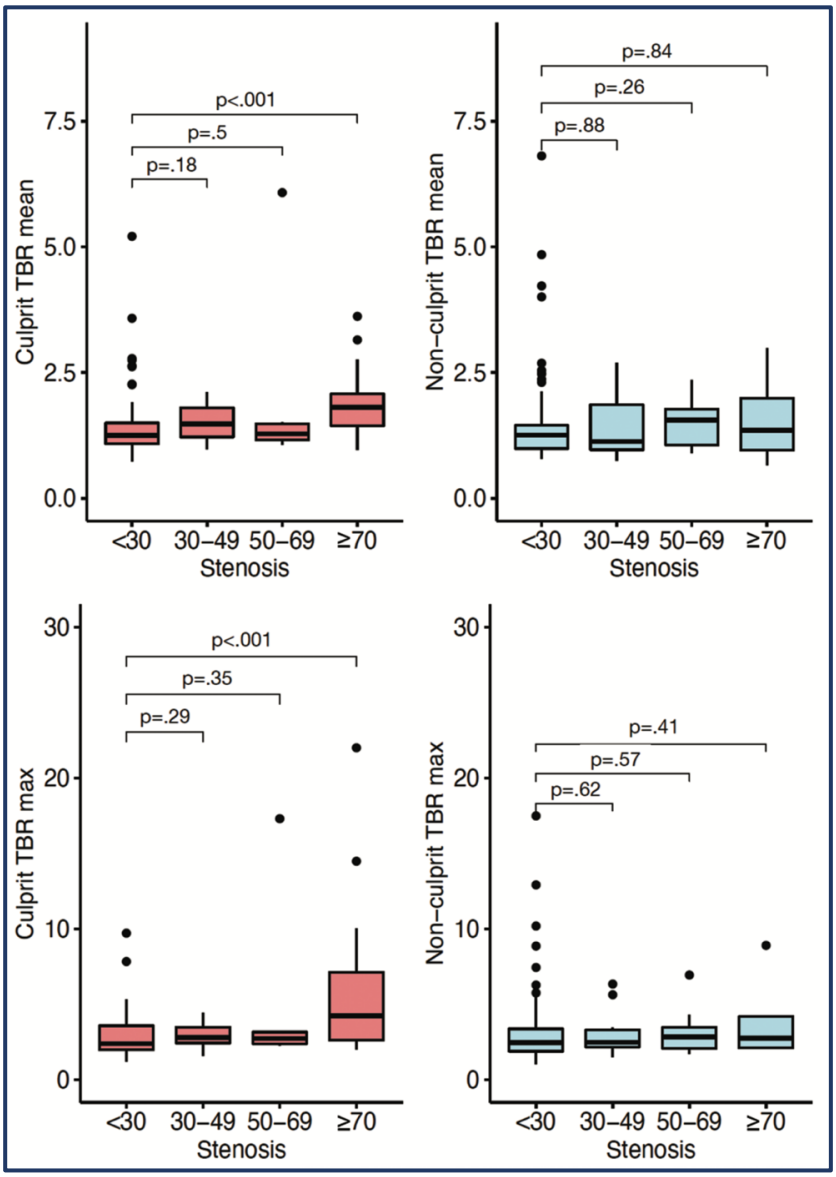
Culprit vessels were more likely to have visually assessed ^{18}F-NaF uptake than non-culprit vessels (n=78/110, 71% versus n=41/110, 37%, p<0.001). Culprit vessels had a higher ^{18}F-NaF uptake than non-culprit vessels (TBR_{max} 1.38 [1.12, 1.82] versus 1.26 [0.99, 1.66], p=0.04; Table 4.4). In the culprit vessel, a stenosis >70% was associated with higher ^{18}F-NaF uptake (TBR_{mean} 1.81 [1.44, 2.07] versus 1.27 [1.09, 1.60], p=0.001; Figure 4.3, Figure 4.4). However, we found no evidence of a difference in ^{18}F-NaF TBR_{mean} in the non-culprit vessel in patients with or without >70% stenosis (TBR_{mean} 1.49 [1.00, 1.95] versus 1.25 [0.99, 1.43], p=0.15; Figure 4.5).). Participants with >70% culprit stenosis had higher ^{18}F-NaF uptake in the culprit vessel than those with <70% culprit stenosis (TBR_{max} 4.23 [2.64, 7.13] versus 2.58 [2.13, 3.57], p<0.001; TBR_{mean} 1.81 [1.44, 2.07] versus 1.27 [1.09, 1.60], p=0.001; Figure 4.4, Figure 4.5, Table 4.7). They also had higher TBR_{max} in the non-culprit vessel than those with <70% culprit stenosis (3.07 [2.15, 4.26] versus 2.27 [1.88, 3.17], p=0.02) and higher TBR_{mean} in the aortic arch (1.62 [1.40, 1.97] versus 1.42 [1.24, 1.62], p=0.03; Figure 4.4, Figure 4.5, Table 4.7).

Table 4.7: ^{18}F-NaF uptake in patients with a culprit vessel stenosis above or below 70%.

Vessels		Culprit <70%	Culprit >70%	p
Number		83	27	
Culprit	SUV_{mean}	1.21 [1.03, 1.46]	1.57 [1.31, 1.92]	**<.001**
	SUV_{max}	2.49 [1.88, 3.04]	3.48 [2.53, 5.96]	**<.001**
	TBR_{mean}	1.27 [1.09, 1.60]	1.81 [1.44, 2.07]	**.001**
	TBR_{max}	2.58 [2.13, 3.57]	4.23 [2.64, 7.13]	**<.001**
Non-culprit	SUV_{mean}	1.15 [0.98, 1.37]	1.22 [1.04, 1.67]	.13
	SUV_{max}	2.33 [1.82, 2.93]	2.59 [2.27, 3.40]	**.02**
	TBR_{mean}	1.25 [0.99, 1.43]	1.49 [1.00, 1.95]	.15
	TBR_{max}	2.27 [1.88, 3.17]	3.07 [2.15, 4.26]	**.02**
Aortic arch	SUV_{mean}	1.34 [1.04, 1.55]	1.48 1.14, 1.77]	.09
	SUV_{max}	2.73 [2.16, 3.38]	2.84 [2.28, 3.90]	.52
	TBR_{mean}	1.42 [1.24, 1.62]	1.62 [1.40, 1.97]	**.04**
	TBR_{max}	3.05 [2.52, 3.76]	2.99 [2.68, 3.78]	.42

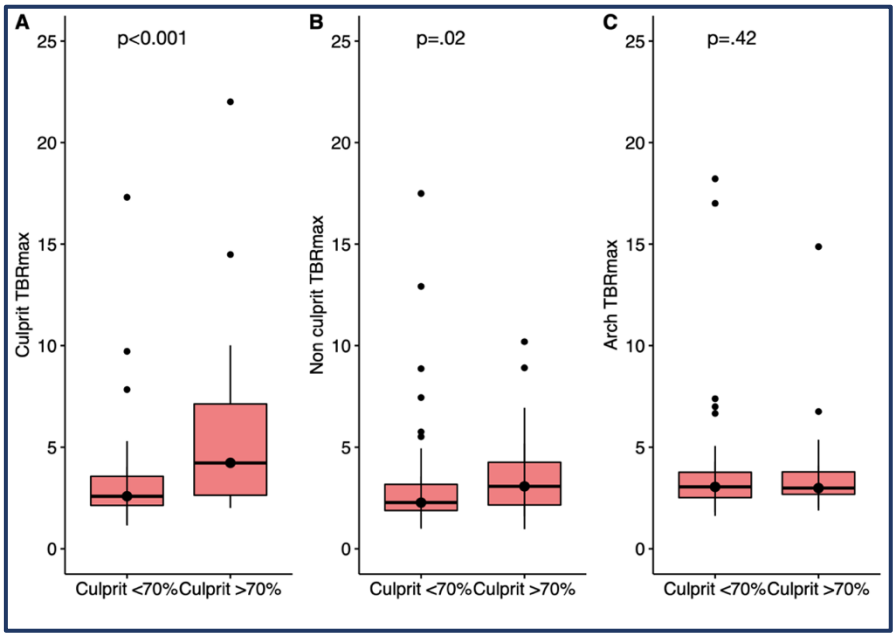
Median [interquartile interval]. SUV_{mean}: mean standardized uptake value; SUV_{max}: maximum standardized uptake value; TBR_{mean}: mean tissue-to-background ratio; TBR_{max}: maximum tissue-to-background ratio.

Figure 4.3: Tukey box and whisker plots show fluorine 18-labelled sodium fluoride uptake (mean tissue-to-background ratio [TBR_{mean}]) stratified by the degree of carotid stenosis (expressed as percentages) in culprit (red) and nonculprit (blue) vessels.



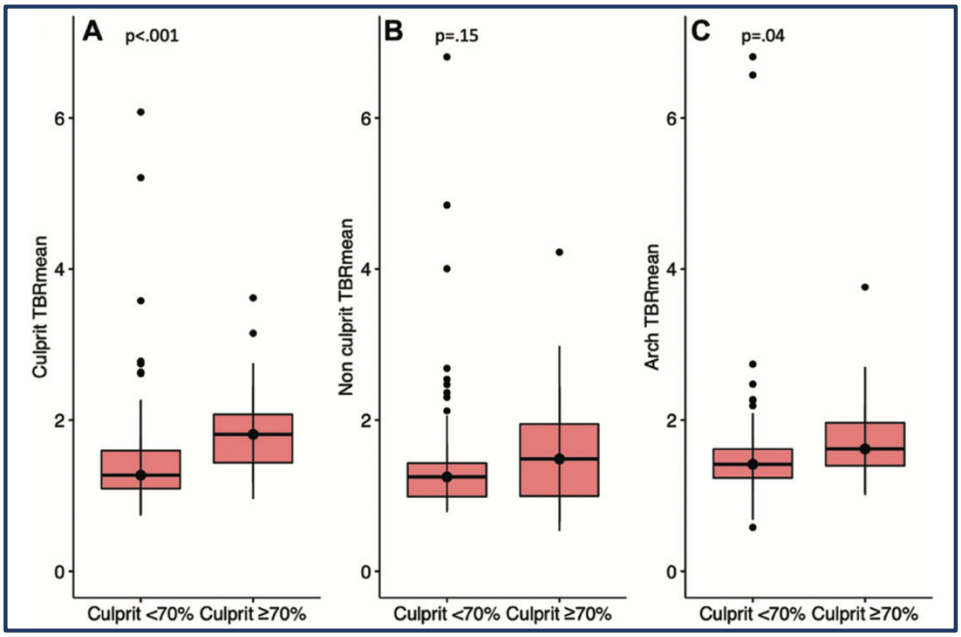
The box bounds the IQR (upper and lower quartile) divided by the median (solid horizontal midline); whiskers extend to the most extreme data points from the edge of the box; outliers beyond the whiskers are individually plotted by the solid dots.

Figure 4.4: ^{18}F-NaF uptake in (A) culprit vessel, (B) non-culprit vessel and (C) aortic arch, in patients with a culprit stenosis above or below 70%.



Median and interquartile range. TBR_{max}: maximum tissue-to-background ratio.

Figure 4.5: Tukey box and whisker plots show fluorine 18-labelled sodium fluoride uptake in the (A) culprit vessel, (B) nonculprit vessel, and (C) aortic arch in patients with stenosis above or below 70% in the culprit vessel.



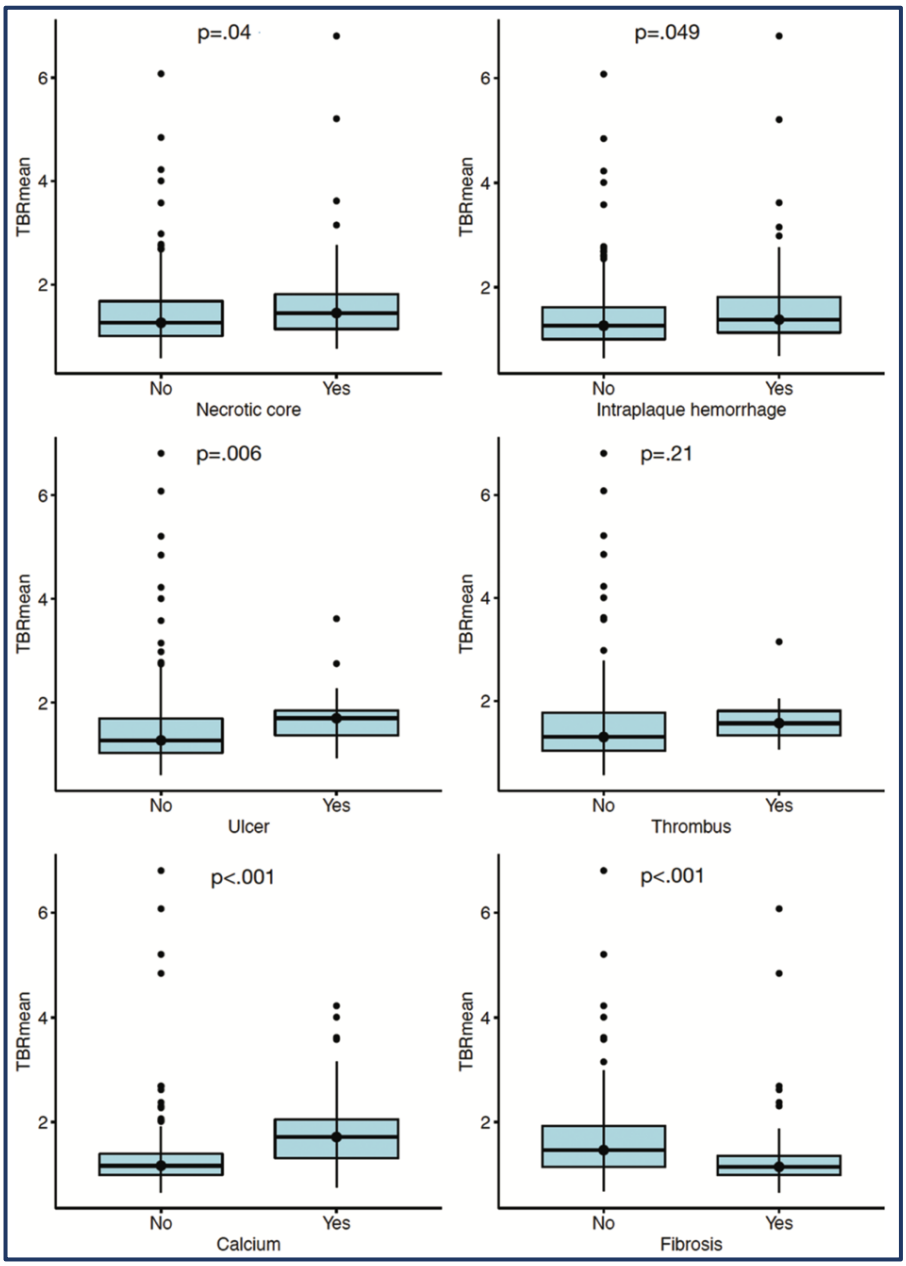
The box bounds the IQR (upper and lower quartile) divided by the median (solid horizontal midline); whiskers extend to the most extreme data points from the edge of the box; outliers beyond the whiskers are individually plotted by the solid dots. TBR_{mean} = mean tissue-to-background ratio.

Combined PET and MRI

^{18}F-NaF TBR_{mean} was higher in all vessels with necrotic core (1.45 [1.14, 1.82] versus 1.26 [1.01, 1.68], p=0.04), intraplaque hemorrhage (1.38 [1.13, 1.82] versus 1.26 [1.01, 1.61], p=0.04), ulcer (1.70 [1.37, 1.85] versus 1.27 [1.03, 1.70], p=0.006) and calcification (1.71 [1.31, 2.05] versus 1.16 [0.98, 1.39], p<0.001), and lower in vessels with fibrosis (1.14 [0.99, 1.35] versus 1.46 [1.14, 1.92], p<0.001; (Figure 4.6, Figure 47, Figure 4.8). Using Youden J statistic the optimum threshold value for the identification of culprit compared with non-culprit vessels was 1.25 for TBR_{mean} and 2.46 for TBR_{max}. Culprit vessels were more likely to have a combination of adverse plaque characteristics and TBR_{mean} >1.25 (80% (n=88/110) versus 55% (n=61/110), p<0.001) or TBR_{max} >2.46 (80% (n=88/110) versus 61% (n=67/110), p=0.003).

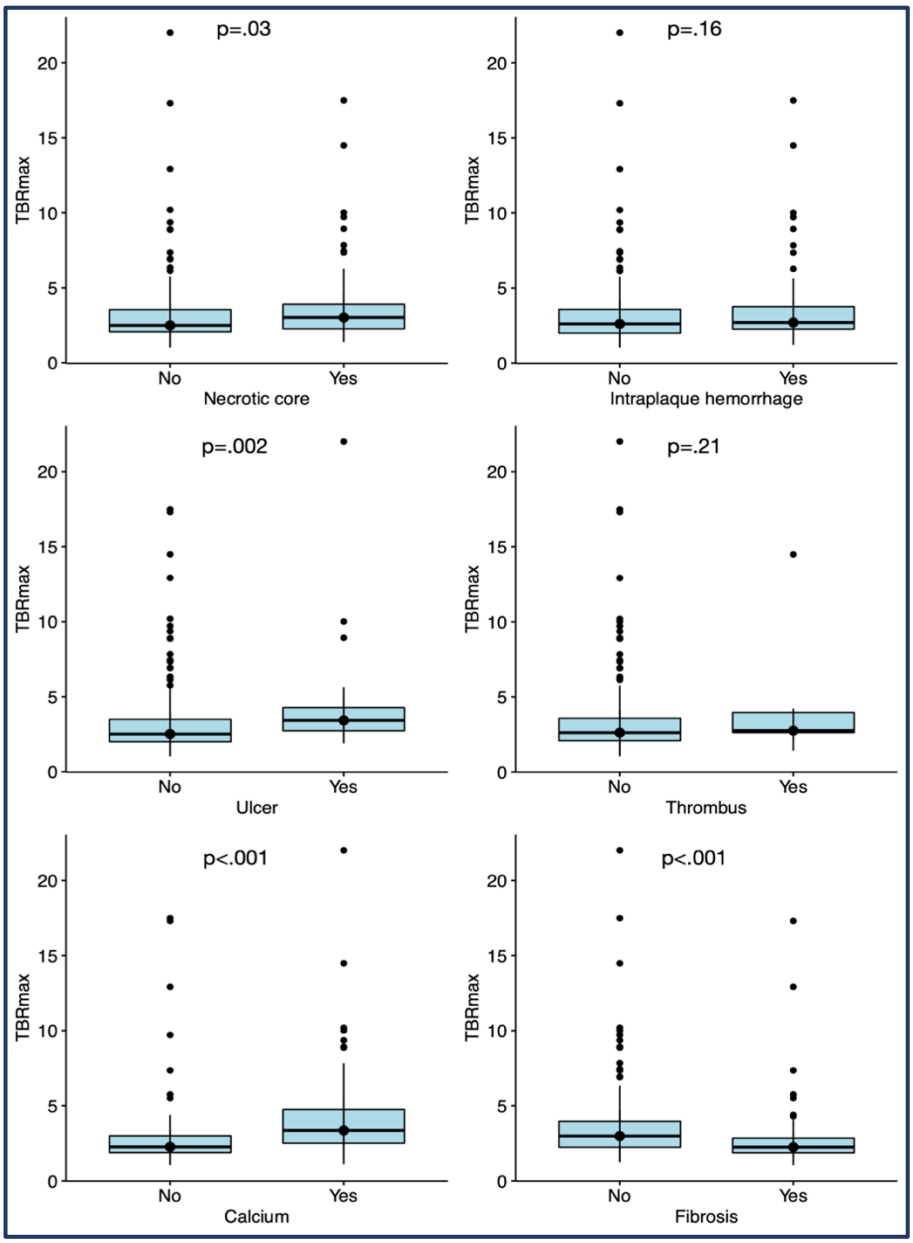
In a multivariable analysis, MRI stenosis >70% (odds ratio 5.72, 95% CI: 2.2, 18, p<0.001) and MRI adverse plaque characteristics (odds ratio 2.2, 95% CI: 1.2, 3.9, p=0.009) were both associated with the culprit vessel compared to the non-culprit vessel, but TBR_{mean} (odds ratio 1.2, 95% CI: 0.7, 1.9, p=0.56) was not. Similarly, in a second model TBR_{max} was not associated with the culprit vessel compared to the non-culprit vessel (odds ratio 1.0, 95% CI: 0.7, 1.6, p=0.91), whereas MRI stenosis >70% (odds ratio 5.8, 95% CI: 2.2, 18, p<0.001) and MRI adverse plaque characteristics were (odds ratio 2.2, 95% CI: 1.2, 3.9, p=0.008, Figure 4.9).

Figure 4.6: Tukey box and whisker plots show fluorine 18-labelled sodium fluoride uptake measured by TBR_{mean} and MRI-defined plaque features.



The box bounds the IQR (upper and lower quartile) divided by the median (solid horizontal midline); whiskers extend to the most extreme data points from the edge of the box; outliers beyond the whiskers are individually plotted by the solid dots. TBR_{mean} = mean tissue-to-background ratio.

Figure 4.7: Tukey box and whisker plots show fluorine 18-labelled sodium fluoride uptake measured by TBR_{max} and MRI-defined plaque features.



The box bounds the IQR (upper and lower quartile) divided by the median (solid horizontal midline); whiskers extend to the most extreme data points from the edge of the box; outliers beyond the whiskers are individually plotted by the solid dots. TBR_{max}: maximum tissue-to-background ratio.

Figure 4.8: Example of false positive ^{18}F-NaF PET-MRI uptake, with uptake seen on axial and sagittal culprit (A, B) and non-culprit (C, D) vessels in a 61-year-old, male with acute neurological syndrome.

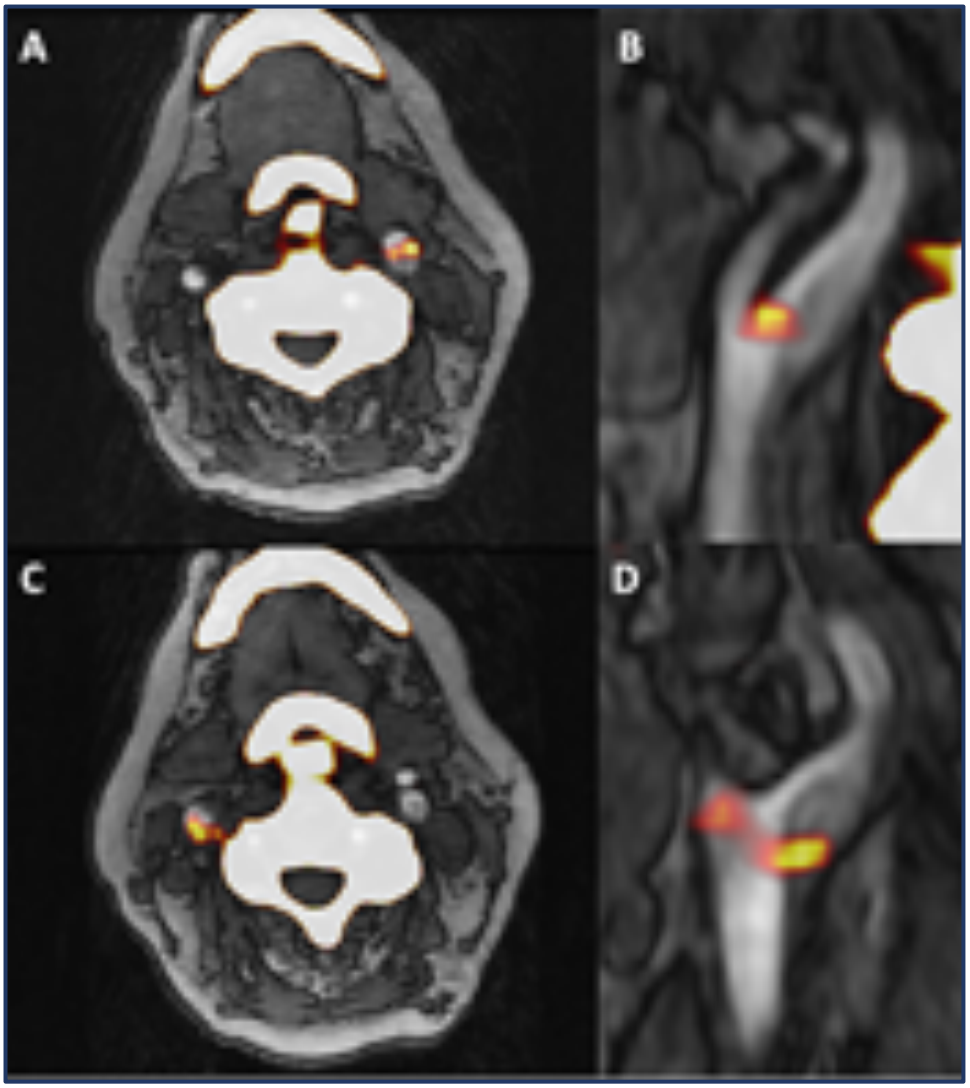
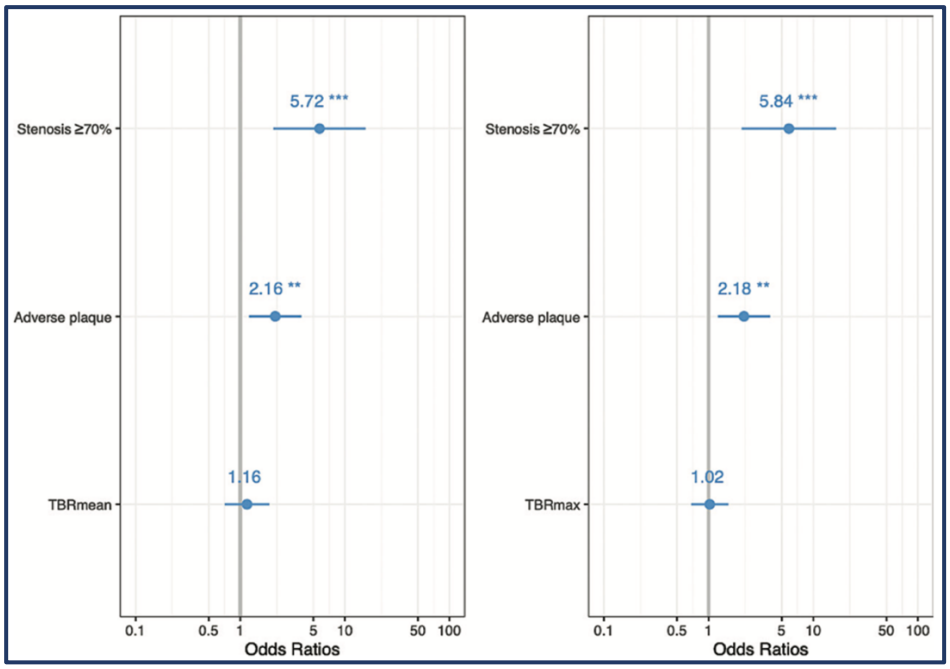


Figure 4.9: Multivariable models were constructed for the identification of culprit compared with nonculprit vessels, which included as covariates the presence of MRI-derived stenosis greater than or equal to 70%, one or more MRI-derived adverse plaque characteristics, and either mean tissue-to-background ratio (TBR_{mean}) or maximum tissue-to-background ratio (TBR_{max}).



Dot plots show odds ratios, with blue lines representing 95% CIs. TBRmean is per doubling [log2(TBRmean)]. ***= P <0.001, **= P <0.01, *= P<0.05, no asterisk= P ≥0.05.

Subsequent Clinical Acute Neurovascular Events

After 1.94±0.61 years of follow-up, only 5 (4.5%) patients experienced a subsequent stroke. There was no difference in demographic characteristics, magnetic resonance angiography stenosis severity or individual magnetic resonance imaging plaque characteristics in the patients who did and did not undergo subsequent stroke. Patients who had a subsequent stroke were more likely to have an adverse plaque in any vessel on the magnetic resonance imaging (60%, n=3/5 versus 55%, n=58/105) and had a higher number of adverse plaque features (3 [0, 4] versus 1 [0, 2]), but these differences were not statistically significant. There was no difference in the ^{18}F-NaF uptake in culprit or non-culprit vessels or in the aortic arch of patients who did or did not have a subsequent stroke. Patients who experienced subsequent stroke appeared to have a numerically higher prevalence of both of adverse plaque characteristics and an elevated TBR_{mean} >1.95 (80%, n=4/5 versus 60%,

n=53/105, p=0.670) or TBR_{max} >2.48 (100%, n=5/5 versus 74%, n=77/105, p=0.439), but these differences were not statistically significant.

4.3.4 SURGICAL VERSUS NON-SURGICAL PARTICIPANTS

Participants (n=20, 18%) who underwent carotid surgery were more likely to present with stroke (45%, n=9/20 versus 23%, n=21/90, p=0.02) but had similar demographic characteristics to participants who did not undergo surgery (Table 4.8).

MRI

In the culprit vessel, participants undergoing surgery were more likely to have stenoses greater than 70% or 50% than those who did not (100%, n=20/20 versus 14%, n=13/90, p<0.001 and 95%, n=19/20 versus 9%, n=8/90, p<0.001 respectively; Table 4.9). In the non-culprit vessel, participants undergoing surgery were more likely to have stenoses greater than 50% than participants who did not undergo surgery (50%, n=10/20 versus 8%, p<0.001), but we found no evidence of a difference in the frequency of stenoses greater than 70% (15%, n=3/20 versus 2%, n=2/90, p=0.06).

In the culprit vessel, participants undergoing surgery were more likely to have a necrotic core, intraplaque hemorrhage, thrombus, ulceration and calcification and less likely to have fibrosis compared with participants who did not undergo surgery (p=.04 to <0.001, Table 4.9). In the non-culprit vessel, participants undergoing surgery were also more likely to have calcification (95%, n=19/20 versus 22%, n=20/90, p<0.001) and less likely to have fibrosis (5%, n=1/20 versus 52%, n=47/90, p<0.001), but we found no evidence of a difference in the other plaque characteristics (Table 4.9). Participants undergoing surgery were more likely to have any (75%, n=15/20 versus 47%, n=42/90, p=0.04), or a higher number of (0 [0, 2] versus 3 [0.75, 5], p<0.001) adverse plaque features in the culprit vessel, we found no evidence of a difference in the presence of adverse plaque characteristics in the non-culprit vessel (30%, n=6/20 versus 30%, n=27/90, p>0.99, Table 4.9).

Table 4.8: Clinical characteristics of patients who underwent carotid endarterectomy (surgical) and patients who did not (non-surgical).

Characteristic	Non-surgical	Surgical	p
Participants	90	20	
Presenting acute neurovascular syndrome			
Amaurosis fugax	19 (21)	7 (35)	**.02**
Transient ischemic attack	50 (56)	4 (20)	
Stroke	21 (23)	9 (45)	
Age (years)	68 ± 10	69 ± 9	.52
Male	57 (63)	13 (65)	>.99
10-Year cardiovascular risk score *	26 [18, 43]	28 [25, 50]	.12
Systolic blood pressure (mmHg)	143 ± 18	147 ± 19	.36
Diastolic blood pressure (mmHg)	81 ± 12	80 ± 8	.47
Heart rate (/min)	71 ± 9	72 ± 11	.89
Body-mass index (kg/m^2)	28 ± 5	29 ± 5	.35
Estimated glomerular filtration rate (mL/min/1.73 m^2)	59 ± 5	59 ± 6	.99
Total cholesterol (mmol/L)	5.2 ± 1.2	5.2 ± 0.9	.88
HDL-Cholesterol (mmol/L)	1.3 [1.1, 1.6]	1.2 [1.1, 1.4]	.28
LDL-Cholesterol (mmol/L)	2.1 [1.7, 3.1]	2.1 [1.6, 2.8]	.36
Triglycerides (mmol/L)	1.4 [0.9, 2.1]	1.3 [1, 1.6]	.57
Hypercholesterolemia	74 (82)	17 (85)	>.99
Smoking status			
Non-smoker	30 (33)	7 (35)	.62
Ex-smoker	28 (31)	8 (40)	
Current smoker	32 (36)	5 (25)	
Chronic Obstructive Pulmonary Disease	6 (7)	3 (15)	.44
Hypertension	62 (69)	15 (75)	.79
Diabetes mellitus	78 (87)	17 (85)	>.99
Ischemic heart disease	11 (12)	4 (20)	.58
Peripheral vascular disease	9 (10)	3 (15)	.80
Previous acute neurovascular syndrome			
Amaurosis fugax	2 (2)	1 (5)	.23
Transient ischemic attack	11 (12)	4 (20)	
Stroke	11 (12)	5 (25)	
Family history of cerebrovascular disease	26 (29)	7 (35)	.79
Clopidogrel	82 (91)	17 (85)	.68
Aspirin	21 (23)	6 (30)	.73
Dual antiplatelet therapy	18 (20)	5 (25)	.85
Statin	86 (96)	20 (100)	.76
Anticoagulant	2 (2)	2 (10)	.31
Beta blocker	14 (16)	3 (15)	>.99
ACE inhibitor	47 (52)	8 (40)	.46
Diuretic	14 (16)	3 (15)	>.99
Calcium channel blocker	23 (26)	7 (35)	.56
Hypoglycaemic therapy	10 (11)	2 (10)	>.99

Number (%), mean ± standard deviation, or median [interquartile interval]. * ASSIGN score. HDL: high-density lipoproteins; LDL: low-density lipoproteins; ACE: angiotensin converting enzyme.

Table 4.9: MRI and ^{18}F-NaF PET findings in patients who underwent carotid endarterectomy (surgical) and those who did not (non-surgical).

Side	MRI		Non-surgical	Surgical	P
Number			90	20	
Culprit	Stenosis	>50%	13 (14)	20 (100)	**<.001**
		>70%	8 (9)	19 (95)	**<.001**
	Necrotic core		28 (31)	12 (60)	**.03**
	Intraplaque haemorrhage		32 (36)	14 (70)	**.01**
	Thrombus		0 (0)	8 (40)	**<.001**
	Ulcer		10 (11)	10 (50)	**<.001**
	Calcium		28 (31)	19 (95)	**<.001**
	Fibrosis		33 (37)	2 (10)	**.04**
	Adverse plaque *		42 (47)	15 (75)	**.04**
	Number of adverse plaque features		0 [0, 2]	3 [0.75, 5]	**<.001**
	TBR_{mean}		1.28 [1.10, 1.72]	1.79 [1.45, 1.95]	**.007**
	TBR_{max}		2.55 [2.12, 3.59]	4.05 [2.68, 6.33]	**.001**
Non-culprit	Stenosis	>50%	7 (8)	10 (50)	**<.001**
		>70%	2 (2)	3 (15)	.06
	Necrotic core		15 (17)	5 (25)	.58
	Intraplaque haemorrhage		20 (22)	5 (25)	>.99
	Ulcer		2 (2)	2 (10)	.31
	Calcium		20 (22)	19 (95)	**<.001**
	Fibrosis		47 (52)	1 (5)	**<.001**
	Adverse plaque *		27 (30)	6 (30)	>.99
	Number of adverse plaque features		0 [0, 1]	0 [0, 1.25]	.66
	TBR_{mean}		1.25 [0.98, 1.51]	1.46 [1.06, 1.87]	.15
	TBR_{max}		2.37 [1.89, 3.30]	3.04 [2.13, 4.23]	.06
Aortic arch	TBR_{mean}		1.44 [1.25, 1.65]	1.58 [1.29, 1.88]	.26
	TBR_{max}		3.07 [2.58, 3.77]	2.89 [2.43, 3.70]	.79

Number (%) or mean ± standard deviation. *intraplaque haemorrhage, necrotic core, ulcer or thrombus.

PET

Participants undergoing surgery had higher ^{18}F-NaF uptake in the culprit vessel (TBR_{mean} 1.79 [1.45, 1.95] versus 1.28 [1.10, 1.72], p=0.007; TBR_{max} 4.05 [2.68, 6.33] versus 2.55 [2.12, 3.59], p=0.001). However, we found no

evidence of a difference in radiotracer uptake in the non-culprit vessel (TBR_{mean} 1.25 [0.98, 1.51] versus 1.46 [1.06, 1.87], p=0.15) or in the arch of the aorta (TBR_{mean} 1.44 [1.25, 1.65] versus 1.58 [1.20, 1.88], p=0.26) between participants who did or did not undergo surgery (Table 4.9).

PET and MRI

Participants undergoing surgery were more likely to have a combination of adverse plaque characteristics and TBR_{mean} >1.25 (100%, n=20/20 versus 71%, n=64/90, p=0.01) or TBR_{max} >2.46 (100%, n=20/20 versus 71%, n=64/90, p=0.01) than those who did not.

4.4 DISCUSSION

Carotid ^{18}F-NaF PET-MRI has the potential to combine information on stenosis severity, MRI adverse plaque characteristics and atherosclerotic disease activity. In this large prospective study including participants with a broad range of acute neurovascular syndromes, culprit carotid vessels had a higher degree of stenosis (>70% stenosis: 25% versus 5%, p<0.001), higher ^{18}F-NaF uptake (maximum TBR 1.38 versus 1.26, p=.04) and more frequent MRI adverse plaque features (52% versus 30%, p=0.002) compared to non-culprit vessels. Moreover, ^{18}F-NaF uptake was higher in vessels with lipid necrotic core (1.45 [1.14, 1.82] versus 1.26 [1.01,1.68], p=0.04), intraplaque hemorrhage (1.38 [1.13, 1.82] versus 1.26 [1.01, 1.61], p=0.04), and ulceration (1.70 [1.37, 1.85] versus 1.27 [1.03, 1.70], p=0.006) and lower in areas of fibrosis (1.14 [0.99, 1.35] versus 1.46 [1.14, 1.92], p<0.001), suggesting complementarity between plaque features and plaque biology. Interestingly, spontaneous microembolisation was detected in one individual only. After two years of follow-up, all patients who experienced a subsequent stroke had either MRI-defined adverse plaque characteristics or elevated ^{18}F-NaF uptake. These findings may lay the ground for future clinical evaluation of strokes with

uncertain etiology and assessment of carotid disease activity to guide the selection of patients for surgical intervention

Previous studies established that adverse carotid plaque characteristics can be identified with MRI, and that these features are more frequent in culprit compared to non-culprit vessels, including in patients without severe stenoses [Kopczak et al., 2020]. The MRI adverse carotid plaque characteristics described in this study were intraplaque hemorrhage, necrotic core, thrombus and ulceration. Identification of these features may therefore help to determine the culprit vessel in cases where this is uncertain. These adverse carotid plaque characteristics have also been linked to an increased risk of subsequent acute events in those with established cerebrovascular disease and asymptomatic patients [Rizvi et al., 2020; Hop et al., 2018; Sun et al., 2017]. A recent meta-analysis found that the carotid MRI features associated with the highest risk of subsequent acute neurovascular syndromes were intraplaque hemorrhage, necrotic core and thinning or rupture of the fibrous cap [Gupta et al., 2013; Rizvi et al., 2020]. Identification of these high-risk plaque features can therefore provide additional information, over and above stenosis severity, which can help to guide management and prognostication. However, lack of spontaneous microembolisation in all but one participant was bewildering. This precluded any meaningful analysis regarding any potential correlates of microembolic signals with adverse plaque phenotypes and the radiotracer uptake.

^{18}F-NaF is a marker of biologically active microcalcification [Irkle et al., 2015; Hop et al., 2018] and we have previously shown that ^{18}F-NaF PET-CT identifies the culprit carotid plaque in patients with stroke or TIA [Vesey et al., 2017]. In our current study, we expanded these findings demonstrating that ^{18}F-NaF can identify the culprit carotid plaque across a wider range of disease severity. We showed that radiotracer uptake is higher in vessels with high-risk MRI characteristics and lower in areas of fibrosis. These findings are consistent with histological assessment, showing that ^{18}F-NaF localizes in areas with macrophage infiltration, apoptosis, necrosis, active calcification and

ulceration [Joshi et al., 2014]. MRI and PET, therefore, provide overlapping and complementary markers of high-risk atherosclerotic disease.
Several small studies have demonstrated the feasibility of PET-MRI of the carotid arteries using ^{18}F-fluorodeoxyglucose [Bachi et al., 2019; Kundel et al., 2018; Kundel et al., 2021; Hyafil et al., 2015a; Li et al., 2016; Ripa et al., 2013; Rajiah et al., 2016; Ungar et al., 2020], ^{64}Cu-DOTATE [Pedersen et al., 2015]and ^{68}Ga-Pentixafor [Li et al., 2019] in patients with previous stroke and a variety of other conditions. Only one previous study assessed ^{18}F-NaF PET-MRI in 12 patients with carotid stenosis ≥50% (6 symptomatic and 6 asymptomatic) [Mechtouff et al., 2020]. They found that ^{18}F-NaF uptake was higher in culprit compared with non-culprit plaques. However, they found no association with MRI features of plaque vulnerability, likely due to the small number of patients. In contrast, this study showed that ^{18}F-NaF uptake was associated with key features of plaque vulnerability, a finding that has not previously been well established in the literature.

In this study we also provide information on the association between ^{18}F-NaF PET/MRI findings in the carotid arteries and risk of subsequent stroke. Patients who experienced subsequent stroke were more likely to have adverse plaques on MRI and elevated TBR, although this difference was not statistically significant. The low rate of recurrent neurovascular events reported in our study likely stems from insufficient sample size and a lack of power. Furthermore, this small number of subsequent strokes represents advanced stages of the atherosclerotic disease that carries a risk of failure to respond to treatment. These findings will require further assessment in larger studies with longer follow-up before any meaningful conclusions can be drawn between these hypothetical associations with subsequent outcomes.

Our study had several limitations. First, it assumes that one culprit vessel was the source of the index acute event, whereas other cardioembolic sources or bilateral carotid disease may be present. Second, the impact of the Circle of Willis architecture or other brain MRI findings was not assessed. Third, ^{18}F-

NaF uptake in adjacent bony structures can cause overestimation of carotid uptake. Fourth, the threshold used to define abnormal ^{18}F-NaF may be higher than the true threshold as a control group is unavailable. Fifth, false negative ^{18}F-NaF uptake may occur with a large plaque rupture event where there is little residual metabolically active plaque in the culprit vessel. Sixth, MRI signal characteristics may overlap, and very small lesions may not be apparent due to the resolution of MRI. Finally, the clinical use of PET-MRI is limited by its lack of widespread availability and the exclusion of patients with metallic implants or claustrophobia.

4.5 CONCLUSIONS

Identifying culprit carotid plaques in patients with acute neurovascular syndromes could improve targeting of medical and surgical management, monitor disease progression and inform future prognostication. This study shows that carotid ^{18}F-NaF PET-MRI is associated with culprit atherosclerotic plaques and features of plaque vulnerability and activity. ^{18}F-NaF uptake was higher in culprit lesions, areas of severe stenosis and locations of adverse plaque characteristics. However, only the presence of severe stenosis and adverse plaque characteristics were independent markers of the culprit compared with the non-culprit vessel. Future research will assess the optimal ^{18}F-NaF uptake threshold to identify culprit lesions with PET-MRI and incorporate follow-up imaging in larger cohorts. Further technical improvements of PET-MRI will require reduction of image acquisition time and improvement of MRI attenuation correction. Further research is warranted to assess how these features of PET-MRI correspond with subsequent clinical outcomes.

CHAPTER FIVE

^{18}F-SODIUM FLUORIDE POSITRON EMISSION TOMOGRAPHY-MAGNETIC RESONANCE IMAGING IN PATIENTS UNDERGOING CAROTID ENDARTERECTOMY – CORRELATION WITH HISTOLOGY

5.1 INTRODUCTION

Over the past three decades, management of acute neurovascular syndrome (ischaemic stroke, transient ischaemic attack, amaurosis fugax) has been dichotomised to either carotid endarterectomy or medical treatment using one aspect of symptomatic carotid disease, the degree of carotid artery stenosis. However, non-invasive cross-sectional imaging of carotid atherosclerosis supported by comprehensive histological data has gathered compelling and irrefutable information that plaque characteristics are a far better predictor of future acute neurovascular events than carotid stenosis alone [Kramer et al., 2020; Saba et al., 2020]. Furthermore, the application of sophisticated hybrid molecular imaging probes elevated our insights into a complex interplay of parallel atherogenic pathways, including chronic degenerative inflammation and vascular microcalcification [Evans et al., 2020]. The latter is associated with increased local stress within the fibrous cap, inflammation, and necrosis [Vesey et al., 2017]. Unlike macrocalcification, this early stage of mineralisation (<50 μm) is beyond the resolution of currently available imaging techniques. Therefore, the ability to detect microscopic nodules of calcium by fluorine-18-labelled sodium fluoride (^{18}F-NaF) molecular imaging may identify carotid plaques that are at high risk of symptomatic transformation with the associated classic tissue changes (inflammation, necrotic lipid core, intraplaque haemorrhage, thin fibrous cap, ulceration, and thrombus). This could pave the way for a new individualised therapeutic dyad for survivors of acute neurovascular syndromes. Patients with the highly stenosed carotid artery and morphologically quiescent plaque could avoid vascular intervention, including procedural risks. Conversely, those with non-surgical grade stenosis but morphologically high-risk carotid atheroma could benefit from stroke-preventative surgery.

Despite promising ^{18}F-NaF positron emission tomography-computed tomography (PET-CT) imaging that identified high-risk ruptured carotid plaques in patients with recent acute neurovascular syndromes [Vesey et al.,

2017], both *in vivo* [Quirce et al., 2013; Quirce et al., 2016; Kim et al., 2018a] and *ex vivo* [Hop et al., 2018] visualisation of carotid plaque is limited by small heterogenous samples, including diverse imaging and histological protocols, rendering clinical correlation unreliable. Likewise, a seminal feasibility report of ^{18}F-NaF PET-MRI following carotid endarterectomy [Mechtouff et al., 2020] due to small sample size (n=12) precluded any form of comparison with our recently published large (n=110) prospective observational single-centre cohort data on the role of ^{18}F-NaF PET-MRI in a broad range of acute neurovascular syndromes [Kaczynski et al., 2022]. Thus, despite years of dedicated research into the topic of intimal calcium dystrophy [Rashdan et al., 2020; Mahmoud et al., 2019; Irkle et al., 2015], our understanding of one of the most exciting molecular hallmarks of atherosclerosis remains incomplete.

There is a need to corroborate the ^{18}F-NaF PET-MRI based molecular map of carotid tissue with histological markers of calcific mineralisation to understand the mechanisms surrounding radiotracer binding within carotid plaques. We aimed to correlate *in vivo* 3T ^{18}F-NaF PET-MRI characterisation of microcalcification and high-risk carotid plaque features with *ex vivo* imaging (^{18}F-NaF microPET-CT and 7T MRI) and histological (reference standard) examination using the same carotid endarterectomy atherosclerotic plaques.

5.2 METHODS

5.2.1 STUDY DESIGN

This prospective observational cohort study was approved by the South-East Scotland Research Ethics Committee (17/SS/0097) and registered with ClinicalTrials.gov (NCT03215550). The study was a subset of a more extensive single-center prospective observational cohort study (17/SS/0098, NCT03215563) as described previously [Kaczynski et al., 2022]. Written informed consent was obtained, and the study was performed in accordance with the Declaration of Helsinki.

5.2.2 STUDY PARTICIPANTS

Participants over 40 years of age who had suffered a recent neurovascular event (14 days) were recruited consecutively from acute neurovascular clinics or hospitals between October 2017 and January 2020. Diagnostic criteria for acute neurovascular events were based on symptoms supported by radiological investigations, in line with published guidelines [Sacco et al., 2013]. The diagnosis of acute ischemic stroke or retinal infarction included clinically evident infarction persisting >24 hours [Sacco et al., 2013]. A transient ischemic attack (TIA) or amaurosis fugax (transient retinal ischemia) was diagnosed when clinical symptoms lasted <24 hours [Sacco et al., 2013]. Inclusion criteria comprised of a clinical presentation compatible with a carotid (anterior) territory event, and carotid Doppler ultrasound confirming carotid stenosis requiring carotid endarterectomy (carotid artery stenosis ≥50% by the North American Symptomatic Carotid Endarterectomy Trial criteria [Rothwell et al., 2003a; Naylor et al., 2018]. Exclusion criteria were a modified Rankin score >3, chronic kidney disease (estimated glomerular filtration rate <30 mL/min/1.73 m^2), atrial fibrillation, pregnancy, prior ipsilateral carotid intervention or neck radiotherapy, inability to tolerate the supine position, inability to comply with study requirements, prior allergic reaction to study agents, contraindications to MRI, or if participation would delay carotid surgery.

Participants received baseline assessment within 14 days of the index event incorporating routine clinical assessment, review of healthcare records, and previous investigations. The attending stroke clinician defined the culprit carotid artery side based on the clinical presentation and medical records, including radiological investigations.

5.2.3 IMAGING

^{18}F-NaF PET-MRI - in vivo 3T

Participants received a target dose of 125 MBq of ^{18}F-NaF intravenously and, after 60 min of rest, were imaged on a 3T PET-MRI scanner (Biograph mMR, Siemens Healthcare GmbH) using a dedicated head and neck coil. A 3-dimensional ^{18}F-NaF PET scan was obtained using list-mode acquisitions with two 15-min beds positions covering the carotid arteries (aortic arch to skull base). MRI from the aortic arch to the Circle of Willis was obtained simultaneously, including black blood T2-SPACE, 3-dimensional time-of-flight (TOF) MRI angiography, and 2-dimensional axial black blood T1-weighted, T2-weighted and proton density (PD) weighted stacks. After PET acquisition, a contrast-enhanced MRI angiogram (gadobutrol 0.1 mL/kg) was performed, covering the carotid bifurcations and aortic arch. PET images were reconstructed with corrections applied for attenuation, dead time, scatter, and random coincidences (matrix size 256x256, ordered subset expectation maximisation reconstruction with point spread function modelling [HD PET, Siemens Healthcare], 3 iterations, 21 subsets, 2mm Gaussian filtration). Head and neck coils were part of the attenuation-correction map.

MRI – ex vivo 7T

Carotid plaques were transferred from 10% formaldehyde to phosphate-buffered saline for at least 24h before scanning in MRI. Carotid plaques were placed in MRI-compatible sample tubes. Imaging was performed on a 7T horizontal bore MRI system equipped with a 60-mm bore gradient insert (Agilent Technologies, Yarnton, UK, maximum gradient strength 1000 mT/m) or a 140-mm gradient insert (Bruker Biospin, GmbH, Germany, 660 mT/m). All tissue samples were scanned using the same MRI magnet, gradient insert, and radiofrequency coils. Depending on sample size, a variable quadrature volume coil (26, 39 or 86 mm^3) was used for signal transmission and reception (Rapid Biomedical GmbH, Rimpar, Germany or Bruker Biospin GmbH, Germany). Scout images were taken to confirm correct positioning, and the magnetic field was optimised using an automated shim. Subsequently, 40-50

slices were obtained using the following parameters for all sequences producing: field of view 19.2 × 19.2 mm (larger for bigger samples), acquisition matrix 192 × 192 and slice thickness 0.5 mm. Repetition Time (TR) and Time to Echo (TE) varied slightly with the different setups used. For T1-weighted, T2-weighted and proton density scans, a fast spin-echo (FSE) protocol was used with an echo train length of 4 T1-weighted or 8 T2-weighted and Proton Density. Thirty-two to sixty-four signal averages were acquired. For T2*-weighted scans, a gradient echo sequence with a flip angle of 20and 32 signal averages was used.

^{18}F-NaF micro-PET-CT – ex vivo

Carotid plaques were incubated in approximately 100 kBq/mL of ^{18}F-NaF for 30 min at 37 °C. After incubation, specimens were washed with phosphate-buffered saline and stored in a humid environment during the microPET-CT imaging procedure to prevent dehydration. Carotid specimens were imaged using high-resolution (0.5-mm) microPET-CT (NanoScan PET-CT, Medisco, Budapest, Hungary). CT imaging was acquired (full semi-circular trajectory, maximum field of view, 480 projections, 50 kVp and 1:4 binning), followed by the microPET imaging (3-dimensional list mode for 30 min). PET images were reconstructed using a 3D Tera-Tomo (4 iterative methods) reconstruction algorithm, including correction for random scatter and attenuation.

5.2.4 TISSUE COLLECTION

Carotid tissue was obtained from participants who underwent carotid surgery following acute neurovascular syndrome. At the time of carotid endarterectomy, plaque tissue was collected immediately, photographed, and fixed in 10% formaldehyde. Subsequently, the carotid specimen was imaged with *ex vivo* 7T MRI and ^{18}F-NaF microPET-CT to co-localise microcalcification with *in vivo* 3T ^{18}F-NaF PET-MRI and histological markers of calcification. Lesion integrity and geometry were preserved as much as possible.

5.2.5 TISSUE ANALYSIS

All carotid samples were evaluated by histology, immunohistochemistry, and micro-computed tomography (micro-CT). To correct for carotid tissue shrinkage and sample division, the individual carotid plaque components (necrotic lipid core and calcium) were defined relative to the total plaque area and recorded as '*index* = number of positive plaque component/total plaque area mm^2' (Figure 2.11 in Chapter 2). An algorithm was used to isolate and quantify elastic fibres and intraplaque haemorrhage (red blood cells and fibrin) (Figure 2.12 in Chapter 2).

Histology and Immunohistochemistry

Images were generated using an Aperio Slide Scanner using Image Scope software (Leica Biosystems, Germany). All carotid specimens were transversely bisected in regions of plaque (Figure 2.13 in Chapter 2). One half was decalcified in Cal-Ex II (Fisher Scientific, CS511) and then processed for subsequent histology with immunohistochemistry. Immediately prior to embedding, the specimen was cut into 2-mm pieces to facilitate transverse orientation. Following embedding, histologic sections were generated and stained with hematoxylin and eosin (H&E), and Movat's pentachrome stains. Slides were evaluated for histological features of atherosclerotic plaque, as described in Table 2.3 (in Chapter 2), by a subspecialty cardiovascular pathologist blinded to patient demographics and history on Haematoxylin and Eosin, and Movat's Pentachrome staining. These features were characterised according to criteria used in the Oxford Plaque Study [Redgrave et al., 2006; Lovett et al., 2004a; Lovett et al., 2004b] and AtheroExpress [Verhoeven et al., 2004] (Table 2.3 in Chapter 2) and aggregated into four plaque phenotypes (Table 2.4in Chapter 2) using a weighted scoring system for the various plaque features confirming progressively greater "severity" phenotypes from A through to D. The pathologist was blinded to clinical characteristics and imaging findings and confirmed a consistent clustering of the four phenotypes (Figure 2.14 in Chapter 2).

Immunohistochemistry was performed on the selected carotid samples for Osteopontin, Runx2 and Caspase 3 to match the tissue pathology (Figure 2.15 in Chapter 2). Scoring was completed from high-resolution slide scans. Immunohistochemistry was completed using OPN (osteopontin; catalog No. 07264; 1:100 dilution; Sigma-Aldrich), cleaved Caspase 3 (No. 9664; 1:100 dilution; Cell Signaling), and RUNX2 (Abcam Catalog No: Ab76956, 1:50 dilution). Staining was performed via automated staining with a Leica Bond Rx system using Bond Epitope Retrieval Solution 1 (pH=6, catalog No. AR9961) for Caspase-3, Runx2, and Osteopontin. Background staining was assessed via assessment of sections processed with the omission of primary antibody.

5.2.6 IMAGING

Micro-Computed Tomography (micro-CT)

Carotid samples were imaged using the Nikon XT H 225 ST micro focus X-ray tomography system (Nikon Metrology, Cambridge, Canada) on whole or bisected samples. Samples were scanned at 100 kV, 350 μA, 177 ms exposure with 1800 projections, 2x averages with a 48-μm resolution. DICOM files were exported and analyzed using ImageJ and a colour scheme with different densities of Hounsfield Units (U) applied throughout the image stack. The criteria were as follows: greyscale (soft tissue) <130 HU, yellow = 130-200 HU, green= 200-300 HU, blue= 300-400, red >400 HU [Ababneh et al., 2014] (Figure 2.11in Chapter 2).

^{18}F-NaF PET-MRI – 3T in vivo

MAGNETIC RESONANCE IMAGING

Visual analysis of carotid plaques was performed by a cardiovascular radiologist (using Carestream Vue Picture Archiving and Communication System (version 11, Carestream) blinded to clinical presentation and imaging. The most severe stenosis in each carotid artery was visually assessed on time of flight or magnetic resonance angiography, and area stenosis was categorised as <30%, 30-49%, 50-69% or >70% stenosis compared with a normal distal reference segment [Naylor et al., 2018]. Consistent with

previously published criteria, signal intensities on T1-weighted, T2-weighted, Proton Density and Time of Flight sequences were used to identify intraplaque haemorrhage, lipid core, calcification, thrombus and rupture/erosion (Table 2.1 in Chapter 2)) [Ota et al., 2009; Briley-Saebo et al., 2007; Yuan et al., 2001b; Cai et al., 2002; Cai et al., 2005]. The sternocleidomastoid muscle was used as a reference for signal intensities [Chu et al., 2004].

Visual analysis of ^{18}F-NaF uptake was performed (MW) using dedicated software (FusionQuant, Ceders-Sinai Medical Center) blinded to clinical presentation and imaging as described previously [Kaczynski et al., 2022]. PET was fused with time of flight or MRI angiography for analysis. ^{18}F-NaF uptake was measured in a spherical volume of interest centred on the most severe stenosis in the culprit carotid plaque. Care was taken to exclude adjacent bony structures by ensuring accurate co-registration and reviewing MRI and PET images. Mean and maximum standardised uptake values (SUV_{mean} and SUV_{max}) were recorded. Mean and maximum target-to-background ratios (TBR_{mean} and TBR_{max}) were calculated by dividing by the mean or maximum background activity averaged from 3 regions of interest within the brachiocephalic or internal jugular veins [Vesey et al., 2017; Tawakol et al., 2013].

MRI – 7T ex vivo

The magnetic resonance micro-images were matched with histological digitalised sections, and visual analysis of carotid plaques was performed (JK and MW) using an OsiriX workstation (OsiriX version 11.0.1, 64-bit, OsiriX Imaging Software, Geneva, Switzerland). blinded to clinical presentation and imaging. The process of matching corresponding images to histology used several previously described landmarks, including carotid bifurcation and gross plaque morphology, such as size, shape, configuration, and calcifications [Saam et al., 2005; Shinnar et al., 1999; Károlyi et al., 2013]. Signal intensities on T1 weighted, T2 weighted, proton density and T2* sequences were used to identify intraplaque haemorrhage, necrotic lipid core,

calcification, thrombus, and rupture or erosion (Table 2.1 in Chapter 2) [Károlyi et al., 2013; Truong et al., 2021; Morrisett et al., 2003].

^{18}F-NaF micro-PET – ex vivo

Images were analysed using an OsiriX workstation (OsiriX version 11.0.1, 64-bit, OsiriX Imaging Software, Geneva, Switzerland). Regions of regions interest were drawn manually around the carotid plaque contours and mapped to corresponding fused PET-CT images to measure concentrations of ^{18}F-NaF. To quantify ^{18}F-NaF uptake, we used the mean (SUV_{mean}) and maximum standardised uptake values (SUV_{max}).

5.2.7 STATISTICAL ANALYSIS

Categorical variables were presented as numbers (percentages). Continuous variables with normal distribution were presented as mean ± standard deviation, whereas non-normally distributed variables were presented as median [interquartile range]. Parametric and non-parametric tests were used, subject to the variables' normality. Shapiro-Wilk's normality test was used, and skewed datasets were log-transformed (log_{10}) to normalise their distribution. Categorical data were compared using Chi-squared and Fisher's exact tests. The correlation was undertaken with either Pearson's or Spearman's as appropriate. To evaluate image-based diagnostic accuracy, the Gwet's AC1 agreement coefficient was calculated and categorised as poor <0.40, good 0.40-0.75, and excellent >0.75 [Dettori et al., 2020; Wongpakaran et al., 2013; Cibulka et al., 2021]. Statistical significance was taken as a two-sided 5% level ($p<0.05$). Statistical analysis was performed using the open-source R statistical software package (version 4.0.3).

5.3 RESULTS

5.3.1 STUDY PARTICIPANTS

The study cohort consisted of 20 participants who underwent clinically indicated carotid endarterectomy after ^{18}F-NaF PET-MRI. Three participants were excluded from the calcium and lipid core analysis due to fragmentation of carotid specimens which precluded reliable tissue analysis. Participants (mean age, 69±9 years; 13 male) had multiple cardiovascular risk factors, especially hypertension, hypercholesterolaemia and smoking habit (Table 5.1).

5.3.2 MAGNETIC RESONANCE IMAGING – DIAGNOSTIC ACCURACY

Direct comparison of *in vivo* and *ex vivo* magnetic resonance scans (Figure 5.1) was completed in all 20 carotid plaques and compared with histology. Identified plaque components included necrotic lipid core, intraplaque haemorrhage, calcium, rupture or erosion, and thrombus (Figure 5.2A).

MRI - 3T in vivo versus 7T ex vivo

The overall percentage of agreement between *in vivo* and *ex vivo* MRI ranged from 60-95% (Table 5.2, Figure 5.2B). The Gwet's AC1 values demonstrated good agreement for the identification of intraplaque haemorrhage (Gwet's AC1=0.46) and rupture or erosion (Gwet's AC1=0.6), whilst an excellent agreement was achieved for the detection of calcified plaque (Gwet's AC1=0.94). A poor agreement was displayed for the necrotic lipid core (Gwet's AC1=0.26).

MRI- 3T in vivo versus Histology

There was excellent agreement (Gwet's AC1 >0.81) for the detection of intraplaque haemorrhage between *in vivo* MRI and histology. Whereas good levels of agreement were found for the identification of necrotic lipid core (Gwet's AC1= 0.46) and thrombus (Gwet's AC1= 0.63). *In vivo* 3T MRI under-

reported rupture or erosion compared to histology resulting in a poor agreement (Gwet's AC1=0.15) (Table 5.3, Figure 5.2C).

MRI- 7T ex vivo versus Histology

There were heterogeneous levels of agreement between *ex vivo* magnetic resonance imaging and histological examination, with the Gwet's AC1 values ranging from 0.26 to 0.88 (Table 5.4, Figure 5.2D). A good agreement was shown for intraplaque haemorrhage (Gwet's AC1= 0.64), necrotic lipid core (Gwet's AC1= 0.5) and excellent for calcium (Gwet's AC1= 0.88). Whereas poor agreement was found for identification of plaque rupture or erosion. *Ex vivo* magnetic resonance imaging failed to identify the presence of any thrombus.

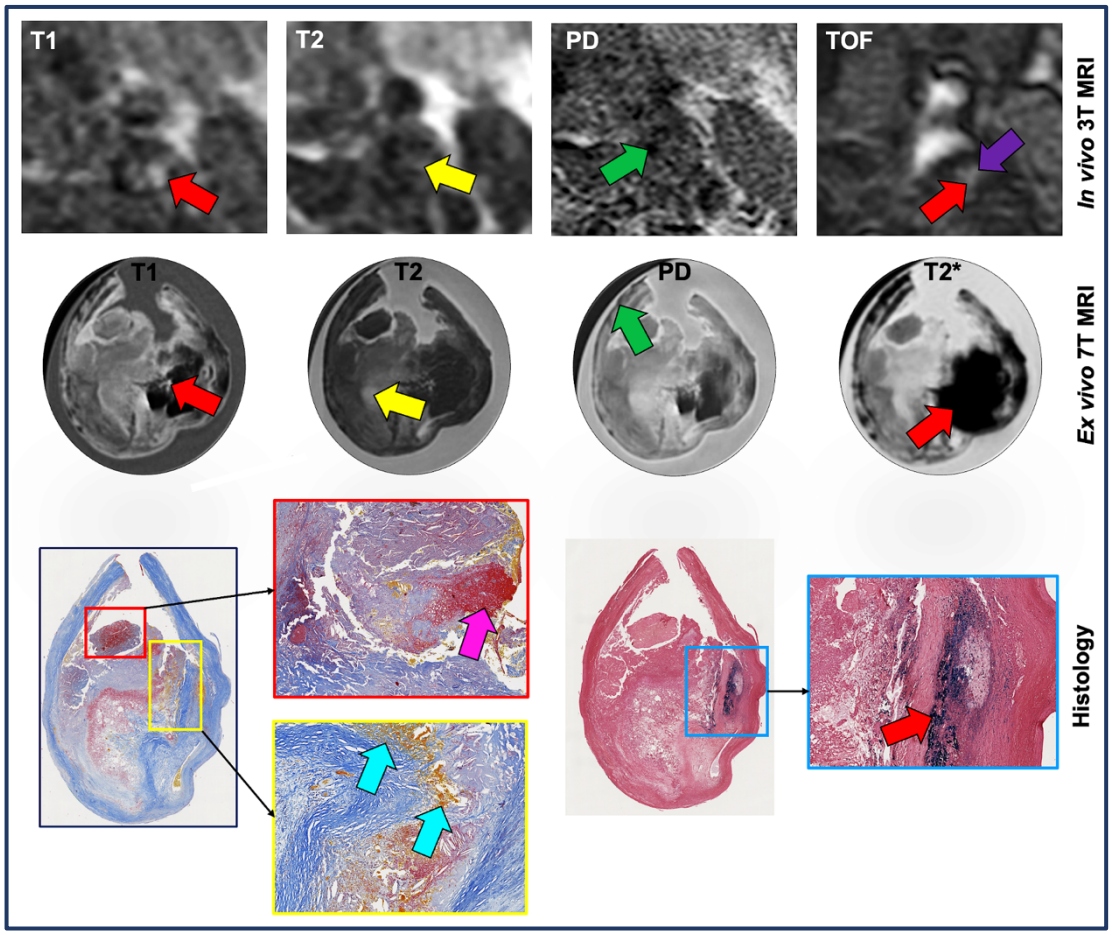
Table 5.1: Baseline characteristics of participants.

Characteristics	Total = 20
Demographics	
Age, years	69 ± 8.6
Men	13 (65%)
ASSIGN score*	37.8 ± 22.3
Vital signs	
Systolic blood pressure (mmHg)	147 ± 18.5
Diastolic blood pressure (mmHg)	80 ± 7.6
Heart rate (/min)	72 ± 11
Body-mass index (kg/m^2)	29 ±4.7
Smoking status	
Non-smoker	7 (35%)
Ex-smoker	8 (40%)
Current smoker	5 (255)
Presenting diagnosis	
Amaurosis fugax	7 (35%)
Transient ischemic attack	4 (20%)
Stroke	9 (45%)
Relevant medical history	
Hypertension	15 (75%)
Diabetes mellitus	3 (15%)
Hypercholesterolemia	17 (85%)
Ischemic heart disease	4 (20%)
Peripheral vascular disease	3 (15%)
Chronic Obstructive Pulmonary Disease	3 (15%)

Previous history of cerebrovascular disease	
Amaurosis fugax	1 (5%)
Transient ischemic attack	4 (20%)
Stroke	5 (25%)
None	10 (50%)
Severity of operated carotid artery stenosis	
Duplex ultrasound	
> 70%	19 (95%)
50-69%	1 (5%)
MRA	
> 70%	19 (95%)
50-69%	1 (5%)
Baseline medication therapy	
Clopidogrel	17 (85%)
Aspirin	6 30%)
Dual antiplatelet therapy	5 (25%)
Statin	20 (100%)
Anticoagulant	2 (10%)
Beta blocker	3 (15%)
ACE inhibitor	8 (40%)
Diuretic	3 (15%)
Calcium channel blocker	7 (35%)
Hypoglycaemic therapy	2 (10%)
Baseline biochemistry	
Total cholesterol (mmol/L)	5.19 ± 0.85
HDL-Cholesterol (mmol/L)	1.23 ± 0.29
LDL-Cholesterol (mmol/L)	2.16 ± 0.74
Triglycerides (mmol/L)	1.42 ± 0.67
eGFR	58.55 ± 6.48

Number (%), mean ± standard deviation, or median [interquartile interval]. *ASSIGN score: 10-Year cardiovascular risk score; MRA: Magnetic Resonance Angiography; HDL: high-density lipoproteins; LDL: low-density lipoproteins; eGFR: Estimated glomerular filtration rate (mL/min/1.73 m^2); ACE: angiotensin-converting enzyme.

Figure 5.1: Carotid plaque imaging with MRI (*in vivo* and *ex vivo*) and histology.



High risk plaque features detected by *in vivo* (top row) and *ex vivo* (middle row) MRI with histological (bottom row) identification of intraplaque haemorrhage:

MRI (*in vivo* and *ex vivo*):

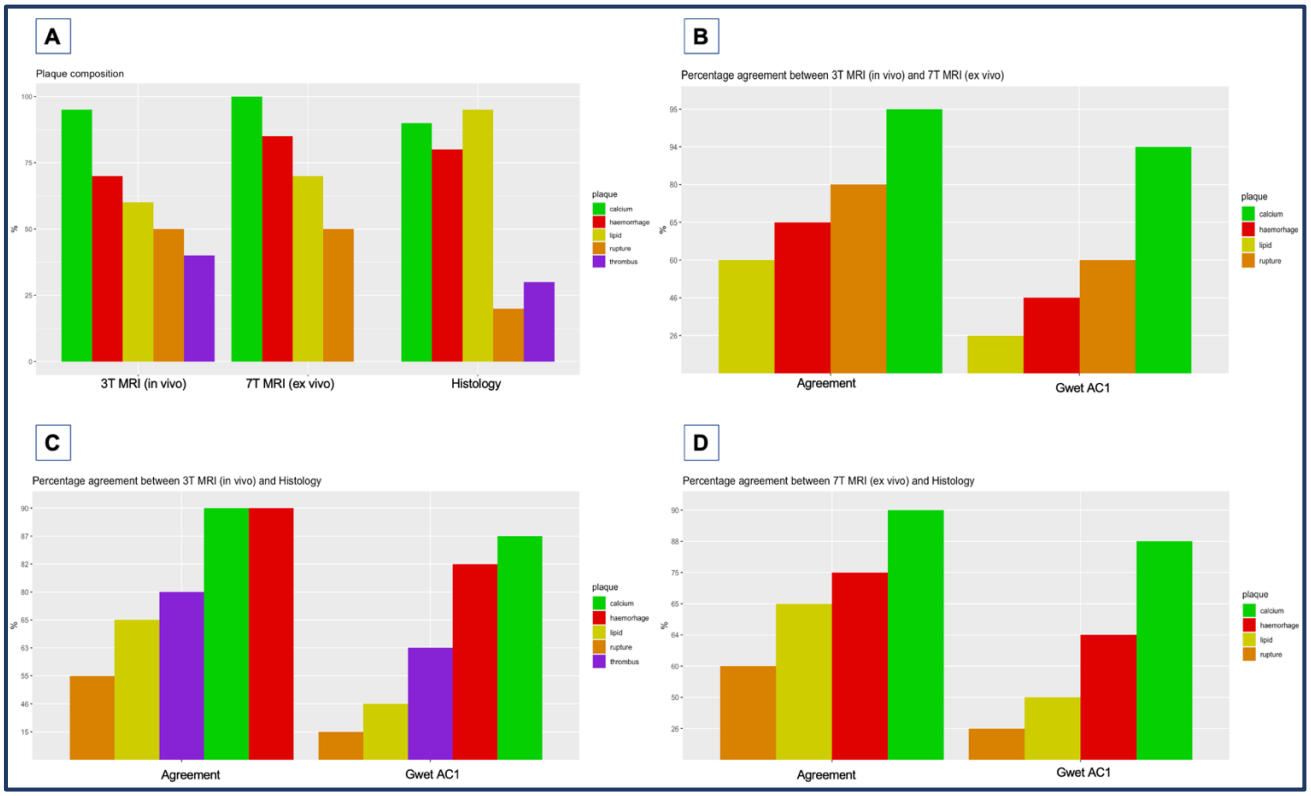
- T1, T2* and TOF: intraplaque haemorrhage (red arrows)
- T2: necrotic lipid core (yellow arrows)
- PD: calcium (green arrows)
- TOF: thrombus (purple arrow)

Histology (Martius Scarlet Blue):

- Red stain: fibrin (pink arrow)
- Yellow stain: red blood cells (turquoise arrows)

MRI: magnetic resonance imaging; T1 and T2: T weighted images; T2*: T star weighted image; PD: proton density, TOF: time of flight.

Figure 5.2: Plaque composition (A) and MRI diagnostic accuracy (B, C, D) with % agreement and Gwet's AC1 agreement coefficient.



A - Frequency distribution (%) of individual plaque components detected by 3T, 7T MRI and histology.
B - MRI diagnostic accuracy (3T versus 7T)
C - MRI diagnostic accuracy (3T versus histology)
D - MRI diagnostic accuracy (7T versus histology)

Table 5.2: MRI - 3T versus 7T and % agreement with Gwet's AC1 coefficient agreement.

In vivo/Ex vivo MRI	% Agreement	Gwet AC1 (CI)
Lipid	60%	0.26 (-0.23-0.76)
Haemorrhage	65%	0.46 (0.01-0.91)
Calcium	95%	0.94 (0.83-1.0)
Rupture/Erosion	80%	0.6 (0.21-0.98)

Table 5.3: MRI - 3T versus Histology and % agreement with Gwet's AC1 coefficient agreement.

In vivo MRI/Histology	% Agreement	Gwet AC1 (CI)
Lipid	65%	0.46 (0.01-0.91)
Haemorrhage	90%	0.82 (0.56-1.0)
Calcium	90%	0.87 (0.68-1.0)
Rupture/Erosion	55%	0.15 (-0.35-0.66)
Thrombus	80%	0.63 (0.25-1.0)

Table 5.4: MRI - 7T versus Histology and % agreement with Gwet's AC1 coefficient agreement.

Ex vivo MRI/Histology	% Agreement	Gwet AC1 (CI)
Lipid	65%	0.5 (0.08-0.93)
Haemorrhage	75%	0.64 (0.29-1.0)
Calcium	90%	0.88 (0.71-1.0)
Rupture/Erosion	60%	0.26 (-0.23-0.76)

5.3.3 HISTOLOGY

The identified carotid plaque components included intraplaque haemorrhage (n=16, 80%), necrotic lipid core (n=19, 95%), calcification (n=18, 90%), thrombus (n=8, 40%), rupture/erosion (n=4, 20%), thin fibrous cap (n=8, 40%), central cap inflammation (n=9, 45%) and cap shoulder inflammation (n=11, 55%). Of 20 carotid plaques, 7 (35%) plaques were graded as phenotype A, 2 (10%) as phenotype B, 6 (30%) as phenotype C and 5 (25%) plaques were described as the most severe phenotype D (Figure 2.12 in Chapter 2).

5.3.4 CORRELATION ANALYSIS - MICROCALCIFICATION

^{18}F-NaF PET - in vivo versus ex vivo

There was a strong correlation between *in vivo* and *ex vivo* ^{18}F-NaF uptake (Figure 5.3) measured by SUV_{mean} (R = 0.62, p=0.004) and SUV_{max} (R=0.78, p<0.001).

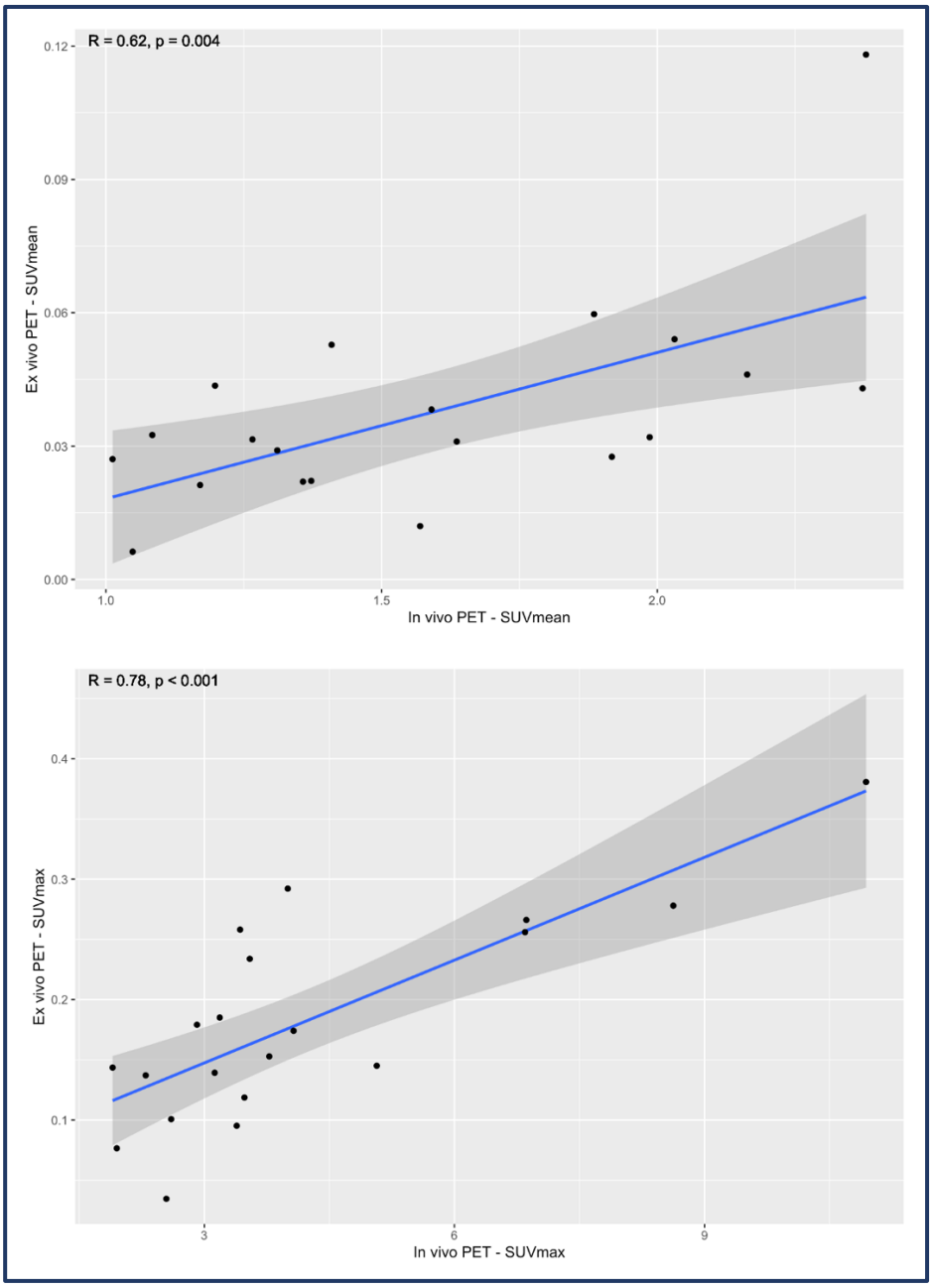
^{18}F-NaF PET – in vivo and ex vivo versus micro-CT (Calcium volume)

The *in vivo* SUV_{max} of ^{18}F-NaF uptake demonstrated a strong correlation with the calcium volume (r=0.73, P<0.001), whilst the *ex vivo* SUV_{max} of ^{18}F-NaF uptake revealed a moderate correlation with the calcium volume (r=0.51, P= 0.03) (Figure 5.4, Tables 5.5 and 5.6).

^{18}F-NaF PET – in vivo and ex vivo versus Histology (Calcium index)

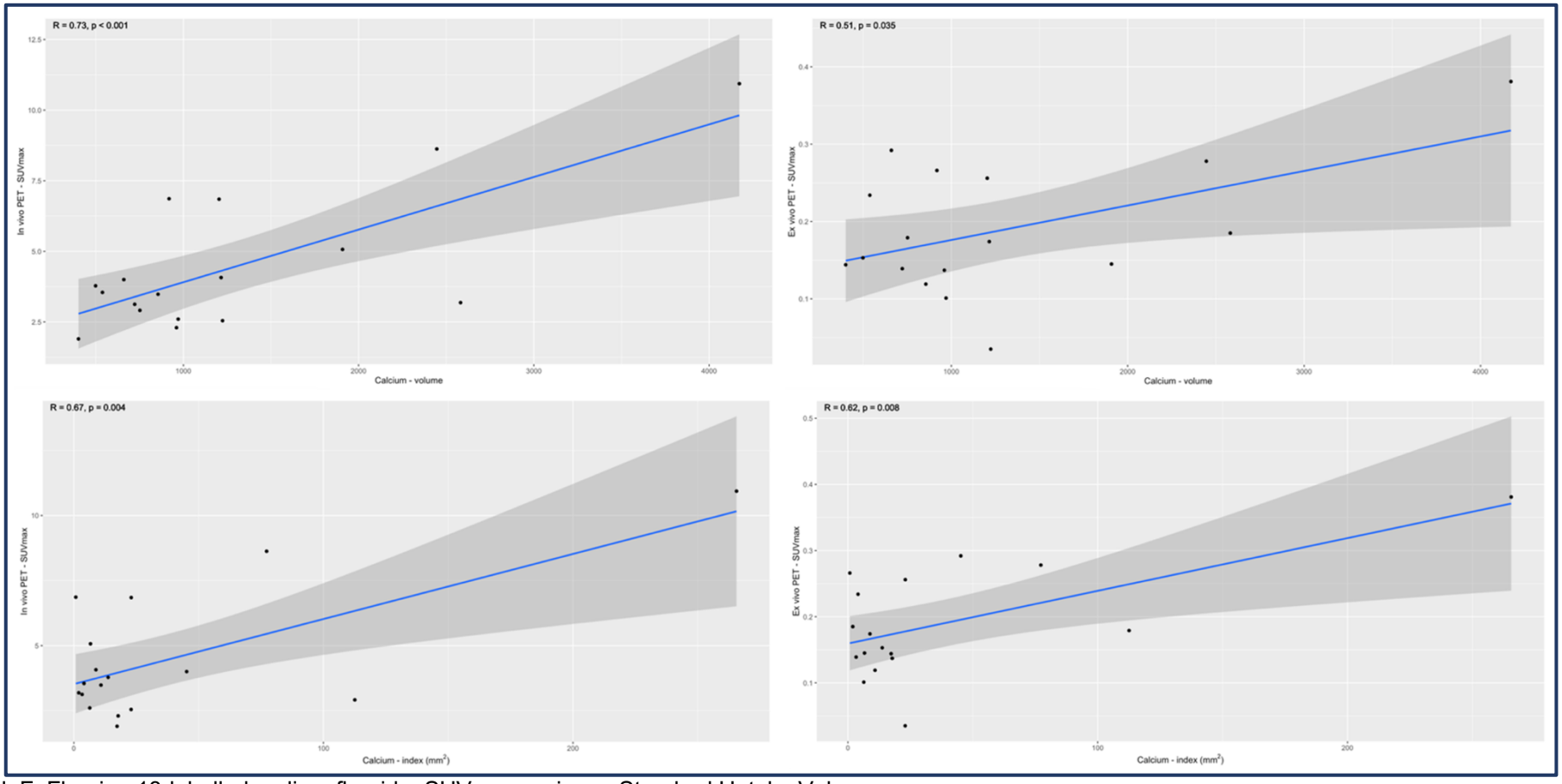
A similar pattern of moderate correlation was observed between the *in vivo* (r=0.67, P=0.004) and *ex vivo* (r=062, p=0.008) SUV_{max} of ^{18}F-NaF uptake and the histologically detected calcium index (Figures 5.4 and 5.5, Tables 5.5 and 5.6).

Figure 5.3: Correlation between *in vivo* and *ex vivo* ^{18}F-NaF uptake.



^{18}F-NaF: Fluorine 18-labelled sodium fluoride; SUV_{mean}: mean Standard Uptake Value; SUV_{max}: maximum Standard Uptake Value.

Figure 5.4: Correlation between ^{18}F-NaF uptake (In vivo and Ex vivo) and calcification detected by microCT (calcium volume) and histology (calcium index).



^{18}F-NaF: Fluorine 18-labelled sodium fluoride; SUV_{max}: maximum Standard Uptake Value.

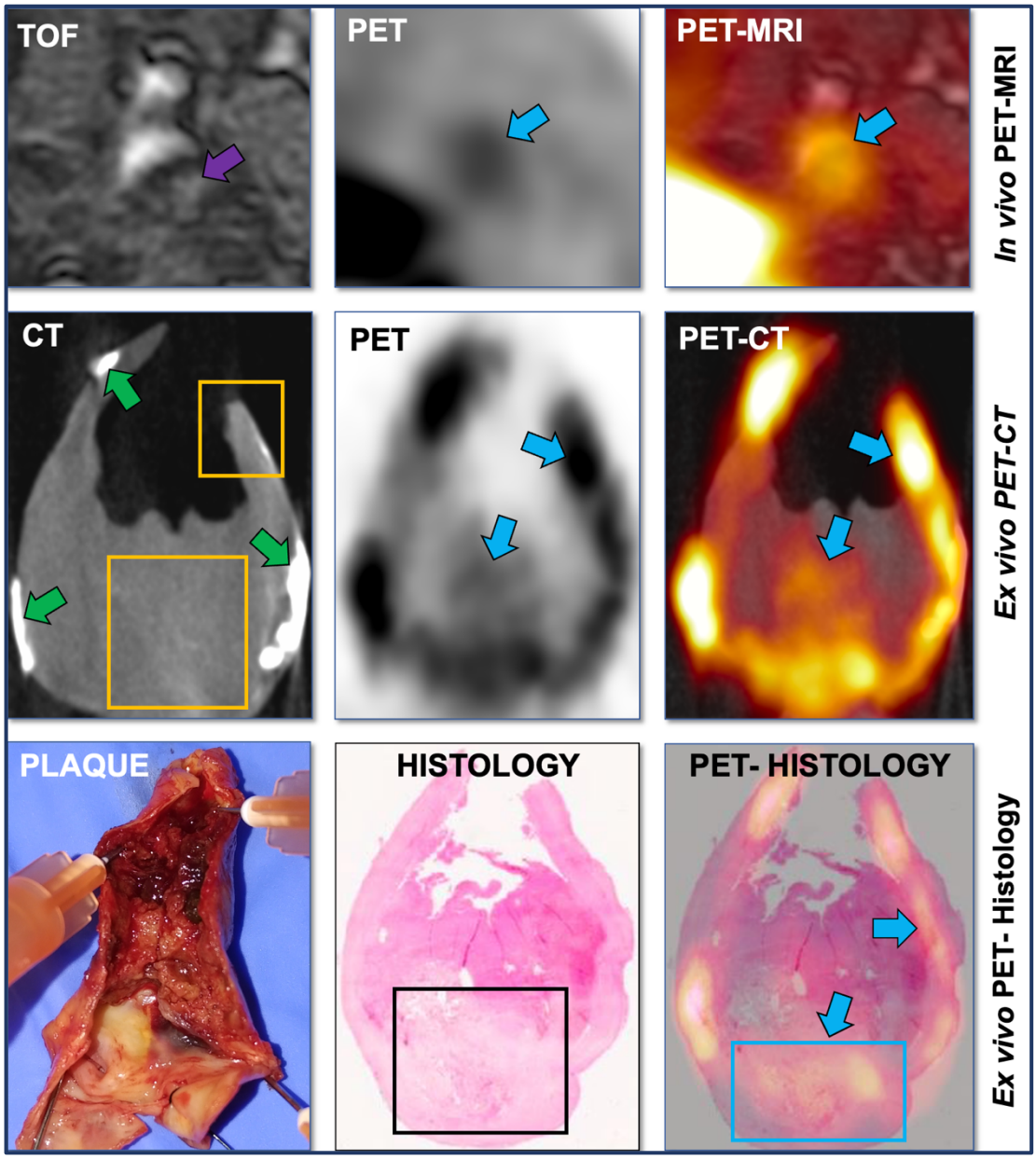
Table 5.5: Correlation between *in vivo* ^{18}F-NaF uptake and histology.

	In vivo PET SUV max			*In vivo PET SUV mean*			*In vivo TBR max*			*In vivo TBR mean*		
Histology	*R*	*95% CI*	*P*	*R*	*95% CI*	*P*	*R*	*95% CI*	*P*	*R*	*95% CI*	*P*
Elastin – index (mm2)	0.44	-0.01-0.74	**0.05**	0.26	-0.2-0.63	0.26	0.30	-0.15-0.66	0.18	0.08	-0.36-0.51	0.70
Calcium – index (mm2)	0.67	0.27-0.86	**0.004**	0.40	-0.09-0.74	0.10	0.63	0.21-0.85	**0.006**	0.35	-0.15-0.71	0.16
Lipid core – index (mm2)	-0.55	-0.82 - -0.10	**0.027**	-0.37	-0.72-0.12	0.13	-0.62	-0.84- -0.19	**0.008**	-0.53	-0.80- -0.07	**0.02**
Fibrin – index (mm2)	-0.17	-0.34-0.53	0.480	-0.16	-0.56-0.30	0.50	0.37	-0.08-0.69	0.10	0.40	-0.04-0.71	0.70
Red blood cells – index (mm2)	-0.25	-0.62-0.22	0.295	-0.32	-0.66-0.14	0.16	-0.05	-0.48-0.40	0.82	0.10	-0.35-0.52	0.65
microCT												
Calcium – volume	0.73	0.39-0.9	**< 0.001**	0.42	-0.06-0.75	0.08	0.70	0.34-0.88	**0.001**	0.41	-0.08-0.74	0.09

Table 5.6: Correlation between *ex vivo* ^{18}F-NaF uptake and histology.

	Ex vivo PET SUV max			*Ex vivo PET SUV mean*		
Histology	*R*	*95% CI*	*P*	*R*	*95% CI*	*P*
Elastin – index (mm2)	0.06	-0.39-0.49	0.80	0.08	-0.37-0.50	0.73
Calcium – index (mm2)	0.62	0.19-0.85	**0.008**	0.83	0.57-0.94	**< 0.001**
Lipid core – index (mm2)	-0.34	-0.7-0.16	0.17	-0.27	-0.66-0.23	0.28
Fibrin – index (mm2)	0.18	-0.3-0.58	0.43	0.35	-0.10-0.68	0.13
Red blood cells – index (mm2)	-0.11	-0.52-0.35	0.67	-0.06	-0.5-0.39	0.78
microCT						
Calcium – volume	0.51	0.04-0.79	**0.03**	0.60	0.18-0.84	**0.009**

Figure 5.5: Meta-imaging of carotid plaque by ^{18}F-NaF PET-MRI, micro-PET-CT and fused PET-Histology.



Meta-imaging:

- **Top row:** TOF detected thrombus (purple arrow) and ^{18}F-NaF uptake localised to culprit internal carotid artery (blue arrows) on PET and fused PET-MRI images
- **Middle row:** *ex vivo* micro-CT with macrocalcified regions (green arrows), undetected microcalcification (orange boxes) and microcalcium (blues arrows) demonstrated by ^{18}F-NaF uptake on micro-PET and fused micro-PET-CT
- **Bottom row:** ruptured carotid plaque with invisible microcalcium on H&E staining (black box) but visible microcalcium deposits following digital fusion of base histology image with micro-PET image (blue box and blue arrows)

^{18}F-NaF PET-MRI: Fluorine 18-labeled sodium fluoride positron emission tomography-magnetic resonance imaging; TOF: time of flight; PET-CT: positron emission tomography-computed tomography; H&E: haematoxylin and eosin.

5.3.5 CORRELATION ANALYSIS – PLAQUE COMPONENTS AND GRADES

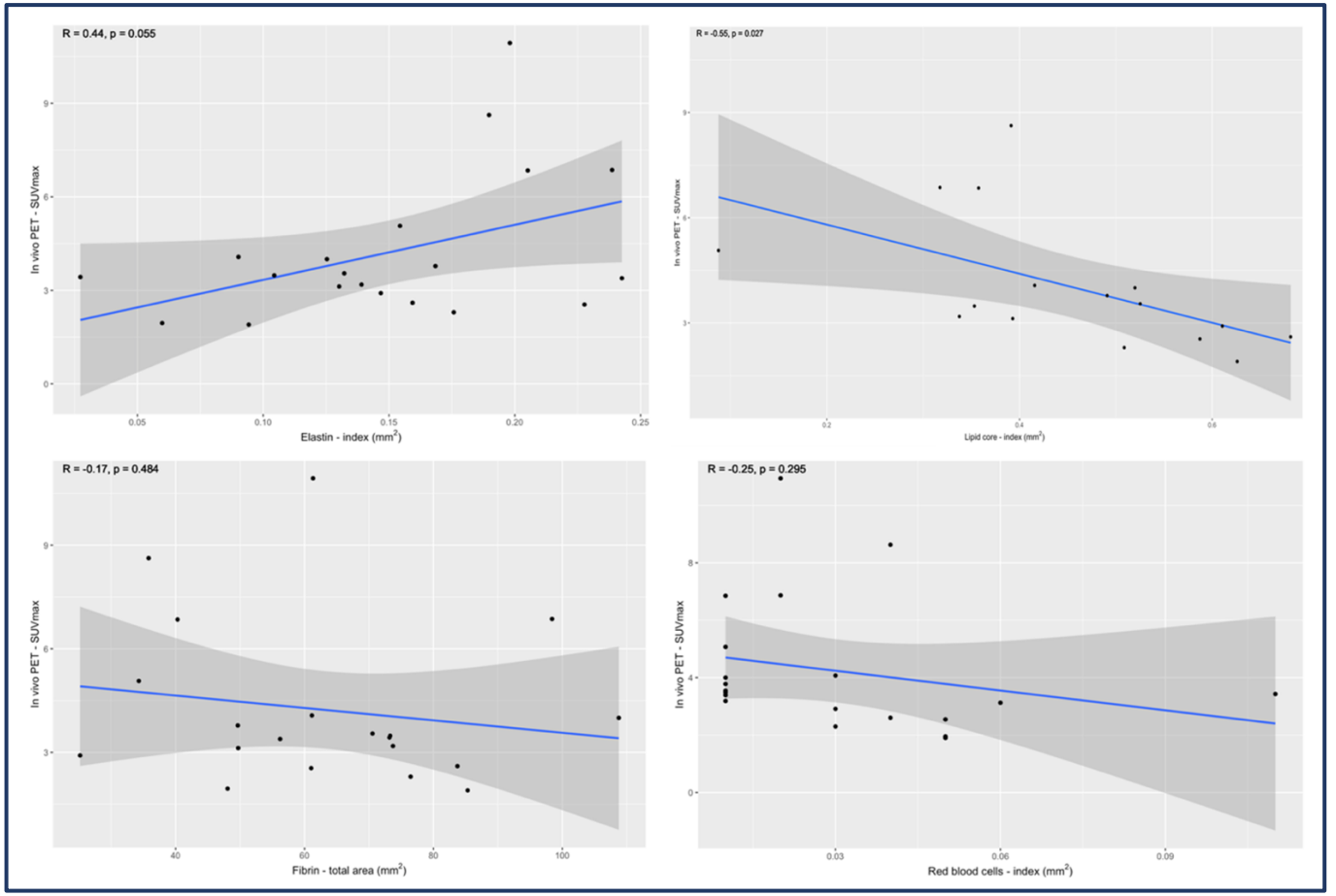
^{18}F-NaF PET – in vivo and ex vivo versus Histology (Plaque components)

The i*n vivo* SUV_{max} of ^{18}F-NaF uptake demonstrated a moderate correlation with the elastin index (r=0.44, P=0.05) and correlated inversely with the lipid core (r= -0.55, P=0.02). The radiotracer did not demonstrate relationships with fibrin index (r=-0.17, P=0.48) and red blood cell index (r=-0.25, P=0.29) (Figure 5.6, Table 5.5). The *ex vivo* SUV_{max} of ^{18}F-NaF uptake did not show demonstrable correlations with plaque features including the elastin index (r=0.06, P=0.8), fibrin index (r=0.17, P=0.48) and red blood cells index (r=-0.11, P=0.66) (Table 5.6).

^{18}F-NaF PET – in vivo and ex vivo versus Histology (Plaque Grades)

The linear regression model demonstrated an association between the *in vivo* SUV_{max} of ^{18}F-NaF uptake and histological carotid plaque grade severity (Figure 5.7). In contrast, no such association was found between *ex vivo* SUV_{max} of ^{18}F-NaF and plaque grade (Figure 5.8).

Figure 5.6: Correlation between *in vivo* ^{18}F-NaF uptake and histological markers of high-risk plaque features (elastin, lipid core, fibrin and red blood cells).



^{18}F-NaF: Fluorine 18-labelled sodium fluoride; SUV_{mean}: mean Standard Uptake Value; SUV_{max}: maximum Standard Uptake Value.

Figure 5.7: Forrest plot demonstrating association between *in vivo* ^{18}F-NaF uptake measured by SUVmax and the most severe plaque grade.

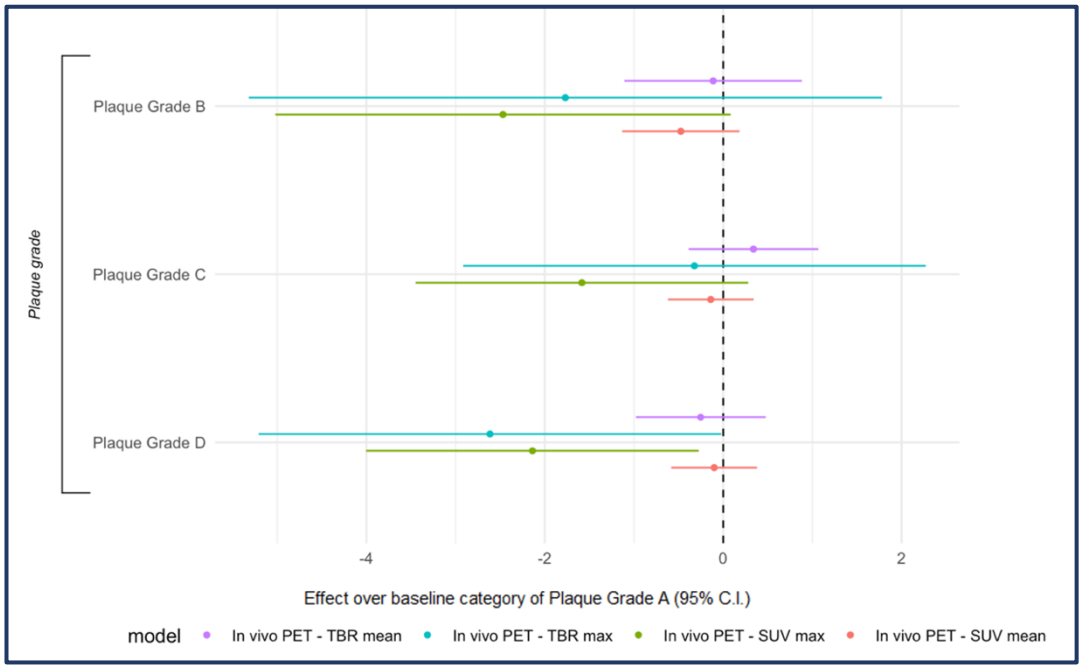
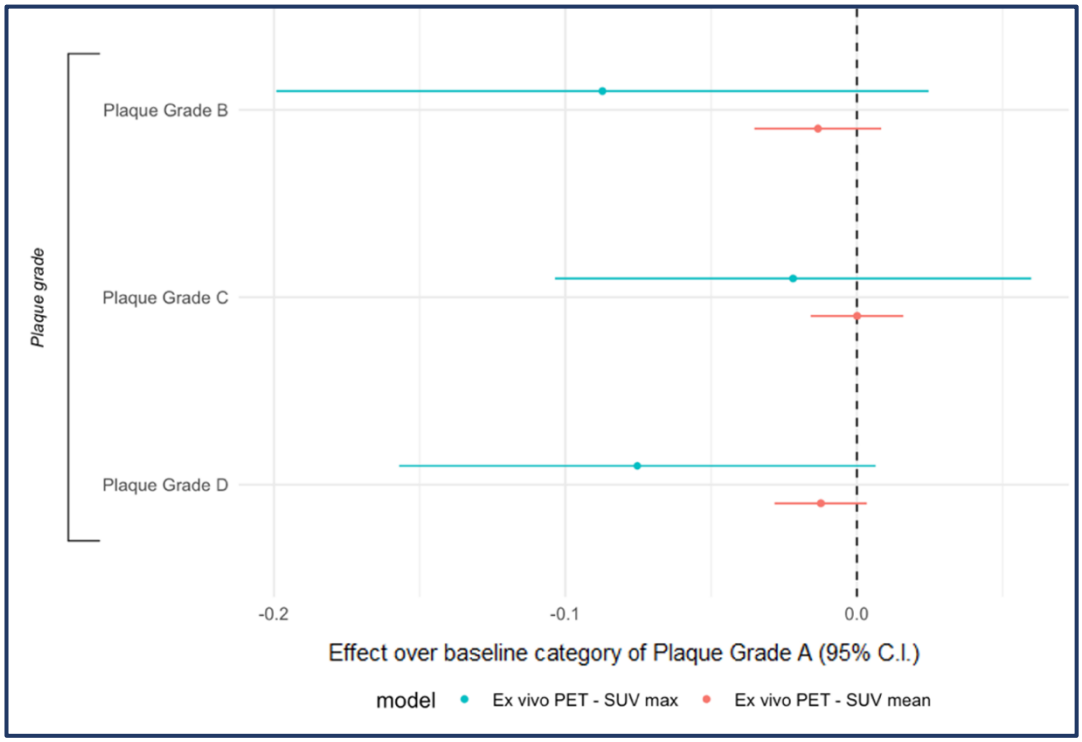


Figure 5.8: Forrest plot demonstrating no association between *ex vivo* ^{18}F-NaF uptake and plaque grades.



5.4 DISCUSSION

^{18}F-NaF PET-MRI of the carotid artery is the only imaging technique which integrates plaque composition with stenosis assessment and identifies areas of microcalcification indicative of high-risk atherosclerotic plaque. In the current study, we demonstrated acceptable diagnostic accuracy of *in vivo* 3T ^{18}F-NaF PET-MRI in detection of high-risk carotid plaque features (intraplaque haemorrhage, lipid core and calcium) compared with *ex vivo* 7T MRI and histological examination. *In vivo* 3T ^{18}F-NaF PET-MRI uptake co-localised with areas of active microcalcification detected by *ex vivo* imaging (micro-CT and ^{18}F-NaF PET) and histological analysis. Furthermore, we found an association between *in vivo* radiotracer binding and plaque subcomponents (elastin and lipid core) indicative of localised tissue degeneration. Finally, we showed that ^{18}F-NaF PET-MRI identified severe histopathological carotid plaque disease denoting its potential role in the dichotomous patient stratification when selecting an individual for high-risk carotid surgical intervention as opposed to the best medical management alone.

A multitude of research devoted to non-invasive cross-sectional imaging of carotid atherosclerosis established that MRI identifies the key tetrad of high-risk carotid plaque features (intraplaque haemorrhage, lipid core, calcification, and thin fibrous cap) that are associated with rapid plaque progression, rupture, and increased risk of future neurovascular events [Kramer et al., 2020; Zhao et al., 2018]. Our study demonstrated that *in vivo* 3T MRI had good or excellent agreement with ex vivo 7T MRI for the identification of adverse plaque features which are prevalent in the culprit plaque, such as intraplaque haemorrhage, rupture or erosion, and calcification. The poor agreement with the lipid core assessment likely reflects specimen shrinkage due to fixation, which causes volume changes and tissue distortion with the largest reported shrinkage of up to 76% [Gonzalez et al., 2016]. Both *in vivo* 3T and *ex vivo* 7T MRI reported good agreement with detailed histological examination for the identification of intraplaque haemorrhage, lipid core and calcification. The

discrepancy between MRI (*in vivo* and *ex vivo*) and histology regarding rupture or erosion and thrombus detection could relate to the spatial resolution differences of *in vivo* 3T versus *ex vivo* 7T MRI and the ultimate gold standard histological examination [Gonzalez et al., 2016]. Additional factors explaining poor agreement for rupture or erosion and no thrombus detection by *ex vivo* 7T MRI point to the interval between *in vivo* and *ex vivo* MRI scans and potential washout of the surface plaque thrombus as all carotid specimens were transferred from 10% formaldehyde to phosphate-buffered saline for at least 24h before scanning in *ex vivo* 7T MRI.

Intimal calcification involves a process resembling osteogenesis, including induction of osteoblasts, representing a healing response to a localised atherosclerotic subintimal wall injury. At present, ^{18}F-NaF is the only radiotracer that has been used to detect and to quantify the degree of this vascular damage as it binds to the earliest precursor of microscopic calcium deposit within the arterial wall, namely the hydroxyapatite (crystallised calcium phosphate) [Irkle et al., 2015]. We have previously reported that ^{18}F-NaF identified the culprit carotid plaque in patients with acute neurovascular syndromes [Vesey et al., 2017] and showed increased uptake in culprit arteries with stenosis >70% [Kaczynski et al., 2022]. In the current study we confirmed strong correlation of radiotracer binding with carotid tissue between *in vivo* and *ex vivo* ^{18}F-NaF PET imaging. These findings were augmented further by calcium co-localisation between ^{18}F-NaF PET (*in vivo* and *ex vivo*) and *ex vivo* micro-CT measured calcium volume (moderate and strong correlation) as well as histologically segmented calcium index (moderate correlation). The ability of ^{18}F-NaF PET-MRI to detect and to quantify biological micronodules of calcium with MRI-detected classical vascular morphological plaque features renders it an ideal hybrid imaging modality capable of identifying carotid plaques that are at high risk of symptomatic transformation (rupture or erosion), thus enabling individualised patient selection for carotid revascularisation. Moreover, these findings indicate a window of therapeutic

opportunity in the context of an early diagnosis, risk prediction and non-surgical therapeutic intervention.

We demonstrated that *in vivo* ^{18}F-NaF exhibited uptake in the histologically detected regions of carotid tissue disruption, including elastin deposition and the lipid core. However, no such association was found in relation to histological markers of intraplaque haemorrhage (fibrin and red blood cells). These findings contrast with the only published report on ^{18}F-NaF PET-MRI in 12 patients with symptomatic carotid disease that found no radiotracer association with MRI high-risk plaque features [Mechtouff et al., 2020]. However, our current observations, excluding the intraplaque haemorrhage, support the findings from our large prospective observational data on the role of ^{18}F-NaF PET-MRI in 110 patients with symptomatic carotid disease which reported radiotracer correlation with the features of plaque vulnerability [Kaczynski et al., 2022]. The lack of meaningful correlation with histological markers (fibrin and red blood cells) of intraplaque haemorrhage could be explained by our surgical cohort data that consisted only of severe carotid disease. As such, correlations may be challenging due to a lack of samples with mild or moderate tissue disease which would provide a broader spectrum of disease and a greater ability to explore potential associations.

The positive correlation of radiotracer uptake with elastin fibers is an interesting finding because increased ^{18}F-NaF uptake implies a loss of tissue integrity. However, elastin fibers disintegration is not a dominant feature of subintimal carotid disease, unlike medial degeneration observed in the aneurysmal aorta that has increased radiotracer uptake in moderately diseased aortic wall [Fletcher et al., 2022a]. Furthermore, there are substantial differences between carotid and aortic circulations including the different amount of native elastin and the unique carotid bifurcation geometry [Beard et al., 2009] that is characterised by the compensatory outward media hypertrophy which harbors elastin producing smooth muscles cell. Thus, whether the radiotracer binding resulted from microcalcific deposits along intact (background ^{18}F-NaF signal) or altered (fragmentation points that

augment ^{18}F-NaF affinity) carotid elastin fibers is unknown and necessitates future research. The negative correlation between the ^{18}F-NaF and lipid core is unsurprising given that the lipid core, which serves as a nidus for deposition of microcalcification, is cleared following plaque rupture. Thus, residual atheromatous carotid plaque content may present little residual metabolic activity. On the other hand, as already mentioned, lack of samples including mild or moderate disease could have prevented unravelling these potential correlations.

Most importantly, we found that *in vivo* ^{18}F-NaF uptake localised to the most severe histological carotid plaque grade severity, a finding that has not been previously reported. The implications are two-fold. First, it confirmed that ^{18}F-NaF identified biological molecular plaque activity in locations of histologically adverse plaque features. Second, it also questions our understanding of the NASCET data which paradoxically and indirectly augmented this long-known premise that MRI derived biomarkers of plaque vulnerability are the key parameters that determine the carotid plaque fate culminating in rupture or erosion. Undoubtedly, NASCET derived luminal arterial stenosis served as a surrogate marker for these complex high-risk atherosclerotic lesions explaining general correlations for such stenotic plaques to predict ipsilateral neurovascular events [Kramer et al., 2020]. Moreover, most of acute neurovascular events occur in carotids with <50% stenoses and perhaps unsurprisingly only about half of symptomatic excised plaques (>50% stenoses) show evidence of a rupture [Howard et al., 2015]. Furthermore, most of highly stenosed carotid arteries remain asymptomatic [Kramer et al., 2020], whilst more prevalent stenoses outside surgical NASCET criteria were responsible for more than 40% of strokes at follow-up in the NASCET trial [Saba et al., 2020]. Finally, non-obstructive (<50%) carotid plaques are increasingly being recognised as the primary cause of acute neurovascular events [Kramer et al., 2020; Kopczak et al., 2020]. Recent meta-analysis found that pooled prevalence of <50% carotid artery stenosis with high-risk plaque features was 32.5% in the ipsilateral vessel compared to 4.6% in the

contralateral carotid [Kamtchum-Tatuene et al., 2021]. Furthermore, higher prevalence of intraplaque haemorrhage has been reported in mildly stenotic plaques compared with moderate and severe carotid artery stenoses [Khenkina et al., 2023]. Nevertheless, the sheer presence of high-risk plaque characteristic does not immediately translate into clinical manifestation of acute neurovascular syndrome: for example, intraplaque haemorrhage can remain present for many years [Saba et al., 2020]. Other factors play a role in symptomatic plaque transformation and undoubtfully microcalcification is an important molecular biomarker that detects biologically active carotid lesions that are at risk of erosion or rupture which represent the most important determinant of thromboembolisation.

Our study is not without limitations. Although presented results reveal important and novel associations between microcalcification and histological plaque grade severity, these data ought to be interpreted cautiously owing to the small sample size devoid of milder degrees of carotid tissue disease. The time frame between *in vivo*, *ex vivo* imaging and histological examinations varied due to logistic reasons, influencing the length of time that harvested tissue was subject to 10% formaldehyde solution (depth of penetration increases with time). *In vivo* 3T MRI resolution may have not enabled accurate detection of small and frequently overlapping regions of carotid atheroma resulting in poor agreement with *ex vivo* 7T MRI. Lastly, although positive correlation between *in vivo* radiotracer uptake and detected calcification by other examinations (*ex vivo* PET, *ex vivo* micro-CT and histology) provided additional confidence when interpreting these associations, passive incubation with radiotracer could be confounded by non-physiological ^{18}F-NaF uptake within carotid specimens.

5.5 CONCLUSIONS

These ^{18}F-NaF PET-MRI study data broaden our understanding of radiotracer binding within carotid plaques by providing an enhanced map of carotid tissue mineralisation supported by relevant *ex vivo* imaging modalities complemented by histological analysis. This study laid the ground for the evaluation of calcified carotid tissue following acute neurovascular events by providing a comprehensive imaging technique which facilitates parallel assessment of cellular (inflammation), molecular (microcalcification) and morphological (macrocalcification, necrotic lipid core, intraplaque haemorrhage, luminal thrombus, and fibrosis) plaque characterisation. Future research is needed to provide data to address the added value of this approach and whether a shift from a traditional luminal stenosis assessment to the one which is based on the carotid atheroma composition has clinical value for our patients.

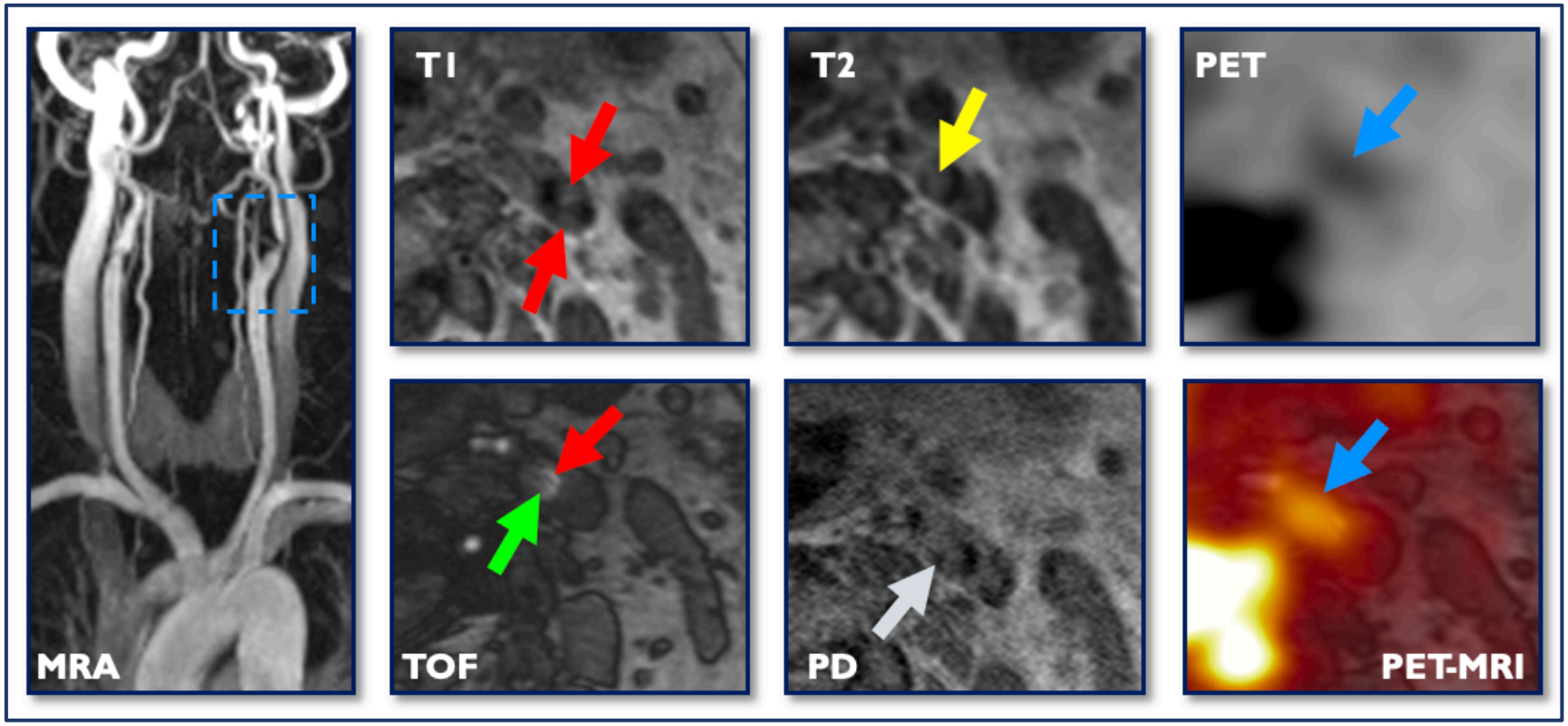
CHAPTER SIX

CONCLUSIONS AND FUTURE DIRECTIONS

6.1. INTRODUCTION

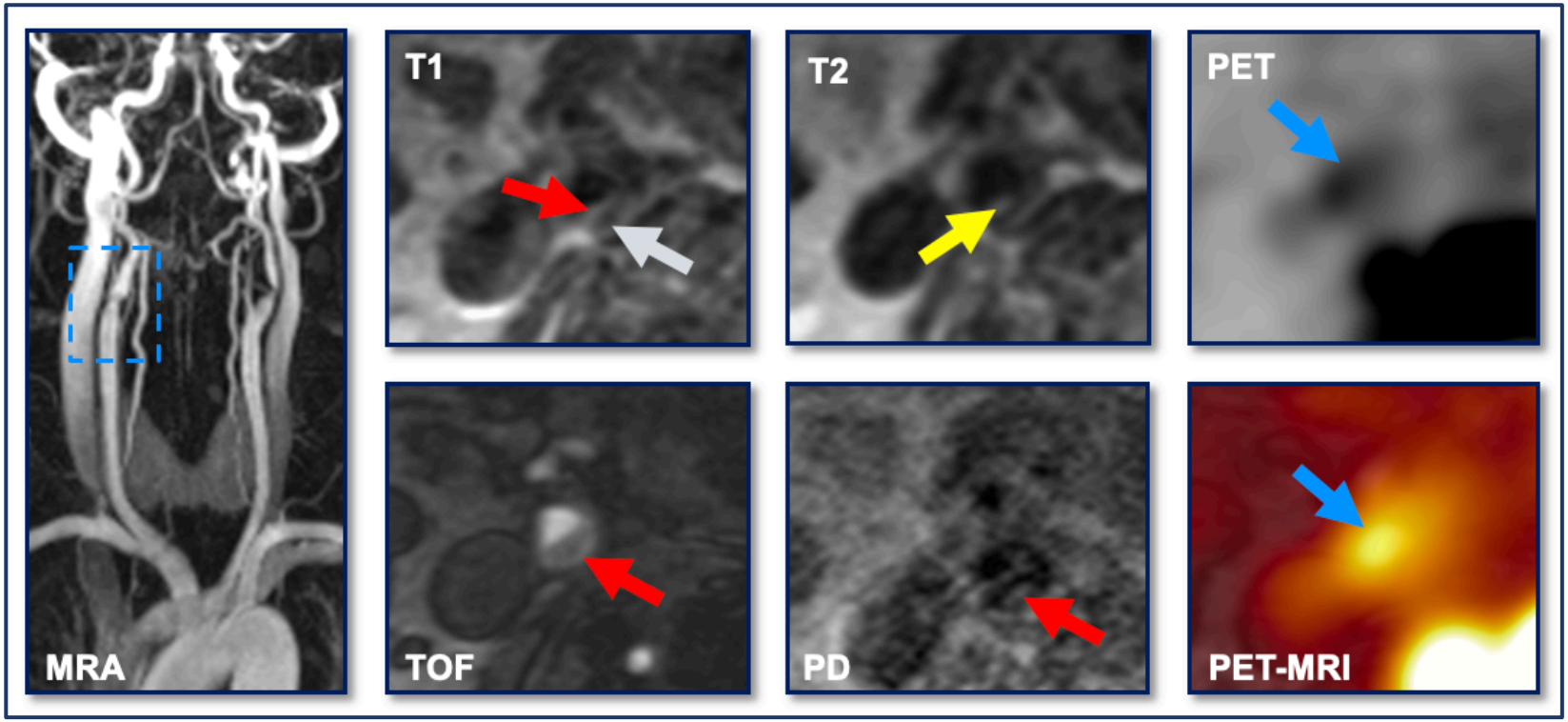
Despite the substantial progress made in understanding that high-risk carotid plaque features are associated with increased risk of acute neurovascular events independently of the degree of stenosis, plaque morphology continues to receive little attention when deciding to intervene. Those suffering from adverse neurovascular events most often display carotid artery stenosis less than the accepted minimal threshold for vascular surgery. In effect, non-obstructive carotid plaques that are highly likely to cause thromboembolic complications are excluded from a stroke preventative intervention (Figure 6.1a). Clinicians around the globe continue to rely on the reduction of luminal diameter of carotid artery as the main parameter that stratifies patients to either surgery or best medical therapy (Figure 6.1b). However, given the plethora of scientific literature, this represents an archaic formula that limits our understanding of atherosclerotic disease and potential therapeutic interventions. Although the mainstay of symptomatic carotid disease treatment is to reduce the incidence of future strokes, the gold standard treatment, namely carotid endarterectomy, can paradoxically lead to a devastating neurovascular outcome. Therefore, almost every technical step of the operation has been subjected to evidence-based scrutiny with large multicentre randomised controlled trials to ensure the best post-operative outcome for an individual patient that is determined by the major adverse neurovascular event that occurs within the first 30 post-operative days. Additionally, the Vascular Society of Great Britain and Ireland advocates that carotid endarterectomy should be performed in high-volume vascular units which undertake a minimum of 40 carotid surgeries in a year [Waton et al., 2020]. Multiple studies have demonstrated lower rates of stroke, death, and reduced hospital stay in higher volume centres [Naylor et al., 2018]. Such vascular centres have dedicated vascular anaesthetists, vascular laboratory technologists and multidisciplinary meetings in line with the Quality Improvement Programme that formulates Vascular Service Provision guidelines [Renton et al., 2018; Waton et al., 2013].

Figure 6.1a: Index acute neurovascular event.



Example of a surgical patient with left hemispheric TIA and >70% stenosis of the left internal carotid artery (MRA blue box) that underwent carotid endarterectomy. MRI plaque analysis identified intraplaque haemorrhage (red arrows), necrotic lipid core (yellow arrow), thrombus (green arrow) and calcification (grey arrow). ^{18}F-NaF PET-MRI showed focal uptake (blue arrows) in the region of the intraplaque haemorrhage and necrotic lipid core.
TIA: Transient ischaemic attack; MRA: magnetic resonance angiography; ^{18}F-NaF PET-MRI: Fluorine 18-labelled sodium fluoride positron emission tomography-magnetic resonance imaging; T1 and T2 weighted imaging; TOF: time-of-flight; PD: proton density.

Figure 6.1b: Contralateral acute neurovascular event.



Example of the same surgical patient (as in Figure 6.1a) which presented at the same time with right amaurosis fugax and 45% stenosis of the right internal carotid artery (MRA blue box) and despite the presence of high-risk plaque features was declined carotid endarterectomy because the degree of stenosis was outside NASCET criteria. MRI plaque analysis identified intraplaque haemorrhage (red arrows), necrotic lipid pool (yellow arrow), necrotic lipid core (yellow arrow) and calcification (grey arrow). ^{18}F-Na PET-MRI showed focal and moderate uptake (blue arrows) in the region of the intraplaque haemorrhage and necrotic lipid core. MRA: magnetic resonance angiography; ^{18}F-NaF PET-MRI: Fluorine 18-labelled sodium fluoride positron emission tomography-magnetic resonance imaging; T1 and T2 weighted imaging; TOF: time-of-flight; PD: proton density.

The pathogenesis of carotid atherosclerosis results from a multifaceted constellation of pathophysiological processes that ultimately lead to plaque rupture. Although detection of the key biological culprit plaque features has not found it's place in standard clinical practice, these can be assessed with the use of one of the most exciting technological developments in the field of cardiovascular imaging, such as the hybrid ^{18}F-NaF PET-MRI. Hybrid ^{18}F-NaF PET-MRI integrates plaque composition with stenosis assessment and identifies areas of microcalcification indicative of high-risk atherosclerotic plaque.

6.1.1 PAST, PRESENT AND THE FUTURE OF CAROTID PLAQUE IMAGING

The past hundred years represent a remarkable era that was astonishingly enriched by the technological development involving a shift towards digital imaging and analysis. The ground-breaking work began in 1895 with the discovery of electromagnetic radiation (x-rays) by Wilhelm Roentgen (Germany), followed by an invention of the very first mobile x-ray unit called *Little Curie* by Marie Curie in 1914 (France). These achievements provided the earliest glimpses into the radiation-based imaging phenomenon and paved the way for subsequent technological advances that have elevated cardiovascular science to a whole different level. In particular, the past decade delivered refined and highly attuned hybrid imaging modalities that seem to be *million light-years* away from the *Little Curies* of the previous century (Figure 6.2).

The present chapter was launched with the foundational publication regarding the role of MRI in cancer diagnosis in the journal of Nature in 1964 by John Millard (that went unnoticed) followed by a first whole-body MRI installation in 1980 in Aberdeen in the United Kingdom, shadowed by a parallel development of PET imaging by co-inventors Edward Hoffman and Michael Phelps in 1974 (United States of America). Finally, decades later, the first installation of a clinical hybrid PET-MRI scanner took place in 2010 (Germany, Switzerland and United States of America) [Muzic et al., 2014], echoed by the participants

recruitment into the first PET-MRI studies at the Edinburgh Imaging Facility (United Kingdom) in 2016.

Figure: 6.2: Little Curie.



Radiological car Massiot (a mobile x-ray unit used by the military health service of the French army and the Red Cross) [Bibliotheque-Nationale-de-France, 1914].

6.1.2 DANCE OF CAROTID PLAQUE PARTLICLES - QUANTUM PHYSICS JOURNEY

The undeniable strength of the hybrid PET-MRI imaging lies in the fact that it combines structural and physiological information that enables identification of specific plaque components with disease activity at a molecular level. More importantly, it lays the ground for a completely different therapeutic dyad based on the plaque morphology and severity of stenosis. The new clinical model may seem like an uninviting option and undoubtfully would be met with scepticism. However, this should not defer practitioners from pursuing such an approach because plaque phenotype classification that enables risk stratification offers the most congruent way of symptomatic carotid atherosclerosis management culminating in the individualised surgical or medical intervention. Thus, if we want to respond to patients' welfare to the best of our abilities, we ought to integrate the biology of an atheroma into the clinical decision paradigm, which is the prime determinant of clinical

neurovascular outcomes. We must be ready to alter our clinical perspective, thereby challenging the current *status quo* based on the stenosis measurement to manage acute neurovascular syndromes on an individual case basis.

Although challenging, a similar narrative has been depicted by other scientific schools when faced with new discoveries. In many ways, the introduction of hybrid PET-MRI scanners parallels the launch of sophisticated telescopes such as the Event Horizon Telescope that allowed us to obtain the first image of a central supermassive black hole within the Messier 87 galaxy (a supergiant elliptical galaxy in the Virgo constellation located 55 million light-years away from Earth) which existence was only theoretically hypothesised within the vast and ever-expanding universe until 2017 (Figure 6.3).

Moreover, such an astounding imaging triumph would not be possible without the most powerful scientific theory - the Quantum Theory, which has gifted us with all technological developments, including hybrid PET-MRI. The Quantum Theory was born at the beginning of the 20th century as an enigma that confused many scientists and was met with disbelief among others. It gradually unravelled peculiar relations between subatomic particles and shaped the very foundations of all machinery, allowing us to comprehend everything from the periodic table to complex medical imaging or nuclear fission [Rovelli, 2020]. The Quantum Theory, with its three core principles (*observation*, *granularity,* and *probability*) [Rovelli, 2020], opened a new direction of viewing the culprit carotid plaque through the lens of hybrid PET-MRI. The *observation* represents the primordial measure of stenosis severity, *granularity* resembles the detection of the plaque grains (plaque components), whilst *probability* refers to the statistical inference of risk of the future acute neurovascular event (Figure 6.4). Hence, plaque rupture which frees its particles as quanta or photons (discrete pockets of energy) that dance intraluminally as emboli (quanta of light) mimics quantum-like phenomena. The Quantum Theory proved once again that "our reality may be profoundly other that we had

imagined" [Rovelli, 2020] because, beyond the simplicity of the NASCET carotid artery stenosis measurement, hybrid PET-MRI presented us with a new capacity of imaging interior strata of the microscopic and molecular world that was invisible for decades.

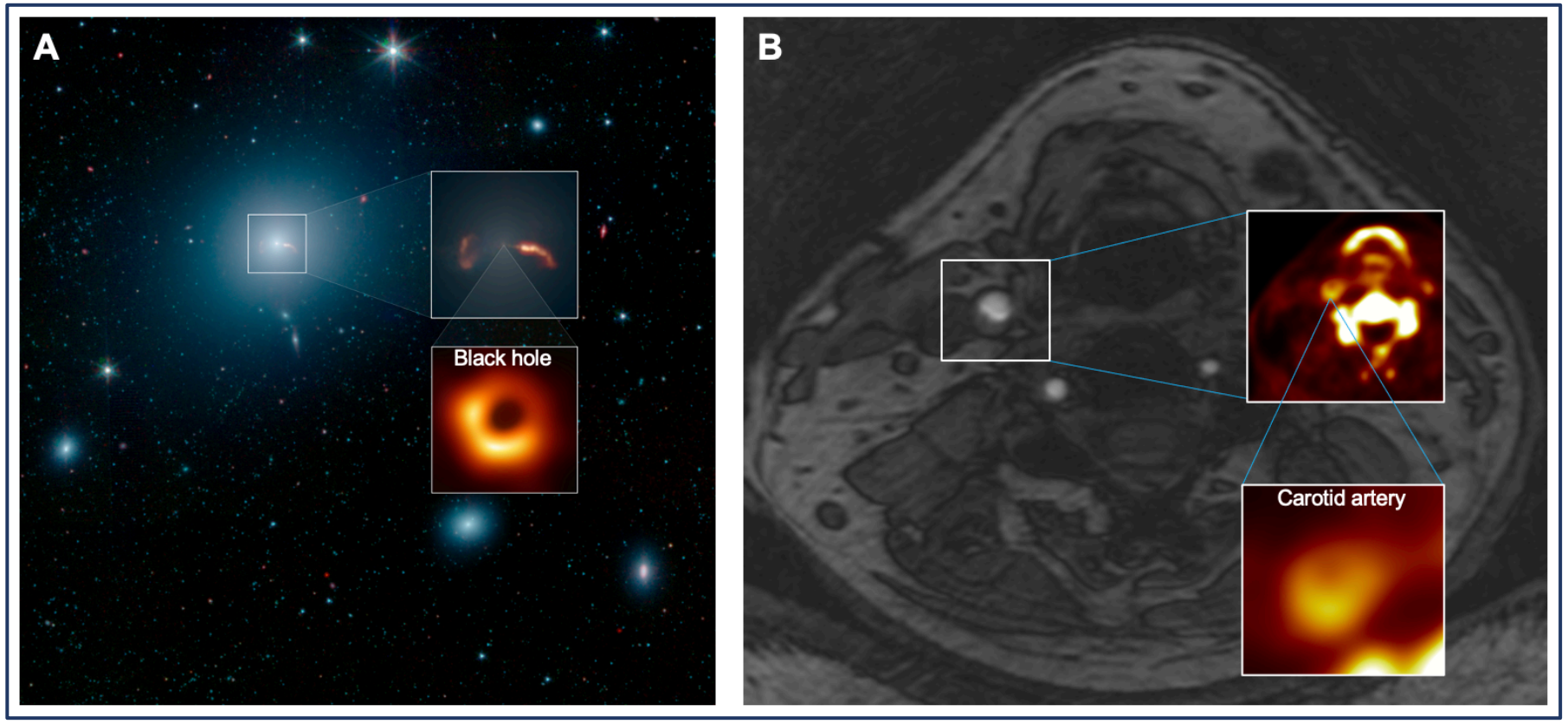
6.1.3 QUANTUM ENTANGELMENT OF CAROTID PLAQUE

"I think that I can safely say that nobody understands quantum mechanics."

- *Richard Feynman (1918-1988)*

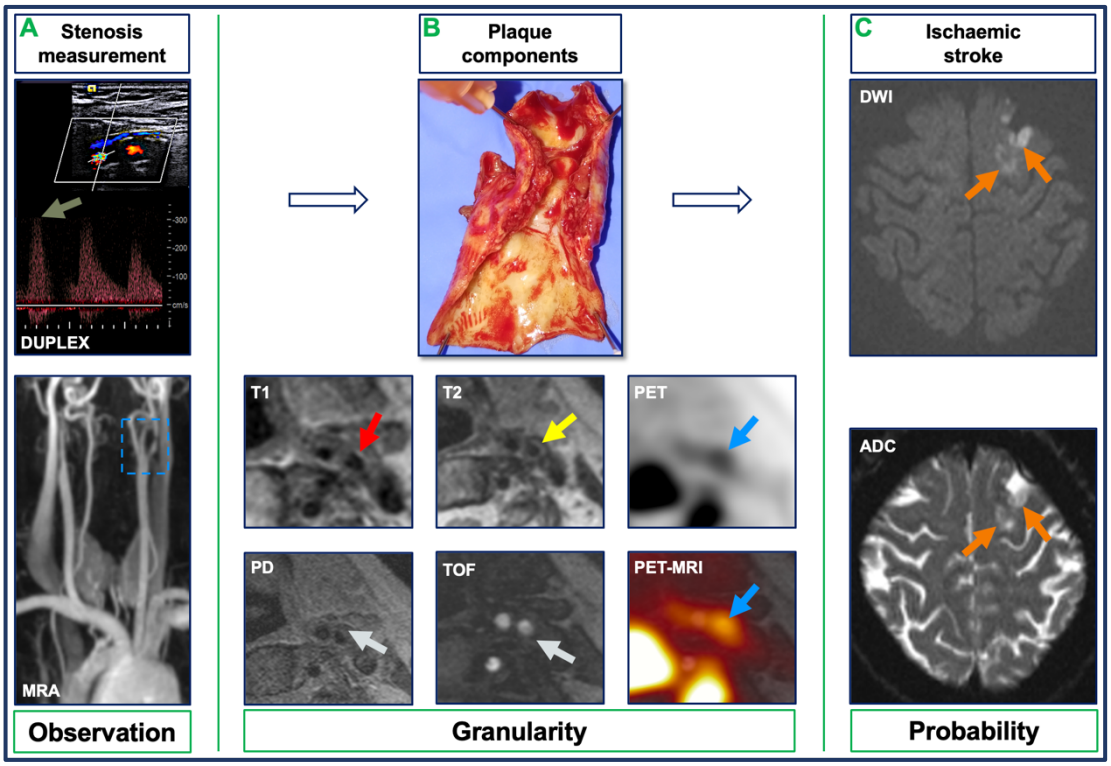
Modern hybrid state-of-the-art imaging, which is largely focused on microcalcification deposition, does not resolve the issue as to why some plaques hibernate for decades, whist others are engaged in a self-reinforcing loop of *regression-progression-rupture*, thus at some point re-emerge as acute neurovascular event. The contingent nature of atheroma represents an exceptional model of quantum entanglement (Figure 6.5) [Moreau et al., 2019] which at its core describes a situation where two particles, objects or systems remain inter-connected (physical properties of one affect the other) irrespective of the distance between them. Thus, carotid plaque consisting of juxta-positioned stable (macrocalcium) and unstable (microcalcium) territories (Figure 1.5a in Chapter 1) represents quantum phenomena as it exists in two different sates at the same time indicating that its overall 'state' remains 'undetermined'; as it might remain indolent or rupture revealing its clinical fate. Plaque progression stems not just from the solitary tract of microcalcium precipitation which is indicative of early yet already established arterial wall injury but from a quantum plaque biology where hypothetically neighbouring carotid region or remote aortic lesion could influence clinically culprit carotid plaque emergent property. This transfer of quantum information from one plaque to another presents us with a fundamentally different, counterintuitive, yet at the same time practical path that might become the quintessential solution that will unravel the ultimate origin of the acute neurovascular syndromes.

Figure 6.3: Carotid hybrid PET- MRI resembling black hole imaging.



A: The Event Horizon Telescope image of a supermassive black hole and its shadow adapted and updated from [Torbet, 2019].
B: Fused axial image of ^{18}F-NaF PET-MRI uptake in the carotid artery.
^{18}F-NaF PET-MRI: Fluorine 18-labelled sodium fluoride positron emission tomography-magnetic resonance imaging.

Figure 6.4: Carotid plaque – a quantum physics journey.



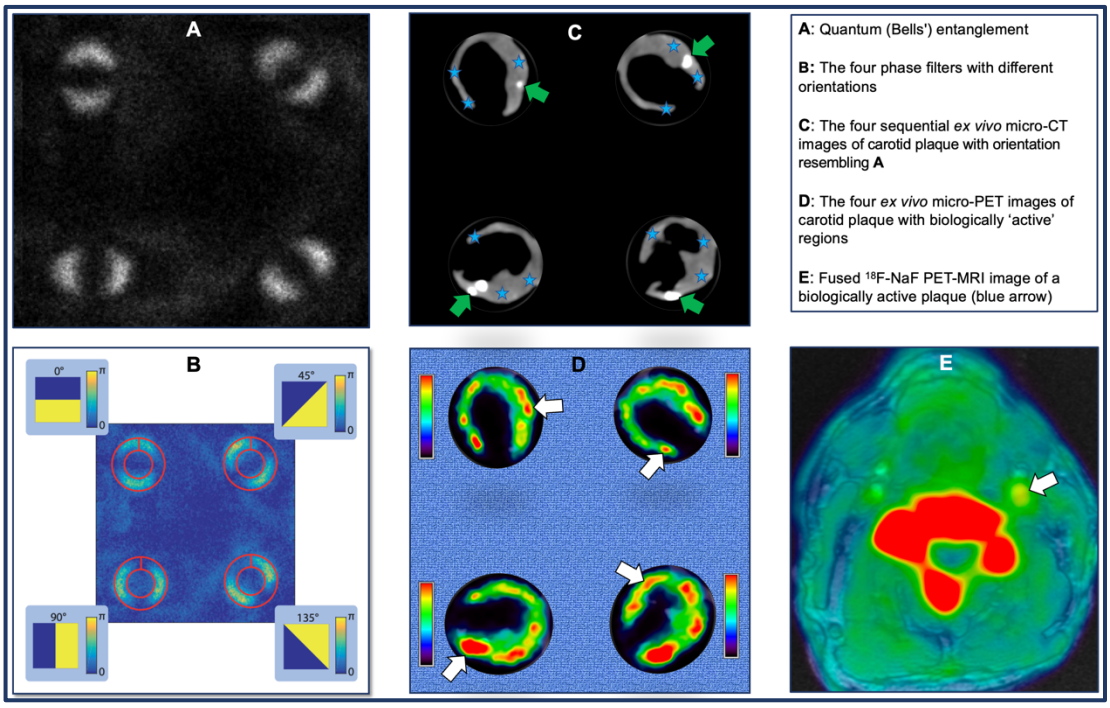
A: Left internal carotid artery stenosis > 90% on MRA (dashed blue box) and Duplex with peak systolic velocity 300 cm/sec (olive arrow)

B: Plaque high risk features: necrotic lipid core (yellow arrow), intraplaque haemorrhage (red arrows), macrocalcification (light grey arrows) and microcalcification (blue arrows)

C: Acute ischaemic left frontal lobe infarct (orange arrows) on brain imaging (DWI and ADC)

MRA: magnetic resonance angiography; ^{18}F-NaF PET-MRI: Fluorine 18-labelled sodium fluoride positron emission tomography-magnetic resonance imaging; T1 and T2 weighted imaging; TOF: time-of-flight; PD: proton density; DWI: diffusion weighted imaging; ADC: apparent diffusion coefficient.

Figure 6.5: Carotid plaque – quantum entanglement.



Adapted and updated from **Imaging Bell-type nonclonal behaviour** [Moreau et al., 2019].

- Quantum entanglement in the single image: **A:** four incidence counting images with **B:** four phase filters demonstrate four ROI (red circles- extracted from A) [Moreau et al., 2019]

- **C:** super-position state of carotid plaque denoted by four sequential *ex vivo* micro-CT images of carotid plaque with orientation resembling **A** and an apparent quantum entanglement (undetermined plaque state) with generally homogenous plaque tissue consisting of visible macrocalcium deposits (green arrows) and concealed microcalcium (blue stars) undetectable by micro-CT, hence giving an impression of a 'stable' plaque

- **D**: The four *ex vivo* micro-PET images of carotid plaque with ^{18}F-NaF detected microcalcium shift plaque destiny from a 'cold'-stable (**C**) to a 'hot'-active (**D** and **E**) one (white arrows)

- **E**: Fused ^{18}F-NaF PET-MRI image of a biologically active plaque (white arrow) that has caused acute neurovascular event

ROI: Region of interest; micro-CT: micro-computed tomography; micro-PET: micro-positron emission tomography; ^{18}F-NaF PET-MRI: Fluorine 18-labelled sodium fluoride positron emission tomography-magnetic resonance imaging.

Whether PET-MRI will direct the meandrous imaging of currently "*undetected*" signalling pathway (lipids, mitochondrial dysregulation, matrix loss, MSC phenotype switch, glycolysis) enmeshed within a complex plaque biochemical

architecture that modulates plaque homeostasis and crucially signals the pre-transition phase, remains unknown; as the Quantum Theory provides only the probability of finding an *observable* parameter (i.e. an electron at one point if observed), for example, a molecular marker denoting an altered particular molecular dynamics indicative of an irreversible shift in a plaque state. Thus, if we are not observing (not imaging) an indicator or object of interest, which is presently undetermined, the Quantum Theory is unable to provide information as to where such biomarker or any particle of matter could be found. Yet, the same quantum physics recognises some exceptions to this rule, namely the phenomenon of *ghost-imaging* which facilitates imaging of photons that reproduce a ghost image but have not interacted with the imaged object [Dogra et al., 2022] or imaging of *undetected* photons which is based on the single-photon interference and doesn't require coincidence detection [Lemos et al., 2014], unlike classical PET molecular imaging (Chapter 2). Most recent journey into quantum physics involves the *inter-action free measurements* where an existence of an object (presence of a target in a region of space) or an event is determined without irreversible photon absorption [Dogra et al., 2022]. In effect, *observation* of a target molecule is possible without excitation by a mediating particle. This promising quantum hypothesis builds on the concept of negative-results measurement of Renninger and Dicke that modified the output probabilities as "projective" even when no photon absorption took place by the target of interest [Dogra et al., 2022]. Novel technological advances including quantum computing, sensing, cryptography, and imaging might overcome hurdles of classical physics, hence open a completely different dimension of future cardiovascular imaging. Nevertheless, even in existing state, PET-MRI offers astonishingly subtle yet powerful observation of a culprit carotid plaque when investigating acute neurovascular syndromes and has every opportunity to aspire to the greatest achievement of medical imaging science in the 21st century.

Likewise, the *Little Curies*, which provided initially rudimentary images that now would be deemed obfuscating and uninterpretable, these *pictures*

ultimately evolved into sophisticated molecular imaging machinery that once again permitted to unfold the previously concealed morphological elements. As we have seen throughout this thesis, hybrid molecular imaging is rich in possibilities. We need to widen our understanding of this work, continuously update it, and render hybrid PET-MRI as the most appropriate imaging modality of the current century.

The management of symptomatic carotid stenosis represents a truly remarkable triumph of science that has lengthened and enhanced the lives of many. The complex wisdom gained from the integrating physiological information woven together with the traditional markers of carotid plaque fabric expands our understanding of paroxysms of unpredictable acute neurovascular syndromes. With the advent of hybrid PET-MRI, we can fully appreciate the full magnificence of scientific medical wonders that will continue to advance healthcare for the benefit of *others*. And it is my hope that the work presented in this thesis will promote discussion on a new model of clinical action and will help to ajar the future scientific doors for a whole range of new opportunities within cardiovascular imaging. After all, the more we understand, the better we will navigate the management of acute neurovascular syndromes.

"*Nothing in life is to be feared, it is only to be understood.*
Now is the time to understand more, so that we may fear less."

-Marie Sklodowska-Curie (1867-1934)

6.2 SUMMARY OF THESIS FINDINGS

This work examined the role of transcranial Doppler ultrasound scan in detecting MES in the MCA in healthy volunteers and patients with symptomatic carotid artery stenosis. It also explored the use of ^{18}F-NaF PET-MRI in detecting clinically culprit carotid plaque in patients with acute neurovascular syndromes.

6.2.1 REPRODUCIBILITY STUDY OF TRANSCRANIAL DOPPLER ULTRASOUND IN THE MIDDLE CEREBRAL ARTERY

In both groups (healthy volunteers and patients), Transcranial Doppler ultrasound demonstrated reproducible middle cerebral artery velocities data. No spontaneous micro-embolisation was detected in either of the examined groups. Future studies need to assess the relationship between the ^{18}F-NaF PET-MRI uptake, MRI-detected plaque features and MES to determine the potential clinical utility of Transcranial Doppler ultrasound in acute neurovascular syndromes, including the identification of clinically culprit plaque.

6.2.2 ^{18}F-NaF PET-MRI - ACUTE NEUROVASCULAR SYNDROME

We have previously demonstrated that ^{18}F-NaF PET-CT identified *in vivo* culprit carotid plaques following acute neurovascular events [Vesey et al., 2017]. *Ex vivo* imaging of carotid specimens revealed that radiotracer co-localised to the site of plaque rupture and tissue regions that histologically were indicative of inflammation, necrosis and microcalcification [Vesey et al., 2017]. The results presented within this thesis validated and augmented further our research group's findings, as above. Additional findings from the MRI component of hybrid imaging expanded our understanding of carotid atherosclerosis and its clinical consequences. More importantly, this work represents the first prospective evaluation of ^{18}F-NaF in a non-carotid vascular bed that has the potential to inflict adverse neurovascular events.

3T MRI CHARACTERISATION

On magnetic resonance angiography, culprit vessels, compared with the contralateral non-culprit vessels, were characterised by a higher degree of carotid arterial stenoses and were associated with increased prevalence of MRI-detected high-risk plaque features (intraplaque haemorrhage, necrotic core, thrombus, and ulceration). Depending on the stenosis severity, an interesting pattern of plaque composition was depicted among the culprit vessels; severely stenosed vessels were more likely to have calcification, ulceration and thrombus and were less likely to have fibrosis. Whilst fibrosis, a protective feature predominantly characterised culprit vessels without severe carotid stenosis. In summary, stenosis severity and adverse MRI plaque characteristics were independent predictors of the culprit vessel.

^{18}F-NaF PET UPTAKE

As expected, culprit vessels, particularly those with severe stenoses, had increased carotid ^{18}F-NaF uptake compared to the non-culprit vessels. In comparison, no difference in the radiotracer uptake was shown in the non-culprit vessels regardless of the degree of carotid stenosis on magnetic resonance angiography. Higher ^{18}F-NaF uptake was positively associated with high-risk plaque features, including necrosis, intraplaque haemorrhage, ulceration, and calcification, and inversely associated with fibrosis. Additionally, no difference was demonstrated in ^{18}F-NaF uptake within the aortic arch. These findings reaffirm that culprit vessels were associated with hostile MRI-detected plaque features, higher stenosis severity on magnetic resonance angiography and increased ^{18}F-NaF PET uptake measured by validated uptake parameters.

CLINICAL ACUTE NEUROVASCULAR EVENTS

Preliminary follow-up data showed that patients who experienced a recurrent stroke were more likely to have adverse plaque features in any vessel on MRI that were associated with an apparent trend of avid ^{18}F-NaF PET uptake.

Those who did not have subsequent strokes had no difference in the radiotracer uptake between culprit, non-culprit and aortic arch vessels.

SUMMARY

The above findings indicate that ^{18}F-NaF PET-MRI identifies culprit carotid plaques and provides detailed plaque morphological information following acute neurovascular events. Patients with culprit vessel stenosis >70% had a greater proportion of high-risk atherosclerotic plaque features on MRI and higher ^{18}F-NaF uptake. Most importantly, patients who experienced subsequent strokes had a high radiotracer uptake with adverse plaque characteristics. Finally, ^{18}F-NaF PET-MRI detected active atherosclerotic plaques within the aorta, highlighting that the acute neurovascular syndromes cannot be solely credited to the carotid circulation. These results also stipulate that ^{18}F-NaF binding outside carotid arteries may signify a global measure of vascular disease that may be a useful imaging parameter predicting recurrent acute neurovascular events. Whether clinical outcomes could be improved using hybrid PET-MRI remains to be established in future clinical studies.

6.2.3 ^{18}F-NaF PET-MRI – CORRELATION WITH HISTOLOGY

7T MRI CHARACTERISATION

The 3T MRI component of hybrid ^{18}F-NaF PET-MRI is capable of detailed carotid atherosclerotic tissue characterisation. However, its performance against ex vivo 7T MRI and gold standard histological examination has not been formally assessed, except for the solitary ^{18}F-NaF PET-MRI feasibility report (n=12 carotid plaques) [Mechtouff et al., 2020], which evaluated the association between hybrid imaging and histological analysis.

In vivo 3T MRI demonstrated satisfactory agreement with *ex vivo* 7T MRI in detecting high-risk carotid plaque features (intraplaque haemorrhage, rupture, or erosion, intraplaque haemorrhage) and histology (lipid core, thrombus, calcium). In contrast, agreement was poor for lipid core on *ex vivo* 7T MRI and rupture or erosion on histology. The overall level of agreement between *ex*

vivo 7T MRI and histology ranged from good (intraplaque haemorrhage, lipid core) to excellent (calcium). Still, again there was a poor agreement for plaque rupture or erosion with no thrombus detection by *ex vivo* 7T MRI. Albeit small data, it represents confidence in ^{18}F-NaF PET-MRI ability to detect established structural arterial wall changes that often mark the end stage of atherosclerosis associated with acute neurovascular syndromes.

^{18}F-NaF PET UPTAKE

Vascular calcification is a complex pathobiological process that begins with hydroxyapatite (microcalcification) deposition, detected by ^{18}F-NaF ions incorporated into the hydroxyapatite by ion exchange with hydroxyl groups at the crystal surface. These micro-deposits of calcium weaken the fibrous cap and may predispose it to rupture. Thus, microcalcification indicates both metabolically active and high-risk or unstable plaque. Subsequently, these micro-nodules grow and merge into larger deposits (macrocalcification), making the atheroma's quiescent yet advanced and irreversible stage biologically stable.

^{18}F-NaF (*in vivo*) uptake corresponded with radiotracer avid regions in all excised carotid plaques that were assessed by both *ex vivo* PET imaging and histological examination. Finally, ^{18}F-NaF binding was highly selective in the most advanced atherosclerotic plaques. These findings suggest that ^{18}F-NaF may be used as a carotid plaque disease severity biomarker.

SUMMARY

The ability of ^{18}F-NaF PET-MRI to detect early signs of the altered vessel wall texture at the molecular level (picomolar concentrations of radiotracer) offers a fundamentally unique observation and direction of management of acute neurovascular syndromes that starts with a precise carotid atherosclerotic disease evaluation. These thesis findings further support the long-held view that plaque biology as a harbinger of neurovascular events is more important than the degree of luminal stenosis and guard against the primacy of stenosis

severity. ^{18}F-NaF PET-MRI technological depth and sophistication fully equip this imaging system to unravel the complicated relationship between repetitive and self-destructive plaque patterns. This may permit the identification of high-risk plaques that may silently rupture. Furthermore, such information could be used to target patients for surgical intervention more appropriately and pave the way for novel pharmacological therapies aimed at plaque stabilisation, providing an opportunity for early treatment to slow the disease progression.

6.3 LIMITATIONS

Although results obtained from this largest and prospective single-centre observational cohort study are very encouraging, they ought to be interpreted cautiously. The recruited sample size was modest; however, a single site may report an overoptimistic picture which is a potential source of bias. Ultimately, the ability of ^{18}F-NaF PET-MRI in predicting future acute neurovascular syndromes or its capacity in establishing a clear threshold for the radiotracer uptake would represent a long-waited pinnacle of imaging-based individualised cardiovascular medicine as opposed to the *one-fits-all-stenosis-based* strategy. At present, none of the above issues can be addressed due to the lack of larger clinical trials that preclude any form of comparisons, including validation of this preliminary work. This is a direct consequence of the limited availability of hybrid PET-MRI scanners due to high costs and highly trained multidisciplinary staff consisting of physicists, radiographers, clinicians, and others. Another barrier relates to radioisotopes' production as the majority of these necessitate on-site cyclotron installation as opposed to the very few radiotracers that can be obtained commercially. Moreover, a complex radiochemistry production process cannot guarantee rapid access to a particular radiotracer, thereby significantly limits its use when a clinical scenario advocates urgent vascular surgical intervention such as carotid endarterectomy.

6.3.1 PET IMAGE ANALYSIS

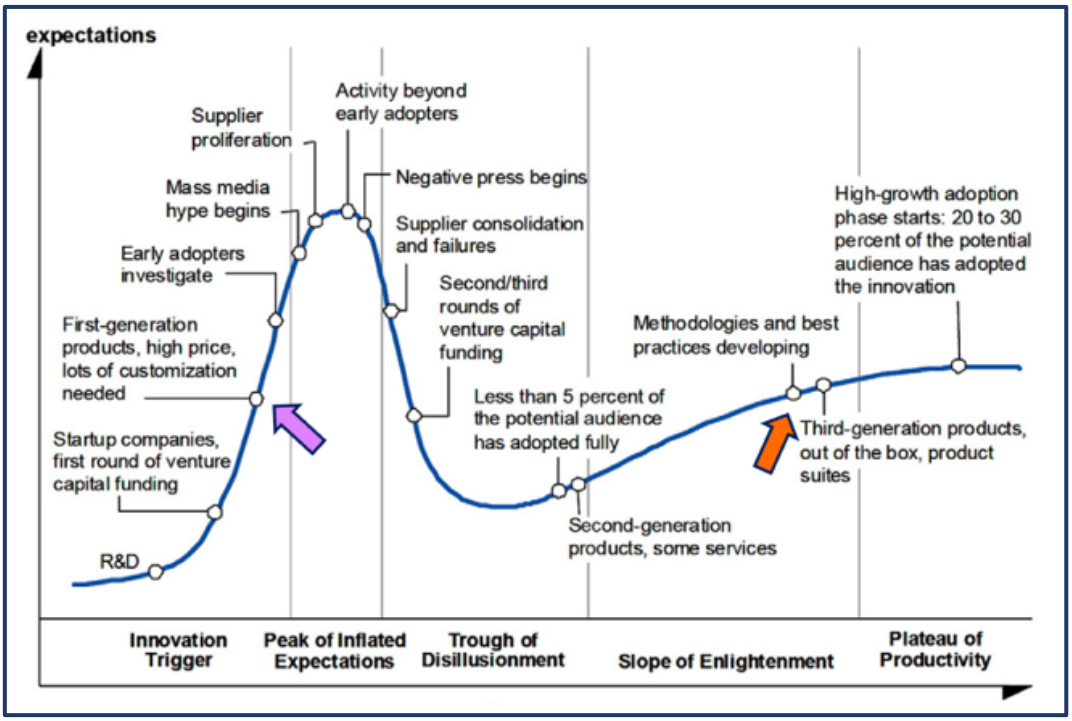
Carotid PET imaging analysis can be performed by either manual or automated methods. The traditional manual approach involves time consuming delineation of the plaque borders (volume of interests) based on visual assessment of increased radiotracer activity. Next, either the highest SUV or TBR or both parameters are used as the primary imaging endpoint. However, these rely on a single *hottest* pixel value which underestimates actual radiotracer burden, thereby global disease activity. An alternative to the above is an automated methodology which is more time efficient. Unfortunately, various studies often use locally designed softwares making robust interpretation of presented data difficult [Marnane et al., 2012; Tawakol et al., 2013; Blomberg et al., 2017]. Finally, our research group proposed a new semiautomated assessment of radiotracer uptake in the whole coronary circulation which utilises 3-dimensional tubular volumes of interest in each of the coronary arteries [Kwiecinski et al., 2020]. The results showed that the global measure of coronary microcalcification activity (CMA) was the strongest predictor of future coronary events in patients with the multilevel disease. Subsequently, the above principles were extrapolated to the ascending and aortic arch vasculature. This novel method, namely the aortic microcalcification activity (AMA), represents a ratio of aortic activity to the background radiotracer activity [Fletcher et al., 2021]. We demonstrated that AMA provided a reproducible summary of the overall burden of aortic disease activity and correlated with the validated stroke risk score. These findings imply that global description of disease activity could be a better prognostic marker of future neurovascular events, although this is yet to be proved. Overall, the measure of all potential foci of disease activity lays the ground for another paradigm shift from the vulnerable single vascular lesion to the vulnerable patient [Arbab-Zadeh et al., 2015]. This could also change the traditional best medical therapy approach which is focused on treating the risk factors. Instead, intensified best medical therapy targeting a particular vessel and based on a subsequent plaque response to the pharmacological treatment could individualise treatment further. The benefits of this “treating arteries”

concept was demonstrated by the carotid plaque regression (measured by ultrasound) and reduced incidence of cardiovascular events with a diminished rate of microemboli on transcranial Doppler [Spence et al., 2010].

6.3.2 HYPE CYCLE

A relatively unknown hybrid PET-MRI with many uncertainties associated with its technology and availability seems like a perplexing experiment to conduct. However, when we look at the *hype cycle,* which describes a dynamic trajectory of any novel technical or procedural innovation, we can see that there is a light at the end of a tunnel. The *hype cycle* forecasts distinct stages of technological evolution from the peak through disappointment, culminating in recovery patterns [Dedehayir et al., 2016]. This allows us to pragmatically brace for this PET-MRI tour of inevitable up and down slopes that occasionally may dim our scientific spirit obscuring new scientific horizons (Figure 6.6). However, the evolution of imaging demonstrated how each time resilience, commitment, and refusal to abdicate among the galaxy of the scientific tribe re-enabled researchers to architect the invention of novel technical solutions that continued to advance the above imaging discoveries. In the future, hybrid PET-MRI will reach the *plateau* of productivity leading to a more prominent role in clinical practice.

Figure 6.6: The hype cycle.



The curve of a hype cycle with its distinct stages [Dedehayir et al., 2016], updated to denote current hybrid PET-MRI technology position (purple arrow) and potential for the development of *reporting standards* (orange arrow).

6.3.3 PET REPORTING STANDARDS

Greater availability of hybrid PET-MRI could facilitate the emergence of *reporting standards* that would embody a set of comprehensive guidelines to comply with when conducting and subsequently publishing data. This would include the developing standardised imaging protocols, thus permitting reliable reproducibility data assessment across different research sites. All the above would ensure good quality multicentre data, combining results for the potential meta-analyses, timely publications, and making hybrid PET-MRI a technique worth investing into. The first step towards a universal agreement on facilitating standardised PET imaging protocols in atherosclerosis has been produced by the Cardiovascular Committee of the European Association of Nuclear Medicine [Bucerius et al., 2016]. However, the document included recommendations regarding the ^{18}F-FDG imaging only, and future optimal standards need to include other radiotracers proposals.

6.4 FUTURE DIRECTIONS

6.4.1 ASSESSMENT OF ^{18}F-GP1 IN THE ROLE AND ORIGIN OF THROMBOEMBOLISM CAUSING ISCHAEMIC STROKE

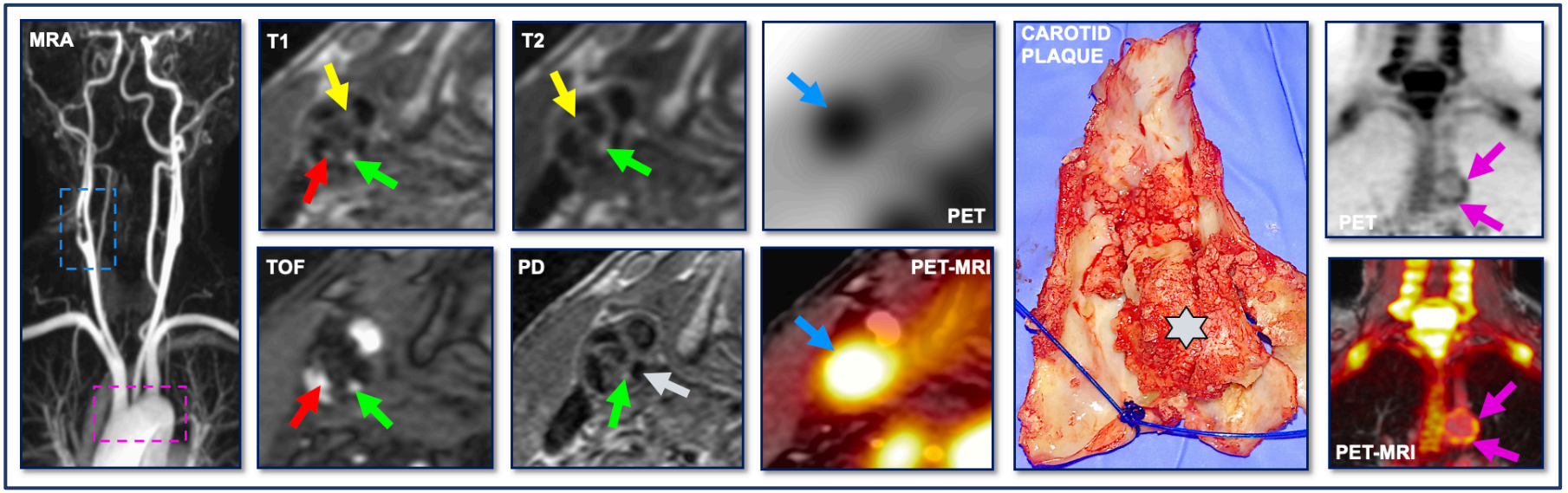
Most strokes are ischaemic (80%) in nature, with underlying thromboembolism as the principal mechanism foreshadowing brain tissue infarction. However, frequently it is difficult to ascertain the true origin of thromboembolism. The research presented within this thesis has proved that contrary to our NASCET driven guidelines, a carotid lesion may not be the solitary culprit source of a thrombus, thus acute neurovascular event. Hybrid PET-MRI detected acute aortic vascular lesions in patients who underwent carotid endarterectomy, implying that the stenosed carotid artery was nothing but a presumed source of thromboembolism (Figure 6.7). This is equally relevant in patients with symptomatic carotid artery stenosis but below the threshold for operative intervention, thereby probing other vascular conduits (aortic arch and intracerebral vessels) as potential explanations for acute neurovascular presentations. In effect, up to 25% of individuals have either several potential overlapping sources or are labelled as *cryptogenic* when despite extensive diagnostic work up no cause has been identified [Saver, 2016].

The current lack of routine assessment of these extra-carotid circulations, including difficulties in visualising thrombus, precludes any form of meaningful evaluation of the role and origin of thromboembolism. This sustains the default position of the carotid artery as the primary culprit vessel in the pathogenesis of ischaemic stroke until proven otherwise. Furthermore, uncertainly exists regarding the exact role of thromboembolism in lacunar stroke, a common subtype of ischaemic stroke. Conflicting data have been published on the role of embolic material affecting lenticulostriate arteries and as such clinical management of these patients remains poorly defined [Wardlaw et al., 2019]. Therefore, there is an urgent need to explore the pathogenesis of ischaemic stroke with its specific subtypes that can lay the ground for the development

of appropriate preventative therapies and, most importantly, assess if this new knowledge will impact on the clinical patients' outcomes.

This new project aims to evaluate a novel clinical grade thrombus-specific radiotracer, ^{18}F-GP1, which has a high specificity for the glycoprotein IIb/IIIa receptor on activated platelets (Chapter 1). Our research group already demonstrated that ^{18}F-GP1 is highly sensitive to *in vivo* thrombus formation and shows avid binding to thrombus associated with pulmonary embolism, left ventricular thrombus and stroke. The new study will involve a contrast-enhanced ^{18}F-GP1 PET-CT scan that will specifically assess multiple vascular beds, including intracranial and extra-cranial neck arteries, aortic arch, and the chambers of the heart, including the left atrial appendage with the left ventricle. The non-invasive *in vivo* thrombus detection could facilitate the detection of a source and the provide basis to influence the management of patients with specific subtypes of strokes that are ill-understood.

Figure 6.7: ^{18}F-Sodium fluoride PET-MRI uptake in carotid and aortic circulations.



Example of a surgical patient with right amaurosis fugax and >70% stenosis of the left internal carotid artery (MRA blue dashed box) that underwent carotid endarterectomy. Hybrid PET-MRI revealed focal and high-grade ^{18}F-NaF uptake in carotid artery (blue arrows) and moderate uptake in aortic arch (MRA pink dashed box, and pink arrows). MRI plaque analysis demonstrated thrombus (green arrows), intraplaque haemorrhage (red arrows), necrotic lipid core (yellow arrows) and calcification (grey arrow).

MRA: magnetic resonance angiography; PET-MRI: positron emission tomography-magnetic resonance imaging; ^{18}F-NaF: Fluorine 18-labelled sodium fluoride; T1 and T2 weighted imaging; TOF: time-of-flight; PD: proton density.

6.4.2 THE EDINVASC STUDY: MicroPET-CT OF THE EX VIVO VASCULAR TISSUE (^{18}F-NaF AND ^{18}F-GALACTO-RDG)

Molecular imaging has been driven mainly by the plethora of studies that have examined the role of PET-CT in coronary, carotid and aortic vessels, including abdominal aortic aneurysms [Vesey et al., 2017; Forsythe et al., 2018; Joshi et al., 2014]. More recently, this form of imaging has been adapted to examine lower limb peripheral arterial disease, which is a global problem. Without treatment, patients with critical limb ischaemia are at risk of limb loss. Up to date, *in vivo* PET-CT imaging enabled a better understanding of atherosclerotic differences among different vascular anatomical beds (carotid versus femoral) [Shaikh et al., 2014], improved detection of infected vascular grafts [Sah et al., 2015] and prediction of re-stenosis following angioplasty treatment of the superficial femoral artery [Chowdhury et al., 2020].

The EdinVasc Study investigates the role of microPET-CT using two radiotracers, ^{18}F-NaF and ^{18}F-Galacto-RGD (Chapter 1), in *ex vivo* human aortic and peripheral arterial tissue (carotid, femoral, tibial) in delineating important pathophysiological processes of atherosclerosis. This could create the foundation platform for subsequent new clinical PET-CT studies to characterise the peripheral arterial disease, predict clinical outcomes and introduce novel treatment strategies.

6.4.3 THE CONUNDRUM OF A RANDOMISED CONTROLLED TRIAL

“An approximate answer to the right question is worth a great deal more than a precise answer to the wrong question.”

- *John Tukey (1915 - 2000)*

Over the past three decades, management of the acute neurovascular syndromes has been dichotomised using one aspect of symptomatic carotid disease, the degree of carotid artery stenosis, leaving aside other facets such

as plaque morphology and its biology that are of even greater importance. In practice, carotid endarterectomy is offered to female patients with symptomatic severe stenosis (>70%) and males with a moderate degree of stenosis (>50%). Therefore, the need for a randomised controlled trial to accurately evaluate carotid treatment choices using the atherosclerotic plaque composition versus the current *stenosis-based* approach would not be just simple idle curiosity. To the contrary, it would best serve our main goal of preventing stroke related disability and death. If advanced modalities such as the combination of PET with either CT or MRI could identify a robust imaging bio-parameter that would demonstrate a clinically meaningful prognostic value in detecting future acute neurovascular syndromes, it could be used as a trigger for subsequent carotid surgical intervention instead of a stenosis severity alone. In practice, patients labelled as high-risk based on non-invasive *in vivo* thrombus detection determined by ^{18}F-GP1 uptake could proceed to stroke preventative surgery regardless of the severity of carotid artery stenosis. Whereas those with severe stenosis but lacking specific adverse plaque texture characteristics could avoid carotid endarterectomy, including surgical risks that cannot be abolished entirely. While such an approach would undoubtedly provoke criticism, we should pursue this course of action as it would cast an objective light on this long-ago hypothesised perspective.

Undoubtfully, well-designed, and executed randomised controlled trials provide information about average risks of harm and benefits under specific conditions. It is precisely the process of randomisation that reduces the risk of selection bias. Randomised controlled trials also underpin the importance of understanding scientific principles, expand our knowledge, and stimulate new discoveries. Medicine, in general, has too often seen an introduction of a novel technology without high-quality scientific evidence. This distorts science and, although not designed to harm participants, carries such potential. Ultimately, as already discussed in this thesis, NASCET and ESCT (despite few drawbacks) delivered a clear message that continues to benefit patients around the globe. On the other hand, we cannot escape the fact that the

debate *for* versus *against* carotid stenting continues despite the completion of 22 randomised controlled trials and data from more than 20 international registries [Müller et al., 2020; Paraskevas et al., 2016]. Moreover, randomised controlled trials can fail to extrapolate information on a treatment efficacy and safety across general population as they may apply only to a specific subgroup of individuals. Thus, certain subpopulations may be overlooked and lost in the global data conclusions [Abbott, 2015; Paraskevas et al., 2019]. We have observed this in NASCET data which dismissed the benefits of carotid surgery in those with <50% stenosis, yet now with the advent of non-invasive cross-sectional and molecular imaging we can appreciate that this subgroup of patients is also worthy of our clinical attention. Furthermore, randomised controlled trials necessitate vast recruitment networks, rigorous recruitment, committed institutions and involve complicated administrative processes that guard ethical principles of this scientific enquiry. Although experts advocate simplification of randomised research process aimed at increasing feasibility by mitigating the above obstacles [Collins et al., 2020; Yusuf et al., 1984], it is unlikely that we will witness such amendments. All these aspects within the resource confined health care system that is currently overwhelmed by the post-pandemic state make the motivation for such trial truly nebulous.

Moreover, acute neurovascular syndromes do not have a one big therapeutic solution, instead improved clinical outcomes are governed by a combination of prompt diagnosis, imaging and best medical or surgical intervention. In the context of increasingly available precision medicine that targets heterogenous and small populations of individuals sharing the same medical condition [Eichler et al., 2021], prospect of large randomised controlled trial seems futile. Thus, randomised data may not be the only feasible or appropriate scientific framework to ask a research question and answer it reliably. Arguably, hybrid PET-MRI based research may require a more pragmatic approach consisting of non-randomised controlled clinical registries based on the large longitudinal prospective observational cohort studies. Large registries allow for an extensive data collection in a shorter time frame than randomised controlled

trials that often take more a decade to complete. Additionally, limited availability and complexity of PET-MRI technology precludes large scale randomised strategy. This leaves non-randomised studies at the forefront of generating knowledge and hypotheses for the future potential trials [Hong, 2021]. Most importantly, scientifically sound, and large observational data that provides longitudinal data across the care continuum [Franklin et al., 2021], facilitates emulation of a target trial [Hernán et al., 2016]. Promising results of 10 trials emulations that evaluated cardiovascular outcomes of antidiabetic (n=8) and antiplatelet (n=2) medications showed that *real-world* data achieved hazard ratio estimate that was within the 95% confidence interval of the corresponding randomised controlled trials (8 out of 10 studies) [Franklin et al., 2021]. Therefore, the *real-world* approach with the population mimicking randomised data may be the best way for making appropriate decisions concerning the harms and benefits associated with clinical interventions. Additionally, this strategy can provide valuable insights into the barriers and challenges of using hybrid imaging in daily practice.

How can we take hybrid PET-MRI based research forward? At present, seven PET-MRI scanners that are available at tertiary centres (United Kingdom) could build foundations for the very first multicentre carotid PET-MRI study. This would require development of hybrid PET-MRI carotid imaging registry to capture all relevant carotid plaque data and facilitate vigorous clinical follow up. In the first instance, shared national experience could standardise hybrid imaging across United Kingdom, and subsequently expand it between international units. In effect, prospective observational cohort studies could generate meaningful and accurate data that could inform clinical decisions.
However, we ought to remember that observational cohort studies can have its own caveats. First, small and heterogenous data limit generalisability. Whilst the failure to adjust for all confounding factors precludes complex emulation of a target trial. Furthermore, to avoid potential pitfalls related to the analysis of the observational data, emulation necessitates structured methodology including standardised data codes, procedures, comprehensive

internal consistency checks with comparisons across data sets and possibly even machine learning tools [Hernán et al., 2016]. Second, plausible data can be reported which at the end finds no confirmation in the randomised controlled trials. This was demonstrated by the observational studies that showed association between statins and slower progression of aortic stenosis. However, randomised data refuted these findings. In effect, observational studies with outcomes from multiple cohorts may be insufficient to drive the practice change [Bing et al., 2020a] and should not be regarded as a substitute for findings from randomised controlled trial [Collins et al., 2020].

Ultimately, understanding the strengths and weakness of these different spectra of scientific enquiry highlights their complementary roles that may pave the way for the future hybrid PET-MRI research. When randomised controlled trials are not feasible (unethical, expensive) the *real-world* approach may be the only viable trade-off to accept. This strategy may allow to establish a precise and unbiased estimate of the truth to comply with the patient's best interests. Afterall it is better to "be approximately right" when a stroke of scientific data serendipity comes from the large and prospective observational cohort studies, "rather than exactly wrong" despite randomised, albeit small, controlled trial data. Whether unresolved questions surrounding complex diseases such as carotid atherosclerosis might be best answered by randomised controlled trials to provide definitive wisdom how best guide carotid surgical intervention remains unknown.

6.4.4 CAROTID PLAQUE AS IMAGING BIO-PARAMETER - AT LAST!

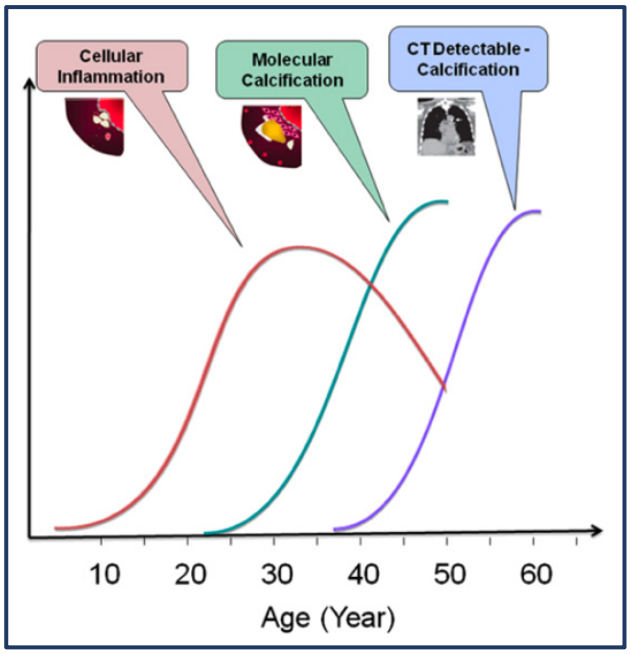
"That's one small step for man, one giant leap for mankind."

- *Neil Armstrong (1930-2012)*

The theme, that plaque phenotype including biological composition more accurately reflects the risk of subsequent acute neurovascular syndrome, and

therefore, patient's clinical outcome, has looped endlessly throughout decades of vascular stroke related research. Furthermore, although CT and MRI can provide complementary plaque characteristics, neither of these cross-sectional imaging modalities can offer a robust insight into the biological status of the clinically culprit plaque. At present, hybrid PET-MRI is the only imaging technique which facilitates parallel assessment of cellular (inflammation), molecular (microcalcification) and morphological (macrocalcification, necrotic lipid core, intraplaque haemorrhage, luminal thrombus, and fibrosis) plaque characterisation (Figure 6.8).

Figure.6.8: Biological sequence of events over time.

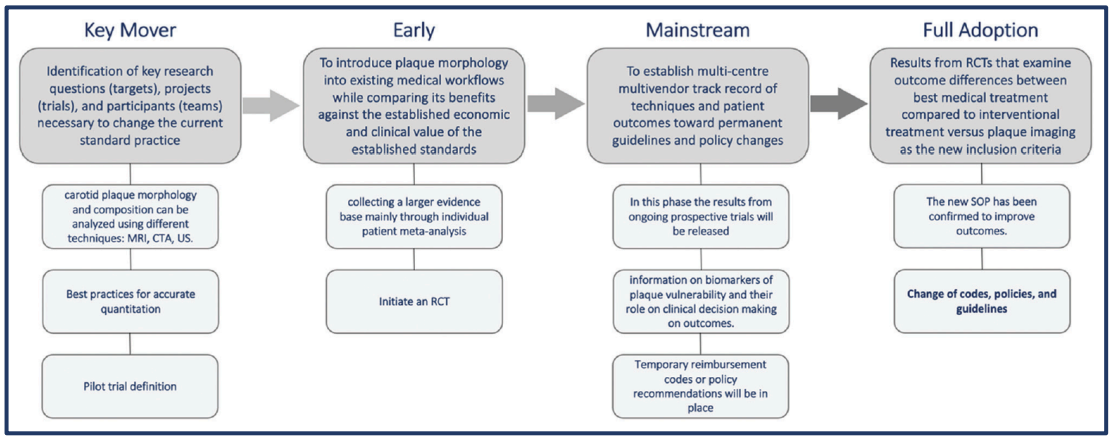


Molecular PET imaging detects and quantifies microcalcification before macrocalcification is detectable by CT years later [Saboury et al., 2011]. PET: positron emission tomography; CT: computed tomography.

Specifically, molecular aspect allows for an early detection of microcalcification before any irreversible structural arterial wall changes are present or cause neurovascular events. This creates a window of opportunity in the context of an early diagnosis, risk prediction and therapeutic intervention (Figure 6.8).

Therefore, how do we instigate the shift from this well-known plaque phenotype *principle* to a *rule* that will guard day-to-day clinical practice?
The first step involved the invention of hybrid PET-MRI, whilst the second step has been recently marked by the landmark publication of a roadmap consensus on carotid plaque imaging [Saba et al., 2021]. An international and multidisciplinary group of experts (including leading figures from the United Kingdom, Professors: Naylor, Wardlaw, Rothwell, and Brown) proposed incorporation of carotid plaque imaging as a core imaging bio-parameter in addition to the stenosis measurement when assessing individuals for a therapeutic option. This document represents a truly giant leap forward as it challenges current guidelines and provides a detailed and pragmatic 4-phase roadmap that can ultimately fundamentally reshape and refine management of acute neurovascular syndromes (Figure 6.9).

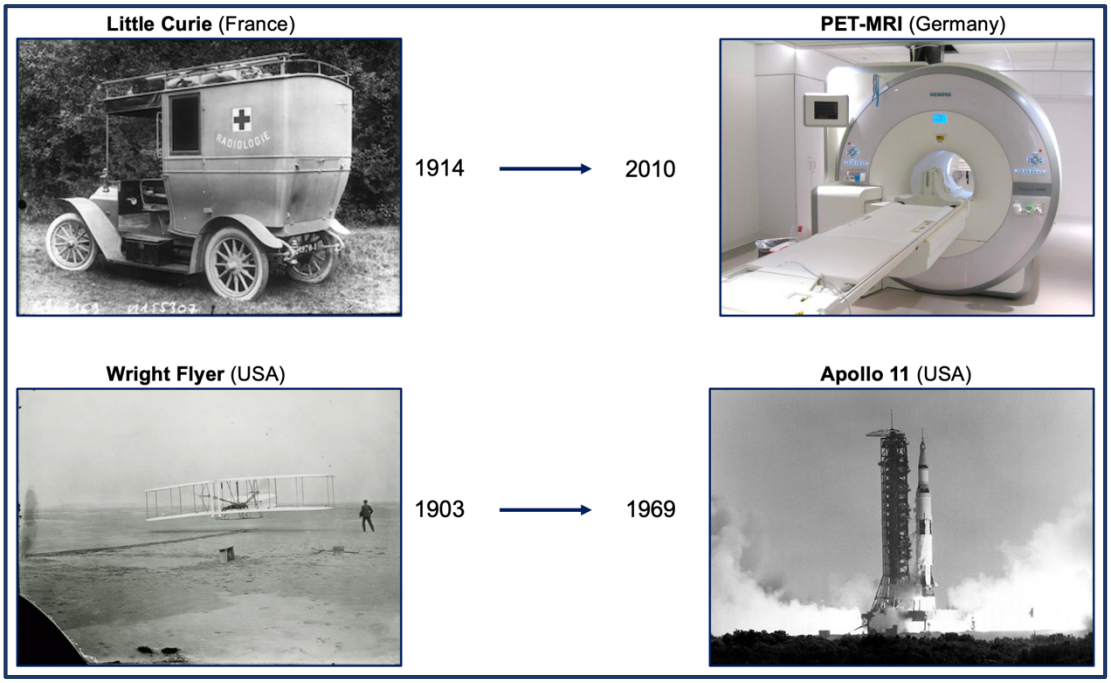
Figure.6.9: A roadmap consensus on carotid plaque imaging.



Four phases of the carotid plaque-based imaging that aim to change the current standard of practice [Saba et al., 2021].

Thus, we are no longer *frozen* by the rigid set of NASCET guidelines, nor can we ignore scientifically established concept of biological plaque composition. Hybrid PET-MRI technology allowed us to view the atherosclerotic plaque through the most comprehensive imaging *oracle* of the 21st century (Figure 6.10) and it is high time that equipped with this knowledge and experience we move forward.

Figure 6.10: Ad Astra per Aspera.



Little Curie - first mobile x-ray unit; [Bibliotheque-Nationale-de-France, 1914]
PET-MRI - first Siemens Biograph mMR; [Muzic et al., 2014]
Wright Flyer - first powered flight at Kitty Hawk, National Air and Space Museum, https://airandspace.si.edu/stories/editorial/first-flight
Apollo 11 - first space launch from Florida on a mission to the Moon; NASA Apollo 11 Image gallery, https://www.nasa.gov/apollo11-gallery

6.4.5 TOOLBOX OF RADIOTRACERS

The roots of many radiotracers originate from oncology, which as a medical speciality pioneered the development of different radiopharmaceuticals, including a *toolbox of radiotracers* targeting different aspects of cancer cell functions [Buscombe, 2015]. A similar approach within the field of cardiovascular imaging could unlock new possibilities. Atheromatous plaque is characterised by a whole range of pathophysiological processes that specific radiotracers can target on cellular and molecular levels (Figure 1.14, Table 1.2 in Chapter 1). At present, published data are limited to the exploration of ^{18}F-FDG with few novel tracers such as ^{18}F-NaF, ^{68}Ga-DOTATATE, ^{18}F-FMSIO and ^{68}Ga-FAPI-04 (Chapter 1). In contrast, pre-clinical studies compared ^{18}F-FDG with ^{18}F-FEDAA1106, ^{18}F-FCH, and ^{18}F-FOL (Chapter 1). Although the

idea of a *toolbox* appears quite remote, it could provide the multifaced way of atherosclerotic plaque assessment. Thromboembolism is a direct consequence of an acute plaque change, however, the exact trigger which shifts molecular pathways towards plaque instability remains unclear. Consequently, the ability to detect culprit carotid plaque at risk of rupture based on molecular and cellular processes in those who have not suffered an acute neurovascular event would hold a remarkable promise for improving atherosclerosis detection and patients risk stratification. However, various factors need to be accounted for when considering using paired or multiple radiotracers, including different half-life time, biodistribution, costs and commercial availability.

6.4.6 PAN-VASCULAR HYBRID IMAGING PLATFORM

A pan-vascular hybrid imaging platform consisting of simultaneous assessment of cephalic, extra-cranial, coronary, and aortic arch circulations could transform vascular assessment of acute neurovascular syndromes [MacAskill et al., 2019]. From a carotid imaging point of view, this could also include concurrent brain evaluation as a *one-stop-shop* or a *smart hybrid pan-vascular* approach reducing the number of hospital appointments. At present, this holistic or meta concept of cardiovascular assessment could be served either by a standard hybrid PET imaging (combined with CT or MRI) or the most recent technological innovation, namely the total-body PET.

Our research group has recently re-analysed images of patients (n=461) with a primary diagnosis of stable coronary artery disease or aortic stenosis who had undergone ^{18}F-NaF PET-CT of the thoracic aorta as part of one of three prospective clinical imaging studies [Fletcher et al., 2022b]. The results showed that AMA was associated with thoracic disease progression and the future risk of ischaemic stroke (n=23). More interestingly, clinical events correlated with the imaged vascular territory. In effect, CMA identified patients at risk of myocardial infarction, whereas AMA detected those at risk of future ischaemic stroke after adjustment for clinical risk factors and thoracic aortic

calcium scoring [Fletcher et al., 2022b]. This simultaneous assessment of coronary and thoracic arteries could improve evaluation and identification of individuals at high risk of acute neurovascular syndromes and adverse cardiac events, prompting more sophisticated treatments. Currently, larger, and prospective observational studies are being conducted at our institution to validate the above preliminary findings.

Imaging that spans the multiple vascular structures from the thorax up to the vertex brings its challenges. The pan-vascular imaging would be time consuming, and the appropriate quality of imaging data would require sufficient body cover by PET. The above can be difficult to achieve, and one potential solution is the total-body PET that measures the distribution of radiotracer in the whole bed rather than from images obtained from multiple bed positions covering limited body parts. In effect, the individual's entire body is surrounded by the PET detectors without the need for the imaging bed movement [Høilund-Carlsen et al., 2019; Schmall et al., 2019]. The total body PET scan could provide the most comprehensive measure of the atherosclerosis burden, which intuitively looks like a more accurate representation of the disease activity than the imaging of a single vascular lesion. More diffuse disease processes (abdominal aortic aneurysm, acute aortic dissection and aortitis) could benefit from the global quantification of the disease using the AMA strategy [Fletcher et al., 2021]. Whether the same would be applicable in the carotid artery is yet to be seen as the most disease segment approach may prove to be more valid when acute adverse events are precipitated by a focally aberrant carotid atheroma (that ruptures) or aortic wall tear [Syed et al., 2022] which is a leading point for the dissection. On the other hand, when each of the high-risk plaques scattered along the arterial tree carries the *culprit* potential, a more global assessment of the disease may provide the ultimate solution to guide subsequent management of such individuals.

As we work with increasing complexity, a new model of *diagnosis-treatment-cure* will become essential where the hybrid PET-MRI would underpin all

elements of this clinical axis. The potential for total body PET is vast. If successful translation (efficacy, applicability) into the clinical area occurred, it would facilitate early detection of atherosclerotic disorder with preventative treatments and monitoring of the course of therapeutic interventions.

6.4.7 ANTICALCIFIC THERAPY

Ultimately, the ability to delay or halt the process of microcalcification could open new avenues of treatment that could potentially avoid the need for any invasive treatment. If mineralisation could be diminished or even reversed, ^{18}F-NaF hybrid imaging would play a vital role in detecting the early disease stages and subsequent assessment of response to the treatment [Doris et al., 2019]. At present, the anti-calcific therapies have not been investigated in carotid atherosclerosis. Our research group has investigated in the single-centre, double-blind, randomised, placebo-controlled trial SALTIRE II (Study Investigating the Effects of Drugs Used to Treat Osteoporosis on the Progression of Calcific Aortic Stenosis) if either a bisphosphonate, denosumab (a human monoclonal antibody) or placebo can attenuate ^{18}F-NaF PET-CT uptake in the aortic valve indicating a reduction in the disease progression [Pawade et al., 2015; Pawade et al., 2021]. Disappointingly, neither of the medications influenced progression of aortic valve calcification suggesting that alternative mechanisms ought to be explored to find disease-modifying therapies. Another potential medication that could ebb away stenotic aortic disease is the dipeptidyl peptidase-4 inhibitor, an oral hypoglycaemic used in diabetes mellitus. An observational study demonstrated reduced disease progression, diminished aortic valve velocities and gradients following administration of dipeptidyl peptidase-4 inhibitor [Bing et al., 2020b]. However, available data suffers from many confounding factors (heterogeneous patient population, no data regarding other medications or compliance to dipeptidyl peptidase-4 inhibitor), hence it should be viewed with caution [Bing et al., 2020b]. Furthermore, despite that both aortic (stenosis) and carotid (atherosclerosis) arterial disorders emerge from a complex interplay of endothelial injury, lipid deposition, inflammation and dystrophic calcification,

the fundamentally different mechanisms underline subsequent adverse clinical complications. Aortic stenosis via the progressive valvular obstruction leads to chronic and progressive myocardial pressure overload (left ventricular hypertrophy) [Bing et al., 2020b]. Whist atherosclerotic plaques manifest as acute neurovascular syndromes by means of thrombo-embolism. Therefore, the potential benefits from the proposed anti-calcific therapies may vary substantially across these anatomically different circulations. Modification of aortic stenosis progression and avoidance for valve replacement is a plausible concept. However, the same cannot be directly extrapolated regarding carotid calcification. The inhibition or reversal of carotid microcalcification could compromise protective macrocalcification, thus destabilise atheroma and lead to a plaque rupture. Additionally, the above would need to be carefully balanced against the potential harms to the healthy skeletal metabolism, which shares the same mineralisation pathways as the vascular calcification [Phadwal et al., 2021]. One possible solution that could be more effective involves the restoration of mitochondrial homeostasis. The most recent comprehensive review highlighted the crucial role of mitochondrial dysfunction in calcific dysregulation, phenotype switching of smooth muscle cells (from a contractile to an osteogenic) and metabolic shift to glycolysis [Phadwal et al., 2021]. In effect, smooth muscle cells containing calcified mitochondria induce a pro-inflammatory state, arterial stiffening and apoptosis leading to atherosclerotic plaque rupture [Phadwal et al., 2021]. However, the actual role of mitochondria as a future target for pharmacological therapy is yet to be presented.

6.4.8 NON-IMAGING BIOMARKERS

It is hard to ignore the research examining the role of altered expression of various molecules and genes by unstable atherosclerotic plaques associated with cardiovascular disease. Among many, these include the work of our research group collaboration on long noncoding RNAs [Hung et al., 2019], long noncoding RNA SMILR [Mahmoud et al., 2019] and osteocalcin [Rashdan et al., 2020]. Further exciting developments include proapoptotic signalling

pathway [Dorweiler et al., 2014], Galectin-3 [Kadoglou et al., 2015], chemokine ligand-19 [Salem et al., 2016] and MMP [Razuvaev et al., 2011]. While others report promising yet limited data on plasma-based biomarkers such as lipoprotein associated phospholipase A2 [Sarlon-Bartoli et al., 2012] and endothelial derived microparticles [Wekesa et al., 2014]. Although these markers and molecules are of major scientific interest and provide mechanistically important data, so far, none of the above biomarkers demonstrated any form of link between image-derived high-risk plaque features or metabolic activity. Therefore, it is doubtful that they will alter clinical practice in the near future.

6.5 FINAL CONCLUSIONS

The work presented in this thesis represents the largest prospective observational data on the role of ^{18}F-NaF PET-MRI in acute neurovascular syndromes. ^{18}F-NaF PET-MRI identified clinically culprit carotid plaques that were characterised by adverse plaque features, higher radiotracer uptake and coexistent active aortic vascular lesions. Hybrid PET-MRI is the only imaging modality that facilitates simultaneous structural and physiological atherosclerotic plaque assessment. This may help better understand the complexities surrounding plaque evolution, responses to new pharmacological therapies with targeted and more effective interventions. Most importantly, hybrid PET-MRI could become the ultimate imaging modality evoking full adoption of the long-waited customised therapeutic intervention centred on the carotid plaque composition. Hence, the translation of hybrid ^{18}F-NaF PET-MRI into the clinical practice is the only way forward.

"Now I feel that it is really time for me to leave,..but is also seems that I've made my point. In fact, I can't think of anything else to say on the subject".

- *Sam Harris (Free Will, 2012)*

BIBLIOGRAPHY

PUBLICATIONS AND BOOK CHAPTER DIRECTLY ARISING FROM THIS THESIS

1.^{18}F-NaF PET-MRI of carotid atheroma in acute neurovascular syndrome. J Kaczynski, S Sellers, M Seidman, M Syed, M Dennis, G Macnaught, M Jansen, S Semple, C Alcaide-Corral, A Tavares, T MacGillivray, S Debono, R Forsythe, A Tambyraja, J Leipsic, M Dweck, W Whiteley, J Wardlaw, E van Beek, D Newby, M Williams. *Journal of Radiology* 2022; 305(1):137-148

My contribution: collected all data, performed statistical analysis, interpreted results, drafted, revised and finalised the manuscript.

2. Emerging techniques in atherosclerosis imaging. MBJ Syed, RO Forsythe, J Kaczynski, DE Newby, MR Dweck, EJR van Beek. *British Journal of Radiology* 2019;92:(1103):20180309

My contribution: drafted and revised the manuscript.

3. Reproducibility of transcranial Doppler ultrasound in the middle cerebral artery. Kaczynski J, Home R, Shields K, Walters M, Whiteley W, Wardlaw J, Newby DE. *Cardiovasc Ultrasound.* 2018;16(1):15

My contribution: collected all data, performed statistical analysis, interpreted results, drafted, revised and finalised the manuscript.

4.^{18}F-Sodium Fluoride Positron Emission Tomography/Computed Tomography Imaging of the Peripheral Vasculature. M Syed, J Kaczynski, D Newby. In: Bomanji JB, Ganansegaran G, Fanti S, Macapinlac HA, eds. Clinicians' Guide to Radionuclide Hybrid Imaging. Springer Nature Switzerland AG; 2020. p. 85-94

My contribution: drafted and revised the book chapter.

PUBLICATION IN PREPARATION

1.^{18}F-NaF PET-MRI in patients undergoing carotid endarterectomy - correlation with ex vivo imaging and histology. J Kaczynski, MA Seidman, T Reed, M Jansen, C Alcaide-Corral, AAS Tavares, M Syed, S Debono, G Macnaught, SI Semple, T MacGillivray, R Forsythe, A Tambyraja, J Leipsic, MR Dweck, W Whiteley, J Wardlaw, M Dennis, EJR van Beek, MC Williams, DE Newby, S Sellers. – submission to *Journal of American College of Cardiology: Basic Translational Science*

My contribution: collected all data, performed statistical analysis, interpreted results, and drafted the manuscript.

PUBLICATIONS RELATED TO THIS THESIS ARISING FROM OTHER RESEARCH ACITIVITIES

1. Thoracic Aortic Microcalcification Activity in Combined Positron Emission Tomography and Magnetic Resonance Imaging. J Nash, S Debono, J Kaczynski, T Clark, G Macnaught, S Semple, EJR van Beek, D Dey, MC Williams, PJ Slomka, M R Dweck, DE Newby, AJ Fletcher. *European Journal of Nuclear Medicine and Molecular Imaging* 2024; DOI: 10.1007/s00259-024-06670-5

My contribution: statistical analysis and manuscript preparation.

2. ^{18}F-Sodium Fluoride Positron Emission Tomography and Computed Tomography in acute aortic syndrome. M Syed, A Fletcher, S Debono, R Forsythe, M Williams, M Dweck, A Shah, M Macaskill, A Tavares, M Denvir, K Lim, W Wallace, J Kaczynski, T Clark, S Sellers, N Masson, O Falah, R Chalmers, A Tambyraja, E van Beek, D Newby. *Journal of American College of Cardiology* 2022; 15(7):1291-1304

My contribution: recruitment with follow up imaging scans and manuscript preparation.

3. Thoracic Aortic ^{18}F-Sodium Fluoride Activity and Ischemic Stroke in Patients with Established Cardiovascular Disease. A Fletcher, Y Tew, E Tzolos, S Joshi, J Kaczynski, J Nash, S Debono, M Lembo, J Kwiecinski, R Bing, M Syed, M Doris, E van Beek, A Moss, W Jenkins, N Walker, N Joshi, T Pawade, P Adamson, W Whiteley, J Wardlaw, P Slomka, M Williams, D Newby, M Dweck. *Journal of American College of Cardiology* 2022; 15(7):1274-1288

My contribution: recruitment and manuscript preparation.

4. A Novel Plaque Enriched Long Non-coding RNA in Macrophage Phagocytosis Regulation (PELATON). J Hung, JP Scanlon, J Rodor, AD Mahmoud, M Fontaine, L Temmerman, J Kaczynski, R Bhushan, EAL. Biessen, DE Newby, JC Sluimer, AH Baker. *Journal of Arteriosclerosis, Thrombosis and Vascular Biology* 2020;40:697-713

My contribution: recruitment, samples with clinical data collection, and manuscript preparation.

5. Osteocalcin Regulates Arterial Calcification via Altered Wnt Signalling and Glucose Metabolism. NA Rashdan, AM Sim, L Cui, K Phadwal, FL Roberts, R Carter, DD Ozdemir, P Hohenstein, J Hung, J Kaczynski, DE Newby, AH Baker, G Karsenty, NM Morton, VE MacRae. *Journal of Bone and Mineral Research* 2020;35(2):357-367

My contribution: recruitment, samples with clinical data collection and manuscript preparation.

6. The Human- and Smooth Muscle Cell-Enriched lncRNA SMILR Promotes Proliferation by Regulating Mitotic CENPF mRNA and Drives Cell-Cycle Progression Which Can Be Targeted to Limit Vascular Remodeling. AD Mahmoud, MD Ballantyne, V Miscianinov, K Pinel, J Hung, JP Scanlon, J Iyinikkel, J Kaczynski, AS Tavares, AC Bradshaw, NL Mills, DE Newby, A Caporali, GW Gould, SJ George, I Ulitsky, JC Sluimer, J Rodor, AH Baker. *Circulation Research* 2019; 125:535-551

My contribution: recruitment, samples with clinical data collection and manuscript preparation.

7.^{18}F-Sodium Fluoride Uptake in Abdominal Aortic Aneurysms. SoFIA^3 Study Investigators: R Forsythe, M Dweck, O McBride, A Vesey, S Semple, A Shah, P Adamson, W Wallace, J Kaczynski, W Ho, E van Beek, C Gray, A Fletcher, C Lucatelli, A Martin, P Burns, A Tambyraja, R Chalmers, G Weir, N Mitchard, A Tavares, J Robson, D Newby. *Journal of the American College of Cardiology* 2018;71(5):513-523

My contribution: reproducibility PET-CT imaging analysis and manuscript preparation.

8.Aortic Wall Inflammation Predicts Abdominal Aortic Aneurysm Expansion, Rupture, and Need for Surgical Repair. MA3RS Study Investigators: Newby D, Forsythe R, McBride O, Robson J, Vesey A, Chalmers R, Burns P, Garden OJ, Dweck M, Gray C, MacGillivray T, Wang C, Koutraki C, Koutraki YG, Mitchard N, Cooper A, van Beek E, McKillop G, Ho W, Fraser L, Cuthbert H, Hoskins P, Doyle B, Conlisk N, Stuart W, Berry C, Roditi G, Murdoch L, Holdsworth R, Scott E, Milne L, Strachan F, Wee F, Oatley K, Graham C, Murray G, Milne G, Bucukoglu M, Goodman K, Kaczynski J, Shah A, Tambyraja A, Brittenden J, Houston G, Lambie R, Norrie J. *Circulation* 2017;136(9):787-797

My contribution: clinical endpoint committee, volumetric AAA imaging analysis and manuscript preparation.

SUBMITTED MANUSCRIPTS

1.Spatial Lipidomic Profiles of Atherosclerotic Plaques: Mass Spectrometry Imaging Study. S Ntshangase, S Khan, T Gazarkova, L Bezuidenhout, J Kaczynski, S Sellers, N Rattray, DE Newby, PWF Hadoke, R Andrew. Journal of the American Society for Mass Spectrometry and Analytical Chemistry.

My contribution: Bio-resource study approval, recruitment, samples with clinical data collection and manuscript preparation.

2. Aortic disease activity in patients with endoleak after endovascular aneurysm repair. S Debono, J Nash, MBJ Syed, AJ Fletcher, J Kaczynski, C Alcaide-Corral, C Gray, EJR van Beek, D Dorward, MC Williams, AL Tambyraja, MG MacAskill, AAS Tavares, MR Dweck, DE Newby, RO Forsythe. *Journal of American College of Cardiology: Cardiovascular Imaging.*

My contribution: manuscript preparation.

ABSTRACTS ARISING DIRECTLY FROM THIS THESIS AND FROM ADDITIONAL RESEARCH WORKS

1. 18F-Fluoride Positron Emission Tomography in Acute Aortic Syndrome. Syed M, Fletcher A, Debono S, Forsythe R, Williams M, Dweck M, Tavares A, Macaskill M, Shah A, Denvir M, Lim K, Wallace W, Kaczynski J, Clark T, Seller S, Masson N, Falah O, Chalmer R, Tambyraja A, van Beek E, Newby D. *Heart* 2021; 107(Suppl 1): A1-A185, doi:10.1136/heartjnl-2021-BCS.158

2. Early experience with ^{18}F-Fluoride Positron Emission Tomography-Magnetic Resonance Imaging in Patients with Symptomatic Carotid artery Stenosis Undergoing Carotid Endarterectomy. Kaczynski J, Williams M, Forsythe R, Tambyraja A, Lucatelli C, van Beek EJR, Whiteley W, Newby DE. *European Journal of Vascular and Endovascular Surgery* 2019;58(6): SUPPL 3: E845-E846676-678

3. **Early experience with ^{18}F-Fluoride Positron Emission Tomography-Magnetic Resonance Imaging in Patients with Acute Neurovascular Syndrome**. Kaczynski J, Williams M, Wardlaw JM, Dweck M, Macnaught G, Forsythe R, Whiteley W, van Beek EJR, Newby DE. *European Society of Radiology*, doi:10.26044/ecr2019/C-0655

4. **Predicting Abdominal Aortic Aneurysm Growth Using ^{18}F-Sodium Fluoride PET-CT**. R Forsythe, M Dweck, O McBride, A Vesey, S Semple, A Shah, P Adamson, W Wallace, J Kaczynski, E van Beek, C Gray, A Fletcher, C Lucatelli, A Martin, P Burns, A Tambyraja, R Chalmers, G Weir, N Mitchard, A Tavares, J Robson, D Newby. *Heart* 2018;104(Suppl 5): A1

5. **Microcalcification predicts abdominal aortic aneurysm expansion and repair: the ^{18}F-Sodium Fluoride Imaging in Abdominal Aortic Aneurysms (SoFIA^3) Study**. R Forsythe, M Dweck, O McBride, A Vesey, S Semple, A Shah, P Adamson, W Wallace, J Kaczynski, W Ho, E van Beek, C Gray, A Fletcher, C Lucatelli, A Martin, P Burns, A Tambyraja, R Chalmers, G Weir, N Mitchard, A Tavares, J Robson, D Newby. *Journal of Vascular Surgery* 2017; 65(Suppl 6): 24S-25S

PRESENTATIONS ARISING DIRECTLY FROM THIS THESIS AND FROM ADDITIONAL RESEARCH WORKS

International

1. ^{18}F-NaF PET-MRI in patients undergoing carotid endarterectomy - correlation with ex vivo imaging and histology. J Kaczynski, M Syed, S Debono, M Williams, D Newby, A Tavares, R Forsythe, S Sellers. European Society for Vascular Surgery (ESVS) Translational Spring Meeting, Stockholm, Sweden, 06/2024

2. Imaging Lipoprotein(a) and its Lipid Cargo in atherosclerosis using Mass Spectrometry. S Ntshangase, S Khan, J Kaczynski, S Sellers, DE Newby, PWF Hadoke, R Andrew. Federation of European Biochemical Societies (FEBS) – 15th European Summer School on Advance Proteomics, Bolzano, Italy, 08/2023

3.Sodium [^{18}F] fluoride and [^{18}F] NOTA-RGDfk uptake in abdominal aortic aneurysm tissue. S Debono, M BJ Syed, J Kaczynski, C Alcaide-Corral, C Gray, D E Newby, M G MacAskill, A AS Tavares, R O Forsythe. PET is Wonderful (PiW) Annual Scientific Meeting, Royal Society of Edinburgh, Edinburgh, UK, 09/2022

4. ^{18}F-Sodium Fluoride positron emission tomography / computed tomography in acute aortic syndrome. M Syed, A Fletcher, R Forsythe, M Williams, M Dweck, A Shah, A Tavarez, M Denvir, K Lim, W Wallace, J Kaczynski, S Sellers, N Masson, O Falah, R Chalmers, A Tambyraja, E van Beek, D Newby. *European Society for Vascular Surgery Annual Meeting (ESVS month)*, 10/2020

5. Early experience with ^{18}F-Fluoride Positron Emission Tomography-Magnetic Resonance Imaging in patients with Symptomatic Carotid Artery Stenosis undergoing carotid endarterectomy. J Kaczynski, MC Williams, RO Forsythe, A Tambyraja, C Lucatelli, EJR van Beek, W Whitely, DE Newby. *European Society for Vascular Surgery (ESVS) Annual Meeting*, Hamburg, Germany, 09/2019

6. A novel macrophage long non-coding RNA in atherosclerosis. Hung J, Rodor J, Scanlon JP, Mahmoud AD, Fontaine M, Temmerman L, Kaczynski J, Tavares A, Ballantyne M, Pinel K, Bhushan R, Newby DE, Biessen EAL, Sluimer JC, Baker AH. *European Society for Microcirculation- European Vascular Biology Organisation (ESM-EVBO)*, Maastricht, Netherlands, 04/2019

7. Early experience with ^{18}F-Fluoride Positron Emission Tomography-Magnetic Resonance Imaging in patients with Acute Neurovascular Syndrome. J Kaczynski, MC Williams, J Wardlaw, M Dweck, G Macnaught, R Forsythe, W Whiteley, EJR van Beek, D Newby. *European Congress of Radiology (ECR)*, Vienna, Austria, 02/2019

8. Assessment of anti-calcific agents with ^{18}F-NaF and Positron Emission Tomography for the treatment of vascular calcification. MacAskill MG, Wu J, Alcaide-Corral CJ, Kaczynski J, Doris M, McDougald W, Hadoke PWF, Maj R, Ivarsson M, Newby DE, Tavares A. *European Molecular Imaging Meeting (EMIM)*, Glasgow, 03/2019

9. Osteocalcin Regulates Arterial Calcification via altered Wnt signalling and Glucose Metabolism. N A Rashdan, A M Sim, P Hohenstein, J Hung, J Kaczynski, D E Newby, A H Baker, G Karsenty, V E MacRae. *Bone Research Society Annual Meeting*, Winchester, UK, 06/2018

10. Predicting Abdominal Aortic Aneurysm Growth Using ^{18}F-Sodium Fluoride PET-CT. Forsythe RO on behalf of the SoFIA^3 Investigators. *British Cardiovascular Imaging Meeting,* Edinburgh, 05/2018

11. Integrative systems approach identifies novel lncRNA transcripts during atherosclerotic plaque development. Bhushan R, Hung J, Rodor J, Kok F, Pinel K, Ballantyne M, Tavares A, Kaczynski J, Sluimer J, Newby D, Baker A. *Non-Coding RNA Biochemistry Society Conference*, Royal College of Surgeons, Edinburgh, 06/2017

12. Microcalcification predicts abdominal aortic aneurysm expansion and repair: the ^{18}F-Sodium Fluoride Imaging in Abdominal Aortic Aneurysms (SoFIA^3) Study. Forsythe RO on behalf of the SoFIA^3 Investigators. *Society for Vascular Surgery Vascular Annual Meeting*, USA, San Diego, 06/2017

National

1. Deciphering Atherosclerosis: Unravelling Spatial Lipid Heterogeneity through Advanced MALDI-MSI Profiling in Rabbit Aortas and Human Carotid Plaques. S Ntshangase, S Khan, T Gazarkova, L Bezuidenhout, J Kaczynski, S Sellers, DE Newby, PWF Hadoke, R Andrew. *British Society of Endocrinology,* Glasgow, 11/2023

2. Lipid-Profiling Atherosclerosis: Mass Spectrometry Imaging Reveals New Insights into Plaque Pathogenesis. S Ntshangase, S Khan, J Kaczynski, S Sellers, DE Newby, PWF Hadoke, R Andrew. *British Mass Spectrometry Society SIG Imaging Symposium*, Sheffield, 05/2023

3. Using Mass Spectrometry imaging to Study the Lipidome of Atherosclerotic Plaques. A Ntshangase, S Khan, J Kaczynski, PWF Hadoke, DE Newby, R Andrew. *British Society of Endocrinology*, Harrogate, 11/2022

4. Early experience with 18F-Fluoride Positron Emission Tomography-Magnetic Resonance Imaging in patients with Acute Neurovascular Syndrome. Kaczynski J, Williams M, Whiteley W, Dennis M, Wardlaw J, Macnaught G, Tavares A, Jansen M, MacGillivray T, Forsythe R, Tambyraja A, Dweck M, Chaudhury R, van Beek E, Newby D. *Scottish Heart and Arterial disease Risk Prevention (SHARP) Meeting*, Crieff, 11/2018

Regional

1. A novel macrophage long non-coding RNA in atherosclerosis. J Hung, R Bhushan, J Rodor, K Pinel, M Ballantyne, A Mahmoud, A Tavares, J Kaczynski, J Sluimer, D Newby, A H Baker. *Cardiovascular Centre Symposium*, Edinburgh, 06/2018

2. Discovery of Novel Long Non-Coding RNAs: Therapeutic Targets in Atherosclerosis. Hung J, Bhushan R, Rodor J, Kok F, Pinel K, Ballantyne M, Tavares A, Kaczynski J, Sluimer J, Newby D, Baker A. *Cardiovascular Centre Symposium*, Edinburgh, 06/2017

PRIZES ARISING FROM ADDITIONAL RESEARCH ACTIVITIES

1. Runner-up (oral): ^{18}F-Sodium fluoride positron emission tomography / computed tomography in acute aortic syndrome. European Society for Vascular Surgery Annual Meeting (ESVS month) (22/10/2020)

2. Runner-up (oral): A novel macrophage long non-coding RNA in Atherosclerosis. Edinburgh Cardiovascular Centre Symposium, Edinburgh (14/06/2018)

3. Winner of the Young Investigator Award (oral): Predicting Abdominal Aortic Aneurysm Growth Using ^{18}F-Sodium Fluoride PET-CT. British Cardiovascular Imaging Meeting, Edinburgh (02/05/2018)

4. Winner of the Thomas Fogarty Award (oral): Microcalcification predicts abdominal aortic aneurysm expansion and repair: the ^{18}F-Sodium Fluoride Imaging in Abdominal Aortic Aneurysms (SoFIA^3) Study. Society for Vascular Surgery Vascular Annual Meeting, San Diego, USA (01/06/2017)

REFERENCES

Aaslid R.Transcranial Doppler sonography, New York, Springer-Verlag, 1986.

Aaslid R, Markwalder T-M, Nornes H.Noninvasive transcranial Doppler ultrasound recording of flow velocity in basal cerebral arteries. *Journal of neurosurgery* 1982;57:769–774.

Ababneh B, Rejjal L, Pokharel Y, Nambi V, Wang X, Tung C-H et al.Distribution of calcification in carotid endarterectomy tissues: comparison of micro-computed tomography imaging with histology. *Vasc medicine Lond Engl* 2014;19:343–50.

Abbott AL.Bias in the use of randomized trials for carotid stenosis management. *Gefässchirurgie* 2015;20:252–257.

Abbott AL, Chambers BR, Stork JL, Levi CR, Bladin CF, Donnan GA.Embolic signals and prediction of ipsilateral stroke or transient ischemic attack in asymptomatic carotid stenosis: a multicenter prospective cohort study. *Stroke* 2005;36:1128–1133.

Abbott AL, Levi CR, Stork JL, Donnan GA, Chambers BR.Timing of Clinically Significant Microembolism after Carotid Endarterectomy. *Cerebrovasc Dis* 2007a;23:362–367.

Abbott AL, Levi CR, Stork JL, Donnan GA, Chambers BR.Timing of clinically significant microembolism after carotid endarterectomy. *Cerebrovascular diseases* 2007b;23:362–367.

Adamson PD, Newby DE, Dweck MR.Translational Coronary Atherosclerosis Imaging with PET. *Cardiol Clin* 2016;34:179–186.

Aidi HE, Mani V, Weinshelbaum KB, Aguiar SH, Taniguchi H, Postley JE et al.Cross-sectional, prospective study of MRI reproducibility in the assessment of plaque burden of the carotid arteries and aorta. *Nat Clin Pract Cardiovasc Medicine* 2009;6:219–28.

Aikawa E.Cardiovascular Imaging, Arterial and Aortic Valve Inflammation and Calcification, 1st edition. Switzerland, Springer International Publishing, 2015.

Aird WC.Phenotypic Heterogeneity of the Endothelium. *Circ Res* 2007;100:174–190.

Aizaz M, Moonen RPM, Pol JAJ van der, Prieto C, Botnar RM, Kooi ME.PET/MRI of atherosclerosis. *Cardiovasc Diagnosis Ther* 2020;10:1120–1139.

Alexandrov AV, Sloan MA, Tegeler CH, Newell DN, Lumsden A, Garami Z et al.Practice standards for transcranial Doppler (TCD) ultrasound. Part II. Clinical indications and expected outcomes. *Journal of Neuroimaging* 2012;22:215–224.

Alexandrov AV, Sloan MA, Wong LK, Douville C, Razumovsky AY, Koroshetz WJ et al.Practice standards for transcranial Doppler ultrasound: part I—test performance. *Journal of Neuroimaging* 2007;17:11–18.

Alexopoulos N, Raggi P.Calcification in atherosclerosis. *Nat Rev Cardiol* 2009;6:681–688.

AlMuhanna K, Hossain MM, Zhao L, Fischell J, Kowalewski G, Dux M et al.Carotid plaque morphometric assessment with three-dimensional ultrasound imaging. *J Vasc Surg* 2014;61:690–7.

Aloya R, Shirvan A, Grimberg H, Reshef A, Levin G, Kidron D et al.Molecular imaging of cell death in vivo by a novel small molecule probe. *Apoptosis* 2006;11:2089–2101.

Alquraini A, Khoury JE.Scavenger receptors. *Curr Biol* 2020;30:R790–R795.

Amarenco P, Bogousslavsky J, Callahan A, Goldstein LB, Hennerici M, Rudolph AE et al.High-Dose Atorvastatin after Stroke or Transient Ischemic Attack. *New Engl J Medicine* 2006;355:549–559.

Andrews JPM, Fayad ZA, Dweck MR.New methods to image unstable atherosclerotic plaques. *Atherosclerosis* 2018;272:118–128.

Antonov AS, Kolodgie FD, Munn DH, Gerrity RG.Regulation of Macrophage Foam Cell Formation by αVβ3 Integrin Potential Role in Human Atherosclerosis. *Am J Pathology* 2004;165:247–258.

Arbab-Zadeh A, Fuster V.The myth of the 'vulnerable plaque': transitioning from a focus on individual lesions to atherosclerotic disease burden for coronary artery disease risk assessment. *J Am Coll Cardiol* 2015;65:846–55.

Arbab-Zadeh A, Nakano M, Virmani R, Fuster V.Acute Coronary Events. *Circulation* 2012;125:1147–1156.

Archie JP.Commentary on 'Risk of Recurrent Stroke in Patients with Symptomatic Mild (20–49% NASCET) Carotid Stenosis'. *Eur J Vasc Endovasc* 2016;52:295.

Armitage J, Holmes MV, Preiss D.Cholesteryl Ester Transfer Protein Inhibition for Preventing Cardiovascular Events JACC Review Topic of the Week. *J Am Coll Cardiol* 2019;73:477–487.

Arnold JA, Modaresi KB, Thomas N, Taylor PR, Padayachee TS.Carotid plaque characterization by duplex scanning: observer error may undermine current clinical trials. *Stroke* 1999;30:61–65.

Arnolds BJ, Reutern G-M von.Transcranial Dopplersonography. Examination technique and normal reference values. *Ultrasound in medicine & biology* 1986;12:115–123.

Artlett CM.Inflammasomes in wound healing and fibrosis. *J Pathology* 2013;229:157–167.

Artul S, Nseir W, Armaly Z, Soudack M.Superb Microvascular Imaging: Added Value and Novel Applications. *J Clin Imaging Sci* 2017;7:45.

Ayala-López W, Xia W, Varghese B, Low PS.Imaging of Atherosclerosis in Apoliprotein E Knockout Mice: Targeting of a Folate-Conjugated Radiopharmaceutical to Activated Macrophages. *J Nucl Med* 2010;51:768–774.

Azarpazhooh MR, Chambers BR.Clinical application of transcranial Doppler monitoring for embolic signals. *Journal of clinical neuroscience* 2006;13:799–810.

Babikian VL, Feldmann E, Wechsler LR, Newell DW, Gomez CR, Bogdahn U et al.Transcranial Doppler ultrasonography: year 2000 update. *Journal of Neuroimaging* 2000;10:101–115.

Bachi K, Mani V, Kaufman AE, Alie N, Goldstein RZ, Fayad ZA et al.Imaging plaque inflammation in asymptomatic cocaine addicted individuals with simultaneous positron emission tomography/magnetic resonance imaging. *World J Radiology* 2019;11:62–73.

Bala G, Blykers A, Xavier C, Descamps B, Broisat A, Ghezzi C et al.Targeting of vascular cell adhesion molecule-1 by 18F-labelled nanobodies for PET/CT imaging of inflamed atherosclerotic plaques. *European Hear J - Cardiovasc Imaging* 2016;17:1001–1008.

Balla G, Jacob HS, Eaton JW, Belcher JD, Vercellotti GM.Hemin: a possible physiological mediator of low density lipoprotein oxidation and endothelial injury. *Arteriosclerosis Thrombosis J Vasc Biology* 2018;11:1700–1711.

Ballotta E, Angelini A, Mazzalai F, Piatto G, Toniato A, Baracchini C.Carotid endarterectomy for symptomatic low-grade carotid stenosis. *J Vasc Surg* 2014;59:25–31.

Barnett HJM, Taylor DW, Haynes RB, Ferguson GG, Fox AJ, Rankin RN et al.Beneficial Effect of Carotid Endarterectomy in Symptomatic Patients with High-Grade Carotid Stenosis. *New Engl J Medicine* 1991;325:445–453.

Baroncini LAV, Nakao LS, Ramos SG, Filho AP, Murta LO, Ingberman M et al.Assessment of MMP-9, TIMP-1, and COX-2 in normal tissue and in advanced symptomatic and asymptomatic carotid plaques. *Thrombosis J* 2011;9:6.

Battle MR, Goggi JL, Allen L, Barnett J, Morrison MS.Monitoring Tumor Response to Antiangiogenic Sunitinib Therapy with 18F-Fluciclatide, an 18F-Labeled αVβ3-Integrin and αVβ5-Integrin Imaging Agent. *J Nucl Med* 2011;52:424–430.

Baumgartner RW, Mathis J, Sturzenegger M, Mattle HP.A validation study on the intraobserver reproducibility of transcranial color-coded duplex sonography velocity measurements. *Ultrasound in medicine & biology* 1994;20:233–237.

Beard J, Gaines PA.Vascular and Endovascular Surgery, 4th edition. Elsevier Health Sciences, 2009.

Beer AJ, Pelisek J, Heider P, Saraste A, Reeps C, Metz S et al.PET/CT Imaging of Integrin αvβ3 Expression in Human Carotid Atherosclerosis. *Jacc Cardiovasc Imaging* 2014;7:178–187.

Benditt EP, Benditt JM.Evidence for a Monoclonal Origin of Human Atherosclerotic Plaques. *Proc National Acad Sci* 1973;70:1753–1756.

Bentzon JF, Otsuka F, Virmani R, Falk E.Mechanisms of Plaque Formation and Rupture. *Circ Res* 2014;114:1852–1866.

Best LM, Webb AC, Gurusamy KS, Cheng SF, Richards T.Transcranial Doppler Ultrasound Detection of Microemboli as a Predictor of Cerebral Events in Patients with Symptomatic and Asymptomatic Carotid Disease: A Systematic Review and Meta-Analysis. *Eur J Vasc Endovasc Surg* 2016;52:565–580.

Bibliotheque-Nationale-de-France.Radiological car Massiot- photography [Internet] 1914;Available from: https://images.bnf.fr/#/detail/549507/10

Bing R, Dweck MR.Management of asymptomatic severe aortic stenosis: check or all in? *Heart* 2020a;heartjnl-2020-317160.

Bing R, Dweck MR.The quest for an aortic stenosis cure. *Heart* 2020b;106:1790–1791.

Bird JLE, Izquierdo-Garcia D, Davies JR, Rudd JHF, Probst KC, Figg N et al.Evaluation of translocator protein quantification as a tool for characterising macrophage burden in human carotid atherosclerosis. *Atherosclerosis* 2010;210:388–391.

Bitto A, Caridi GD, Polito F, Calò M, Irrera N, Altavilla D et al.Evidence for markers of hypoxia and apoptosis in explanted human carotid atherosclerotic plaques. *J Vasc Surg* 2010;52:1015–1021.

Blomberg BA, Thomassen A, Jong PA de, Lam MGEH, Hess S, Olsen MH et al.Reference values for fluorine-18-fluorodeoxyglucose and fluorine-18-sodium fluoride uptake in human arteries: a prospective evaluation of 89 healthy adults. *Nuclear medicine communications* 2017;38:998–1006.

Boswijk E, Bauwens M, Mottaghy FM, Wildberger JE, Bucerius J.Potential of α7 nicotinic acetylcholine receptor PET imaging in atherosclerosis. *Methods* 2017;130:90–104.

Bot I, Biessen E.Mast cells in atherosclerosis. *Thromb Haemostasis* 2011;106:820–826.

Bot I, Shi G-P, Kovanen PT.Mast Cells as Effectors in Atherosclerosis. *Arteriosclerosis Thrombosis Vasc Biology* 2015;35:265–271.

Boyle JJ, Harrington HA, Piper E, Elderfield K, Stark J, Landis RC et al.Coronary Intraplaque Hemorrhage Evokes a Novel Atheroprotective Macrophage Phenotype. *Am J Pathology* 2009;174:1097–1108.

Bragoni M, Feldmann E.Transcranial Doppler indices of intracranial hemodynamics. *Neurosonology Boston: Mosby* 1996;129–140.

Briley-Saebo KC, Mulder WJM, Mani V, Hyafil F, Amirbekian V, Aguinaldo JGS et al.Magnetic resonance imaging of vulnerable atherosclerotic plaques: Current imaging strategies and molecular imaging probes. *J Magn Reson Imaging* 2007;26:460–479.

Brinjikji W, Huston J, Rabinstein AA, Kim G-M, Lerman A, Lanzino G.Contemporary carotid imaging: from degree of stenosis to plaque vulnerability. *J Neurosurg* 2016;2016:27–42.

Broisat A, Hernot S, Toczek J, Vos JD, Riou LM, Martin S et al.Nanobodies Targeting Mouse/Human VCAM1 for the Nuclear Imaging of Atherosclerotic Lesions. *Circ Res* 2012;110:927–937.

Bucerius J, Hyafil F, Verberne HJ, Slart RHJA, Lindner O, Sciagra R et al.Position paper of the Cardiovascular Committee of the European Association of Nuclear Medicine (EANM) on PET imaging of atherosclerosis. *Eur J Nucl Med Mol I* 2016;43:780–792.

Buscombe JR.Exploring the nature of atheroma and cardiovascular inflammation in vivo using positron emission tomography (PET). *Br J Radiology* 2015;88:20140648.

Cai J, Hatsukami TS, Ferguson MS, Kerwin WS, Saam T, Chu B et al.In Vivo Quantitative Measurement of Intact Fibrous Cap and Lipid-Rich Necrotic Core Size in Atherosclerotic Carotid Plaque: Comparison of High-Resolution,

Contrast-Enhanced Magnetic Resonance Imaging and Histology. *Circulation* 2005;112:3437–3444.

Cai J-M, Hatsukami TS, Ferguson MS, Small R, Polissar NL, Yuan C.Classification of Human Carotid Atherosclerotic Lesions With In Vivo Multicontrast Magnetic Resonance Imaging. *Circulation* 2002;106:1368–1373.

Calcagno C, Fayad ZA.Clinical imaging of cardiovascular inflammation. *Q J Nucl Medicine Mol Imaging* 2020;64. DOI: 10.23736/s1824-4785.20.03228-8

Campbell LA, Rosenfeld ME.Infection and Atherosclerosis Development. *Arch Med Res* 2015;46:339–350.

Caplan LR.Caplan's Stroke: a clinical approach, 5th edition. Cambridge, Cambridge University Press, 2016.

Carrea R, Molins M, Murphy G.[Surgery of spontaneous thrombosis of the internal carotid in the neck; carotido-carotid anastomosis; case report and analysis of the literature on surgical cases]. *Medicina* 1955;15:20–9.

Carroll BA.Carotid sonography. *Radiology* 1991;178:303–313.

Castellanos M, Serena J, Segura T, Pérez-Ayuso MJ, Silva Y, Dávalos A.Atherosclerotic Aortic Arch Plaques in Cryptogenic Stroke: A Microembolic Signal Monitoring Study. *Eur Neurol* 2001;45:145–150.

Castillo M, of LKAJ.Clinical applications of proton MR spectroscopy. *pdfs.semanticscholar.org* 1996;

Chae SY, Kwon T-W, Jin S, Kwon SU, Sung C, Oh SJ et al.A phase 1, first-in-human study of 18F-GP1 positron emission tomography for imaging acute arterial thrombosis. *Ejnmmi Res* 2019;9:3.

Chai JT, Biasiolli L, Li L, Alkhalil M, Galassi F, Darby C et al.Quantification of Lipid-Rich Core in Carotid Atherosclerosis Using Magnetic Resonance T2 Mapping: Relation to Clinical Presentation. *JACC: Cardiovascular Imaging* 2017;10:747–756.

Chambless LE, Heiss G, Shahar E, Earp MJ, Toole J.Prediction of Ischemic Stroke Risk in the Atherosclerosis Risk in Communities Study. *Am J Epidemiol* 2004;160:259–269.

Chappell FM, Wardlaw JM, Young GR, Gillard JH, Roditi GH, Yip B et al.Carotid artery stenosis: accuracy of noninvasive tests--individual patient data meta-analysis. *Radiology* 2009;251:493–502.

Chen L, Deng H, Cui H, Fang J, Zuo Z, Deng J et al.Inflammatory responses and inflammation-associated diseases in organs. *Oncotarget* 2017;9:7204–7218.

Chobanian AV, Bakris GL, Black HR, Committee NHBPEPC.The seventh report of the Joint National Committee on prevention, detection, evaluation, and treatment of high blood pressure. The JNC 7 report. *Acc Curr J Rev* 2003;12:31–32.

Chorath A, Choi Y, Turkbey EB, Ahlman MA, Sibley CT, Liu S et al.Coronary CT Angiography and Carotid MRI Improve Phenotyping of Disease Extent Compared with ACC/AHA Risk Score Alone. *Radiology Cardiothorac Imaging* 2020;2:e190068.

Chowdhury MM, Tarkin JM, Albaghdadi MS, Evans NR, Le EPV, Berrett TB et al.Vascular Positron Emission Tomography and Restenosis in Symptomatic Peripheral Arterial Disease A Prospective Clinical Study. *Jacc Cardiovasc Imaging* 2020;13:1008–1017.

Chu B, Kampschulte A, Ferguson MS, Kerwin WS, Yarnykh VL, O'Brien KD et al.Hemorrhage in the Atherosclerotic Carotid Plaque: A High-Resolution MRI Study. *Stroke J Am Hear Assoc* 2004;35:1079–1084.

Cibulka MT, Strube MJ.The Conundrum of Kappa and Why Some Musculoskeletal Tests Appear Unreliable Despite High Agreement: A Comparison of Cohen Kappa and Gwet AC to Assess Observer Agreement When Using Nominal and Ordinal Data. *Phys Ther* 2021;101. DOI: 10.1093/ptj/pzab150

Cohen A, Shirvan A, Levin G, Grimberg H, Reshef A, Ziv I.From the Gla domain to a novel small-molecule detector of apoptosis. *Cell Res* 2009;19:625–637.

Collins R, Bowman L, Landray M, Peto R.The Magic of Randomization versus the Myth of Real-World Evidence. *New Engl J Med* 2020;382:674–678.

Connor MD, Walker R, Modi G, Warlow CP.Burden of stroke in black populations in sub-Saharan Africa. *Lancet Neurology* 2007;6:269–278.

Conti-Fine BM, Navaneetham D, Lei S, Maus ADJ.Neuronal nicotinic receptors in non-neuronal cells: new mediators of tobacco toxicity?11The work reviewed here carried out in the authors' laboratory was partially supported by NIDA grants DA05698, DA08131 and DA11806. *Eur J Pharmacol* 2000;393:279–294.

Cooley DA.Carotid endarterectomy: from first recorded case to present. *Tex Heart I J* 1988;15:139–41.

Cooley DA, Al-Naaman YD, Carton CA.Surgical Treatment of Arteriosclerotic Occlusion of Common Carotid Artery. *J Neurosurg* 1956;13:500–506.

Coull AJ, Lovett JK, Rothwell PM, Study OV.Population based study of early risk of stroke after transient ischaemic attack or minor stroke: implications for public education and organisation of services. *Bmj* 2004;328:326.

Cronenwett JL, Johnston KW.Rutherford's Vascular Surgery, 7th edition. Philadelphia, Elsevier Health Sciences, 2014.

Crouse JR, Byington RP, Furberg CD.HMG-CoA reductase inhibitor therapy and stroke risk reduction: an analysis of clinical trials data. *Atherosclerosis* 1998;138:11–24.

Cuccurullo C, Fazia M, Mezzetti A, Cipollone F.COX-2 Expression in Atherosclerosis: The Good, the Bad or the Ugly? *Curr Med Chem* 2007;14:1595–1605.

Cuhlmann S, Gsell W, Heiden KV der, Habib J, Tremoleda JL, Khalil M et al.In Vivo Mapping of Vascular Inflammation Using the Translocator Protein Tracer 18F-FEDAA1106. *Mol Imaging* 2014;13:7290.2014.00014.

Cullinane M, Reid G, Dittrich R, Kaposzta Z, Ackerstaff R, Babikian V et al.Evaluation of new online automated embolic signal detection algorithm, including comparison with panel of international experts. *Stroke* 2000;31:1335–1341.

Curtis SB, Hewitt J, Yakubovitz S, Anzarut A, Hsiang YN, Buchan AMJ.Somatostatin receptor subtype expression and function in human vascular tissue. *Am J Physiol-heart C* 2000;278:H1815–H1822.

Davies AH, Beard JD, Wyatt MG.Essential Vascular Surgery, London, WB Saunders Complany Limited, 1999.

Davies AH, Brophy CM.Vascular Surgery, United States of America, Springer Science, 2006.

Davies JR, Rudd JHF, Fryer TD, Graves MJ, Clark JC, Kirkpatrick PJ et al.Identification of Culprit Lesions After Transient Ischemic Attack by Combined 18F Fluorodeoxyglucose Positron-Emission Tomography and High-Resolution Magnetic Resonance Imaging. *Stroke* 2005;36:2642–2647.

Dawson DL, Zierler RE, Strandness DE, Clowes AW, Kohler TR.The role of duplex scanning and arteriography before carotid endarterectomy: A prospective study. *J Vasc Surg* 1993;18:673–683.

DeBakey ME.Successful Carotid Endarterectomy For Cerebrovascular Insufficiency: Nineteen-Year Follow-up. *Jama* 1975;233:1083–1085.

Dedehayir O, Steinert M.The hype cycle model: A review and future directions. *Technol Forecast Soc* 2016;108:28–41.

Degnan AJ, Young VEL, Gillard JH.Advances in noninvasive imaging for evaluating clinical risk and guiding therapy in carotid atherosclerosis. *Expert Rev Cardiovasc Ther* 2012;10:37–53.

Dellen D van, Tiivas CAS, Jarvi K, Marshall C, Higman DJ, Imray CHE.Transcranial Doppler ultrasonography-directed intravenous glycoprotein IIb/IIIa receptor antagonist therapy to control transient cerebral microemboli before and after carotid endarterectomy. *Brit J Surg* 2008;95:709–713.

Demirkaya S, Uluc K, Bek S, Vural O.Normal blood flow velocities of basal cerebral arteries decrease with advancing age: a transcranial Doppler sonography study. *Tohoku J Exp Med* 2008;214:145–149.

Deng F, Hao X, Tang Z, Mu C, Li K, Li H.Carotid plaque magnetic resonance imaging and recurrent stroke risk: A protocol for systematic review and meta-analysis. *Medicine* 2019;98:e15410.

Derlin T, Habermann CR, Lengyel Z, Busch JD, Wisotzki C, Mester J et al.Feasibility of 11C-Acetate PET/CT for Imaging of Fatty Acid Synthesis in the Atherosclerotic Vessel Wall. *J Nucl Med* 2011;52:1848–1854.

Derlin T, Sedding DG, Dutzmann J, Haghikia A, König T, Napp LC et al.Imaging of chemokine receptor CXCR4 expression in culprit and nonculprit coronary atherosclerotic plaque using motion-corrected [68Ga]pentixafor PET/CT. *Eur J Nucl Med Mol I* 2018;45:1934–1944.

Dettori JR, Norvell DC.Kappa and Beyond: Is There Agreement? *Global Spine J* 2020;10:499–501.

Devuyst G, Karapanayiotides T, Ruchat P, Pusztaszeri M, Lobrinus JA, Jonasson L et al.Ultrasound measurement of the fibrous cap in symptomatic and asymptomatic atheromatous carotid plaques. *Circulation* 2005;111:2776–2782.

Diegelmann RF, Evans MC.Wound healing: an overview of acute, fibrotic and delayed healing. *Front Biosci* 2004;9:283.

Dittrich R, Ritter MA, Droste DW.Microembolus detection by transcranial doppler sonography. *Eur J Ultrasound* 2002;16:21–30.

Dogra S, McCord JJ, Paraoanu GS.Coherent interaction-free detection of microwave pulses with a superconducting circuit. *Nat Commun* 2022;13:7528.

Donkor ES.Stroke in the 21st Century: A Snapshot of the Burden, Epidemiology, and Quality of Life. *Stroke Res Treat* 2018;2018:1–10.

Donnan G, Davis S, Chambers B, Gates P.Surgery for prevention of stroke. *Lancet* 1998;351:1372–1373.

Doris MK, Everett RJ, Shun-Shin M, Clavel M-A, Dweck MR.The Role of Imaging in Measuring Disease Progression and Assessing Novel Therapies in Aortic Stenosis. *Jacc Cardiovasc Imaging* 2019;12:185–197.

Dorweiler B, Grechowa I, Wallrath A, Vahl CF, Horke S.Activation of the Proapoptotic Unfolded Protein Response in Plaques of the Human Carotid Artery. *Eur J Vasc Endovasc* 2014;48:248–257.

Duivenvoorden R, Wijk D van, Klimas M.Detection of liquid phase cholesteryl ester in carotid atherosclerotic lesions by 1H-magnetic resonance spectroscopy in humans. *JACC Cardiovasc Imaging* 2013;

Dweck MR, Aikawa E, Newby DE, Tarkin JM, Rudd JHF, Narula J et al.Noninvasive Molecular Imaging of Disease Activity in Atherosclerosis. *Circ Res* 2016;119:330–40.

Eastcott HHG, Pickering GW, Rob CG.Reconstruction of internal carotid artery in a patient with intermittent attacks of hemiplegia. *Lancet* 1954;264:994–996.

Eesa M, Hill MD, Al-Khathaami A, Al-Zawahmah M, Sharma P, Menon BK et al.Role of CT Angiographic Plaque Morphologic Characteristics in Addition to Stenosis in Predicting the Symptomatic Side in Carotid Artery Disease. *American Journal of Neuroradiology* 2010;31:1254–1260.

Ehlers S, Schaible UE.The Granuloma in Tuberculosis: Dynamics of a Host–Pathogen Collusion. *Front Immunol* 2013;3:411.

Eichler H, Pignatti F, Schwarzer-Daum B, Hidalgo-Simon A, Eichler I, Arlett P et al.Randomized Controlled Trials Versus Real World Evidence: Neither Magic Nor Myth. *Clin Pharmacol Ther* 2021;109:1212–1218.

Estol CJ.Dr C. Miller Fisher and the History of Carotid Artery Disease. *Stroke* 1996;27:559–566.

Evans NR, Tarkin JM, Buscombe JR, Markus HS, Rudd JHF, Warburton EA.PET imaging of the neurovascular interface in cerebrovascular disease. *Nat Rev Neurol* 2017;13:676–688.

Evans NR, Tarkin JM, Chowdhury MM, Warburton EA, Rudd JHF.PET Imaging of Atherosclerotic Disease: Advancing Plaque Assessment from Anatomy to Pathophysiology. *Curr Atheroscler Rep* 2016;18:30.

Evans NR, Tarkin JM, Le EP, Sriranjan RS, Corovic A, Warburton EA et al.Integrated cardiovascular assessment of atherosclerosis using PET/MRI. *Br J Radiology* 2020;93:20190921.

Evrard SM, Lecce L, Michelis KC, Nomura-Kitabayashi A, Pandey G, Purushothaman K-R et al.Endothelial to mesenchymal transition is common in atherosclerotic lesions and is associated with plaque instability. *Nat Commun* 2016;7:11853.

Faggiotto A, Ross R.Studies of hypercholesterolemia in the nonhuman primate. II. Fatty streak conversion to fibrous plaque. *Arteriosclerosis Official J Am Hear Assoc Inc* 2018;4:341–356.

Feigin VL, Forouzanfar MH, Krishnamurthi R, Mensah GA, Connor M, Bennett DA et al.Global and regional burden of stroke during 1990–2010: findings from the Global Burden of Disease Study 2010. *Lancet* 2014;383:245–255.

Feigin VL, Norrving B, Mensah GA.Global Burden of Stroke. *Circ Res* 2017;120:439–448.

Feldmann E, Wilterdink JL, Kosinski A, Lynn M, Chimowitz MI, Sarafin J et al.The Stroke Outcomes and Neuroimaging of Intracranial Atherosclerosis (SONIA) trial. *Neurology* 2007;68:2099–2106.

Ferguson GG, Eliasziw M, Barr HWK, Clagett GP, Barnes RW, Wallace MC et al.The North American Symptomatic Carotid Endarterectomy Trial: Surgical Results in 1415 Patients. *Stroke* 1999;30:1751–1758.

Fisher M.Occlusion of the internal carotid artery. *M Archives Neurology Psychiatry* 1951;65:346–377.

Fletcher AJ, Lembo M, Kwiecinski J, Syed MBJ, Nash J, Tzolos E et al.Quantifying microcalcification activity in the thoracic aorta. *J Nucl Cardiol* 2021;1–14.

Fletcher AJ, Nash J, Syed MBJ, Macaskill MG, Tavares AAS, Walker N et al.Microcalcification and Thoracic Aortopathy: A Window Into Disease Severity. *Arter, Thromb, Vasc Biol* 2022a;42:1048–1059.

Fletcher AJ, Tew YY, Tzolos E, Joshi SS, Kaczynski J, Nash J et al.Thoracic Aortic 18F-Sodium Fluoride Activity and Ischemic Stroke in Patients With Established Cardiovascular Disease. *Jacc Cardiovasc Imaging* 2022b; DOI: 10.1016/j.jcmg.2021.12.013

Forsythe RO, Dweck MR, McBride OMB, Vesey AT, Semple SI, Shah ASV et al.18 F–Sodium Fluoride Uptake in Abdominal Aortic Aneurysms. *J Am Coll Cardiol* 2018;71:513–523.

Franklin JM, Patorno E, Desai RJ, Glynn RJ, Martin D, Quinto K et al.Emulating Randomized Clinical Trials With Nonrandomized Real-World Evidence Studies: First Results From the RCT DUPLICATE Initiative. *Circulation* 2021;143:1002–1013.

Friedman SG.The first carotid endarterectomy. *J Vasc Surg* 2014;60:1703-1708.e4.

Fujimoto S, Hartung D, Ohshima S, Edwards DS, Zhou J, Yalamanchili P et al.Molecular Imaging of Matrix Metalloproteinase in Atherosclerotic Lesions

Resolution With Dietary Modification and Statin Therapy. *J Am Coll Cardiol* 2008;52:1847–1857.

Fujitani RM, Mills JL, Wang LM, Taylor SM.The effect of unilateral internal carotid arterial occlusion upon contralateral duplex study: Criteria for accurate interpretation. *J Vasc Surg* 1992;16:459–468.

Gaemperli O, Shalhoub J, Owen DRJ, Lamare F, Johansson S, Fouladi N et al.Imaging intraplaque inflammation in carotid atherosclerosis with 11C-PK11195 positron emission tomography/computed tomography. *Eur Heart J* 2012;33:1902–1910.

Garrard J, Ummur P, Nduwayo S, Kanber B, Hartshorne T, West K et al.Shear Wave Elastography May Be Superior to Greyscale Median for the Identification of Carotid Plaque Vulnerability: A Comparison with Histology. *Ultraschall Der Medizin - European J Ultrasound* 2015;36:386–390.

Giannakou S, Angelidis G, Tsougos I, Valotassiou V, Kappas K, Georgoulias P.Pet tracers for vulnerable plaque imaging. *Ann Nucl Med* 2020;34:305–313.

Goldberger ZD, Valle JA, Dandekar VK, Chan PS, Ko DT, Nallamothu BK.Are changes in carotid intima-media thickness related to risk of nonfatal myocardial infarction? A critical review and meta-regression analysis. *Am Heart J* 2010;160:701–14.

Golledge J, Siew DA.Identifying the Carotid 'High Risk' Plaque: Is it Still a Riddle Wrapped up in an Enigma? *European Journal of Vascular and Endovascular Surgery* 2008;35:2–8.

Gonzalez MRL, Foo SY, Holmes WM, Stewart W, Muir KW, Condon B et al.Atherosclerotic Carotid Plaque Composition: A 3T and 7T MRI-Histology Correlation Study: Atherosclerotic Carotid Plaque Composition. *J Neuroimaging* 2016;26:406–413.

Gorelick PB.The global burden of stroke: persistent and disabling. *Lancet Neurology* 2019;18:417–418.

Griffin MB, Kyriacou E, Pattichis C, Bond D, Kakkos SK, Sabetai M et al.Juxtaluminal hypoechoic area in ultrasonic images of carotid plaques and hemispheric symptoms. *J Vasc Surg* 2010;52:69–76.

Grolimund P, Seiler RW.Age dependence of the flow velocity in the basal cerebral arteries—a transcranial Doppler ultrasound study. *Ultrasound in medicine & biology* 1988;14:191–198.

Gronholdt ML, Nordestgaard BG, Schroeder TV, Vorstrup S, Sillesen H.Ultrasonic echolucent carotid plaques predict future strokes. *Circulation* 2001;104:68–73.

Grotta JC, Alexandrov AV.Preventing Stroke 2001;

Guerci B, Böhme P, Kearney-Schwartz A, Zannad F, Drouin P.Endothelial dysfunction and type 2 diabetes. Part 2: altered endothelial function and the effects of treatments in type 2 diabetes mellitus. *Diabetes Metab* 2001;27:436–47.

Guo S, Shen S, Wang J, Wang H, Li M, Liu Y et al.Detection of High-Risk Atherosclerotic Plaques with Ultrasound Molecular Imaging of Glycoprotein IIb/IIIa Receptor on Activated Platelets. *Theranostics* 2015;5:418–430.

Guo W, Morrisett JD, Lawrie GM, DeBakey ME, Hamilton JA.Identification of different lipid phases and calcium phosphate deposits in human carotid artery plaques by MAS NMR spectroscopy. *Magnetic Resonance in Medicine* 1998;39:184–189.

Gupta A, Baradaran H, Schweitzer AD, Kamel H, Pandya A, Delgado D et al.Carotid Plaque MRI and Stroke Risk. *Stroke* 2013;44:3071–3077.

Guyton JR.MR Spectroscopy of Cholesteryl Ester in Human Atherosclerosis 2013;

Hans SS.Extracranial Carotid and Vertebral Artery Disease, Contemporary Management, Springer, 2018.

Hartog AG den, Bovens SM, Koning W, Hendrikse J, Luijten PR, Moll FL et al.Current Status of Clinical Magnetic Resonance Imaging for Plaque Characterisation in Patients with Carotid Artery Stenosis. *European Journal of Vascular and Endovascular Surgery* 2013;45:7–21.

Hayashi K, Mani V, Nemade A, Aguiar S, Postley JE, Fuster V et al.Variations in atherosclerosis and remodeling patterns in aorta and carotids. *J Cardiovasc Magnetic Reson Official J Soc Cardiovasc Magnetic Reson* 2010;12:10.

Heeschen C, Weis M, Aicher A, Dimmeler S, Cooke JP.A novel angiogenic pathway mediated by non-neuronal nicotinic acetylcholine receptors. *J Clin Invest* 2002;110:527–536.

Hennerici M, Rautenberg W, Sitzer G, Schwartz A.Transcranial Doppler ultrasound for the assessment of intracranial arterial flow velocity--Part 1. Examination technique and normal values. *Surg Neurol* 1987;27:439–448.

Hernán MA, Robins JM.Using Big Data to Emulate a Target Trial When a Randomized Trial Is Not Available. *Am J Epidemiol* 2016;183:758–764.

Hillmer AT, Li S, Zheng M-Q, Scheunemann M, Lin S, Nabulsi N et al.PET imaging of α7 nicotinic acetylcholine receptors: a comparative study of [18F]ASEM and [18F]DBT-10 in nonhuman primates, and further evaluation of [18F]ASEM in humans. *Eur J Nucl Med Mol I* 2017;44:1042–1050.

Hjelmgren O, Holdfeldt P, Johansson L, Fagerberg B, Prahl U, Schmidt C et al.Identification of vascularised carotid plaques using a standardised and reproducible technique to measure ultrasound contrast uptake. *Eur J Vasc Endovasc Surg* 2013;46:21–28.

Høilund-Carlsen PF, Moghbel MC, Gerke O, Alavi A.Evolving Role of PET in Detecting and Characterizing Atherosclerosis. *Pet Clin* 2019;14:197–209.

Hong JC.Strategies to Turn Real-world Data Into Real-world Knowledge. *Jama Netw Open* 2021;4:e2128045.

Hoogeveen RM, Opstal TSJ, Kaiser Y, Stiekema LCA, Kroon J, Knol RJJ et al.PCSK9 Antibody Alirocumab Attenuates Arterial Wall Inflammation Without Changes in Circulating Inflammatory Markers. *Jacc Cardiovasc Imaging* 2019;12:2571–2573.

Hop H, Boer SA de, Reijrink M, Kamphuisen PW, Borst MH de, Pol RA et al.<Superscript>18</Superscript>F-sodium fluoride positron emission tomography assessed microcalcifications in culprit and non-culprit human carotid plaques. *Journal of Nuclear Cardiology* 2018;361:1–12.

Hoshiga M, Alpers CE, Smith LL, Giachelli CM, Schwartz SM.α v β 3 Integrin Expression in Normal and Atherosclerotic Artery. *Circ Res* 1995;77:1129–1135.

Howard DPJ, Lammeren GW van, Redgrave JN, Moll FL, Vries J-PPM de, Kleijn DPV de et al.Histological Features of Carotid Plaque in Patients With Ocular Ischemia Versus Cerebral Events. *Stroke* 2013;44:734–739.

Howard DPJ, Lammeren GW van, Rothwell PM, Redgrave JN, Moll FL, Vries J-PPM de et al.Symptomatic Carotid Atherosclerotic Disease: Correlations Between Plaque Composition and Ipsilateral Stroke Risk. *Stroke* 2015;46:182–189.

Huibers A, Borst GJ de, Wan S, Kennedy F, Giannopoulos A, Moll FL et al.Non-invasive Carotid Artery Imaging to Identify the Vulnerable Plaque: Current Status and Future Goals. *European Journal of Vascular and Endovascular Surgery* 2015;50:563–572.

Hung J, Scanlon JP, Mahmoud AD, Rodor J, Ballantyne M, Fontaine MAC et al.Novel Plaque Enriched Long Noncoding RNA in Atherosclerotic Macrophage Regulation (PELATON). *Arteriosclerosis Thrombosis Vasc Biology* 2019;40:697–713.

Hunink MG, Polak JF, Barlan MM, O'Leary DH.Detection and quantification of carotid artery stenosis: efficacy of various Doppler velocity parameters. *Am J Roentgenol* 1993;160:619–625.

Hyafil F, Pelisek J, Laitinen I, Schottelius M, Mohring M, Döring Y et al.Imaging the Cytokine Receptor CXCR4 in Atherosclerotic Plaques with the Radiotracer 68Ga-Pentixafor for PET. *J Nucl Med* 2017;58:499–506.

Hyafil F, Schindler A, Sepp D, Obenhuber T, Bayer-Karpinska A, Boeckh-Behrens T et al.High-risk plaque features can be detected in non-stenotic carotid plaques of patients with ischaemic stroke classified as cryptogenic using combined (18)F-FDG PET/MR imaging. *Eur J Nucl Med Mol I* 2015a;43:270–9.

Hyafil F, Tran-Dinh A, Burg S, Leygnac S, Louedec L, Milliner M et al.Detection of Apoptotic Cells in a Rabbit Model with Atherosclerosis-Like Lesions Using the Positron Emission Tomography Radiotracer [18F]ML-10. *Mol Imaging* 2015b;14:7290.2015.00017.

Iking J, Staniszewska M, Kessler L, Klose JM, Lückerath K, Fendler WP et al.Imaging Inflammation with Positron Emission Tomography. *Biomed* 2021;9:212.

Ikram MA, Seshadri S, Bis JC, Fornage M, DeStefano AL, Aulchenko YS et al.Genomewide Association Studies of Stroke. *New Engl J Medicine* 2009;360:1718–1728.

Imray CH, Tiivas CA.Are some strokes preventable? The potential role of transcranial doppler in transient ischaemic attacks of carotid origin. *The Lancet Neurology* 2005;4:580–586.

Ionita MG, Borne P van den, Catanzariti LM, Moll FL, Vries J-PPM de, Pasterkamp G et al.High Neutrophil Numbers in Human Carotid Atherosclerotic Plaques Are Associated With Characteristics of Rupture-Prone Lesions. *Arteriosclerosis Thrombosis Vasc Biology* 2010;30:1842–1848.

Irkle A, Vesey AT, Lewis DY, Skepper JN, Bird JLE, Dweck MR et al.Identifying active vascular microcalcification by ^{18}F-sodium fluoride positron emission tomography. *Nature Communications* 2015;6:7495.

Ishai A, Tawakol A.Imaging Plaque Inflammation in Higher-Risk Patients: What Do We Know and What Are We Looking For? *Curr Cardiovasc Risk Reports* 2015;9:31.

Itoh T, Matsumoto M, Handa N, Maeda H, Hougaku H, Hashimoto H et al.Rate of successful recording of blood flow signals in the middle cerebral artery using transcranial Doppler sonography. *Stroke* 1993;24:1192–1195.

Jager NA, Westra J, Golestani R, Dam GM van, Low PS, Tio RA et al.Folate Receptor-β Imaging Using 99mTc-Folate to Explore Distribution of Polarized Macrophage Populations in Human Atherosclerotic Plaque. *J Nucl Med* 2014;55:1945–1951.

Jenkins WS, Vesey AT, Vickers A, Neale A, Moles C, Connell M et al.In vivo alpha-V beta-3 integrin expression in human aortic atherosclerosis. *Heart* 2019;105:1868.

Johnson CO, Nguyen M, Roth GA, Nichols E, Alam T, Abate D et al.Global, regional, and national burden of stroke, 1990–2016: a systematic analysis for the Global Burden of Disease Study 2016. *Lancet Neurology* 2019;18:439–458.

Johnson JL, Newby AC.Macrophage heterogeneity in atherosclerotic plaques. *Curr Opin Lipidol* 2009;20:370–378.

Johnston SC, Mendis S, Mathers CD.Global variation in stroke burden and mortality: estimates from monitoring, surveillance, and modelling. *Lancet Neurology* 2009;8:345–354.

Johri AM, Spence JD.Barometer in the Storm—Carotid Artery Plaque Quantified by Three-Dimensional Ultrasound. *J Am Soc Echocardiog* 2013;26:A20.

Joshi FR, Manavaki R, Fryer TD, Figg NL, Sluimer JC, Aigbirhio FI et al.Vascular Imaging With 18F-Fluorodeoxyglucose Positron Emission Tomography Is Influenced by Hypoxia. *J Am Coll Cardiol* 2017;69:1873–1874.

Joshi NV, Vesey AT, Williams MC, Shah ASV, Calvert PA, Craighead FHM et al.18F-fluoride positron emission tomography for identification of ruptured and high-risk coronary atherosclerotic plaques: a prospective clinical trial. *The Lancet* 2014;383:705–713.

Kaczynski J, Sellers S, Seidman MA, Syed M, Dennis M, Mcnaught G et al.18 F-NaF PET/MRI for Detection of Carotid Atheroma in Acute Neurovascular Syndrome. *Radiology* 2022;212283.

Kadoglou NPE, Sfyroeras GS, Spathis A, Gkekas C, Gastounioti A, Mantas G et al.Galectin-3, Carotid Plaque Vulnerability, and Potential Effects of Statin Therapy. *Eur J Vasc Endovasc* 2015;49:4–9.

Kairemo HA, Macapinlac H.Sodium Fluoride PET/CT in Clinical Use, Springer, 2020.

Kakkos SK, Griffin MB, Nicolaides AN, Kyriacou E, Sabetai MM, Tegos T et al.The size of juxtaluminal hypoechoic area in ultrasound images of asymptomatic carotid plaques predicts the occurrence of stroke. *J Vasc Surg* 2013;57:609-618.e1; discussion 617-8.

Kamtchum-Tatuene J, Nomani AZ, Falcione S, Munsterman D, Sykes G, Joy T et al.Non-stenotic Carotid Plaques in Embolic Stroke of Unknown Source. *Front Neurol* 2021;12:719329.

Kanaoka Y, Koga M, Sugiyama K, Ohishi K, Kataoka Y, Yamauchi A.Varenicline enhances oxidized LDL uptake by increasing expression of LOX-1 and CD36 scavenger receptors through α7 nAChR in macrophages. *Toxicology* 2017;380:62–71.

Kanber B, Hartshorne TC, Horsfield MA, Naylor AR, Robinson TG, Ramnarine KV.A novel ultrasound-based carotid plaque risk index associated with the presence of cerebrovascular symptoms. *Ultraschall in der Medizin-European Journal of Ultrasound* 2015;36:480–486.

Karlsson L, Kangefjärd E, Hermansson S, Stromberg S, Österberg K, Nordanstig A et al.Risk of Recurrent Stroke in Patients with Symptomatic Mild (20–49% NASCET) Carotid Artery Stenosis. *European Journal of Vascular and Endovascular Surgery* 2016;52:287–294.

Károlyi M, Seifarth H, Liew G, Schlett CL, Maurovich-Horvat P, Stolzmann P et al.Classification of Coronary Atherosclerotic Plaques Ex Vivo With T1, T2, and Ultrashort Echo Time CMR. *Jacc Cardiovasc Imaging* 2013;6:466–474.

Kawasaki M, Takatsu H, Noda T, Ito Y, Kunishima A, Arai M et al.Noninvasive quantitative tissue characterization and two-dimensional color-coded map of human atherosclerotic lesions using ultrasound integrated backscatter. *J Am Coll Cardiol* 2001;38:486–492.

Kayani I, Conry BG, Groves AM, Win T, Dickson J, Caplin M et al.A Comparison of 68Ga-DOTATATE and 18F-FDG PET/CT in Pulmonary Neuroendocrine Tumors. *J Nucl Med* 2009;50:1927–1932.

Kelly PJ, Camps-Renom P, Giannotti N, Martí-Fàbregas J, Murphy S, McNulty J et al.Carotid Plaque Inflammation Imaged by 18F-Fluorodeoxyglucose Positron Emission Tomography and Risk of Early Recurrent Stroke. *Stroke* 2019;50:1766–1773.

Khenkina N, Aimo A, Fabiani I, Masci PG, Sagris D, Williams SE et al.Magnetic resonance imaging for diagnostic workup of embolic stroke of undetermined source: A systematic review. *Int J stroke : Off J Int Stroke Soc* 2023;17474930231189946.

Kietselaer BLJH, Reutelingsperger CPM, Heidendal GAK, Daemen MJAP, Mess WH, Hofstra L et al.Noninvasive Detection of Plaque Instability with Use of Radiolabeled Annexin A5 in Patients with Carotid-Artery Atherosclerosis. *New Engl J Medicine* 2004;350:1472–1473.

Kim C, Lee JS, Han Y, Chae SY, Jin S, Sung C et al.Glycoprotein IIb/IIIa Receptor Imaging with 18F-GP1 PET for Acute Venous Thromboembolism: An Open-Label, Nonrandomized, Phase 1 Study. *J Nucl Med* 2019;60:244–249.

Kim J, Park JE, Nahrendorf M, Kim D-E.Direct Thrombus Imaging in Stroke. *J Stroke* 2016;18:286–296.

Kim J-M, Lee ES, Park K-Y, Seok JW, Kwon O-S.Comparison of [18F]-FDG and [18F]-NaF Positron Emission Tomography on Culprit Carotid Atherosclerosis A Prospective Study. *Jacc Cardiovasc Imaging* 2018a;12:370–372.

Kim M-J, Shrestha SS, Cortes M, Singh P, Morse C, Liow J-S et al.Evaluation of Two Potent and Selective PET Radioligands to Image COX-1 and COX-2 in Rhesus Monkeys. *J Nucl Med* 2018b;59:1907–1912.

Kimura K, Minematsu K, Koga M, Arakawa R, Yasaka M, Yamagami H et al.Microembolic signals and diffusion-weighted MR imaging abnormalities in acute ischemic stroke. *American Journal of Neuroradiology* 2001;22:1037–1042.

King A, Markus HS.Doppler embolic signals in cerebrovascular disease and prediction of stroke risk. *Stroke* 2009a;40:3711–3717.

King A, Markus HS.Doppler embolic signals in cerebrovascular disease and prediction of stroke risk: a systematic review and meta-analysis. *Stroke* 2009b;40:3711–3717.

King D, Wittenberg R, Patel A, Quayyum Z, Berdunov V, Knapp M.The future incidence, prevalence and costs of stroke in the UK. *Age Ageing* 2020;49:277–282.

Kol A, Libby P.The Mechanisms by Which Infectious Agents May Contribute to Atherosclerosis and Its Clinical Manifestations. *Trends Cardiovas Med* 1998;8:191–199.

Kooi ME, Cappendijk VC, Cleutjens KBJM, Kessels AGH, Kitslaar PJEHM, Borgers M et al.Accumulation of Ultrasmall Superparamagnetic Particles of Iron Oxide in Human Atherosclerotic Plaques Can Be Detected by In Vivo Magnetic Resonance Imaging. *Circulation* 2003;107:2453–2458.

Kopczak A, Schindler A, Bayer-Karpinska A, Koch ML, Sepp D, Zeller J et al.Complicated Carotid Artery Plaques as a Cause of Cryptogenic Stroke. *J Am Coll Cardiol* 2020;76:2212–2222.

Kramer CM, Treiman GS.Vulnerable Plaque in Carotid Arteries Without "Significant" Stenosis Unmasking the Hidden Links to Stroke ∗. *J Am Coll Cardiol* 2020;76:2223–2225.

Krejza J, Mariak Z, Walecki J, Szydlik P, Lewko J, Ustymowicz A.Transcranial color Doppler sonography of basal cerebral arteries in 182 healthy subjects: age and sex variability and normal reference values for blood flow parameters. *AJR American journal of roentgenology* 1999;172:213–218.

Kruth HS.The fate of lipoprotein cholesterol entering the arterial wall. *Curr Opin Lipidol* 1997;8:246–252.

Kuge Y, Takai N, Ogawa Y, Temma T, Zhao Y, Nishigori K et al.Imaging with radiolabelled anti-membrane type 1 matrix metalloproteinase (MT1-MMP) antibody: potentials for characterizing atherosclerotic plaques. *Eur J Nucl Med Mol I* 2010;37:2093–2104.

Kundel V, Reid M, Fayad Z, Ayappa I, Mani V, Rueschman M et al.Sleep duration and vascular inflammation using hybrid positron emission tomography/magnetic resonance imaging: results from the Multi-Ethnic Study of Atherosclerosis (MESA). *J Clin Sleep Med* 2021; DOI: 10.5664/jcsm.9382

Kundel V, Trivieri MG, Karakatsanis NA, Robson PM, Mani V, Kizer JR et al.Assessment of atherosclerotic plaque activity in patients with sleep apnea using hybrid positron emission tomography/magnetic resonance imaging (PET/MRI): a feasibility study. *Sleep Breath* 2018;22:1125–1135.

Kwiecinski J, Cadet S, Daghem M, Lassen ML, Dey D, Dweck MR et al.Whole-vessel coronary 18F-sodium fluoride PET for assessment of the global coronary microcalcification burden. *Eur J Nucl Med Mol I* 2020;47:1736–1745.

Labropoulos N, Mansour MA, Kang SS, Oh DS, Buckman J, Baker WH.Viscoelastic properties of normal and atherosclerotic carotid arteries. *European Journal of Vascular and Endovascular Surgery* 2000;19:221–225.

Lairez O, Robson PM, Fayad ZA.Time to move to PET-MR for cardiovascular imaging. *J Nucl Cardiol* 2016;23:1112–1113.

Laitinen I, Marjamäki P, Någren K, Laine VJO, Wilson I, Leppänen P et al.Uptake of inflammatory cell marker [11C]PK11195 into mouse atherosclerotic plaques. *Eur J Nucl Med Mol I* 2008;36:73.

Laitinen I, Saraste A, Weidl E, Poethko T, Weber AW, Nekolla SG et al.Evaluation of αvβ3 Integrin-Targeted Positron Emission Tomography Tracer 18F-Galacto-RGD for Imaging of Vascular Inflammation in Atherosclerotic Mice. *Circulation Cardiovasc Imaging* 2009;2:331–338.

Lammie GA, Wardlaw J, Allan P, Ruckley CV, Peek R, Signorini DF.What pathological components indicate carotid atheroma activity and can these be identified reliably using ultrasound? *Eur J Ultrasound* 2000;11:77–86.

Lappalainen H, Laine P, Pentikäinen MO, Sajantila A, Kovanen PT.Mast Cells in Neovascularized Human Coronary Plaques Store and Secrete Basic Fibroblast Growth Factor, a Potent Angiogenic Mediator. *Arteriosclerosis Thrombosis Vasc Biology* 2004;24:1880–1885.

Lavra F, Cecco CND, Varga-Szemes A, Santis DD, Albrecht MH, Lesslie VW et al.New Imaging Techniques for Atherosclerotic Plaque Characterization. *Curr Radiology Reports* 2017;5:55.

Lee RH, Vazquez G.Evidence for a prosurvival role of alpha-7 nicotinic acetylcholine receptor in alternatively (M2)-activated macrophages. *Physiological Reports* 2013;1:e00189.

Lemos GB, Borish V, Cole GD, Ramelow S, Lapkiewicz R, Zeilinger A.Quantum Imaging with Undetected Photons. *Arxiv* 2014; DOI: 10.48550/arxiv.1401.4318

Lennard N, Smith J, Dumville J, Abbott R, Evans DH, London NJ et al.Prevention of postoperative thrombotic stroke after carotid endarterectomy: the role of transcranial Doppler ultrasound. *J Vasc Surg* 1997a;26:579–584.

Lennard N, Smith J, Dumville J, Abbott R, Evans DH, London NJ et al.Prevention of postoperative thrombotic stroke after carotid endarterectomy: the role of transcranial Doppler ultrasound. *J Vasc Surg* 1997b;26:579–584.

Lennard N, Smith JL, Gaunt ME, Abbott RJ, London NJ, Bell PR et al.A policy of quality control assessment helps to reduce the risk of intraoperative stroke during carotid endarterectomy. *European Journal of Vascular and Endovascular Surgery* 1999a;17:234–240.

Lennard N, Smith JL, Hayes P, Evans DH, Abbott RJ, London N et al.Transcranial Doppler directed dextran therapy in the prevention of carotid thrombosis: three hour monitoring is as effective as six hours. *European Journal of Vascular and Endovascular Surgery* 1999b;17:301–305.

Lennard NS, Vijayasekar C, Tiivas C, Chan CW, Higman DJ, Imray CH.Control of emboli in patients with recurrent or crescendo transient ischaemic attacks using preoperative transcranial Doppler-directed Dextran therapy. *Br J Surg* 2003;90:166–170.

Li X, Bauer W, Israel I, Kreissl MC, Weirather J, Richter D et al.Targeting P-Selectin by Gallium-68–Labeled Fucoidan Positron Emission Tomography for Noninvasive Characterization of Vulnerable Plaques. *Arteriosclerosis Thrombosis Vasc Biology* 2014;34:1661–1667.

Li X, Heber D, Rausch I, Beitzke D, Mayerhoefer ME, Rasul S et al.Quantitative assessment of atherosclerotic plaques on 18F-FDG PET/MRI: comparison with a PET/CT hybrid system. *Eur J Nucl Med Mol I* 2016;43:1503–1512.

Li X, Samnick S, Lapa C, Israel I, Buck AK, Kreissl MC et al.68Ga-DOTATATE PET/CT for the detection of inflammation of large arteries: correlation with18F-FDG, calcium burden and risk factors. *Ejnmmi Res* 2012;2:52.

Li X, Yu W, Wollenweber T, Lu X, Wei Y, Beitzke D et al.[68Ga]Pentixafor PET/MR imaging of chemokine receptor 4 expression in the human carotid artery. *Eur J Nucl Med Mol I* 2019;46:1616–1625.

Libby P, Buring JE, Badimon L, Hansson GK, Deanfield J, Bittencourt MS et al.Atherosclerosis. *Nat Rev Dis Primers* 2019;5:56.

Libby P, Egan D, Skarlatos S.Roles of Infectious Agents in Atherosclerosis and Restenosis: An Assessment of the Evidence and Need for Future Research. *Circulation* 1997;96:4095–4103.

Libby P, Hansson GK.Inflammation and immunity in diseases of the arterial tree: players and layers. *Circ Res* 2015;116:307–11.

Libby P, Loscalzo J, Ridker PM, Farkouh ME, Hsue PY, Fuster V et al.Inflammation, Immunity, and Infection in Atherothrombosis JACC Review Topic of the Week. *J Am Coll Cardiol* 2018;72:2071–2081.

Libby P, Ridker PM, Hansson GK, Atherothrombosis LTN on.Inflammation in Atherosclerosis: From Pathophysiology to Practice. *Journal of the American College of Cardiology* 2009;54:2129–2138.

Libby P, Ridker PM, Maseri A.Inflammation and Atherosclerosis. *Circulation* 2002;105:1135–1143.

Libby P, Simon DI.Inflammation and Thrombosis. *Circulation* 2001;103:1718–1720.

Libby P, Theroux P.Pathophysiology of Coronary Artery Disease. *Circulation* 2005;111:3481–3488.

Lindegaard K-F, Bakke SJ, Aaslid R, Nornes H.Doppler diagnosis of intracranial artery occlusive disorders. *J Neurol Neurosurg Psychiatry* 1986;49:510–518.

Lindegaard K-F, Bakke SJ, Grolimund P, Aaslid R, Huber P, Nornes H.Assessment of intracranial hemodynamics in carotid artery disease by transcranial Doppler ultrasound. *Journal of neurosurgery* 1985;63:890–898.

Lindegaard K-F, Lundar T, Wiberg J, Sjøberg D, Aaslid R, Nornes H.Variations in middle cerebral artery blood flow investigated with noninvasive transcranial blood velocity measurements. *Stroke* 1987;18:1025–1030.

Lovett JK, Gallagher PJ, Hands LJ, Walton J, Rothwell PM.Histological Correlates of Carotid Plaque Surface Morphology on Lumen Contrast Imaging. *Circulation* 2004a;110:2190–2197.

Lovett JK, Gallagher PJ, Rothwell PM.Reproducibility of Histological Assessment of Carotid Plaque: Implications for Studies of Carotid Imaging. *Cerebrovasc Dis* 2004b;18:117–123.

Lu R, Meng Y, Zhang Y, Zhao W, Wang X, Jin M et al.Superb microvascular imaging (SMI) compared with conventional ultrasound for evaluating thyroid nodules. *Bmc Med Imaging* 2017;17:65.

Luo Y, Pan Q, Yang H, Peng L, Zhang W, Li F.Fibroblast Activation Protein–Targeted PET/CT with 68 Ga-FAPI for Imaging IgG4-Related Disease: Comparison to 18 F-FDG PET/CT. *J Nucl Med* 2020;62:266–271.

MacAskill MG, Newby DE, Tavares AAS.Frontiers in positron emission tomography imaging of the vulnerable atherosclerotic plaque. *Cardiovasc Res* 2019;115:1952–1962.

Mackinnon AD, Aaslid R, Markus HS.Long-term ambulatory monitoring for cerebral emboli using transcranial Doppler ultrasound. *Stroke* 2004;35:73–78.

Mackinnon AD, Aaslid R, Markus HS.Ambulatory transcranial Doppler cerebral embolic signal detection in symptomatic and asymptomatic carotid stenosis. *Stroke* 2005;36:1726–1730.

Maeda H, Etani H, Handa N, Tagaya M, Oku N, Kim B-H et al.A validation study on the reproducibility of transcranial Doppler velocimetry. *Ultrasound in medicine & biology* 1990;16:9–14.

Magnussen JH, Ettrup A, Donat CK, Peters D, Pedersen MHF, Knudsen GM et al.Radiosynthesis and in vitro validation of 3H-NS14492 as a novel high affinity alpha7 nicotinic receptor radioligand. *Eur J Pharmacol* 2015;762:35–41.

Mahmoud AD, Ballantyne MD, Miscianinov V, Pinel K, Hung J, Scanlon JP et al.The Human- and Smooth Muscle Cell-Enriched lncRNA SMILR Promotes Proliferation by Regulating Mitotic CENPF mRNA and Drives Cell-Cycle Progression Which Can Be Targeted to Limit Vascular Remodeling. *Circ Res* 2019;125:535–551.

Malik R, Chauhan G, Traylor M, Sargurupremraj M, Okada Y, Mishra A et al.Multiancestry genome-wide association study of 520,000 subjects identifies 32 loci associated with stroke and stroke subtypes. *Nat Genet* 2018;50:524–537.

Malik R, Traylor M, Pulit SL, Bevan S, Hopewell JC, Holliday EG et al.Low-frequency and common genetic variation in ischemic stroke. *Neurology* 2016;86:1217–1226.

Marinoni M, Ginanneschi A, Forleo P, Amaducci L.Technical limits in transcranial Doppler recording: Inadquate acoustic windows. *Ultrasound in medicine & biology* 1997;23:1275–1277.

Markl M, Wegent F, Zech T, Bauer S, Strecker C, Schumacher M et al.In Vivo Wall Shear Stress Distribution in the Carotid Artery. *Circulation Cardiovasc Imaging* 2010;3:647–655.

Markus H.Monitoring embolism in real time. *Circulation* 2000a;102:826–828.

Markus H, Bland JM, Rose G, Sitzer M, Siebler M.How good is intercenter agreement in the identification of embolic signals in carotid artery disease? *Stroke* 1996;27:1249–1252.

Markus HS.Transcranial Doppler detection of circulating cerebral emboli. A review. *Stroke* 1993;24:1246–1250.

Markus HS.Transcranial Doppler ultrasound. *Br Med Bull* 2000b;56:378–388.

Markus HS, Ackerstaff R, Babikian V, Bladin C, Droste D, Grosset D et al.Intercenter agreement in reading Doppler embolic signals. *Stroke* 1997;28:1307–1310.

Markus HS, Droste DW, Kaps M, Larrue V, Lees KR, Siebler M et al.Dual antiplatelet therapy with clopidogrel and aspirin in symptomatic carotid stenosis evaluated using Doppler embolic signal detection. *Circulation* 2005;111:2233–2240.

Markus HS, Harrison MJ.Microembolic signal detection using ultrasound. *Stroke* 1995;26:1517–1519.

Marnane M, Merwick A, Sheehan OC, Hannon N, Foran P, Grant T et al.Carotid plaque inflammation on 18F-fluorodeoxyglucose positron emission tomography predicts early stroke recurrence. *Annals of neurology* 2012;71:709–718.

Mateo J, Izquierdo-Garcia D, Badimon JJ, Fayad ZA, Fuster V.Noninvasive Assessment of Hypoxia in Rabbit Advanced Atherosclerosis Using 18F-fluoromisonidazole Positron Emission Tomographic Imaging. *Circulation Cardiovasc Imaging* 2018;7:312–320.

Matter CM, Wyss MT, Meier P, Späth N, Lukowicz T von, Lohmann C et al.18F-Choline Images Murine Atherosclerotic Plaques Ex Vivo. *Arteriosclerosis Thrombosis Vasc Biology* 2006;26:584–589.

McMahon CJ, McDermott P, Horsfall D, Selvarajah JR, King AT, Vail A.The reproducibility of transcranial Doppler middle cerebral artery velocity measurements: implications for clinical practice. *British journal of neurosurgery* 2007;21:21–27.

Mechtouff L, Sigovan M, Douek P, Costes N, Bars DL, Mansuy A et al.Simultaneous assessment of microcalcifications and morphological criteria of vulnerability in carotid artery plaque using hybrid 18F-NaF PET/MRI. *J Nucl Cardiol* 2020;1–11.

Mitchell CC, Stein JH, Cook TD, Salamat S, Wang X, Varghese T et al.Histopathologic Validation of Grayscale Carotid Plaque Characteristics Related to Plaque Vulnerability. *Ultrasound Medicine Biology* 2017;43:129–137.

Moreau P-A, Toninelli E, Gregory T, Aspden RS, Morris PA, Padgett MJ.Imaging Bell-type nonlocal behavior. *Sci Adv* 2019;5:eaaw2563.

Moreno PR, Muller JE.Identification of high-risk atherosclerotic plaques: a survey of spectroscopic methods. *Current Opinion in Cardiology* 2002;17:638.

Mori H, Finn AV, Kolodgie FD, Davis HR, Joner M, Virmani R.Physiological Assessment of Coronary Stenoses and the Microcirculation 2017;21–37.

Morrisett J, Vick W, Sharma R, Lawrie G, Reardon M, Ezell E et al.Discrimination of components in atherosclerotic plaques from human carotid endarterectomy specimens by magnetic resonance imaging ex vivo1 1Abbreviations: TBS = Tris buffered saline; MRI = magnetic resonance imaging; CHA = calcium hydroxyapatite; OCT = imbedding medium for frozen tissue specimens; RC = ruptured cap; FC = fibrous cap; EM = extracellular matrix; HB = hemorrhaged blood; SS = surgical slit; LU = lumen; T1 = spin lattice relaxation time; T2 = spin-spin relaxation time. *Magn Reson Imaging* 2003;21:465–474.

Müller MD, Lyrer P, Brown MM, Bonati LH.Carotid artery stenting versus endarterectomy for treatment of carotid artery stenosis. *Cochrane Db Syst Rev* 2020;2:CD000515.

Murshid A, Borges TJ, Lang BJ, Calderwood SK.The Scavenger Receptor SREC-I Cooperates with Toll-Like Receptors to Trigger Inflammatory Innate Immune Responses. *Front Immunol* 2016;7:226.

Muzic RF, DiFilippo FP.Positron Emission Tomography-Magnetic Resonance Imaging: Technical Review. *Semin Roentgenol* 2014;49:242–254.

Naghavi M, Libby P, Falk E, Casscells SW, Litovsky S, Rumberger J et al.From Vulnerable Plaque to Vulnerable Patient. *Circulation* 2003;108:1664–1672.

Nakamura I, Hasegawa K, Wada Y, Hirase T, Node K, Watanabe Y.Detection of early stage atherosclerotic plaques using PET and CT fusion imaging targeting P-selectin in low density lipoprotein receptor-deficient mice. *Biochem Bioph Res Co* 2013;433:47–51.

Naylor AR.Interventions for carotid artery disease: time to confront some ‘inconvenient truths’. *Expert Rev Cardiovasc Ther* 2007;5:1053–1063.

Naylor AR.Carotid artery disease: clinical features and management. *Surgery* 2015a;33:340–344.

Naylor AR.Why is the management of asymptomatic carotid disease so controversial? *Surgeon* 2015b;13:34–43.

Naylor AR, Hayes PD, Allroggen H, Lennard N, Gaunt ME, Thompson MM et al.Reducing the risk of carotid surgery: a 7-year audit of the role of monitoring and quality control assessment. *J Vasc Surg* 2000;32:750–759.

Naylor AR, Ricco JB, Borst GJ de, Debus S, Haro J de, Halliday A et al.Editor's Choice - Management of Atherosclerotic Carotid and Vertebral Artery Disease: 2017 Clinical Practice Guidelines of the European Society for Vascular Surgery (ESVS). *Eur J Vasc Endovasc Surg* 2018;55:3–81.

Naylor R.Carotid webinar 2021;

New SEP, Aikawa E.Role of Extracellular Vesicles in De Novo Mineralization. *Arteriosclerosis Thrombosis Vasc Biology* 2013a;33:1753–1758.

New SEP, Goettsch C, Aikawa M, Marchini JF, Shibasaki M, Yabusaki K et al.Macrophage-Derived Matrix Vesicles. *Circ Res* 2013b;113:72–77.

Nicolaides A, Beach KW, Kyriacou E, Pattichis CS.Ultrasound and carotid bifurcation atherosclerosis, London, Springer-Verlag, 2012.

Niederkorn K, Myers LG, Nunn CL, Ball MR, McKinney WM.Three-dimensional transcranial Doppler blood flow mapping in patients with cerebrovascular disorders. *Stroke* 1988;19:1335–1344.

Nilsen ML.A Historical Account of Stroke and the Evolution of Nursing Care for Stroke Patients. *J Neurosci Nurs* 2010;42:19–27.

Niu C, Wang X, Zhao M, Cai T, Liu P, Li J et al.Macrophage Foam Cell–Derived Extracellular Vesicles Promote Vascular Smooth Muscle Cell Migration and Adhesion. *J Am Heart Assoc* 2016;5. DOI: 10.1161/jaha.116.004099

Noritomi T, Sigel B, Gahtan V, Swami V, Justin J, Feleppa E et al.In vivo detection of carotid plaque thrombus by ultrasonic tissue characterization. *J Ultras Med* 1997;16:107–111.

O'Donnell TF, Erdoes L, Mackey WC, McCullough J, Shepard A, Heggerick P et al.Correlation of B-Mode Ultrasound Imaging and Arteriography With Pathologic Findings at Carotid Endarterectomy. *Arch Surg-chicago* 1985;120:443.

Oliver TB, Lammie GA, Wright AR, Wardlaw J, Patel SG, Peek R et al.Atherosclerotic Plaque at the Carotid Bifurcation: CT Angiographic Appearance with Histopathologic Correlation. *American Journal of Neuroradiology* 1999;20:897–901.

Ota H, Yu W, Underhill HR, Oikawa M, Dong L, Zhao X et al.Hemorrhage and large lipid-rich necrotic cores are independently associated with thin or ruptured fibrous caps: an in vivo 3T MRI study. *Arteriosclerosis Thrombosis Vasc Biology* 2009;29:1696–701.

Paoli FD, Staels B, Chinetti-Gbaguidi G.Macrophage Phenotypes and Their Modulation in Atherosclerosis. *Circ J* 2014;78:1775–1781.

Paraskevas KI, Borst GJ de, Veith FJ.Why randomized controlled trials do not always reflect reality. *J Vasc Surg* 2019;70:607-614.e3.

Paraskevas KI, Kalmykov EL, Naylor AR.Stroke/Death Rates Following Carotid Artery Stenting and Carotid Endarterectomy in Contemporary Administrative Dataset Registries: A Systematic Review. *Eur J Vasc Endovasc* 2016;51:3–12.

Paulos CM, Varghese B, Widmer WR, Breur GJ, Vlashi E, Low PS.Folate-targeted immunotherapy effectively treats established adjuvant and collagen-induced arthritis. *Arthritis Res Ther* 2006;8:R77.

Pawade TA, Doris MK, Bing R, White AC, Forsyth L, Evans E et al.Effect of Denosumab or Alendronic Acid on the Progression of Aortic Stenosis: A Double-Blind Randomized Controlled Trial. *Circulation* 2021;143:2418–2427.

Pawade TA, Newby DE, Dweck MR.Calcification in Aortic Stenosis The Skeleton Key. *J Am Coll Cardiol* 2015;66:561–577.

Pearlman JD, Zajicek J, Merickel MB, Carman CS, Ayers CR, Brookeman JR et al.High-resolution H NMR spectral signature from human atheroma. *Magnetic Resonance in Medicine* 1988;7:262–279.

Pearson TA, Dillman JM, Solex K, Heptinstall RH.Clonal markers in the study of the origin and growth of human atherosclerotic lesions. *Circ Res* 2018;43:10–18.

Pedersen SF, Sandholt BV, Keller SH, Hansen AE, Clemmensen AE, Sillesen H et al.64Cu-DOTATATE PET/MRI for Detection of Activated Macrophages in Carotid Atherosclerotic Plaques. *Arteriosclerosis Thrombosis Vasc Biology* 2015;35:1696–1703.

Perler BA.The Effect of Statin Medications on Perioperative and Long-Term Outcomes Following Carotid Endarterectomy or Stenting. *Semin Vasc Surg* 2007;20:252–258.

Pfeifer A, Knigge U, Mortensen J, Oturai P, Berthelsen AK, Loft A et al.Clinical PET of Neuroendocrine Tumors Using 64Cu-DOTATATE: First-in-Humans Study. *J Nucl Med* 2012;53:1207–1215.

Phadwal K, Vrahnas C, Ganley IG, MacRae VE.Mitochondrial Dysfunction: Cause or Consequence of Vascular Calcification? *Frontiers Cell Dev Biology* 2021;9:611922.

Poole JC, Goss SJ, Harris H.Monoclonal theory of atheroma. *Brit Med J* 1977;1:1596.

Powell J.Vascular News [Internet] 2015;Available from: https://vascularnews.com/janet-powell/

Pozo JL, Ringelstein EB.Noninvasive detection of occlusive disease of the carotid siphon and middle cerebral artery. *Annals of neurology* 1990;28:640–647.

Qiu J.Charles Warlow: a career of "successive flukes". *Lancet Neurology* 2008;7:478.

Quirce R, Martínez-Rodríguez I, Banzo I, Jiménez-Bonilla J, Martínez-Amador N, Ibáñez-Bravo S et al.New insight of functional molecular imaging into the atheroma biology: 18F-NaF and 18F-FDG in symptomatic and asymptomatic carotid plaques after recent CVA. Preliminary results. *Clin Physiol Funct Imaging* 2016;36:499–503.

Quirce R, Martínez-Rodríguez I, Torres MDA, Jiménez-Bonilla JF, Banzo I, Rebollo M et al.Contribution of 18F-sodium fluoride PET/CT to the study of the carotid atheroma calcification. *Revista espanola de medicina nuclear e imagen molecular* 2013;32:22–25.

Rafailidis V, Chryssogonidis I, Xerras C, Grisan E, Cheimariotis G-A, Tegos T et al.An Ultrasonographic Multiparametric Carotid Plaque Risk Index Associated with Cerebrovascular Symptomatology: A Study Comparing Color Doppler Imaging and Contrast-Enhanced Ultrasonography. *Ajnr Am J Neuroradiol* 2019;40:1022–1028.

Rajiah P, Hojjati M, Lu Z, Kosaraju V, Partovi S, O'Donnell JK et al.Feasibility of carotid artery PET/MRI in psoriasis patients. *Am J Nucl Medicine Mol Imaging* 2016;6:223–33.

Rangasamy L, Geronimo BD, Ortín I, Coderch C, Zapico JM, Ramos A et al.Molecular Imaging Probes Based on Matrix Metalloproteinase Inhibitors (MMPIs). *Molecules* 2019;24:2982.

Rashdan NA, Sim AM, Cui L, Phadwal K, Roberts FL, Carter R et al.Osteocalcin Regulates Arterial Calcification Via Altered Wnt Signaling and Glucose Metabolism. *J Bone Miner Res* 2020;35:357–367.

Razuvaev A, Ekstrand J, Folkersen L, Agardh H, Markus D, Swedenborg J et al.Correlations Between Clinical Variables and Gene-expression Profiles in Carotid Plaque Instability. *Eur J Vasc Endovasc* 2011;42:722–730.

Redgrave JNE, Lovett JK, Gallagher PJ, Rothwell PM.Histological assessment of 526 symptomatic carotid plaques in relation to the nature and timing of ischemic symptoms: the Oxford plaque study. *Circulation* 2006;113:2320–2328.

Reimann C, Brangsch J, Colletini F, Walter T, Hamm B, Botnar RM et al.Molecular imaging of the extracellular matrix in the context of atherosclerosis. *Adv Drug Deliver Rev* 2017;113:49–60.

Renton S, Varty K, Loftus I, Garnham A, Imray C, Boyle J et al.The Provision of Services for Patients with Vascular Disease 2018 [Internet], The Vascular Society of Great Britain and Ireland, 2018, [cited 2020 Dec 13].Available from: https://vascularsociety.org.uk/_userfiles/pages/files/Document%20Library/VS%202018%20Final.pdf

Rerkasem K, Rothwell PM.Systematic Review of Randomized Controlled Trials of Patch Angioplasty Versus Primary Closure and Different Types of Patch Materials During Carotid Endarterectomy. *Asian J Surg* 2011;34:32–40.

Ringelstein EB, Droste DW, Babikian VL, Evans DH, Grosset DG, Kaps M et al.Consensus on microembolus detection by TCD. *Stroke* 1998;29:725–729.

Ringelstein EB, Kahlscheuer B, Niggemeyer E, Otis SM.Transcranial Doppler sonography: anatomical landmarks and normal velocity values. *Ultrasound in medicine & biology* 1990;16:745–761.

Ripa RS, Knudsen A, Hag AMF, Lebech A-M, Loft A, Keller SH et al.Feasibility of simultaneous PET/MR of the carotid artery: first clinical experience and comparison to PET/CT. *Am J Nucl Medicine Mol Imaging* 2013;3:361–71.

Ritter MA, Dittrich R, Thoenissen N, Ringelstein EB, Nabavi DG.Prevalence and prognostic impact of microembolic signals in arterial sources of embolism. A systematic review of the literature. *Journal of neurology* 2008a;255:953–961.

Ritter MA, Dittrich R, Thoenissen N, Ringelstein EB, Nabavi DG.Prevalence and prognostic impact of microembolic signals in arterial sources of embolism. *Journal of neurology* 2008b;255:953–961.

Rizvi A, Seyedsaadat SM, Alzuabi M, Murad MH, rd JH, Lehman VT et al.Carotid plaque vulnerability on magnetic resonance imaging and risk of future ischemic events: a systematic review and meta-analysis. *J Neurosurg Sci* 2020;64:480–486.

Roach REJ, Helmerhorst FM, Lijfering WM, Stijnen T, Algra A, Dekkers OM.Combined oral contraceptives: the risk of myocardial infarction and ischemic stroke. *Cochrane Db Syst Rev* 2015;CD011054.

Robson PM, Dey D, Newby DE, Berman D, Li D, Fayad ZA et al.MR/PET Imaging of the Cardiovascular System. *Jacc Cardiovasc Imaging* 2017;10:1165–1179.

Rorick MB, Nichols FT, Adams RJ.Transcranial Doppler correlation with angiography in detection of intracranial stenosis. *Stroke* 1994;25:1931–1934.

Rötering S, Deuther-Conrad W, Cumming P, Donat CK, Scheunemann M, Fischer S et al.Imaging of α7 nicotinic acetylcholine receptors in brain and cerebral vasculature of juvenile pigs with [18F]NS14490. *Ejnmmi Res* 2014;4:43.

Rötering S, Scheunemann M, Fischer S, Hiller A, Peters D, Deuther-Conrad W et al.Radiosynthesis and first evaluation in mice of [18F]NS14490 for molecular imaging of α7 nicotinic acetylcholine receptors. *Bioorgan Med Chem* 2013;21:2635–2642.

Rothwell P, Eliasziw M, Gutnikov S, Fox A, Taylor D, Mayberg M et al.Analysis of pooled data from the randomised controlled trials of endarterectomy for symptomatic carotid stenosis. *Lancet* 2003a;361:107–116.

Rothwell P, Eliasziw M, Gutnikov S, Warlow C, Barnett H, Collaboration for the CET.Endarterectomy for symptomatic carotid stenosis in relation to clinical subgroups and timing of surgery. *Lancet* 2004;363:915–924.

Rothwell PM, Giles MF, Chandratheva A, Marquardt L, Geraghty O, Redgrave JNE et al.Effect of urgent treatment of transient ischaemic attack and minor stroke on early recurrent stroke (EXPRESS study): a prospective population-based sequential comparison. *Lancet* 2007;370:1432–1442.

Rothwell PM, Gutnikov SA, Warlow CP, Collaboration ECST.Reanalysis of the Final Results of the European Carotid Surgery Trial. *Stroke J Am Hear Assoc* 2003b;34:514–523.

Rovelli C.Helgoland, Dublin, Penguin Books, 2020.

Ruberg FL, Viereck J, Phinikaridou A, Qiao Y, Loscalzo J, Hamilton JA.Identification of cholesteryl esters in human carotid atherosclerosis by ex vivo image-guided proton MRS. *Journal of Lipid Research* 2006;47:310–317.

Rudd JHF, Warburton EA, Fryer TD, Jones HA, Clark JC, Antoun N et al.Imaging Atherosclerotic Plaque Inflammation With [18F]-Fluorodeoxyglucose Positron Emission Tomography. *Circulation* 2002;105:2708–2711.

Russell DA, Wijeyaratne SM, Gough MJ.Relationship of carotid plaque echomorphology to presenting symptom. *Eur J Vasc Endovasc Surg* 2010;39:134–138.

Saam T, Ferguson MS, Yarnykh VL, Takaya N, Xu D, Polissar NL et al.Quantitative Evaluation of Carotid Plaque Composition by In Vivo MRI. *Arteriosclerosis Thrombosis Vasc Biology* 2005;25:234–239.

Saba L, Brinjikji W, Spence JD, Wintermark M, Castillo M, Borst GJD et al.Roadmap Consensus on Carotid Artery Plaque Imaging and Impact on Therapy Strategies and Guidelines: An International, Multispecialty, Expert Review and Position Statement. *Am J Neuroradiol* 2021;42:1566–1575.

Saba L, Mallarini G.Fissured fibrous cap of vulnerable carotid plaques and symptomaticity: are they correlated? Preliminary results by using multi-detector-row CT angiography. *Cerebrovasc Dis Basel Switz* 2009;27:322–7.

Saba L, Moody AR, Saam T, Kooi ME, Wasserman BA, Staub D et al.Vessel Wall–Imaging Biomarkers of Carotid Plaque Vulnerability in Stroke Prevention Trials. *Jacc Cardiovasc Imaging* 2020;13:2445–2456.

Sabeti S, Schillinger M, Mlekusch W, Willfort A, Haumer M, Nachtmann T et al.Quantification of Internal Carotid Artery Stenosis with Duplex US: Comparative Analysis of Different Flow Velocity Criteria. *Radiology* 2004;232:431–439.

Saboury B, Ziai P, Alavi A.Detection and Quantification of Molecular Calcification by PET/Computed Tomography: A New Paradigm in Assessing Atherosclerosis. *Pet Clin* 2011;6:409–415.

Sacco RL, Kasner SE, Broderick JP, Caplan LR, Connors JJB, Culebras A et al.An Updated Definition of Stroke for the 21st Century: A Statement for Healthcare Professionals From the American Heart Association/American Stroke Association. *Stroke* 2013;44:2064–2089.

Saedon M, Dilshad A, Tiivas C, Virdee D, Hutchinson CE, Singer DRJ et al.Prospective validation study of transorbital Doppler ultrasound imaging for the detection of transient cerebral microemboli. *Brit J Surg* 2014;101:1551–1555.

Sah B-R, Husmann L, Mayer D, Scherrer A, Rancic Z, Puippe G et al.Diagnostic Performance of 18F-FDG-PET/CT in Vascular Graft Infections. *Eur J Vasc Endovasc* 2015;49:455–464.

Saito D, Oka T, Kajiyama A, Ohnishi N, Shiraki T.Factors predicting compensatory vascular remodelling of the carotid artery affected by atherosclerosis. *Heart* 2002;87:136–139.

Saito H, Kuroda S, Hirata K, Magota K, Shiga T, Tamaki N et al.Validity of Dual MRI and 18F-FDG PET Imaging in Predicting Vulnerable and Inflamed Carotid Plaque. *Cerebrovasc Dis* 2013;35:370–377.

Salem MK, Bown MJ, Sayers RD, West K, Moore D, Nicolaides A et al.Identification of patients with a histologically unstable carotid plaque using ultrasonic plaque image analysis. *Eur J Vasc Endovasc Surg* 2014;48:118–125.

Salem MK, Butt HZ, Choke E, Moore D, West K, Robinson TG et al.Gene and Protein Expression of Chemokine (C-C-Motif) Ligand 19 is Upregulated in Unstable Carotid Atherosclerotic Plaques. *Eur J Vasc Endovasc* 2016;52:427–436.

Salem MK, Sayers RD, Bown MJ, Eveson DJ, Robinson TG, Naylor AR.Rapid Access Carotid Endarterectomy can be Performed in the Hyperacute Period without a Significant Increase in Procedural Risks. *Eur J Vasc Endovasc* 2011;41:222–228.

Salem MK, Sayers RD, Bown MJ, West K, Moore D, Robinson TG et al.Features of unstable carotid plaque during and after the hyperacute period following TIA/stroke. *Eur J Vasc Endovasc Surg* 2013a;45:114–120.

Salem MK, Vijaynagar B, Sayers RD, West K, Moore D, Robinson TG et al.Histologically unstable asymptomatic carotid plaques have altered expression of genes involved in chemokine signalling leading to localised plaque inflammation and rupture. *Eur J Vasc Endovasc Surg* 2013b;45:121–127.

Santilli SM, Stevens RB, Anderson JG, Payne WD, Caldwell MD.Transarterial wall oxygen gradients at the dog carotid bifurcation. *Am J Physiol-heart C* 1995;268:H155–H161.

Sarkar S, Ghosh S, Ghosh SK, Collier A.Role of transcranial Doppler ultrasonography in stroke. *Postgrad Med J* 2007;83:683–689.

Sarlon-Bartoli G, Boudes A, Buffat C, Bartoli MA, Piercecchi-Marti MD, Sarlon E et al.Circulating Lipoprotein-associated Phospholipase A2 in High-grade Carotid Stenosis: A New Biomarker for Predicting Unstable Plaque. *Eur J Vasc Endovasc* 2012;43:154–159.

Saver JL.Cryptogenic Stroke. *New Engl J Medicine* 2016;374:2065–2074.

Schäfers M, Riemann B, Kopka K, Breyholz H-J, Wagner S, Schäfers KP et al.Scintigraphic Imaging of Matrix Metalloproteinase Activity in the Arterial Wall In Vivo. *Circulation* 2004;109:2554–2559.

Schmall JP, Karp JS, Alavi A.The Potential Role of Total Body PET Imaging in Assessment of Atherosclerosis. *Pet Clin* 2019;14:245–250.

Schmidkonz C, Rauber S, Atzinger A, Agarwal R, Götz TI, Soare A et al.Disentangling inflammatory from fibrotic disease activity by fibroblast activation protein imaging. *Ann Rheum Dis* 2020;79:1485–1491.

Schulthess GK von, Kuhn FP, Kaufmann P, Veit-Haibach P.Clinical Positron Emission Tomography/Magnetic Resonance Imaging Applications. *Semin Nucl Med* 2013;43:3–10.

Semenza GL.Hypoxia-Inducible Factors in Physiology and Medicine. *Cell* 2012;148:399–408.

Shahidi S, Owen-Falkenberg A, Gottschalksen B, Ellemann K.Risk of early recurrent stroke in symptomatic carotid stenosis after best medical therapy and before endarterectomy. *Int J Stroke* 2015;11:41–51.

Shaikh S, Welch A, Ramalingam SL, Murray A, Wilson HM, McKiddie F et al.Comparison of fluorodeoxyglucose uptake in symptomatic carotid artery and stable femoral artery plaques. *Brit J Surg* 2014;101:363–370.

Shen Q, Stuart J, Venkatesh B, Wallace J, Lipman J.Inter observer variability of the transcranial Doppler ultrasound technique: impact of lack of practice on the accuracy of measurement. *Journal of clinical monitoring and computing* 1999;15:179–184.

Shinnar M, Fallon JT, Wehrli S, Levin M, Dalmacy D, Fayad ZA et al.The Diagnostic Accuracy of Ex Vivo MRI for Human Atherosclerotic Plaque Characterization. *Arteriosclerosis Thrombosis Vasc Biology* 1999;19:2756–2761.

Silvola JMU, Li X-G, Virta J, Marjamäki P, Liljenbäck H, Hytönen JP et al.Aluminum fluoride-18 labeled folate enables in vivo detection of atherosclerotic plaque inflammation by positron emission tomography. *Sci Rep-uk* 2018;8:9720.

Simon A, Megnien J-L, Chironi G.The Value of Carotid Intima-Media Thickness for Predicting Cardiovascular Risk. *Arteriosclerosis Thrombosis Vasc Biology* 2010;30:182–185.

Sitzer M, Fürst G, Fischer H, Siebler M, Fehlings T, Kleinschmidt A et al.Between-method correlation in quantifying internal carotid stenosis. *Stroke* 1993;24:1513–1518.

Sitzer M, Muller W, Siebler M, Hort W, Kniemeyer HW, Jancke L et al.Plaque ulceration and lumen thrombus are the main sources of cerebral microemboli in high-grade internal carotid artery stenosis. *Stroke* 1995;26:1231–1233.

Skagen K, Johnsrud K, Evensen K, Scott H, Krohg-Sorensen K, Reier-Nilsen F et al.Carotid plaque inflammation assessed with (18)F-FDG PET/CT is higher in symptomatic compared with asymptomatic patients. *Int J Stroke* 2015;10:730–736.

Skagen K, Skjelland M, Zamani M, Russell D.Unstable carotid artery plaque: new insights and controversies in diagnostics and treatment. *Croat Med J* 2016a;57:311–320.

Skagen K, Skjelland M, Zamani M, Russell D.Unstable carotid artery plaque: new insights and controversies in diagnostics and treatment. *Croatian medical journal* 2016b;57:311–320.

Sol AI del, Moons KGM, Hollander M, Hofman A, Koudstaal PJ, Grobbee DE et al.Is Carotid Intima-Media Thickness Useful in Cardiovascular Disease Risk Assessment? *Stroke* 2001;32:1532–1538.

Spence JD.The importance of distinguishing between diffuse carotid intima-media thickening and focal plaque. *Can J Cardiol* 2008;24:61C-64C.

Spence JD.Measurement of Carotid Plaque Burden. *Jama Neurol* 2015;72:383.

Spence JD.Transcranial Doppler monitoring for microemboli: a marker of a high-risk carotid plaque. *Semin Vasc Surg* 2017;30:62–66.

Spence JD, Hackam DG.Treating Arteries Instead of Risk Factors. *Stroke* 2010;41:1193–1199.

Spence JD, Koschinsky M.Mechanisms of Lipoprotein(a) Pathogenicity. *Arteriosclerosis Thrombosis Vasc Biology* 2012;32:1550–1551.

Sriranjan RS, Tarkin JM, Evans NR, Le EPV, Chowdhury MM, Rudd JHF.Atherosclerosis imaging using PET: Insights and applications. *Brit J Pharmacol* 2019; DOI: 10.1111/bph.14868

Stiekema LCA, Stroes ESG, Verweij SL, Kassahun H, Chen L, Wasserman SM et al.Persistent arterial wall inflammation in patients with elevated lipoprotein(a) despite strong low-density lipoprotein cholesterol reduction by proprotein convertase subtilisin/kexin type 9 antibody treatment. *Eur Heart J* 2018;40:2775–2781.

Stork JL, Kimura K, Levi CR, Chambers BR, Abbott AL, Donnan GA.Source of microembolic signals in patients with high-grade carotid stenosis. *Stroke* 2002a;33:2014–2018.

Stork JL, Levi CR, Chambers BR, Abbott AL, Donnan GA.Possible Determinants of Early Microembolism After Carotid Endarterectomy. *Stroke* 2002b;33:2082–2085.

Stroke-Association.Stroke statistics [Internet] 2020;Available from: https://www.stroke.org.uk/what-is-stroke/stroke-statistics#UK%20summary

Stroobant N, Vingerhoets G.Test-retest reliability of functional transcranial Doppler ultrasonography. *Ultrasound in medicine & biology* 2001;27:509–514.

Sugiyama S, Kugiyama K, Aikawa M, Nakamura S, Ogawa H, Libby P.Hypochlorous Acid, a Macrophage Product, Induces Endothelial Apoptosis and

Tissue Factor Expression. *Arteriosclerosis Thrombosis Vasc Biology* 2004;24:1309–1314.

Sun J, Zhao X-Q, Balu N, Neradilek MB, Isquith DA, Yamada K et al.Carotid Plaque Lipid Content and Fibrous Cap Status Predict Systemic CV Outcomes The MRI Substudy in AIM-HIGH. *Jacc Cardiovasc Imaging* 2017;10:241–249.

Syed MB, Fletcher AJ, Forsythe RO, Kaczynski J, Newby DE, Dweck MR et al.Emerging techniques in atherosclerosis imaging. *Br J Radiology* 2019;92:20180309.

Syed MBJ, Fletcher AJ, Debono S, Forsythe RO, Williams MC, Dweck MR et al.18F-Sodium Fluoride Positron Emission Tomography and Computed Tomography in Acute Aortic Syndrome. *Jacc Cardiovasc Imaging* 2022; DOI: 10.1016/j.jcmg.2022.01.003

Tada S, Tarbell JM.Oxygen Mass Transport in a Compliant Carotid Bifurcation Model. *Ann Biomed Eng* 2006;34:1389–1399.

Tahara N, Kai H, Ishibashi M, Nakaura H, Kaida H, Baba K et al.Simvastatin Attenuates Plaque Inflammation. *J Am Coll Cardiol* 2006;48:1825–1831.

Takai H, Uemura J, Yagita Y, Ogawa Y, Kinoshita K, Hirai S et al.Plaque Characteristics of Patients with Symptomatic Mild Carotid Artery Stenosis. *J Stroke Cerebrovasc Dis* 2018;27:1930–1936.

Tarbell J, Mahmoud M, Corti A, Cardoso L, Caro C.The role of oxygen transport in atherosclerosis and vascular disease. *J Roy Soc Interface* 2020;17:20190732.

Tarkin JM, Joshi FR, Evans NR, Chowdhury MM, Figg NL, Shah AV et al.Detection of Atherosclerotic Inflammation by 68Ga-DOTATATE PET Compared to [18F]FDG PET Imaging. *J Am Coll Cardiol* 2017;69:1774–1791.

Tawakol A, Fayad ZA, Mogg R, Alon A, Klimas MT, Dansky H et al.Intensification of statin therapy results in a rapid reduction in atherosclerotic inflammation: results of a multicenter fluorodeoxyglucose-positron emission tomography/computed tomography feasibility study. *J Am Coll Cardiol* 2013;62:909–17.

Tellides G, Pober JS.Inflammatory and Immune Responses in the Arterial Media. *Circ Res* 2015;116:312–322.

Thapar A, Jenkins IH, Mehta A, Davies AH.Diagnosis and management of carotid atherosclerosis. *BMJ* 2013;346:f1485–f1485.

Thompson M.Oxford Textbook of Vascular Surgery, Oxford, Oxford University Press, 2016.

Thrush, Hartshorne, Colin D.Vascular Ultrasound: how, why and when, ed 4th. 2023.

Torbet G.Supermassive black hole resides inside a supermassive galaxy [Internet] 2019;Available from: https://www.digitaltrends.com/cool-tech/messier-87-black-hole-galaxy/

Totaro R, Marini C, Cannarsa C, Prencipe M.Reproducibility of transcranial Dopplersonography: a validation study. *Ultrasound in medicine & biology* 1992;18:173–177.

Truong M, Lennartsson F, Bibic A, Sundius L, Persson A, Siemund R et al.Classifications of atherosclerotic plaque components with T1 and T2* mapping in 11.7 T MRI. *European J Radiology Open* 2021;8:100323.

Tsuruda JS, Saloner D, Anderson C.Noninvasive evaluation of cerebral ischemia. Trends for the 1990s. *Circulation* 1991;83:I176-89.

Tzolos E, Dweck MR.18F-NaF for Imaging Microcalcification Activity in the Cardiovascular System. *Arteriosclerosis Thrombosis Vasc Biology* 2020;40:1620–1626.

Udesh R, Natarajan P, Thiagarajan K, Wechsler LR, Crammond DJ, Balzer JR et al.Transcranial Doppler Monitoring in Carotid Endarterectomy: A Systematic Review and Meta-analysis. *J Ultrasound Med* 2017;36:621–630.

Underhill HR, Yuan C, Zhao X-Q, Kraiss LW, Parker DL, Saam T et al.Effect of rosuvastatin therapy on carotid plaque morphology and composition in moderately hypercholesterolemic patients: A high-resolution magnetic resonance imaging trial. *Am Heart J* 2008;155:584.e1-584.e8.

Ungar B, Pavel AB, Robson PM, Kaufman A, Pruzan A, Brunner P et al.A Preliminary 18F-FDG-PET/MRI Study Shows Increased Vascular Inflammation in Moderate-to-Severe Atopic Dermatitis. *J Allergy Clin Immunol Pract* 2020;8:3500–3506.

Valk FM van der, Sluimer JC, Vöö SA, Verberne HJ, Nederveen AJ, Windhorst AD et al.In Vivo Imaging of Hypoxia in Atherosclerotic Plaques in Humans. *Jacc Cardiovasc Imaging* 2015;8:1340–1341.

Valton L, Larrue V, Traon AP le, Massabuau P, Géraud G.Microembolic signals and risk of early recurrence in patients with stroke or transient ischemic attack. *Stroke* 1998;29:2125–2128.

Varasteh Z, Mohanta S, Robu S, Braeuer M, Li Y, Omidvari N et al.Molecular Imaging of Fibroblast Activity After Myocardial Infarction Using a 68Ga-Labeled Fibroblast Activation Protein Inhibitor, FAPI-04. *J Nucl Med* 2019;60:1743–1749.

Vavra AK, Eskandari MK.Treatment options for symptomatic carotid stenosis: timing and approach. *Surgeon* 2015;13:44–51.

Venkatesh B, Shen Q, Lipman J.Continuous measurement of cerebral blood flow velocity using transcranial Doppler reveals significant moment-to-moment variability of data in healthy volunteers and in patients with subarachnoid hemorrhage. *Critical care medicine* 2002;30:563–569.

Verhoeven B, Vries J de, Pasterkamp G, Ackerstaff R, Schoneveld AH, Velema E et al.Carotid atherosclerotic plaque characteristics are associated with microembolization during carotid endarterectomy and procedural outcome. *Stroke* 2005a;36:1735–1740.

Verhoeven BAN, Velema E, Schoneveld AH, Vries JPPM de., Bruin P de, Seldenrijk CA et al.Athero-express: Differential atherosclerotic plaque expression of mRNA and protein in relation to cardiovascular events and patient characteristics. Rationale and design. *Eur J Epidemiol* 2004;19:1127–1133.

Verhoeven N, Vries JPPM de, Pasterkamp G, Ackerstaff RGA, Schoneveld AH, Velema E et al.Carotid Atherosclerotic Plaque Characteristics Are Associated With Microembolization During Carotid Endarterectomy and Procedural Outcome. *Stroke* 2005b;36:1735–1740.

Vesey AT, Jenkins WSA, Irkle A, Moss A, Sng G, Forsythe RO et al.18F-Fluoride and 18F-Fluorodeoxyglucose Positron Emission Tomography After Transient Ischemic Attack or Minor Ischemic StrokeCLINICAL PERSPECTIVE: Case–Control Study. *Circulation: Cardiovascular Imaging* 2017;10:e004976.

Vingerhoets G, Stroobant N.Lateralization of cerebral blood flow velocity changes during cognitive tasks. A simultaneous bilateral transcranial Doppler study. *Stroke* 1999;30:2152–2158.

Vingerhoets G, Stroobant N.Reliability and validity of day-to-day blood flow velocity reactivity in a single subject: an fTCD study. *Ultrasound in medicine & biology* 2002;28:197–202.

Vinitski S, Consigny PM, Shapiro MJ, Janes N, Smullens SN, Rifkin MD.Magnetic resonance chemical shift imaging and spectroscopy of atherosclerotic plaque. *Investigative radiology* 1991;26:703–714.

Virmani R, Kolodgie FD, Burke AP, Finn AV, Gold HK, Tulenko TN et al.Atherosclerotic Plaque Progression and Vulnerability to Rupture. *Arteriosclerosis Thrombosis Vasc Biology* 2005;25:2054–2061.

Vöö S, Kwee RM, Sluimer JC, Schreuder FHBM, Wierts R, Bauwens M et al.Imaging Intraplaque Inflammation in Carotid Atherosclerosis With 18F-Fluorocholine Positron Emission Tomography–Computed Tomography. *Circulation Cardiovasc Imaging* 2018;9:e004467.

Vorst EPC van der, Döring Y, Weber C.Chemokines and their receptors in Atherosclerosis. *J Mol Med* 2015;93:963–971.

Waissi F, Dekker M, Timmerman N, Hoogeveen RM, Bennekom J van, Dzobo KE et al.Elevated Lp(a) (Lipoprotein[a]) Levels Increase Risk of 30-Day Major Adverse Cardiovascular Events in Patients Following Carotid Endarterectomy. *Stroke* 2020;51:2972–2982.

Walker LJ, Ismail A, McMeekin W, Lambert D, Mendelow AD, Birchall D.Computed Tomography Angiography for the Evaluation of Carotid Atherosclerotic Plaque. *Stroke* 2002;33:977–981.

Wan MYS, Endozo R, Michopoulou S, Shortman R, Rodriguez-Justo M, Menezes L et al.PET/CT Imaging of Unstable Carotid Plaque with 68Ga-Labeled Somatostatin Receptor Ligand. *J Nucl Med* 2017;58:774–780.

Wang D, Chen X, Yang T, Guo F, Liang CW and Y-K.The availability of the fibroblast activation protein receptor in early identification of vulnerable atherosclerotic plaques: A preclinical study using a 68Ga-FAPI PET. *Journal of Nuclear Medicine* 2021;62:1395.

Wang Y, Yao M, Zou M, Li S, Ge Z, Hong Y et al.Assessment of Carotid Intraplaque Neovascularization Using Superb Microvascular Imaging in High Risk of Stroke Individuals: Results From a Community-Based Study. *Front Neurol* 2019;10:1146.

Wardlaw JM, Chappell FM, Best JJ, Wartolowska K, Berry E, Research NHS et al.Non-invasive imaging compared with intra-arterial angiography in the diagnosis of symptomatic carotid stenosis: a meta-analysis. *Lancet* 2006a;367:1503–1512.

Wardlaw JM, Chappell FM, Stevenson M, Nigris ED, Thomas S, Gillard J et al.Accurate, practical and cost-effective assessment of carotid stenosis in the UK. *Health Technol Assess* 2006b;10:iii-iv-ix-x-1–182.

Wardlaw JM, Smith C, Dichgans M.Small vessel disease: mechanisms and clinical implications. *Lancet Neurology* 2019;18:684–696.

Wasserman BA, Wityk RJ, Trout HH, Virmani R.Low-Grade Carotid Stenosis. *Stroke* 2005;36:2504–2513.

Waton S, Johal A, Birmpili P, Li Q, Cromwell D, Boyle J et al.National Vascular Registry 2020 Annual Report [Internet], The Royal College of Surgeons of England, 2020, [cited 2020 Dec 9].Available from: https://www.vsqip.org.uk/content/uploads/2020/11/NVR-2020-Annual-Report.pdf

Waton S, Johal A, Groene O, Cromwell D, Mitchell D, Loftus I.UK Carotid Endarterectomy Audit. Round 5., London, The Royal College of Surgeons of England, 2013.

Wehrum T, Dragonu I, Strecker C, Schuchardt F, Hennemuth A, Drexl J et al.Aortic atheroma as a source of stroke – assessment of embolization risk using 3D CMR in stroke patients and controls. *J Cardiov Magn Reson* 2017;19:67.

Wekesa AL, Cross KS, O'Donovan O, Dowdall JF, O'Brien O, Doyle M et al.Predicting Carotid Artery Disease and Plaque Instability from Cell-derived Microparticles. *Eur J Vasc Endovasc* 2014;48:489–495.

Wessels T, Harrer JU, Stetter S, Mull M, Klötzsch C.Three-Dimensional Assessment of Extracranial Doppler Sonography in Carotid Artery Stenosis Compared With Digital Subtraction Angiography. *Stroke* 2004;35:1847–1851.

Wijnhoud AD, Franckena M, Lugt A van der, Koudstaal PJ, Dippel ED.Inadequate acoustical temporal bone window in patients with a transient ischemic attack or minor stroke: role of skull thickness and bone density. *Ultrasound in medicine & biology* 2008;34:923–929.

Wintermark M, Jawadi SS, Rapp JH, Tihan T, Tong E, Glidden DV et al.High-resolution CT imaging of carotid artery atherosclerotic plaques. *Ajnr Am J Neuroradiol* 2008;29:875–82.

Wolf O, Heider P, Heinz M, Poppert H, Sander D, Greil O et al.Microembolic signals detected by transcranial Doppler sonography during carotid endarterectomy and correlation with serial diffusion-weighted imaging. *Stroke* 2004a;35:e373–e375.

Wolf O, Heider P, Heinz M, Poppert H, Sander D, Greil O et al.Microembolic signals detected by transcranial Doppler sonography during carotid endarterectomy and correlation with serial diffusion-weighted imaging. *Stroke* 2004b;35:e373–e375.

Wong DF, Kuwabara H, Pomper M, Holt DP, Brasic JR, George N et al.Human Brain Imaging of α7 nAChR with [18F]ASEM: a New PET Radiotracer for Neuropsychiatry and Determination of Drug Occupancy. *Mol Imaging Biol* 2014;16:730–738.

Wongpakaran N, Wongpakaran T, Wedding D, Gwet KL.A comparison of Cohen's Kappa and Gwet's AC1 when calculating inter-rater reliability coefficients: a study conducted with personality disorder samples. *Bmc Med Res Methodol* 2013;13:61–61.

World-Stroke-Organization.The Global Stroke Fact Sheet [Internet], 2019.Available from: https://www.world-stroke.org/assets/downloads/WSO_Global_Stroke_Fact_Sheet.pdf

Wu M, Ning J, Li J, Lai Z, Shi X, Xing H et al.Feasibility of in vivo Imaging of Fibroblast Activation Protein in Human Arterial Walls. *J Nucl Med* 2021;jnumed.121.262863.

Wüst RCI, Calcagno C, Daal MRR, Nederveen AJ, Coolen BF, Strijkers GJ.Emerging Magnetic Resonance Imaging Techniques for Atherosclerosis Imaging. *Arteriosclerosis Thrombosis Vasc Biology* 2019;39:841–849.

Xia J, Yin A, Li Z, Liu X, Peng X, Xie N.Quantitative Analysis of Lipid-Rich Necrotic Core in Carotid Atherosclerotic Plaques by In Vivo Magnetic Resonance Imaging and Clinical Outcomes. *Medical Sci Monit Int Medical J Exp Clin Res* 2017;23:2745–2750.

Xu F, Ji J, Li L, Chen R, Hu W.Activation of adventitial fibroblasts contributes to the early development of atherosclerosis: A novel hypothesis that complements the "Response-to-Injury Hypothesis" and the "Inflammation Hypothesis". *Med Hypotheses* 2007;69:908–912.

Yang F, Wang C.Consistency of superb microvascular imaging and contrast enhanced ultrasonography in detecting intraplaque neovascularization: a meta-analysis. *Biorxiv* 2020;2020.03.13.990374.

Yao L, Heuser-Baker J, Herlea-Pana O, Iida R, Wang Q, Zou M et al.Bone Marrow Endothelial Progenitors Augment Atherosclerotic Plaque Regression in a Mouse Model of Plasma Lipid Lowering. *Stem Cells* 2012;30:2720–2731.

Yoshida K, Fukumitsu R, Kurosaki Y, Nagata M, Tao Y, Suzuki M et al.Carotid Endarterectomy for Medical Therapy-Resistant Symptomatic Low-Grade Stenosis. *World Neurosurg* 2019;123:e543–e548.

Yoshida K, Sadamasa N, Narumi O, Chin M, Yamagata S, Miyamoto S.Symptomatic Low-Grade Carotid Stenosis With Intraplaque Hemorrhage and Expansive Arterial Remodeling Is Associated With a High Relapse Rate Refractory to Medical Treatment. *Neurosurgery* 2012;70:1143–1151.

Yu C-M, Zhang Q, Lam L, Lin H, Kong S-L, Chan W et al.Comparison of intensive and low-dose atorvastatin therapy in the reduction of carotid intimal-medial thickness in patients with coronary heart disease. *Heart* 2007;93:933–939.

Yuan C.Vessel Based Imaging Techniques: Diagnosis, Treatment, and Prevention, Springer Nature, 2019.

Yuan C, Mitsumori LM, Beach KW, Maravilla KR.Carotid Atherosclerotic Plaque: Noninvasive MR Characterization and Identification of Vulnerable Lesions. *Radiology* 2001a;221:285–299.

Yuan C, Mitsumori LM, Ferguson MS, Polissar NL, Echelard D, Ortiz G et al.In Vivo Accuracy of Multispectral Magnetic Resonance Imaging for Identifying

Lipid-Rich Necrotic Cores and Intraplaque Hemorrhage in Advanced Human Carotid Plaques. *Circulation* 2001b;104:2051–2056.

Yusuf S, Collins R, Peto R.Why do we need some large, simple randomized trials? *Stat Med* 1984;3:409–420.

Zajicek J, Pearlman JD, Merickel MB, Ayers CR, Brookeman JR, Brown MF.High-resolution proton NMR spectra of human arterial plaque. *Biochemical and Biophysical Research Communications* 1987;149:437–442.

Zamani M, Skagen K, Scott H, Russell D, Skjelland M.Advanced ultrasound Methods in assessment of carotid plaque instability: A prospective multimodal study 2020; DOI: 10.21203/rs.2.9292/v4

Zhao X-Q, Hatsukami TS.Risk Factors for Development of Carotid Plaque Components ∗. *Jacc Cardiovasc Imaging* 2018;11:193–195.

Zhu Y-C, Zhang Y, Deng S-H, Jiang Q.Diagnostic Performance of Superb Microvascular Imaging (SMI) Combined with Shear-Wave Elastography in Evaluating Breast Lesions. *Medical Sci Monit Int Medical J Exp Clin Res* 2018;24:5935–5942.